The surface properties effect on bacterial attachment and biofilm formation

A thesis submitted to the Faculty of Science, Agriculture and Engineering for the Degree of Doctor of Philosophy

By

YuFeng Zhu

School of Engineering, Newcastle University

2023

To my dear family and beloved friends who supported me on this journey

Abstract

Many microorganisms form sessile communities, called biofilms, in self-produced extracellular polymeric substances (EPS), which often attach to solid surfaces. Biofilms are central to addressing the most pressing global challenges in every sector application, from medicine to industry to the environment, and play a considerable economic and social influence. The surface roughness and wettability can affect bacterial attachment and biofilm formation. However, there was a lack of studies about how the surface roughness and wettability will affect bacterial attachment and biofilm formation in both static and flow conditions.

In this Ph.D. project, we started with studying the surface roughness and wettability effect of typical biomaterials polydimethylsiloxane (PDMS) on bacterial attachment and biofilm formation of the key biofilm-forming pathogens *Staphylococcus epidermidis* and *Pseudomonas aeruginosa*. The plain PDMS was cast on a petri dish and different sandpapers (P240 and P120) to create different roughness (0.0768 to 15.51μm). These surfaces with different roughness led to contact angles of 117.5 ± 1.1°, 129 ± 5.0° and 115.0 ± 3.1°, respectively. And their corresponding contact angle hysteresis is 21.4 ±2.1°, 20.6 ± 3.5°, and 17.1 ± 5.8°. The results have demonstrated that the roughened surfaces led to much dense and thicker biofilms for both bacteria, although the initial bacterial attachment on rough surfaces with Ra=15.51μm did not differ much. This could be due to stronger adhesion of bacterial attachment on rougher surfaces.

Then, we use both plain PDMS and roughened PDMS to prepare slippery surfaces (with very low contact angle hysteresis) by infusing silicone oil. We fabricated the materials with varied oil thicknesses (50, 20, 5, 2μm) atop the surface. In the static conditions, all slippery surfaces only have little bacterial adhesion for *Staphylococcus epidermidis* and *Pseudomonas aeruginosa*, even for the 14days long-term culture. However, the significant bacterial attachment was found for surfaces with initial thin oil (5, 2μm) after 7 days of dynamic culture (the wall shear stress=0.01Pa). This is due to flow shear-induced oil depletion.

Finally, we fabricated another two slippery surfaces with very low contact angle hysteresis: Slippery Omnipobic Covalently Attached Liquid-like (SOCAL) surface, and Polyethylene glycol (PEG) surface. As silver nanoparticles (AgNPs) are commercially used antimicrobial surfaces. We also prepared AgNPs-coated PDMS as comparisons. All these surfaces have demonstrated excellent resistance against biofilm formation under static and dynamic conditions (with a reduction of biofilm by 2-4 orders of magnitude) compared to plain PDMS, even after 14 days of culture. Notably, the total biomass of *Staphylococcus epidermidis on* SOCAL is 1-2 orders of magnitude larger than that on PEG in static and dynamic culture, and vice versa when culturing *Pseudomonas aeruginosa*. This suggests that *Staphylococcus epidermidis* may be preferable to the hydrophilic surface and it is vice versa for *Pseudomonas aeruginosa*. In addition, when cultured *Pseudomonas aeruginosa* after 2 days, 7 days, and 14 days in static, much EPS has produced on AgNPs-coated PDMS surface. Since the adhesion between EPS and the coating is stronger than that between the coating and the PDMS surface, the coating will be easily peeled off when using the Phosphate Buffered Saline (PBS) to wash the surface. However, silver ions are still present in the solution, which can also kill bacteria. These slippery surfaces offer a new anti-biofilm strategy for medical device applications, while other areas where biofilm development is problematic. The liquid-like solid surfaces demonstrated better antibiofilm performance in flow conditions, compared to liquid-infused surfaces.

Acknowledgments

Throughout my PhD at Newcastle University, I had the opportunity to meet a lot of kind and wonderful people here who have supported me a lot in my life and my research.

Firstly, I would like to express my sincere gratitude to my supervisors Dr. Jinju Chen, Prof. Nicholas S Jakubovics, and Prof Waldemar Vollmer. They provided me with lab space and their office door was always open to answer my questions. I am most deeply grateful to the three mentors who shared a wealth of knowledge and expertise to steer my research in the right direction. Without their patience, advice, and encouragement, I would not have been able to complete my Ph.D. and become an independent researcher.

I thank Dr. Rolando Berlinguer-Palmini, Dr. Alex Laude, Ross Laws and Tracey Davey for technical support of imaging. I also acknowledge the technical assistance from Mr. Dave Race, Mrs. Ekaterina Kozhevnikova and Dr Nadia Rostami. I also acknowledge Dr. George Roberts and Prof. Anthony O'Neill for their technical support on ellipsometry. I also acknowledge Prof. Lidija Siller at NEXUS, Newcastle University for the XPS measurements. Especially thanks to Prof Glen McHale, Dr. Gary Wells, Dr. Hernan Barrio-Zhang and Dr Steven Armstrong for preparing SOCAL on glass and PEG samples on glass.

Heartfelt thanks to my friends HuiDong Wei, Adam West, and JiaLu Lu who helped me to proofread the thesis and gave me good modification suggestions. I would like to thank my family, especially my Dad, Mum, for their endless support in my Ph.D. study mentally and financially. They gave me faith, motivation and backing in life, making me feel like I have a strong pillar when I need it.

Contents

List of Figure

List of Table

List of Abbreviations

AgNPs	silver nanoparticles
AFM	Atomic force microscopy
CA	contact angle
CAH	Contact angle hysteresis
CPD	critical point drying
CF	Cystic fibrosis
DLVO theory	Derjaguin–Landau–Verwey–Overbeek theory
EPS	extracellular polymeric substance
HMDS	Hexamethyltiisilizane
PAO1	*Pseudomonas aeruginosa*
PBS	Phosphate Buffered Saline
PDMS	polydimethylsiloxane
PEG	Polyethylene glycol
S. epidermidis	*Staphylococcus epidermidis*
SLIPS	slippery liquid infused surfaces
SEM	scanning electron microscope
S-PDMS	swollen polydimethylsiloxane
SOCAL	Slippery Omnipobic Covalently Attached Liquid-like
TSB	Trypticase Soy Broth

List of publications

A first-authored paper published in ACS AMI in 2022. Zhu, Y.; McHale, G.; Dawson, J.; Armstrong, S.; Wells, G.; Han, R.; Liu, H.; Vollmer, W.; Stoodley, P.; Jakubovics, N., Slippery Liquid-Like Solid Surfaces with Promising Antibiofilm Performance in both Static and Flow Conditions. *ACS Applied Materials & interfaces*, 2022, 14(5), 6307-6319.

Co-authored a paper published in Langmuir in 2020. Cao, Y.; Jana, S.; Tan, X.; Bowen, L.; **Zhu, Y**.; Dawson, J.; Han, R.; Exton, J.; Liu, H.; McHale, G., Antiwetting and antifouling performances of different Lubricant-Infused slippery surfaces. *Langmuir* 2020, 36 (45), 13396-13407.

1 Introduction

Bacterial biofilms are communities of microorganisms attached to moist surfaces and encapsulated in a self-produced matrix called extracellular polymeric substance (EPS) [25]. Biofilm associated infections have dramatic economic and societal impacts. For instance, it was estimated that biofilm infections cost about $94 billion p.a. in the United States healthcare system [26]. Moreover, around 6–14% of hospitalised patients suffer from biofilm infections associated with medical devices, such as urinary catheters, peritoneal dialysis catheters, tracheal prostheses, pacemakers, endotracheal tubes, dental implants, and orthopaedic implants [27]. Among these, catheter-associated urinary tract infections (CAUTI) in hospitals, are estimated to cause additional health-care costs of £1–2.5 billion in the UK alone [28]. Catheter-related bloodstream infections (CRBSIs) are mainly responsible for nosocomial infection in intensive care units (ICUs), resulting in morbidity, mortality, and significant economic cost [29, 30].

Methods to prevent biofilm formation and growth on medical devices surfaces include immobilisation of antimicrobial agents [31] (i.e., antibiotics, peptide, silver nanoparticles or nitric oxide), the use of special surface texture [32-36], surface grafting with poly (ethylene glycol) (PEG) or zwitterionic polymers [37, 38], quaternary ammonium salt functionalized fluorinated copolymers [39] and the use of biofilm-dispersing enzymes [40]. All anti-biofilm surfaces have their own challenges. For instance, surfaces based on antimicrobial agents lose their efficacy over time and they can potentially trigger antimicrobial resistance [32, 40]. Antibiofilm surface textures have either nanospears to mechanically rupture the bacterial cell wall, causing cell lysis [32-34, 36], or they trap air within micro- or nanostructures to restrict direct contact between the solid surface and micro-organisms [41-43]. For the former, the fast-growing surviving bacteria mask the nanospear structures which restricts their long-term antimicrobial efficiency [32]. For the latter, the anti-biofilm efficacy strongly depends on the lifetime of the non-wetting (Cassie) state, which is often short in submerged environments [41, 44, 45]. The antibiofilm performance of surfaces grafted with poly (ethylene glycol) (PEG) or zwitterionic polymers is also transient because the adsorption of proteins and surfactants secreted by bacteria can mask the underlying surface [46]. Although these surfaces are promising, new developments are required to improve their durability.

Recently, anti-biofilm approaches have been developed based on endowing the surface with a liquid lubricant [47]. There are many physical and chemical methods which can potentially maintain a stable lubricant layer by capillary force, chemical interactions, swelling and employing microcapsules to lock the lubricants [48]. Typically, a porous or textured solid surface is infused with a liquid lubricant locked-in to the structure by capillary forces to create a stable hemi-solid/hemi-liquid surface or a continuous lubricant coating (a slippery liquid-infused porous surface – SLIPS) [49, 50]. Another complementary liquid lubricant-based approach uses a polydimethylsiloxane (PDMS) matrix infused with silicone oil (known as S-PDMS) causing it to swell and locking in a large reservoir of oil in the polymer chains [51, 52]. These liquid lubricant-based surfaces inhibit the surface attachment of bacteria and have great promise as antibiofilm surfaces [53-62]. However, the potential loss of lubricant through repeated usage or shear [63-65] remains a key limiting factor to wider adoption as a practical solution. In clinical settings, this may be a safety risk for patients. Although many factors are involved in the formation of biofilms, the antimicrobial effects of surface roughness and chemical surface coatings have been largely debated in the scientific community [2]. While the exact mechanism of inhibition is not fully understood, many opposing, and widely varying results have been published regarding the degree of biofilm prevention of these two factors.

In this project, we proposed to investigate the effects of surface properties such as wettability and roughness on bacterial attachment and biofilm formation. We also examined the antibiofilm efficiency of a commonly used antimicrobial agents (silver nanoparticles) and various slippery surfaces. Growth of clinically relevant bacterial strains (*Staphylococcus epidermidis* or *Pseudomonas aeruginosa*) was assessed on different surfaces. Quantitative analysis of bacterial growth by confocal microscopy demonstrates anti-biofilm efficacy, as well as observation of cell distribution/arrangement within surface structures by scanning electron microscope (SEM).

1.1 Aim and Objective

The primary aim of this study is to investigate the bacteria adhesion and biofilm formation on different surfaces under static and dynamic conditions with different time scales.

The specific objectives are to:

- Examine the effect of roughness and surface wetting on bacterial attachment and biofilm formation.
- Reveal how the thickness of silicon oil atop S-PDMS may affect the antibiofilm efficacy.
- Examine the antibiofilm efficiency of commonly used antimicrobial agents (silver nanoparticles) and some novel slippery coatings (e.g., SOCAL and PEG)

1.2 Thesis structure

To achieve the objectives of this study, the thesis is divided into seven chapters.

Chapter 1 A brief introduction to the beginning of the thesis, including the main aims and objectives, and a description of the structure of the thesis.

Chapter 2 A detailed literature review of the biofilms, including their history, importance of controlling biofilm formation, biofilm structure, the difference between Gram-positive and Gram-negative bacterial, biofilm formation and lifecycles, mechanisms of bacterial attachment, factors (i.e., surface charge, hydrophobicity, roughness, topography, bacterial surface and appendages) affecting initial bacterial adhesion. In addition, the current development of antibacterial surfaces (either bactericidal or anti-fouling) was discussed.

Chapter 3 summarized the general methodology and techniques used in this study. The main protocol of bacterial culture, antibiofilm test and flow cell design were described. the main characterization techniques: wettability, confocal microscopy, critical point drying, and SEM analysis were described with sufficient details.

Chapter 4 investigated the bacterial adhesion and biofilm formation of *S. epidermidis* and *P. aeruginosa* on different roughness PDMS (Plain PDMS, P240, P120 and P400) under static and dynamic conditions with different time scales. We described the fabrication method of rough PDMS and measured wettability and roughness on different surfaces.

Chapter 5 investigated the bacterial adhesion and biofilm formation of *S.epidermidis* and *P.aeruginosa* on different oil thicknesses (50, 20, 5, 2μm) roughened PDMS surfaces (plain PDMS, P240 and P120) under static and dynamic conditions with different time scales. We described the fabrication method of the different oil thickness slippery surfaces and measured wettability.

Chapter 6 presented the antibiofilm performance of liquid-like solid surfaces and Ag nanoparticles coated surfaces with *S.epidermidis* and *P.aeruginosa* under static and dynamic conditions after 2 hours, 2 days, 7 days and 14 days. We also described the fabrication method of the SOCAL, PEG and AgNPs-coated PDMS surfaces.

Chapter 7 concluded the research work in this thesis and provides an outlook for future work.

2 Literature review

2.1 History of biofilm

As early as April 24, 1676, several kinds of microorganisms have been discovered in steeped-pepper preparation by the Dutch scientist Anthony van Leeuwenhoek, which included bacteria. It is a "great wonder" at that time [2, 66]. And there is a letter sent to the Royal Society which reported the discovery of bacteria and dated at Delft on October 9, 1676, [67]. Until 1684, van Leeuwenhoek used his primitive microscope to observe the biofilms, describing many accumulations of microorganisms on teeth surfaces, which he called "microorganisms in the scurf" [68]. In 1864, the French scientist Louis Pasteur who is the pioneer of microbiology observed and sketched aggregates of bacteria as the cause of wine becoming acetic [69, 70].

The earliest description of bacterial adhesion, aggregation, and multiplication on surfaces is called "slime" or "film" [67]. In 1933, it was introduced in marine microbiology. It is used to distinguish adhering bacteria from free-swimming 'planktonic' bacteria [71]. While in 1922, Angst had already observed there are vast 'slime' on the bottom of ships caused by bacteria [70]. Henrici studied biofouling in freshwater, he discovered that most of the water bacteria are not free-floating organisms, they grow attached to the submerged surface [71]. In 1935, Zobell and Allen first proposed the concept of 'biofilm' through their research on adherence and growth of bacteria on submerged glass slides in seawater [72]. They also found that biofouling was caused by bacteria that grew on biofilms and, to a lesser extent, by other microorganisms, which were conducive to the subsequent attachment of large, more harmful organisms [67, 72].

The first case in medicine linked between the etiology of a persistent (chronic) infection and aggregated bacteria is from 1970 to 1972. In cystic fibrosis (CF) patients who died of chronic *P.aeruginosa* lung infection [73]. In 1980, J. W. Costerton's group published postmortem electron microscopic observation of *P. aeruginosa* microcolonies in CF lung and investigation of the bacterial glycocalyx in nature and disease, and later he replaced 'glycocalyx' with 'biofilms' in his next survey [74-76].

The first biofilm publication which used ‘biofilm’ as the query word is in 1975. It described a technical biofilm problem [77]. In 1981, the first two medical reports published the word ‘biofilm’ by dentists from the University of Lund, Sweden [78, 79]. In the same year, J. W. Costerton first used the term ‘biofilm’ in a technical microbiology report [80, 81]. Since J. W. Costerton introduced the word ‘biofilm’ in medical microbiology in 1985, it has gradually become the most appropriate term for the description of the growth of the body [81, 82].

To summarise the history of biofilm development, in the period before 1980, the research of biofilm mainly used various conventional methods of light microscope and electron microscope to study the culture of bacteria on a solid surface in nature and laboratory [73, 75]. In the next decade, the research on the sequence and growth rate of biofilm development was promoted by the "Robins device biofilm sampler" and continuous culture chemical state instruments [80, 83-85]. Since 1990, confocal laser scanning microscopy has been used to study single or multiple bacterial biofilms labeled with green/yellow/blue fluorescent protein in small flow cells, automatic image analysis of biofilms in flow cells [86-88], Live-Dead staining [89], biofilm formation of various bacterial mutants, transcription analysis, and measurement. In the current period, the formation of biofilm will have a great impact on people's daily life and has become an important research topic.

2.2 Importance of controlling biofilm formation

Bacteria can grow on almost every surface, forming architecturally complex communities which are called biofilm. In biofilms, cells grow in the form of multicellular aggregates, which are encapsulated in the extracellular matrix produced by bacteria [90]. Even though the advantages of biofilm are proposed in many works of literature such as degrading hazardous substances/chemicals in soil [91] and purifying industrial wastewater [92], its harm cannot be underestimated which includes in natural, medical, and industrial settings [92, 93]. For example, chronic infections are very difficult to treat which are caused by biofilm formation on medical devices such as catheters or implants [94]. In addition, infection is also associated with biofilm formation on the surface of the human body, such as teeth, skin, and urinary tract [95]. Thus, it is a great upsurge to study the anti-biofilm surface which can reduce the risk of infections. In industry, for instance, biofilms form on the hull and inside pipes of ships, causing increased drag and energy loss [96]. Also, the pathogens microflora

in the biofilms can cause contamination of food/drink [97]. However, biofilm formation is not always detrimental. In many natural settings, biofilm formation often allows mutualistic symbioses. For example, actinomycetes usually grow on ants to keep them fungus-free [98].

In daily life, biofilm formation is harmful to medical care, drinking water distribution systems, food, and marine industries [22]. So, it is important to control and prevent biofilms. In the United States, over 700 waterborne disease outbreaks were recorded between 2009 and 2017. At least 15 cases were caused by *E. coli* and/or *Salmonella*. In the same period and 10,596 illnesses related to *E. coli* infection, including more than 2,000 hospitalizations and nearly 4,000 deaths. Other data shows that in untreated surface water samples collected from 27 locations in North America, approximately 80% of the sample contained human pathogens, such as *E. coli* [22]. Biofilm-associated infections not only have societal impacts but also have dramatic economic impacts. For instance, catheter-associated urinary tract infections (CAUTI) in hospitals cause extra health care costs of £1-2.5 billion in the UK alone [22, 99]. In addition, there are many types of patients with biofilm infections related to medical devices, such as urinary catheters, peritoneal dialysis catheters, tracheal prostheses, pacemakers, endotracheal tubes, dental implants, and orthopedic implants [99].

From a public health perspective, England's annual report shows that the prevalence in 1,000,000 cases is 6.4% [100]. Particularly, medical device-related infections make a huge negative financial impact on healthcare services and are relevant to increase patient morbidity and mortality [94]. As for medical device-related infections, the most important reason is the impaired immunity of the implant and tissue interface which is caused by bacteria adhesion and biofilm formation on the surface of medical devices (Table 2.1) [94, 101]. Some of the medical devices which are used in the body and easy to form biofilms such as sutures, heart valves, vascular grafts, catheters, and orthopedic implants. As reported, 87% of bloodstream infections are associated with intravascular devices, 80% of pneumonia are relevant to mechanical ventilation, and 95% of urinary tract infections are related to a urinary catheter [102]. These biofilm-related infections are clinically important because the structure of the biofilm can protect the encapsulated bacteria from the host immune response and antibiotic treatment. This special feature allows bacteria to exist in

the human body for a long time. Thus, an effective strategy to inhibit biofilm formation is imperative and required to avoid infection.

Table 2.1 Biofilm of indwelling medical devices

Medical device	Main microorganisms
Contact lens	*P. aeruginosa*, Gram-positive cocci [103]
Urinary catheter	*E.coli*, *Candida spp.*, *E. faecalis*, *P. mirabilis* [104]
Central venous catheter	CoNS, *S. aureus* [105, 106]
Mechanical heart valve	CoNS, *S. aureus* [105, 106]
Artificial hip prothesis	CoNS, *S. aureus* [105, 106]
Voice prostheses	CoNS, *C. Albicans* [106]

CoNS: coagulase-negative staphylococci (e.g., S. epidermidis)

2.3 Biofilm structure

Since biofilms have been discovered and studied, it has been defined as quite complex systems which are an aggregation of single or multiple microorganisms that are attached to many kinds of surfaces which have a common and the most important defining property is wet environment [107-109]. Microorganisms commonly include bacteria, fungi, and protists which can form biofilms [107]. The structure of biofilms is not only composed of many microbial cells but also extracellular polymeric substances (EPS). EPS is considered as the primary matrix material of the biofilm because it takes 50% to 90% of parts of the total organic carbon [110, 111]. Some of the substances confer the anionic property such as uronic acids or ketal-linked pyruvates. Because this significant property allows the combination of divalent cations like Ca^{2+} and Mg^{2+}, which provides a stronger binding force in a developed biofilm [111, 112]. On the other parts, some of the gram-positive cells such as the staphylococci, the chemical composition of EPS may be quite different and may confer cationic. And some of the coagulase-negative bacteria secreted the slime which consists of a teichoic acid with small quantities of proteins [113].

As EPS can incorporate large amounts of water into its structure through hydrogen bonding that confirms it is highly hydrated that can prevent desiccation. Two important properties of EPS can influence the biofilm and its solubility [112]. First, the different compositions and structures of the polysaccharides determine the EPS conformation. For example, many EPS has skeleton structures that contain 1, 3- or 1, 4-β-linked hexose residues and then gain more rigid, less deformable, and hardly soluble or insoluble under certain situations. And the others may easily be soluble in water [112]. Different organisms can produce different quantities of EPS, and the EPS amount increases with the age of the biofilm [114]. EPS may also impede the mass transport of antibiotics through the biofilm to promote the antimicrobial resistance properties of the biofilms [115].

Above all, EPS is a complex structure made up of different components including carbohydrates, proteins, lipids, and nucleic acid [116, 117]. And the EPS serves many functions for the biofilm such as adhesion to the surface, structural integrity, protection from invasion, and intercellular communication.

2.4 Difference between Gram-Positive and Gram-Negative Bacterial

Most bacteria are broadly classified as Gram-positive and Gram-negative by gram staining, while some organisms consistently have Gram-variation. Their apparent large difference is the structural organization outside the plasma membrane but below the capsule (Figure 2.1)[5].

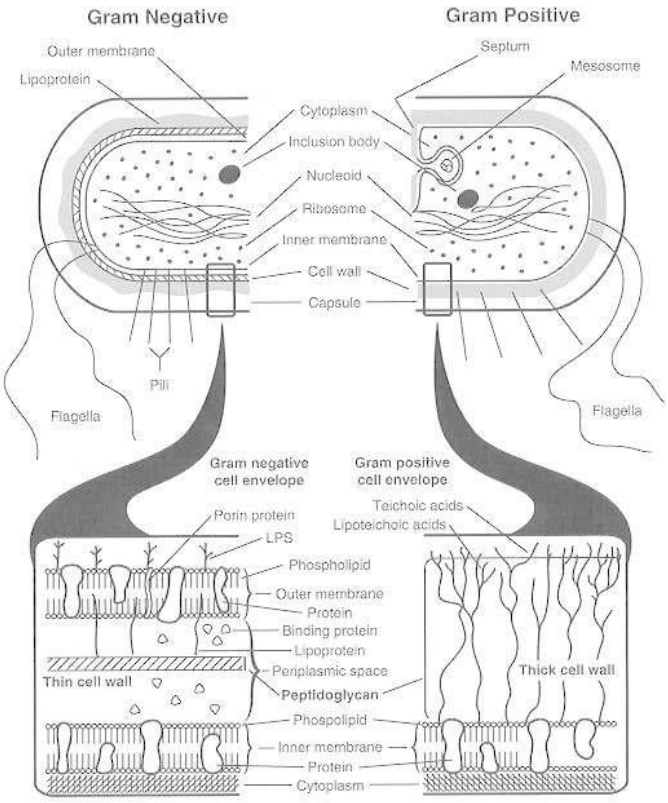

Figure 2.1 Gram-positive bacteria with the comparatively thin cell wall of Gram-negative bacteria. [5]

Gram-positive bacteria form a cell wall, mainly composed of multiple layers of peptidoglycan, forming a hard and thick structure. Its cell walls also contain teichoic acid and phosphate. There are two types of teichoic acid present in Gram-positive bacteria - lipoteichoic acid and teichoic acid [5]. In Gram-negative bacteria, the cell wall consists of an outer membrane and several layers of peptidoglycan. The outer membrane is composed of lipoproteins, phospholipids and LPS. Peptidoglycan remains intact with outer membrane

lipoproteins located in the fluid-like periplasm between the plasma membrane and the outer membrane. The periplasm contains proteins and degrading enzymes that help transport molecules [5]. The other detailed differences between Gram-positive and Gram-negative bacteria have been summarized in Table 2.2.

For example, *S. epidermidis* is primarily associated with infections indwelling in medical devices. The prevalence of *S. epidermidis* in this infection may be due to its abundance on human skin and its ability to adhere to duct surfaces and form biofilms. Biofilm formation is one of the mechanisms to protect *S. epidermidis* from antibiotics and host defenses [118, 119]. In addition, *P. aeruginosa* forms prolific biofilms in aquatic environments, soils, and clinical settings. This species uses two distinct signaling systems to initiate biofilm formation: the second messenger c-di-GMP, regulated by the Wsp system, and the second messenger cyclic AMP (cAMP), which is Pil-Chp/Vfr system for regulation. For example, *P.aeruginosa* PAO1 is relatively rapidly committed to surface attachment and extracellular matrix secretion through the Wsp system-mediated increase in c-di-GMP production [120].

Table 2.2 Difference between Gram-Positive and Gram-Negative Bacteria [121]

Gram-Positive bacteria	Gram-Negative bacteria
Cell Wall	
A single-layered, smooth cell wall	A double-layered, wavy cell-wall
Cell Wall thickness	
The thickness of the cell wall is 20 to 80 nanometres	The thickness of the cell wall is 8 to 10 nanometres
Peptidoglycan Layer	
It is a thick layer/ also can be multilayered	It is a thin layer/ often single-layered.
Teichoic acids	
Presence of teichoic acids	Absence of teichoic acids
Outer membrane	
The outer membrane is absent	The outer membrane is present (mostly)
Porins	
Absent	Occurs in the Outer Membrane
Mesosome	
It is more prominent.	It is less prominent.
Morphology	
Cocci or spore-forming rods	Non-spore forming rods.
Flagella Structure	
Two rings in the basal body	Four rings in the basal body
Lipid content	
Very low	20 to 30%
Lipopolysaccharide	
Absent	Present
Toxin Produced	
Exotoxins	Endotoxins or Exotoxins
Resistance to Antibiotic	
More susceptible	More resistant
Example	
Staphylococcus, *Streptococcus*, etc.	*Pseudomonas aeruginosa*, *Escherichia*, etc.

2.5 Biofilm formation and lifecycles

The processes of biofilm formation are very complex in which microbial cells change the growth mode from planktonic to sessile [122]. Biofilm formation not only has effects on the characteristics of the substratum and the cell surface but also depends on the expression of specific genes which guide the constitution of biofilm [123-125]. There are five important steps of biofilm formation shown below (Figure 2..2) [22, 126]:

1) The reversible attachment phase. Bacteria attach to the surface non-specifically.
2) The irreversible attachment phase involves the interaction between bacterial cells and the surface using bacteria adhesin such as fimbriae and lipopolysaccharide (LPS).
3) Resident bacterial cells produce extracellular polymers (EPS).
4) Biofilm maturation phase, during which bacterial cells synthesize and release signal molecules to sense each other's presence, thereby promoting the formation of microcolonies and the maturation of biofilms.
5) In the dispersal/detachment phase, the bacterial cells break away from the biofilm and return to an independent planktonic lifestyle.

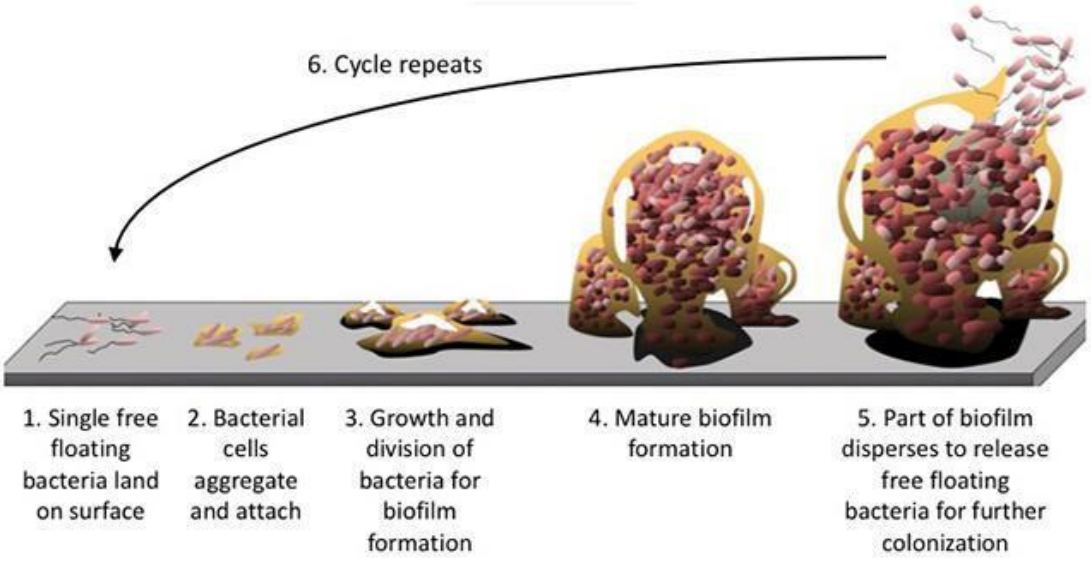

Figure 2.2 The Biofilm life cycle [22]

The initial step to form biofilms has been widely reported which is the development of surface-conditioning films [92, 127, 128]. Loeb et al. first observed the formation of conditioning films, which formed on the surface after a few minutes of exposure to seawater, then they continued to grow for several hours [129]. Conditioning films affect the bacterial adhesion on biomaterials which mainly contain polysaccharides and proteinaceous from blood, urine, tears, and saliva respiratory secretions, it was observed by Mittelman [130]. Conditioning film formation needs adequate nutrients which can absorb macromolecules or proteins onto surfaces, then change the physical and chemical properties of the substrate surface (e.g., surface charge, potential, and tensions, etc.). Especially according to the exposure environment of the substrate, the performance of the conditioning films is very different, which changes the substrate and promotes the accessibility of microorganisms, thereby affecting the initial adhesion of bacteria [127].

Secondly, planktonic bacterial cells attach to the surface depending on physical force or bacterial appendages (flagella) when moving near the conditioned surface [92]. Initially, bacterial cells reach the surface through their motion or Brownian motion and remain attached. Several physical forces contribute to bacterial adhesion, such as the attractive van der Walls interaction and the repulsive electric double-layer interaction [131]. While because of the weakness of the bond, if the attractive force is less than the repulsive force, the bacterial cells will escape from the substrate surface [132]. However, bacterial cells have physical appendages (such as flagella, fimbriae, and fimbriae) and the ability to produce EPS, which can bridge the substrate and overcome the physical repulsion of double electricity [1, 92]. Finally, the bacterial cells can anchor themselves irreversibly to the surface.

Once the microbial cells have irreversibly attached to the surface, the biofilm will begin to mature. The growth and division of initially attached cells will form the bacterial cluster. This process involves the duplication of stationary cells called binary division. The daughter cells spread from the attachment point to the surroundings to clusters [92]. Gradually, the bacterial clusters expand and merge into multi-layered cells with a mushroom-like structure but consume a large amount of liquid and surrounding nutrients in the matrix [133]. Usually, this mushroom-like structure acts as a channel to help distribute nutrients to bacteria deep in the biofilm. At this stage, biological processes begin to replace physical

and chemical factors and dominate. Particularly, the proximity of cells within or between bacterial clusters can provide an ideal environment for creating nutrient gradients, gene exchanges and quorum sensing, to affecting the formation of biofilms [110].

The final stage of biofilm formation is critical to the biofilm life cycle of cell proliferation, which is dispersion. Enzymes are produced by the community itself which can degrade the extracellular matrix of biofilms, such as disperse B and deoxyribonuclease, actively releasing bacterial cells. Subsequently, after a biofilm is formed in the new environment, these separated cells will spread and colonize the new surface. In the different stages of biofilm formation, the regulation of molecular mechanisms differs greatly between different bacterial species, and due to the environmental conditions of the same species [134, 135].

2.6 Mechanisms of bacterial attachment

Before bacteria attach to the surface, many of them are freely suspended in the bulk liquid. There are three regions of fluids, and the motile bacteria will occupy one of them which are [136]:

(1) Bulk liquid, where the bacteria cannot be affected by the surface

(2) Near-surface bulk liquid, where the cells experience the hydrodynamic effects from the surface

(3) Near-surface constrained, where the bacteria are affected by both the hydrodynamic and physicochemical (van der Waals and electrostatic) from the surface

While under the low and moderate fluid velocities condition, non-motile bacteria can adhere to the surface, but in the high-rate fluid velocity which means high wall shear stress, non-motile bacteria are transported with the fluids and do not attach. Otherwise, motile bacteria can attach to the surfaces regardless of fluid velocity. The difference between motile bacteria and nonmotile bacteria is only caused by the activated flagella, and bacteria with non-functional flagella adhere similarly to bacteria without flagella[137].

Bacterial attachment occurs in two periods when it is contacting surfaces. The first one is reversible, it occurs rapidly (around 1min) and includes hydrodynamic and electrostatic

interactions. During this period, the adhesive force between bacteria and surfaces is increased. This phenomenon is caused by physicochemical effects which include interface water loss, surface molecules structural change, and repositioning of the cell body to maximize attachment to the surface. The second period of attachment is irreversible, occurs for several hours, and involves van der Waals interactions between the hydrophobic region of the outer cell wall and the surface [138, 139].

Reversible bacterial adhesion is regarded as a situation in which the distance between the bacterium and surface is very close within the same plane of focus for a light microscope. It is speculated that by introducing a swimming or Brownian motion, reversibly antagonistic bacteria will keep their ability to move laterally along the surface, and these cells may eventually leave the surface. Cells that exhibit features in this manner are observed in many experiments and typically travel very continuously (> 1 minute) near the surface. Alternatively, in irreversible adhesion, by contrast, the bacteria in the duration of observation adhering to the surface cannot move, even by swimming or Brownian motion. In general, bacteria that have already immobilized on the surface are described as irreversibly adhered to the surface, while bacteria that can still move along the surface are regarded as reversibly adhered when a flagellum adheres to the surface, but the bacteria body can still rotate freely which illustrated in Figure 2.3 [16].

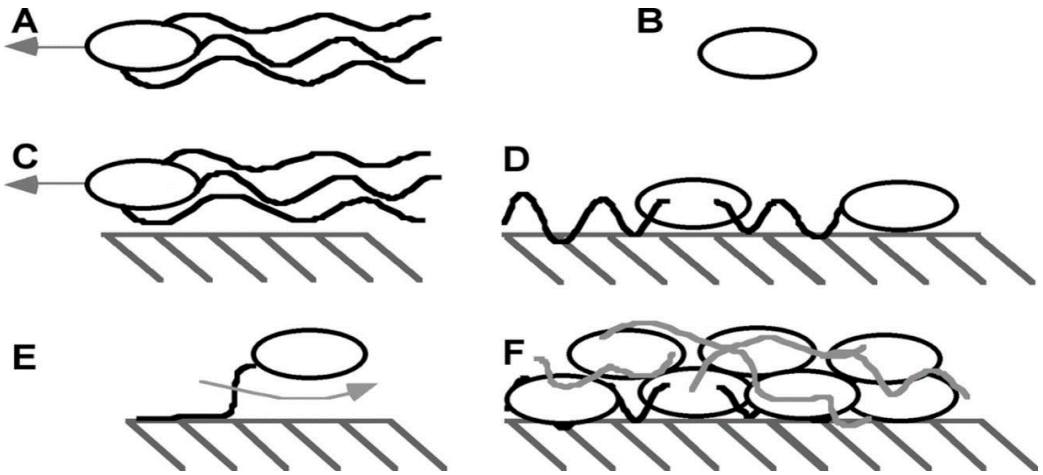

Figure 2.3 Representations of different bacterium-surface interactions. (A) Motile bacterium swimming in bulk fluid; (B) nonmotile bacterium; (C) reversibly adhering bacterium, translating along a surface; (D) irreversibly adhered bacterium; (E) tethered bacterium; (F) biofilm [16]

2.7 Different physical models for bacterial adhesion

Bacteria adhesion is the initial step to form biofilms which include the reversible and irreversible attachment on the surface. It is important to demonstrate the mechanisms of bacterial adhesion biofilm cells can disperse and reach structural maturity with the growth and division of the bacteria. Among microorganisms, the size of the bacteria which consists of biofilms is about 0.5-2um [1]. Thus, the first time to explain bacteria adhesion is based on the classical Derjaguin-Landau-Verwey-Overbeek (DLVO) theory which was initially developed for colloid particles. And other adhesion models such as the thermodynamic approach and the extended DLVO theory are used to investigate bacterial adhesion on the surface [131].

2.7.1 DLVO model

The DLVO model forms the basis of modern colloid and interface technology which can be applied to the attachment of bacteria to solid interface and employed to predict colloid stability. The DLVO model has been used to measure the interaction energy of flat surfaces directly using spherical bodies or crossed cylinders. And Derjaguin and Landau used the complete Debye-Huckel equation for electrical potential distributions between two similarly charged plates when applied to strong electrolytes [131].

In the DLVO model, the sum of the electrostatic interactions and the Lifshitz-van der Waals consists of the energy of the system comprising two particles immersed in the medium, the equation is (Equation 1) [131]:

$$\Delta \mathbf{G^{TOT}}(\mathbf{d}) = \Delta \mathbf{G^{LW}}(\mathbf{d}) + \Delta \mathbf{G^{EL}}(\mathbf{d}) \qquad (1)$$

Where $\Delta \boldsymbol{G^{TOT}}$ is the total interaction energy between the bacteria and the surface, $\Delta \mathbf{G^{LW}}$ is the total long-range Van der Waals force which has electromagnetic nature and originates from second-order perturbation theory to dipoles as first published by London in 1930 and $\Delta \boldsymbol{G^{EL}}$ is the total short-range electrostatic force caused by the overlapping of electrons that form the double election layer.

Van der Waals forces apply to all forms of atoms and molecules, and because of the fluctuating electron positioning within molecules, intermolecular will produce attractive and repulsive forces. If the Van de Waals attractive force dominated near surfaces, then

bacteria cells can adhere irreversibly and cannot detach from the substrate by Brownian motion. Otherwise, while the Van der Waals force decreases rapidly with distance, the double-layer interactions dominate when the bacteria are far away from the substrate [1, 131].

The formation of an electric double layer is due to counter ions against the surface charge attracted by the particles in an aqueous solution. As bacteria and natural surfaces in an aqueous solution are usually negatively charged, the overlap of the electrical double layers of bacterial cells and the substratum caused repulsive electrostatic energy. While decreasing the ionic strength of an aqueous solution, the repulsive energy increases because shielding of the surface charges by the ions in the electrical double layers lessens. At low ionic strengths, when the bacteria close to the surface, bacterial cells cannot swim, or Brownian motion overcome the energy barrier (Figure 2.4). In these conditions, the ionic strength depended on the distance from the surface to the secondary energy minimum which is usually within several nanometers. In the first step of cell adhesion, a bacterial cell comes to this position by its motility or Brownian motion and adheres to the surface reversibly (Figure 2.4). Subsequently, bacterial cells can usually penetrate the energy barrier or produce EPS through nanofibers (i.e., flagella and pili), which are interfering with each other due to their small size. The energy barrier becomes higher, and the critical distance is farther from the substrate (Figure 2.5). Bacterial cells cannot be aligned to the surface because nanofibers and EPS are difficult to reach the bottom layer. Conversely, at high ionic strength, the energy barrier disappears. Therefore, reducing the ionic strength of bacteria and reducing the correlation between their bacteria has been well documented in the literature, which is consistent with the prediction of DLVO theory [1].

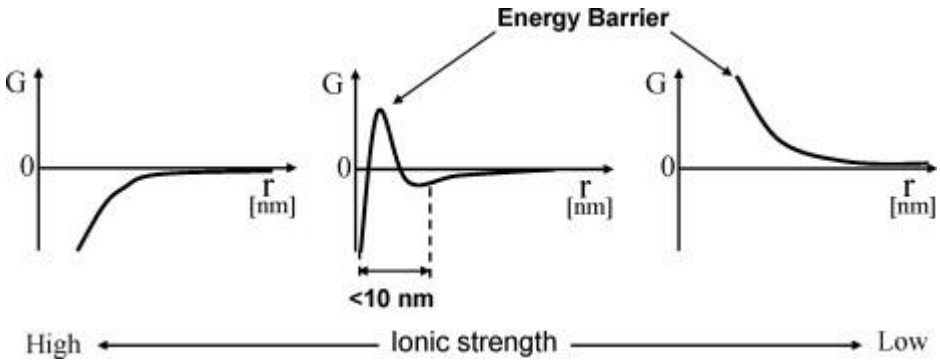

Figure 2.4 Total interaction energy between a bacterial cell and a surface depending on ionic strength. [1, 2]

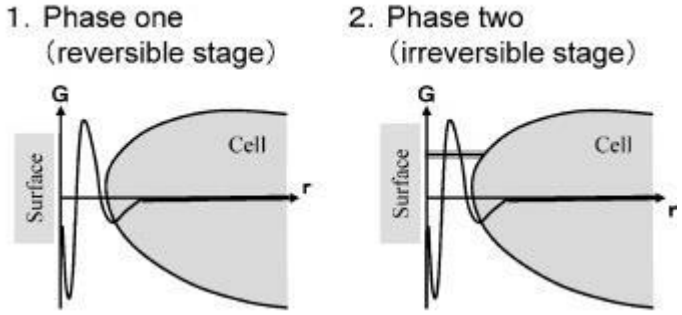

Figure 2.4 Schematic of bacterial adhesion usual two-step process. [1]

2.7.2 Thermodynamic approach

The thermodynamic approach is the second method developed to investigate bacterial adhesion on the surface. It includes contact angle measurement which has been used as a measure of the surface energy of the cell surface that can calculate the Gibbs adhesion energy for bacteria adhesion. The thermodynamic approach equation shows below (Equation 2) [1]:

$$\Delta \mathbf{G^{adh}} = \boldsymbol{\gamma_{BS}} - \boldsymbol{\gamma_{BL}} - \boldsymbol{\gamma_{SL}} \qquad (2)$$

Where ΔG^{adh} is the Gibbs free energy for bacterial adhesion, and γ_{BS}, γ_{BL}, γ_{SL} is the interfacial energy of the bacterium-substratum, bacterium-liquid, and substratum-liquid interfaces, respectively.

If the Gibbs free energy is negative, the adhesion is favored. However, thermodynamics principally assumes that the process is reversible which often not the case is. Based on the DLVO model, bacterial adhesion has been described as a two-phase process. Phase one is an initial, instantaneous and reversible physical phase and phase two is a time-dependent and irreversible molecular and cellular phase. If the bacterial adhesion in phase one at the secondary energy minimum cannot form a new cell-substratum interface, the thermodynamic approach cannot be applied. Therefore, using the thermodynamic approach to calculate the formation of a new cell-substratum interface at the expense of the substratum-medium and cell-medium interfaces. Compared with the DLVO model, in which the interaction energy is dependent on the distance. Even the thermodynamic approach has limitations, while it still can explain a common observation: bacteria with hydrophilic cell surfaces prefer hydrophilic material surfaces, whereas hydrophobic ones prefer hydrophobic surfaces [131].

2.7.3 The extended DLVO model

As mentioned before, neither the DLVO nor the thermodynamic approach can fully explain bacterial adhesion. The extended DLVO model is suggested by van Oss which includes the hydrophobic/hydrophilic interactions and osmotic interactions. For cells osmotic interactions were very small which can be ignored, so the total adhesion energy can be expressed as (Equation 3) [131]:

$$\Delta \boldsymbol{G}^{\boldsymbol{adh}} = \Delta \boldsymbol{G}^{\boldsymbol{vdW}} + \Delta \boldsymbol{G}^{\boldsymbol{dl}} + \Delta \boldsymbol{G}^{\boldsymbol{AB}} \qquad (3)$$

Where $\Delta \boldsymbol{G}^{\boldsymbol{vdW}}$ and $\Delta \boldsymbol{G}^{\boldsymbol{dl}}$ are the 'classical' van der Waals and double layer interactions and $\Delta \boldsymbol{G}^{\boldsymbol{AB}}$ relates to acid-base interactions. The latter component introduces a component that describes attractive hydrophobic interaction and repulsive hydration effects. According to van Oss, it is 10-100 times stronger than the van der Waals interactions of surfaces in direct contact. In some cases, the extended DLVO theory seems better than the classic DLVO theory to predict experimental adhesion results. The extended DLVO theory predicts such strong interactions due to acid-base interactions that lead to an extremely deep minimum without an energy barrier, while in the classical DLVO theory, bacterial adhesion cannot occur. As the distance dependence of acid-base interactions is short-ranged, both acid-base interaction and the electric double-layer interaction exponentially decay from the value at

close contact. Based on the calculation, the distance between the interacting surfaces must be less than 5nm before acid-base interactions can become operative[1].

2.8 Factors affecting initial bacterial attachment

According to the two periods of bacterial attachment which are reversible adhesion and irreversible adhesion, it is generally accepted that the initial bacterial attachment with surface colonization is a key in triggering the growth of biofilms on the surface. For the initial bacterial attachment, we mainly consider two factors here: the solid surface and the bacteria themselves. And few factors affect initial bacterial attachment such as surface charge, surface hydrophobicity, surface roughness, surface topography, and bacterial surface and appendages**.**

2.8.1 Surface charge

It has long been known that surface charge affects bacteria adhesion onto material surfaces and the subsequent formation of biofilms. Most bacterial cells are negatively charged, so generally, positively charged surfaces are more conducive to bacterial adhesion while negatively charged surfaces have resistance to bacteria adhesion [140, 141]. It is discovered that some surfaces with cationic groups, such as quaternary ammonium compounds, cationic peptides, chitosan, lysozyme, and antibiotics have antibacterial effects and may also kill attached bacteria [140-142]. However, modifying the surface charge in a static system may not affect bacterial adhesion because the dead cells may act as a barrier to reduce the surface charge, which may hinder antibacterial efficiency and even promote the attachment of bacteria to positively charged surfaces [141]. If the surface is in a dynamic and force existed environment, dead bacteria could be removed in certain conditions [140]. For example, it can be used in certain oral applications because of the shear stress from rising or brushing [141].

2.8.2 Surface hydrophobicity

Both substrate surface hydrophobicity and cell surface hydrophobicity (CSH) affect bacterial adhesion, either promoting or inhibiting [131]. For example, Mabboux et al. reported that compared with the hydrophilic Streptococcus constellation, hydrophobic Streptococcus sanguinis had much higher bacterial adhesion on saliva-coated pure titanium 2 (cp-Ti) and Ti-6A-5V alloy [143]. Bacteria are generally moderately hydrophilic, but the extent of the CSH is a factor in the greater number of substrate types that colonize biofilms

[144]. Hydrophobic bacteria are easier to attach to hydrophobic substrates than hydrophilic substrates [144]. The relationship between surface and adhesion depends on surface contact angle (CA), for most experiments, hydrophilic and modified superhydrophobic surface CA>150° seem to inhibit adhesion while CA in 70-105°, the increasing hydrophobicity appears to produce the strongest adhesion attachment [145]. For example, although glass predicts the strength of cell-matrix van der Waals interaction stronger than that of Teflon, another clear sign of CSH is that the adhesion of hydrophobic Teflon to bacteria increases compared with glass [131]. On the other hand, more contemporary studies have shown that superhydrophobic or super hydrophilic surfaces can inhibit bacterial adhesion and biofilm formation. The main inspiration for the design of the super-hydrophobic surface comes from the natural lotus leaf, which has a water contact angle of more than 150°. The contact angles are very important because they can quantify the surface wettability which is the property of solid-fluid intermolecular interaction based on the Cassie-Baxter model. As indicated by the Cassie-Baxter model, microscale and nanoscale patterned heterogeneous surface, air could be trapped in the grooves between the surface features to prevent wetting. Most superhydrophobic surfaces have been designed based on these principles, such as silicone elastomer, and TiO_2 nanotubes [140, 146, 147]. Besides, due to the formation of a dense layer of water molecules, the super hydrophilic surface is non-fouling, thereby weakening the interaction between the cell surface and the matrix material and reducing cell adhesion. Many non-fouling materials have been developed such as zwitterionic polymers, tightly charged neutral molecules with positive and negative charges, which are super hydrophilic and reduce fouling caused by proteins and bacteria [140, 141].

One of the important parameters to evaluate the wettability of liquid to a solid surface is CA[148]. It is defined as the angle between the tangent of the gas-liquid interface at the intersection of gas, liquid, and solid through the liquid phase, and the solid-liquid interface (Figure 2.6) [15]. Due to the Young equation, a nonreactive liquid droplet on an ideal flat solid surface form a unique angle which is determined by the mechanical force equilibrium of three interfacial tensions at the three-phase contact line and they can be described as (Equation 4) [149]:

$$\gamma_{sv} = \gamma_{sl} + \gamma_{lv}cos\theta_Y \quad (4)$$

Where γ_{sv}, γ_{sl}, γ_{lv} are the solid-vapor interface tension, solid-liquid interface tension, and vapor-liquid interface tension, respectively. θ_Y is called the Young contact angle which is the same as the equilibrium contact angle (θ_e) obtained based on thermodynamic principles in an ideal wetting system. From the Young equation, it is obvious to say the wetting contact angle is the unique value for the particular solid-liquid-vapor systems. However, in actual systems, most surfaces are not ideal because the manufacturing process may produce pores, streaks, or micro grooves, and even some solids themselves contain the above-mentioned defects like minerals. Therefore, this value is not unique but is in a more or less wide range between the advancing contact angle (θA) and the receding contact angle (θR) [150]. And their difference is called contact angle hysteresis. It is generally believed that the surface roughness and/or chemical heterogeneity of the solid substrate has a great influence on the contact angle hysteresis [151, 152].

Although the most common method to improve solid surface hydrophobicity is chemical modification, both theoretical and experimental studies have shown that it has limitations [153, 154]. Because in the case of water, the maximum advancing contact angle can only reach about 130° which means that the influence of chemical heterogeneity on contact angle hysteresis on contact angle hysteresis may also be limited [155]. Another way to improve surface hydrophobicity is to introduce random or precisely patterned surface roughness into hydrophobic substrates [156]. For example, the two factors that determine the superhydrophobic surface of the lotus leaf are chemical hydrophobicity and micron- or nanometre-sized surface roughness [157, 158]. The combination of low surface energy and micron and/or nanoscale surface roughness to trap an air layer on the surface results in the formation of an air-water interface between the peaks of the surface roughness. The existence of the air-water interface can produce a large static advancing contact angle (θ> 150°), and the contact angle hysteresis is small [159].

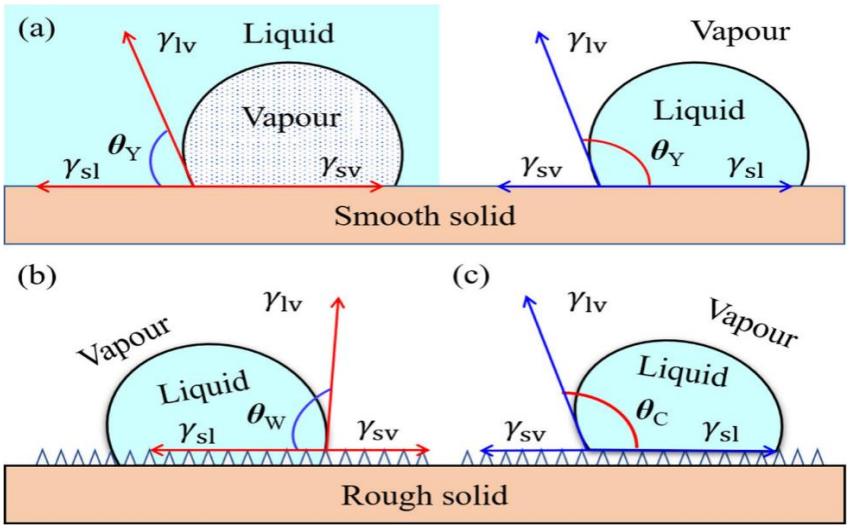

Figure 2.5 Schematic diagram of the relationship between equilibrium contact angle and interfacial tension in gas/liquid/solid system. (a) Young contact angle (θ_Y), (b) Wenzel contact angle (θ_W), and (c) Cassie contact angle (θ_C) [15]

2.8.3 Surface roughness

The surface roughness could have a significant impact on microbial colonization and biofilm formation. Generally, surface structure can be characterized by roughness (two-dimensional measurement based on the average distance between peaks and valleys) and topography (three-dimensional measurement) [141]. Both experiments and computational modeling work have shown that the increase in surface roughness (such as scratches and pores and other irregularities) can promote bacterial adhesion because the surface area is also increased, which may provide more favorable sites for colonization and reduce bacterial deposition energy barrier on the surface of the material [160]. However, there are two different conclusions have emerged from recent research on the relationship between surface roughness and bacterial adhesion. Researchers have reported that when the surface roughness is increased, a greater cell adhesion occurs due to the rougher surface and in turn the adhesion force increases also [101, 102, 161]. For example, the experimental results show that on the rougher surface of poly (methyl methacrylate (PMMA)), the adhesion of *Staphylococcus epidermidis* and *Pseudomonas aeruginosa* increases significantly, and the

average roughness value (i.e., Ra) increases from 0.04 μm increases slightly to 1.24 μm [160]. And Subash et al. reported that the attachment ability of *Streptococcus gordonii* DL1 (NCTC 7868) on flat stainless steel surfaces is significantly less than that on rough surfaces, it is shown in Figure 2.7 [21]. However, others argued that increasing surface roughness cannot promote or inhibit bacterial adhesion [162-165]. The two different results are due to the lack of comprehensive topographic features describing the surface. The most frequently used parameters for characterizing surface topography are average surface roughness (Ra) and root-mean-square surface roughness (Rrms), and many efforts have been made to study the correlation between bacterial adhesion and these two parameters [166]. However, both cannot provide information about the spatial distribution or shape of the surface features. Completely different two surfaces may get similar Ra and Rrms values (Figure 2.8) [9]. Thus, new parameters are needed to fully characterize the surface topography.

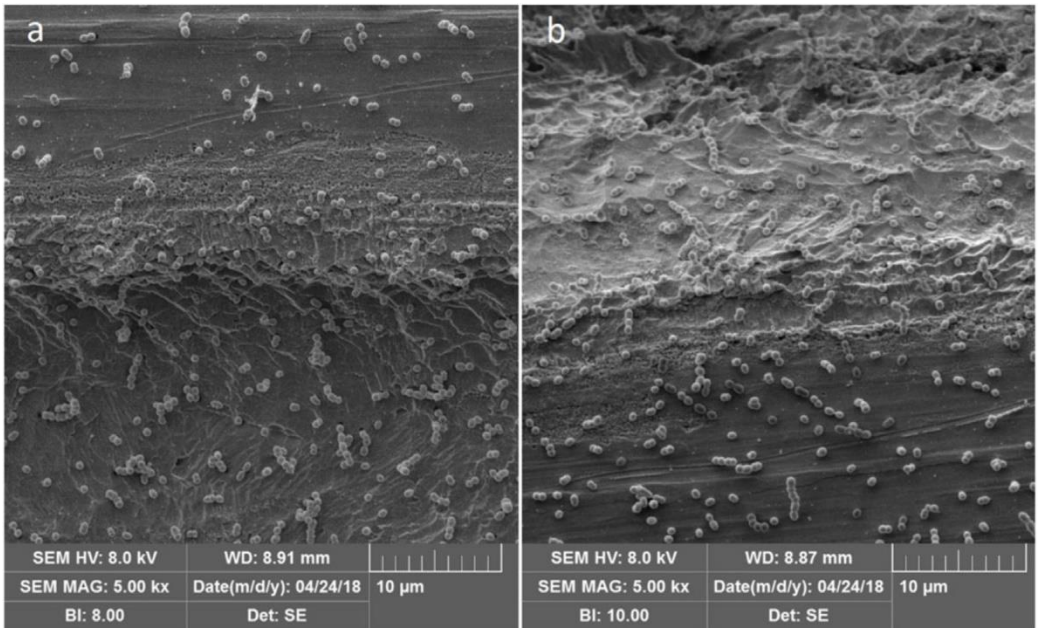

Figure 2.6 Typical SEM images of bacteria attached to stainless steel surfaces: (a) 10 µm surface, (b) 40 µm surfaces [21]

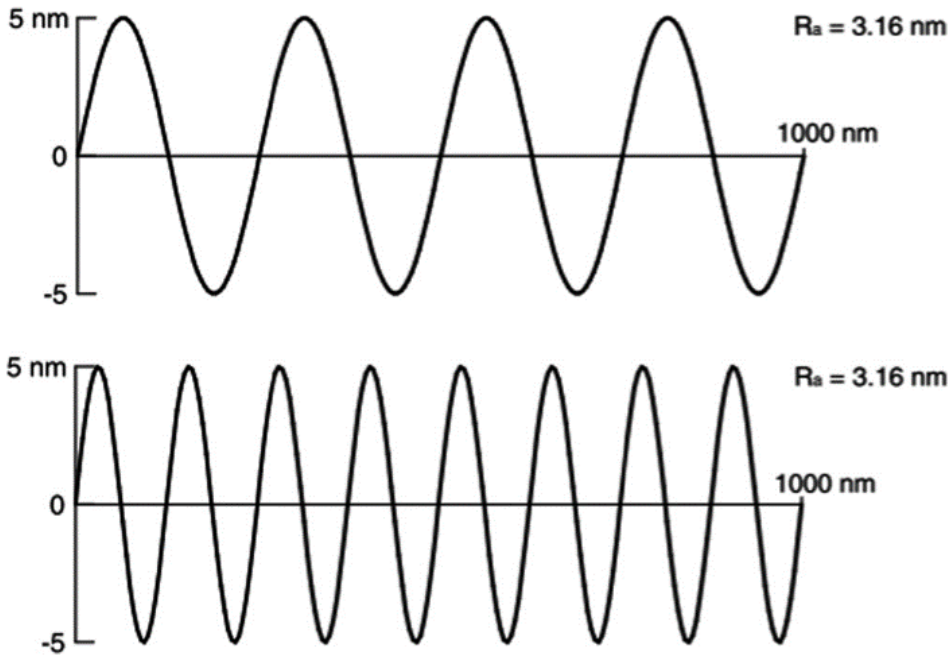

Figure 2.7 Example of two different surfaces with identical Ra values. [9]

In addition, surface roughness is also an important factor that can affect surface hydrophobicity. There are two general theoretical models to explain the mechanism of improving hydrophobicity by increasing the surface roughness of hydrophobic surface: the Wenzel model and the Cassie model [167, 168].

In the Wenzel model, when increasing the surface roughness of the hydrophobic surface will form a larger solid-liquid interface which makes a higher apparent contact appears (Figure 2.6b) [169]. It is assumed that the droplet size is significantly larger than the roughness scale, and the liquid completely penetrates the rough grooves on the solid surface [170]. The Wenzel equation can be expressed as (Equation 5) [171]:

$$\mathbf{cos\theta_w = rcos\theta_\gamma} \qquad (5)$$

Where θ_w is Wenzel contact angle and r is the roughness factor that is the ratio between the real surface area and the projected surface area of a rough surface. For a smooth surface, r=1, otherwise r>1. While the roughness factor is greater than 1, as the surface roughness increases, the hydrophilic solid surface becomes more hydrophilic, otherwise more hydrophobic [172]. Notably, the equilibrium contact angle will increase in the Wenzel state for hydrophobic surfaces. But the contact angle hysteresis is usually also very large. This is because the contact line is fixed to each wetting feature as it recedes [173]. In addition, it has been shown that even if the surface features are properly spaced, on small scales, the roughness cannot sufficiently "trap" the air and will increase the hysteresis [159].

In the Cassie model, increasing the surface roughness of a hydrophobic solid can increase the hydrophobicity. The reason is the air pockets are formed in the peak of the surface roughness, resulting in the existence of part of the liquid-vapor interface and part of the solid-liquid interface (Figure 2.6c) [169]. In the case of heterogeneous surfaces, the composite surface consists of two different areas, including solids and trapped air. Both regions have certain area fractions ϕ_s and ϕ_v, and specific contact angles θs and θv, which are the contact angles of the liquid relative to the pure solid phase and the vapor phase, respectively. The concept that roughness affects contact angle was extended by Cassie and Baxter in 1944 when they focused on porous media where liquids do not penetrate grooves on rough surfaces and leave air gaps [174]. They devised the Cassie- Baxter equation (Equation 6):

$$\mathbf{cos\theta_C = \emptyset_S cos\theta_S - \emptyset_v} \qquad (6)$$

Where θC is the Cassie contact angle. When ϕs+ϕv=1, ϕs=θr, and assuming a water contact angle for the air of 180°, it will become (Equation 7) [175]:

$$\cos\theta_C = \emptyset_S(1 + \cos\theta_Y) - 1 \qquad (7)$$

In 1948 Cassie refined this for two materials with different chemistries on both smooth and rough surfaces, resulting in the aforementioned Cassie's law. The Cassie equation can be expressed as (Equation 8) [175]:

$$\cos\theta_C = \emptyset_S \cos\theta_S + \emptyset_v cos\theta_V \qquad (8)$$

Notably, the advancing and receding contact angles are very large, which causes the contact angle hysteresis in the Cassie state to be almost negligible.

2.8.4 Surface topography

Specific patterns on the surface topography can modify the surface hydrophobicity which is a key parameter for the initial bacterial adhesion [25]. In addition, it is believed that bacterial adhesion is largely dependent on surface topography, rather than micro or nanoscale roughness [176, 177]. Most of the surface topography with specific patterns is enlightened by a natural surface such as Sharkskin [178], worm skin [179], lotus leaves [180], taro leaves [42], butterfly wings [181], and damselfly wings [182]. Due to the development of surface engineering technologies, precise surfaces have been patterned to study cell-surface interactions and design antibacterial surfaces. Also, a few parameters have been investigated to affect the bacteria adhesion, like plateau dimensions [2], shapes and heights [19], and spacing between the plateaus [73]. Polydimethylsiloxane (PDMS) is a widely used material for this purpose due to its innocuity, satisfied elasticity, and workability. For example, Perera-Costa et al. designed protruded or recessed surface topography of different shapes and heights on PDMS surfaces (Figure 2.9a) [19]. Compared to the flat surfaces, all patterned surfaces show an overall decrease in bacterial adhesion. Hou et al. 10μm high square protruding features were produced on the PDMS surface by soft lithography, with different platform sizes [2]. It was observed that E. coli tended to preferentially select valleys among the square features to settle and form a biofilm, even though the size of the platform is much bigger than the valley (Figure 2.9b) [2]. The PDMS surface made by Friedlander et al. has an array of hexagon features with different spacing. Bacterial adhesion on the patterned surface is suppressed at an early stage, but compared to a flat surface, bacterial

adhesion is promoted [183]. Gu et al. studied the adhesion behaviour of Escherichia coli on PDMS. The surface has a 5μm high line pattern with different widths [184]. Narrow patterns with smaller pattern spacing show a more obvious ability to inhibit bacterial adhesion.

For a micro or nano-patterned surface, different bacterial responses according to the different cell-material contacts with the scaling of surface topography, also inspired researchers to design novel surface patterns to inhibit the initial bacterial attachment. These man-made artifacts are made of different materials, different methods, and different surface topography [140]. In addition, the tested bacterial strains are different, and the experimental process (flow cell or static, different incubation time) also varies from study to study. With the increase in research on the surface of various materials and bacterial systems, a clearer consensus on the influence of microstructure or nanostructured surfaces on bacterial adhesion may emerge [140].

For bacterial cells, as discovered in experimental work and computational models, surface irregularities promote the adhesion of bacteria and the formation of biofilms, while ultra-smooth surfaces may not be conducive to bacterial adhesion and biofilm deposition [140]. This may be because the rough surface has a larger surface area, and the gaps in the rough surface may provide a more favorable location for settlement and lower the energy barrier for bacteria to deposit on the material surface. For example, Jahed et al. studied the adhesion of *S. aureus* to nanocrystalline nickel nanostructures with different shapes. It was found that bacterial cells preferentially adhere to the interface between the feature and the substrate or the junction between different parts of the feature, thereby protecting the bacteria from external shearing forces and maximizing the contact area (Figure 2.9c) [185].

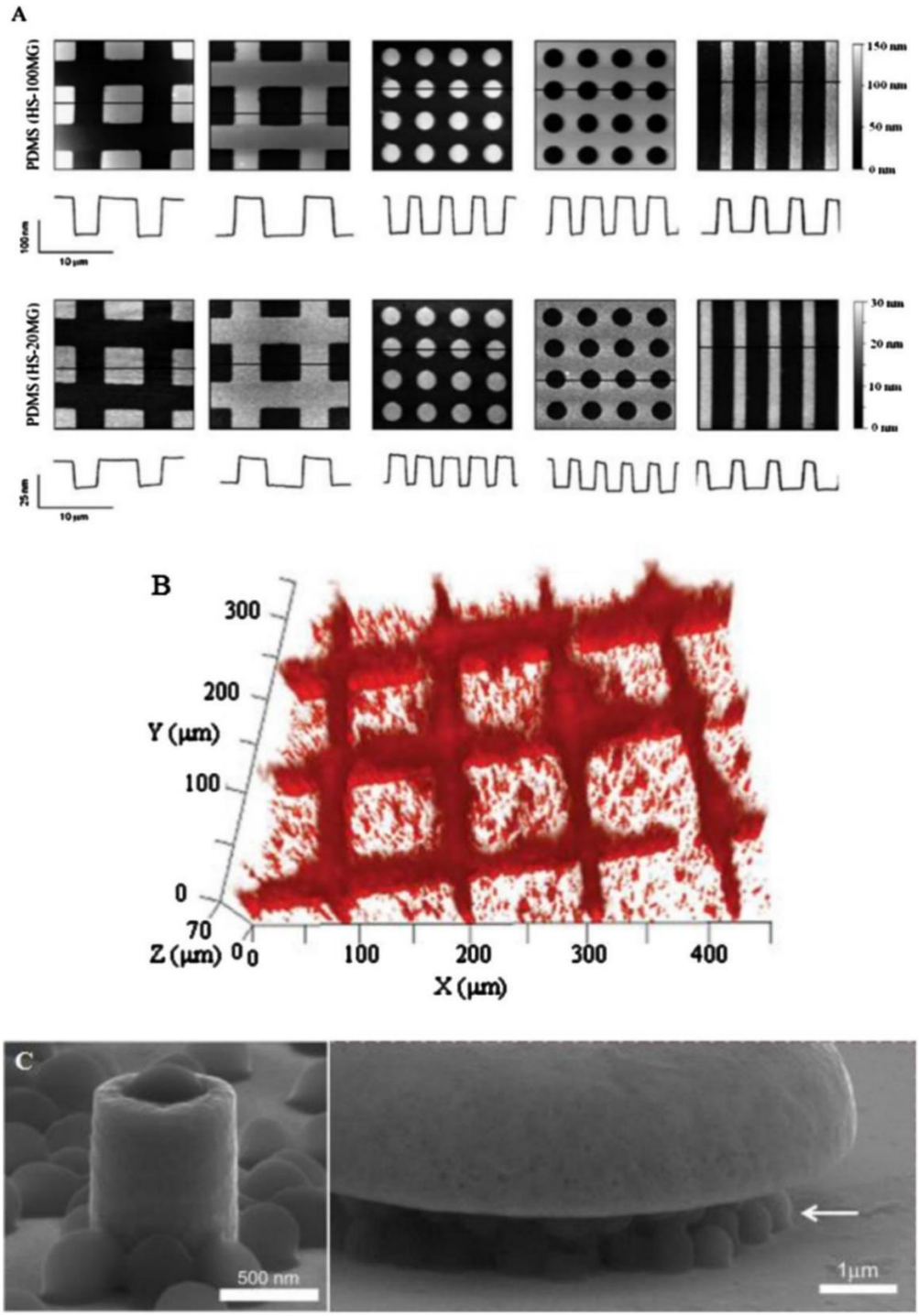

Figure 2.8 (a) Atomic force microscopy (AFM) images of the topographic features produced on PDMS surfaces. (b) Preference of *E. coli* adhesion on a patterned PDMS surface. Bacteria tended to choose valleys instead of protruding square features. (c) SEM micrographs showing the adhesion of S. aureus cells on nickel nanostructures. [19]

2.8.5 Bacterial surface and appendages

The cell envelope can exhibit different charges and hydrophobicity around the cell body due to the bacterial cell surface is highly heterogeneous and contains differently exposed lipids, proteins, exopolysaccharides, non-pilus, or fimbriae structures which mainly depends on the environmental pH and ionic strength (Figure 2.10) [25, 186, 187]. It is worth noting that hydrophobic components of the cell envelope can promote the hydrophobic interaction between bacteria and surface at the microscopic level such as polymer brushes, proteins, and extracellular polysaccharides [25]. These different biopolymers on the cell surface can help bacterial cells overcome the interface water to reach the surface tightly (Figure 2.10a). While if the distance between the bacteria and the surface is close to the nanometer scale, the bacterial cell appendages and the adhesin produced by the bacteria can interact with the solid surface to promote cell adhesion (Figure 2.10b) [25].

The motility of the bacterial flagella can not only actively push the bacteria to the surface, but also help the bacteria to anchor irreversibly on the surface [188]. The presence of active flagella helps surface wetting and masks surface chemicals as a conditioning film for bacterial adhesion[183]. Through surface binding and rotation, the flagella can help the cell body to reposition from the polar to the longitudinal attachment. Therefore, the longitudinal positioning can maximize the contact area between the bacterial cells and the surface, then enhance the cell attachment [189]. In addition, bacterial flagella can provide substantial benefits for cell adhesion in topographical environments [183]. For example, compared with a flat surface, the attachment of wild-type *E. coli* with flagella on the micro hillocks is significantly increased. And flagella filaments help adhesion by entering additional surface cracks. While bacteria attach to the surface, they may use their flagella to explore and try to access the extra surface topography, or to overcome unfavorable surface topography. Then will forming a dense fibrous network [183]. However, it is recently reported that the flagella of *E. coli* can actively sense the hardness of the substance and determine whether the attachment is beneficial, thereby reducing motility and starting colonization [190].

Except for flagella, other cell surfaces extensions like fimbriae, curls, and pili have been found to help bacteria adhere to the solid surface [25]. Generally, the pili function in different types of various bacterial species has been well studied in the first step of adhesion, such

as E. coli type I pili and *P.aeruginosa* type IV pili (T4P) [191, 192]. T4P allows P. aeruginosa cells to quickly explore the microenvironment by crawling horizontally and walking vertically on the surface [191]. The length of T4P can be extended by polymerization and contracted by depolymerization along the surface[193]. According to the bacterial convulsions in fluid flow work, the number of pili and the distribution angle of pili can be used to select the nature of bacterial convulsions depending on the environmental conditions. When the pili attach to the object during the contraction process, they will exert a greater slingshot speed, causing the bacteria to move in the host cell and trigger downstream signals, thereby effectively spreading during the formation of biofilm. In addition, when bacteria twitch on the surface of groove, they tend to gather on the downstream side of the groove wall [194].

For example, Yasmine et al. considered the effect of bacterial appendages by modeling bacteria as rough spheres, that is, reconstructing the topography of surface appendages. And used Surface Element Integration to compute the DLVO interactions between particles and a simulated surface. They demonstrated that the effect of appendages on the bacterial cell surface on deposition was examined in terms of appendage radius. Finer appendages result in a lower net interaction energy barrier and therefore a higher deposition rate (Figure 2.10). From Figure 2.11, it shows that the presence of appendages reduces the height of the barrier since the heir's appendage radius is extremely small compared to the entire bacterial cell without appendages, but increasing the number of appendages per unit area (or surface coverage) of the bacterial cell slightly increases the potential for high rejection barrier under conditions [12].

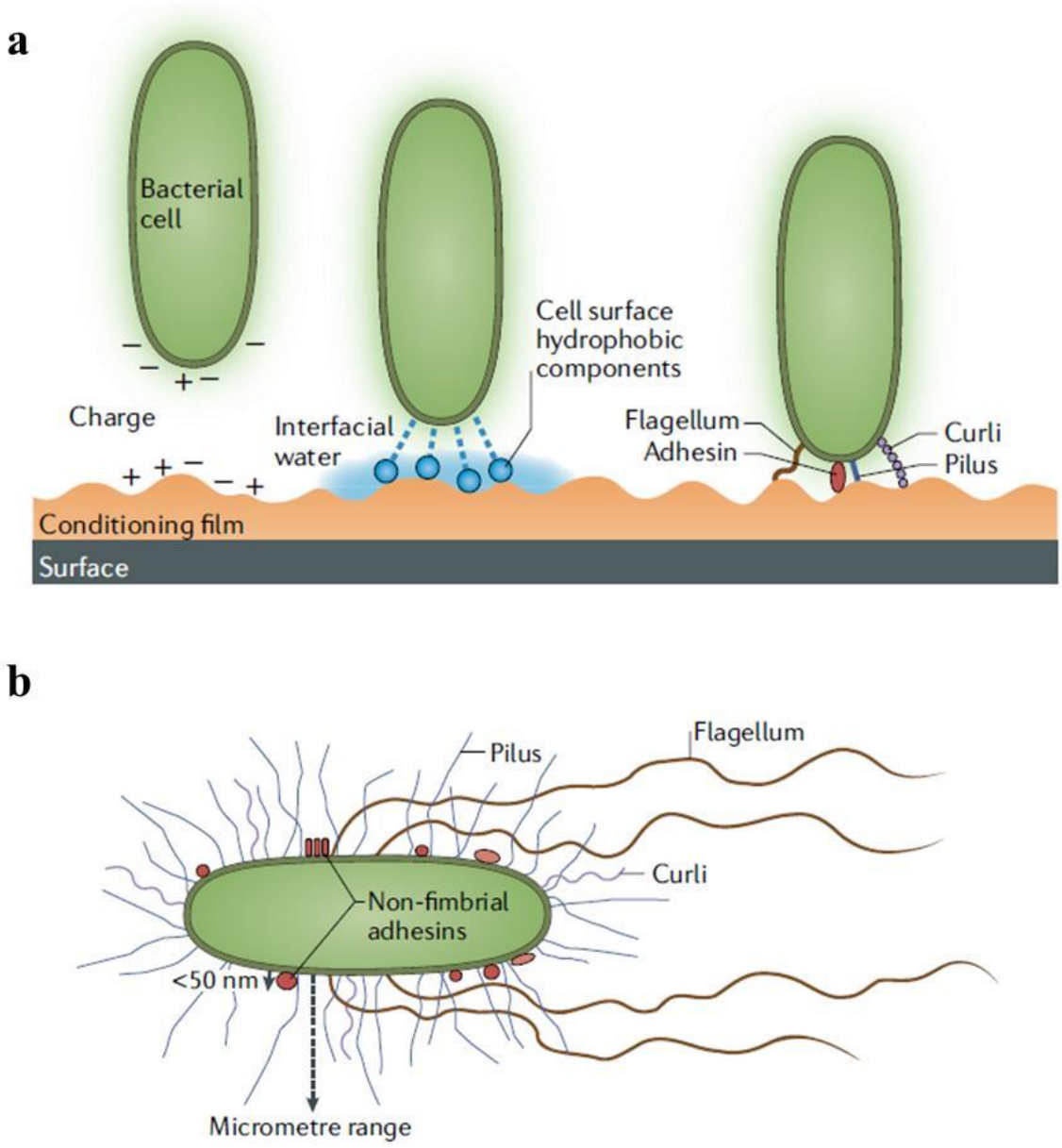

Figure 2.9 (a): the interactions between the cell envelope and solid surface. Orange: the conditioning film; light blue: interfacial water; dark blue: hydrophobic components on the cell surface; (b): adhesins (red) and bacterial cell appendages (such as flagella (brown), pili (blue) and curli (purple)) on cell envelope. [12]

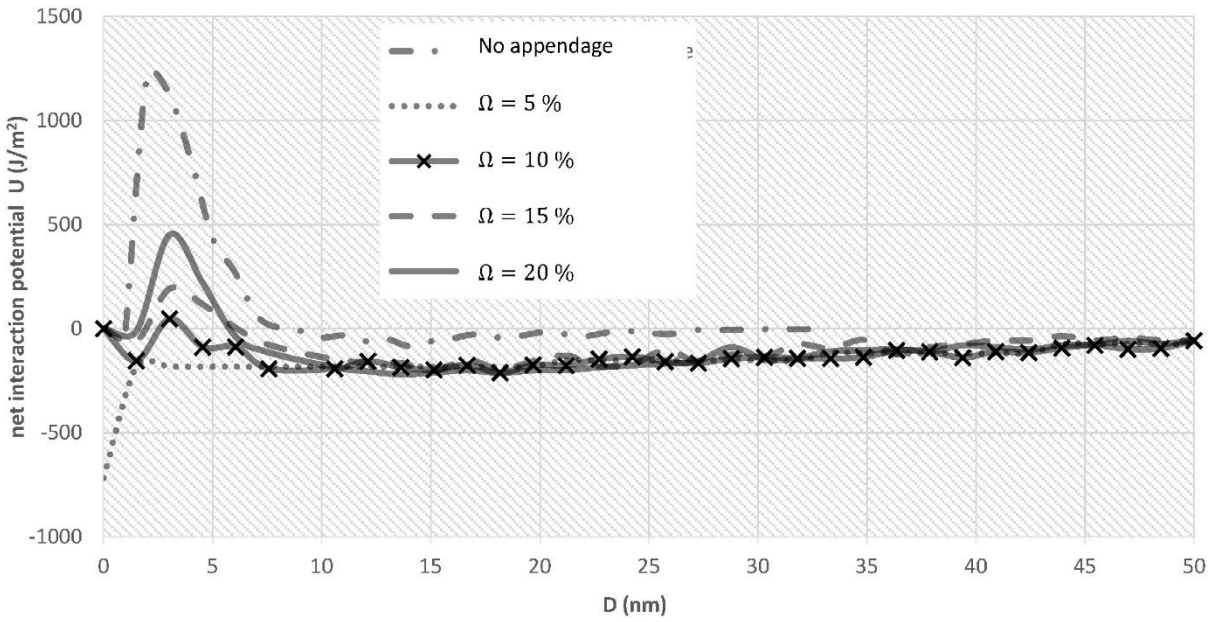

Figure 2.10 Net interaction potential between the 500 nm radius bacterial cell with different appendage surface coverage and materials surface at an ionic strength of 10 mM. [12]

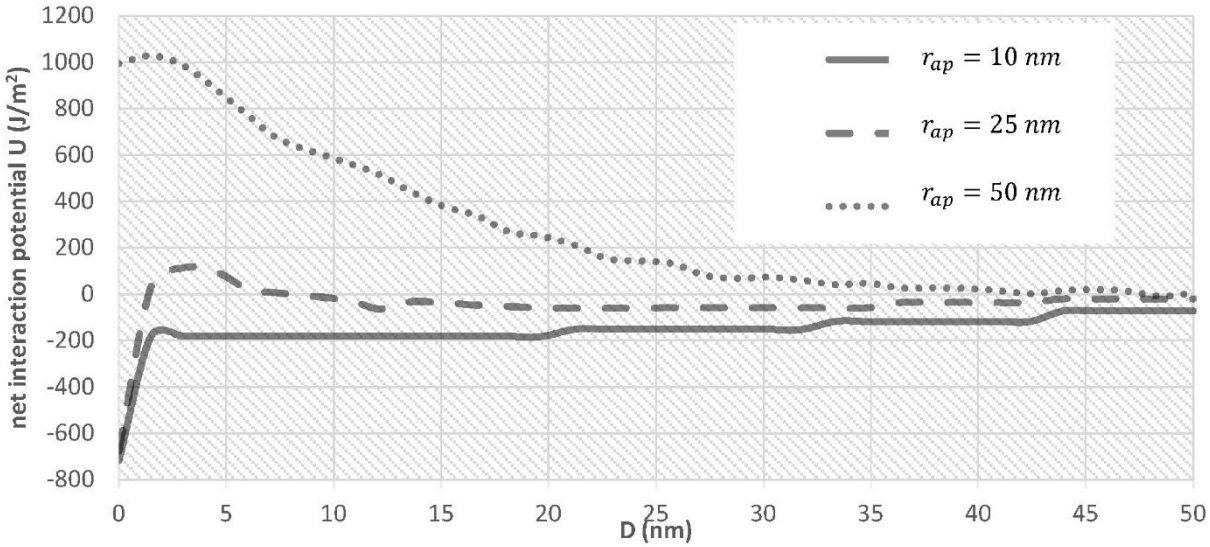

Figure 2.11 Net interaction potential between the 500 nm radius bacterial cell and the surface for the different appendage radii at an ionic strength of 10 mM. [12]

2.9 Antibiofilm surfaces

In general, there have different strategies to prevent biofilm formation such as chemical killing-based methods and surface architecture-based methods. For chemical killing-based methods, the most two common methods are to use antibiotics to kill bacteria and antimicrobial nanoparticles. For surface architecture-based methods, cicada wings were the first example of a bactericidal surface, lotus leaves and shark skins were the example of anti-biofouling surface, Sharklet AFTM was the example of microtopography on the surface and other nanostructured bactericidal surfaces include Silicon-based and Titania based.

2.9.1 Chemical killing-based approaches

If the bacteria adhesion and growth can be prevented on the surface in the early stage, bacterial biofilm formation will be inhibited [195]. Once the biofilm begins to form, tackling bacterial colonies will become harder [196]. There are a variety of chemical methods to eliminate the bacteria which are using antibiotics, the photodynamic inactivation of bacteria, reactive oxygen species and antimicrobial nanoparticles like Ag nanoparticles.

While applying antibiotics to the typical biofilm population (Figure 2.13) [10]. its efficacy in killing the bacteria is limited to the top layer of the biofilm, with almost no effect on the bacteria located deeper within the microcolonies [197]. Thus, there appeared more and more antibiotic-resistant bacteria and caused 700,000 deaths each year in the whole world [198]. In 2007, Tim Maisch et al. demonstrated when exposed to light, photosensitizers in bacteria produce singlet oxygen, which oxidizes proteins or lipids, causing the bacteria to die [199]. In recent work, reactive oxygen species (ROS) is one of the most popular chemical methods to degrade chemicals or prevent biological contaminants [200]. For example, Hanna et al. demonstrated that ROS production is an important mechanism for *G. mellonella* to fight bacterial infection and validate the host as a relevant model for studying host-pathogen interactions [201].

The application of nanoparticles in the recent period has been widely used in medical and pharmaceutical nano-engineering for the delivery of therapeutic agents, chronic disease diagnostics, and sensors. For example, Ag nanoparticles (Figure 2.13) can reduce microbial infections in skin and burn wounds and also prevent bacterial colonization on different surface devices [8]. And Ag nanoparticles can prevent biofilm formation due to their unique physical-chemical properties like the high surface area, mass ratio, high reactivity, and sizes in the nanometer range. Surprisingly, Ag nanoparticles can impact biofilm only in the absence of Suwannee River fulvic acid (SRFA). Because SRFA can prevent bacterial membranes face significant damage from nanoparticles by covering the nanoparticles or by intrinsic antioxidant activity. As for marine biofilms, the reduction of marine biofilms is dependent on the concentration of Ag nanoparticles. And Ag nanoparticles may prevent new bacteria membranes attach to the biofilm and decrease the development and succession of the biofilm by exposing them [202, 203].

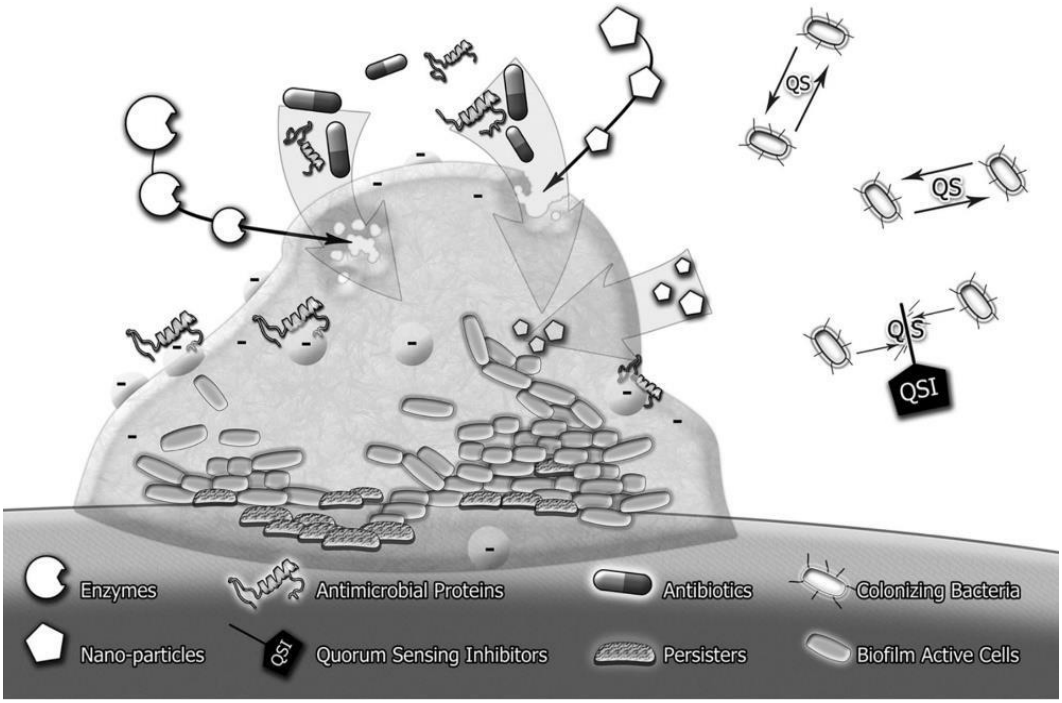

Figure 2.12 Persistence of microbial pathogens in biofilms requires a sophisticated arsenal of killing machines to break their party. [10]

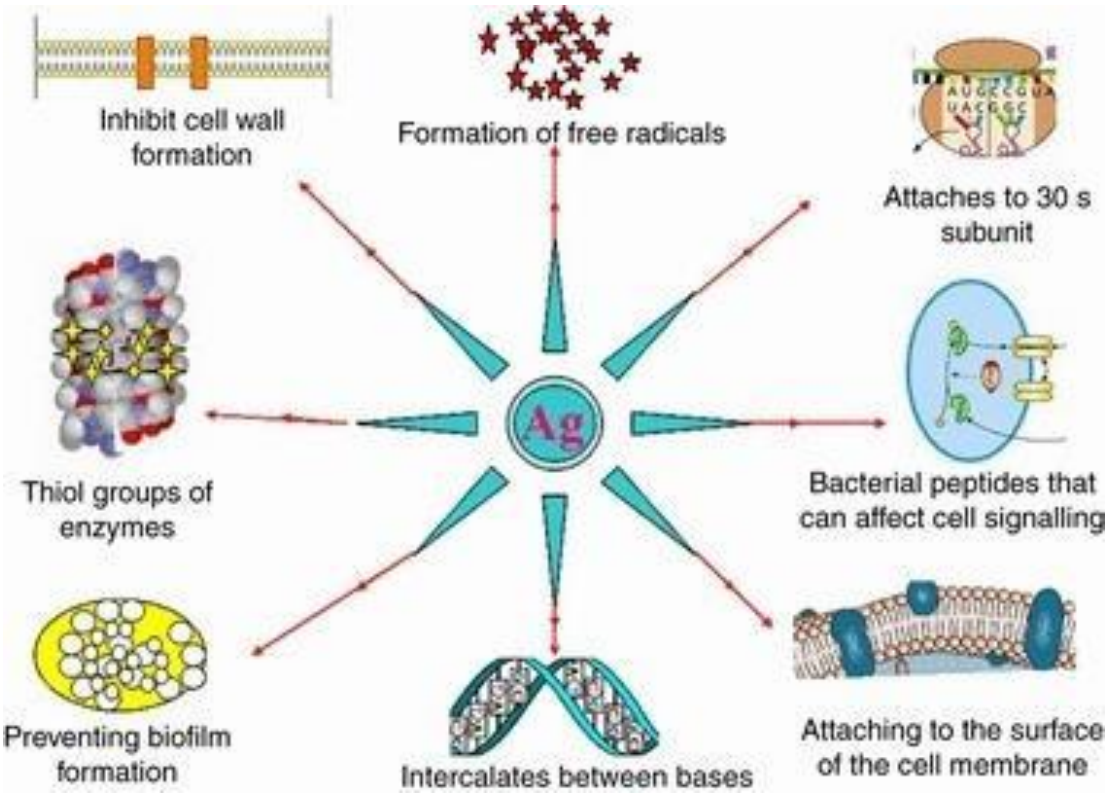

Figure 2.13 Sliver nanoparticles showing multiple bactericidal actions [8]

2.9.2 Different Methods to Fabricate Silver Nanoparticles

Two main processes can be divided for fabrication methods of AgNPs: top-down and bottom-up (Figure 2.15) [23]. The top-down approach, mainly the physical method, refers to the synthesis of AgNPs using various physical forces to form AgNPs from bulk materials. The physical synthesis of AgNPs involves both mechanical and steam-based processes [204, 205]. While the resulting AgNPs are uniform in size distribution, high in purity, and free from chemical agents that could be harmful to humans and the environment, it poses a great challenge to prevent caking due to the lack of stabilizers or capping agents. Furthermore, these methods require complex equipment and external energy during the process. Energy is used to reduce particle size, including mechanical energy (ball milling method) [206], electrical energy (arc discharge method) [206, 207], light energy (laser ablation method) [208], and thermal energy (physical vapor deposition method) [209]. The bottom-up approach involves building complex clusters to obtain NPs from molecular components by employing nucleation and growth processes. Common bottom-up approaches include

chemical synthesis and biosynthesis, both of which can be used to obtain NPs by reducing precursor salts [205]. Chemical synthesis can be coupled with alternative energy sources such as photochemical, electrochemistry, microwave-assisted, and sonochemical methods [23]. Although chemical methods can be employed to rapidly obtain NPs of various shapes, the use of harmful chemical additives may limit the medical treatment of NPs applications. Instead, the biological method can overcome the disadvantages of chemical methods. Biological methods often rely on macromolecular substances such as exopolysaccharides, cellulose and enzymes in bacteria, fungi and algae, and organic components in plant extracts such as enzymes, alcohols, flavonoids, alkaloids, quinine, terpenoids, and phenolic compounds. Biosynthesis is an economical, environmentally friendly, simple and reliable method, but the composition of the nanoparticle surface must be fully considered in the application [23].

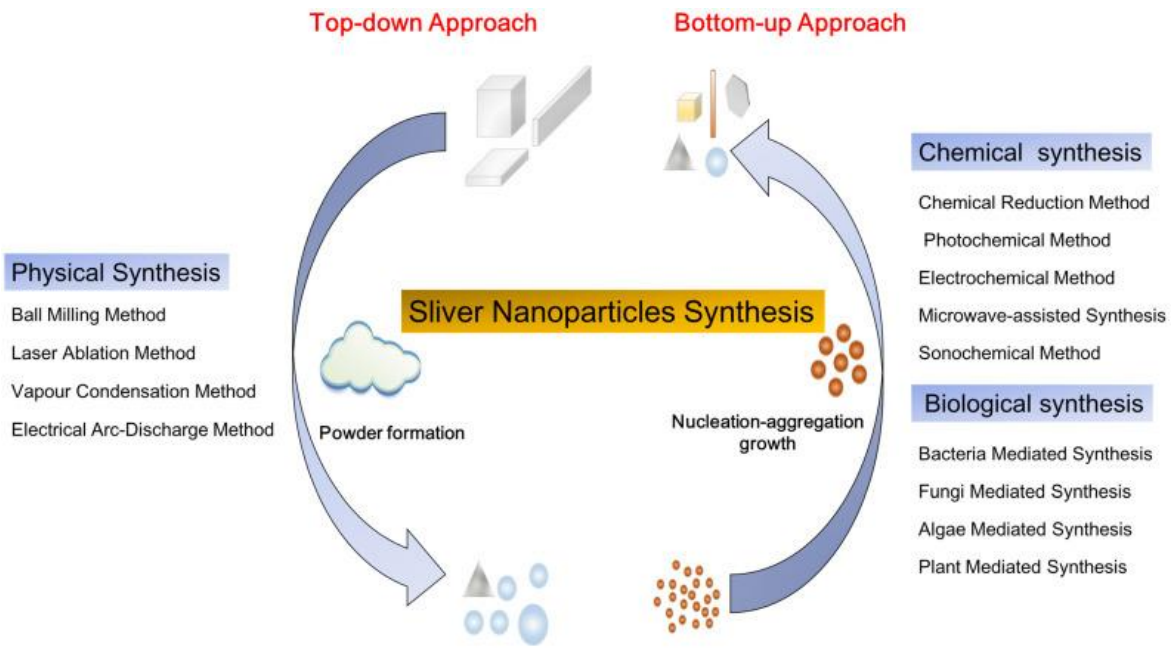

Figure 2.14 Silver nanoparticles synthesis: top-down approach and bottom-up approach [23].

2.9.3 Antibacterial Mechanism of Silver Nanoparticles

The exact mechanism of the antibacterial effect of silver nanoparticles has not been fully elucidated, but there are a variety of antibacterial effects that have been proposed in Figure 2.16 [24]. The mechanism of silver nanoparticles is most likely identified with killing microbes as it can continually release silver ions [210].

Due to the electrostatic attraction and affinity for sulphur proteins, silver ions can easily adhere to cell walls and cytoplasmic membranes. Adhering ions enhances the permeability of the cytoplasmic membrane and lead to bacterial envelope disruption [211]. After free silver ions are taken up into cells, respiratory enzymes are inactivated, producing reactive oxygen species, but interrupting the production of adenosine triphosphate. Reactive oxygen species may be the main factor triggering cell membrane rupture and deoxyribonucleic acid (DNA) modification. Since sulfur and phosphorus are important components of DNA, the interaction of silver ions with sulfur and phosphorus in DNA can cause problems with DNA replication, cell reproduction, and even the death of microorganisms. In addition, silver ions can inhibit protein synthesis by denaturing ribosomes in the cytoplasm [212].

In addition to being able to release silver ions, silver nanoparticles themselves can kill bacteria. Once anchored to the cell surface, silver nanoparticles accumulate in pits formed in the cell wall [213]. Accumulated silver nanoparticles can cause cell membrane degeneration. Silver nanoparticles also can penetrate bacterial cell walls and subsequently alter the structure of cell membranes because of their nanoscale dimensions [213]. Degeneration of the cytoplasmic membrane can rupture organelles and even lead to cell lysis. In addition, silver nanoparticles can be involved in bacterial signal transduction. Bacterial signaling is affected by phosphorylation of protein substrates, and nanoparticles can dephosphorylate tyrosine residues on peptide substrates. Disruption of signal transduction can lead to apoptosis and termination of cell proliferation [214].

The dissolution state of silver nanoparticles in the exposure medium strongly affects their antibacterial effects and mechanisms. The dissolution efficiency depends on synthesis and processing factors, such as the intrinsic silver nanoparticle properties and the surrounding medium [215]. Theoretically, the Ostwald-Freundlich equation describes the effect of particle size and shape on the release of silver ions. Smaller silver nanoparticles that are spherical

or quasi-spherical are more likely to release silver due to their larger surface area. This also explains the lower silver release from aggregated nanoparticles relative to isolated nanoparticles [215]. Capping agents are used to modifying the surface silver nanoparticles, which can alter their dissolution behavior [216]. In addition to these inherent properties of silver nanoparticles, the surrounding medium also affects the release of silver ions. The presence of organic or inorganic components in the medium can affect the dissolution of silver nanoparticles by agglomerating with silver nanoparticles or complexing with silver ions. The researchers also demonstrated that silver nanoparticles released silver ions faster in acidic solutions than in neutral solutions [217].

Gram-negative bacteria are more sensitive to silver nanoparticles [218]. Gram-negative bacteria have narrower cell walls than Gram-positive bacteria. Thicker cell walls may reduce nanoparticle penetration into cells [218]. Different antibacterial effects of silver nanoparticles against Gram-negative and Gram-positive bacteria suggest that the uptake of silver nanoparticles is important for the antibacterial effect. It is widely believed that silver nanoparticles smaller than 10 nanometers can directly alter cell permeability, enter bacterial cells and cause cell damage [216].

Biofilms form rapidly in the oral environment and protect bacteria from silver ions and nanoparticles by hindering their transport. The researchers found that when all the planktonic bacteria were killed with the same concentration of silver nanoparticles, no 100 percent loss of bacterial viability occurred in the biofilm [219]. Therefore, biofilms are resistant to silver nanoparticles due to their complex structure. The diffusion coefficients of silver nanoparticles are generally related to size and physicochemical properties, which determine their mobility and bioavailability in biofilms. First, these coefficients decrease with increasing molar mass, which means that larger silver nanoparticles are more difficult to penetrate biofilms [220]. For particles larger than 50 nm, transport through biofilms can be significantly hindered. Second, the chemical composition of nanoparticles can induce the adsorption and accumulation of silver nanoparticles in biofilms, thereby reducing their diffusion. Third, electrostatic interactions between bacteria and silver nanoparticles can affect the penetration of charged nanoparticles into biofilms [221].

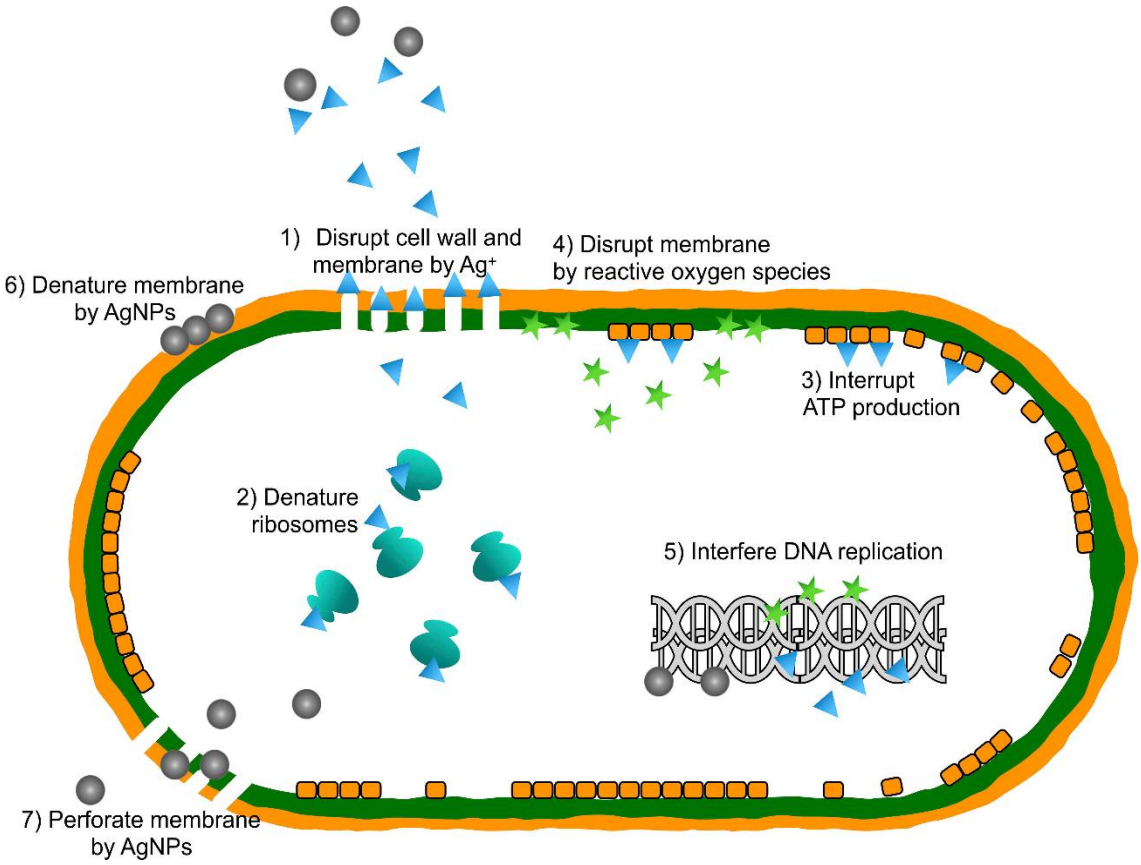

Figure 2.15 Antibacterial effects of silver nanoparticles (AgNPs). 1) Destruction of cell wall and cytoplasmic membrane: silver ions (Ag+) released from silver nanoparticles adhere to or pass through the cell wall and cytoplasmic membrane. 2) Denaturation of ribosomes: silver ions denature ribosomes and inhibit protein synthesis. 3) Interrupt Production of Adenosine Triphosphate (ATP): The production of ATP is terminated due to the inactivation of respiratory enzymes on the cytoplasmic membrane by silver ions. 4) Destruction of the membrane by reactive oxygen species: The reactive oxygen species generated by the broken electron transport chain can cause the destruction of the membrane. 5) Interfere with deoxyribonucleic acid (DNA) replication: Silver and reactive oxygen species bind to DNA, preventing its replication and cell proliferation. 6) Membrane degeneration: Ag nanoparticles accumulate in the cell wall pits, causing membrane degeneration. 7) Membrane perforation: Silver nanoparticles pass directly through the cytoplasmic membrane, which can release organelles from cells. [24]

2.9.4 Surface architecture-based methods

In the current year, many biomaterials with the anti-biofouling surface are based on the structures of some natural systems, such as lotus leaves and shark skins (Figure 2.17) [13, 222-224]. These surfaces are composed of hydrophobic materials with unique topographic features which contribute to the observed self-cleaning effect [184]. For example, lotus leaves have a super-hydrophobic surface (water contact angle is around 154° [225]) which affords the surface the ability to self-clean. When a water droplet encounters the multifunctional surface nanostructure of the top surface of a lotus leaf, it behaves at a very high contact angle and small sliding angle, both are a condition for super-hydrophobicity and low-adhesion functions. After contact, near-spherical water droplets form and rollover, and eventually fall off the blade, collecting and removing foreign matter in the process [18, 224]. Another one is sharkskin which was found to be arranged in a distinct diamond pattern with tiny ribs [226, 227]. These kinds of tiny ribs, together with a mucous layer on the surface allow the shark to remain flexible and clean. As Brennan and colleagues' study demonstrated biomimetic topography inspired by shark skin on PDMS surfaces (with features 2 μm wide and 3 μm height) using standard photolithography to create antifouling surfaces [14, 227]. The rejection rate of *P. aeruginosa* and *S. epidermidis* reached 99.86% and 99.78%, respectively [228].

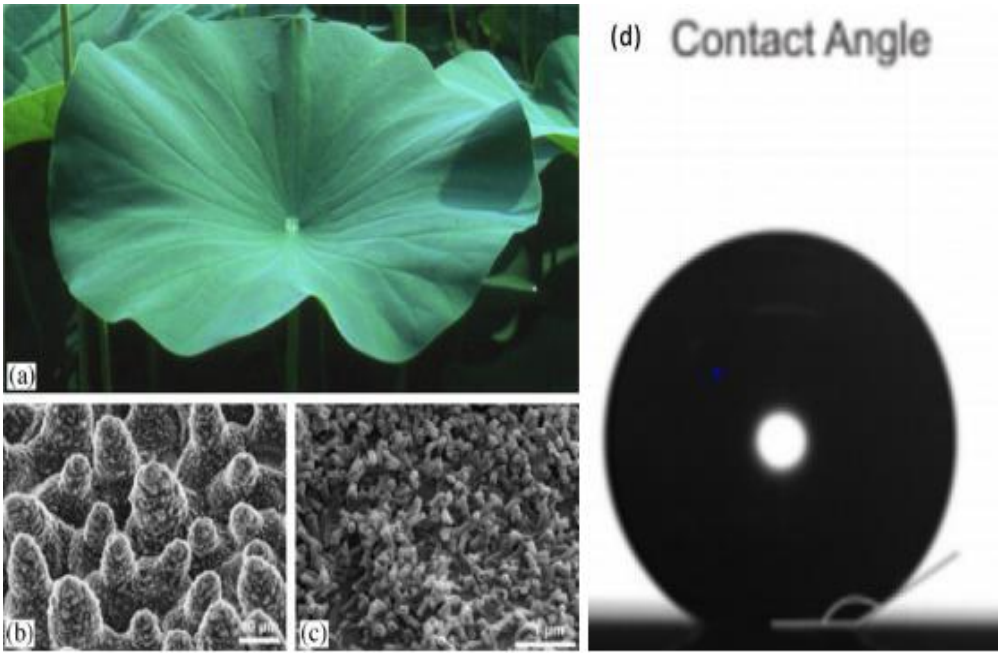

Figure 2.16 (a) Lotus leaves, which exhibit extraordinary water repellence on their upper side. (b) Scanning Electron Microscope (SEM) image of the upper leaf side prepared by 'glycerol substitution' shows the hierarchical surface structure consisting of papillae, wax clusters, and wax tubules. (c) Wax tubules on the upper leaf side (d) the contact angle of lotus leaf [13]

The most successful design to date is Sharklet AFTM which is mimic the sharkskin. This specific microtopography is typically tailored to the critical dimensions of the fouling organism due to non-random and clearly defined surface features. For the recent results on the Sharklet AFTM and other engineered microtopographies which were designed at a 2-um feature width and spacing, 3 um feature height have shown a strong correlation between the engineered roughness index and the inhibition of settlement by the zoospores of the most common ship fouling alga, Ulva. It was assumed that these kinds of dimensions of the topography would be slightly too large to effectively reduce the bacteria attachment in the size range of around 1-2 um. However, it could be affected physically disrupting the further colonization of additional bacteria and subsequent formation of biofilm in Figure 2.17 [14].

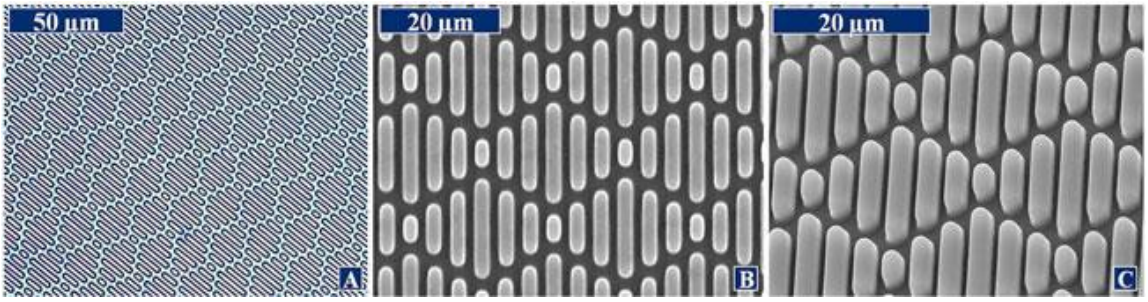

Figure 2.17 Sharklet AF™ topography on PDMS elastomer with 2 um feature width and spacing and 3 um feature height. (A) Light micrograph with top-down view. (B) Scanning electron micrograph with top-down view. (C) Scanning electron micrograph taken at 35° tilt to show protruding features [14]

In addition, several studies have explored alternative physical methods through the contact-killing mechanism. These developments have in part been inspired by nature where nanostructures on the wings of several insects are known to be capable to kill bacteria that are in contact. For instance, the nanopillars on cicada wings (Figure 2.18) have demonstrated strong antimicrobial efficacy against a wide range of bacteria (see Figure 2.18) [18, 229]. Later, similar surface structures have been fabricated on different engineering materials such as silicon and Ti, which have also shown very good antimicrobial performance [198]. However, the long-term antibiofilm performance of these structures is still questionable.

Therefore, we aim to develop novel surfaces which would potentially enable more sustainable antibiofilm performance. To achieve this, first, we need to gain a better understanding of how surface physics may affect bacteria attachment and biofilm formation. Furthermore, most of the existing studies are limited to bacteria attachment and biofilm formation in a static culture environment which may not represent the real scenario. Therefore, we will also study the bacteria attachment and biofilm formation with the flow.

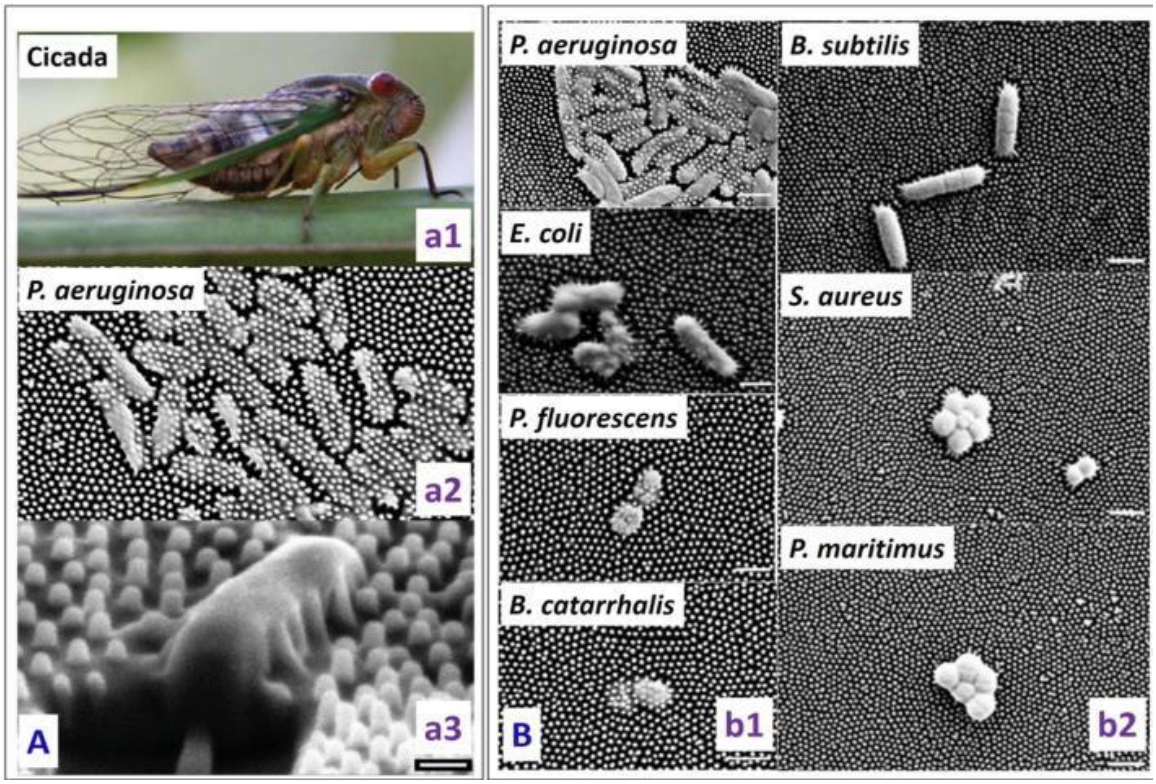

Figure 2.18 (a1) Photograph of cicada insect (Psaltoda claripennis). (a2) *Pseudomonas aeruginosa* cells on the nanostructured cicada wing penetrated by the nanopillar structures. (a3) Representative SEM image of a *Pseudomonas aeruginosa* cell sinking between the nanopillars on the cicada wing surface (53° view angle) (scale bar = 1 μm). (B) Selective bactericidal activity of the Cicada wing surface against (b1) gram negative (*P. aeruginosa*, *E. coli*, *P. fluorescens*, *B. catarrhalis*) and (b2) gram positive bacteria (*B. subtilis*, *S. aureus*, *P. maritimus*) (Scale bars = 1 μm). [18]

2.9.5 Liquid-like surface

McCarthy's group has demonstrated that low contact-angle hysteresis (CAH) surfaces can be achieved by exploiting the "liquid-like" nature of surface-bound functional groups (Figure 2.19). In the "liquid-like" state, the surface functions are flexible and mobile, and the probe liquid in contact experiences a low energy barrier between metastable states and is not easily pinned. From a practical surface modification standpoint, it is easy to form such a smooth/flat "liquid-like" (low CAH) surface without relying on surface roughening or subsequent perfluorination using long-chain perfluorinated compounds, low-cost,

repeatable and environmentally friendly - friendly matches. However, despite these attractive advantages of "liquid-like" (low CAH) surfaces, there are a limited number of papers describing the preparation of such surfaces, showing excellent liquid flow properties, in contrast to topographically modified super-dewetting surfaces and “liquid” surfaces such as smooth liquid-infused porous surfaces (SLIPS). For example, a Slippery Omnipobic Covalently Attached Liquid-like (SOCAL) surface, obtained through acid-catalyzed graft polycondensation of dimethyldimethoxysilane, was first proposed by Wang & McCarthy as an ultra-slippery non-pinning surface for sessile droplets. This SOCAL surface displays similar wetting properties to SLIPS through its grafted PDMS coating that behaves as a liquid phase approximately 150 °C above its glass transition temperature. The wetting properties of SOCAL coatings have been increasingly cited, but only a handful of groups have implemented the techniques and successfully fabricated SOCAL with contact angle hysteresis (CAH) below 3 degrees [17].

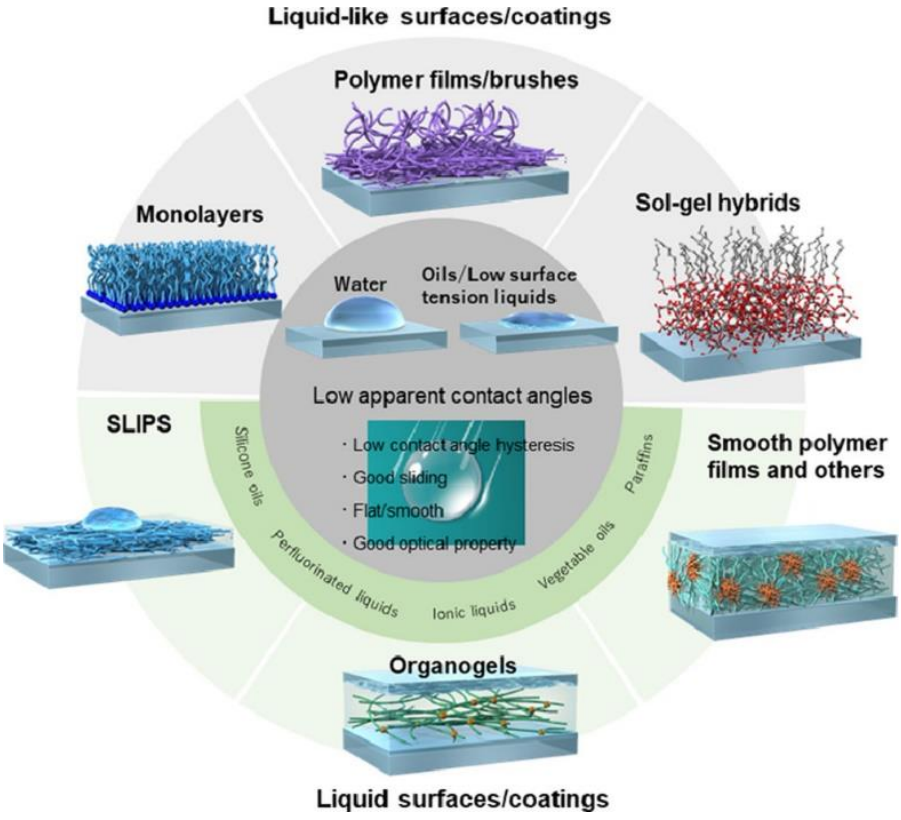

Figure 2.19 Liquid-like surfaces or coatings [17]

2.9.6 Slippery liquid-infused porous surface (SLIPS)

In 2004, a superhydrophobic surface (SHS) was first proposed which is inspired by the surface of the lotus leaf [230]. In the current period, most SHSs are established by creating rough structures on low surface energy materials or reducing the surface energy of existing rough structures [231]. These surfaces can trap air into a specific structure to form an air barrier to protect the substrate from external liquids. Therefore, SHSs are widely used in various scientific and technological fields, including anti-icing, anti-corrosion, drag reduction, liquid transport, and anti-fouling marine devices [231]. However, the manufacture of traditional SHS needs complicated technology and very expensive reagents and is overly dependent on specific substrates. Also, the air barriers are usually impermanent and vulnerable [232]. In addition, the fine structure of SHS is easily damaged by external shocks due to adhesive defects or low mechanical strength. Although some studies on durable SHS have been proposed in the past few years, organic adhesives cannot withstand high temperatures and solvents, which limits their scope of application. Even in a recent report, SHSs are also easy to frost in high humidity environments [233]. Thereby, the slippery liquid-infused porous surface (SLIPS) can replace SHS to protect substrates from damage.

The SLIPS was first proposed in 2011 by Aizenberg et al. which is biomimicking the Nepenthes pitcher plant and confirmed that it is conceptually different from the lotus effect [47]. Compared to SHS, the SLIPSs obtained by the liquid-infused technology are more stabilized because the gas barrier layer in SHS cannot withstand the harsh external environment as effectively as the lubricating layer in SLIPS [234]. Thus, SLIPS has better liquid repellence, anti-icing, anti-fouling, anti-corrosion, pressure stability, and self-healing properties [231]. In recent years, a variety of SLIPS with various properties has been developed to protect the original metal substrate. For example, Li et al. successfully manufactured a porous metal structure (Zn-Ni-Co) and obtained SLIPS through further modification and perfusion, showing excellent anti-corrosion and self-healing properties [235]. Chen et al. Use polyamide 6 to prepare SLIPS through silicone oil and femtosecond laser direct writing method, which has stable liquid repellence and self-healing properties [58]. To further improve the durability of SLIPS, Guo et al. reported that ZnO nanowires were prepared on the micro-pyramid by hydrothermal method and then combined with PDMS and silicone oil to successfully obtain durable SLIPS [236]. In addition, Snehasish et

al. reported that the SLIPS coating based on PDMS showed excellent antifouling ability against aquatic mussels, one of the most aggressive large fouling organisms, both in the laboratory and in the field. It also greatly reduces the adhesive strength of the mussel attachment line after settling, which facilitates their easy removal [237].

For prepared SLIPS, the lubricating fluid is added to the surface through a pipette to form an outer coating. With matching surface chemistry and roughness, the fluid will spontaneously diffuse across the substrate through capillary wicking. Given the known surface area of the sample, the thickness of the outer coating can be controlled by the fluid volume Figure 2.21 [20].

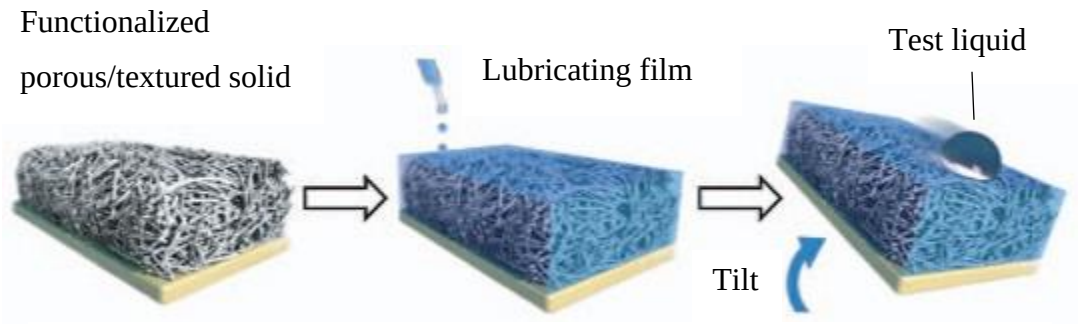

Figure 2.21 Schematics showing the fabrication of a SLIPS by infiltrating a functionalized porous/textured solid with a low-surface energy, chemically inert liquid to form a physically smooth and chemically homogeneous lubricating film on the surface of the substrate [20]

2.9.7 Biofilm detachment

Biofilm detachment is the least known stage in the accumulation of biofilms which is determined by the balance of attachment, growth, and detachment processes [238]. Detachment is defined as the release of microbial cells and their related matrix polymers from the biofilm to the bulk fluid immersed in the film. Many important factors have been suggested, such as matrix-degrading enzymes [239], microbially generated gas bubbles [240], nutrient levels and microbial growth status [241], availability of multivalent cross-linking cations [241], fluid shear stress [242]18, contact attrition [243], quorum-sensing signals [239], and the activation of a lytic bacteriophage [244]. Most of these detachment mechanisms are purely physical, but others may be primarily biological. Two possible factors that may trigger the

detachment process which is the accumulation of a metabolic product and the depletion of a metabolic substrate because they have the potential to explain the observation of biofilm cell cluster hollowing [245].

The mechanism of biofilm detachment is controlled by quorum-sensing signals. It is assumed that when the signal molecule (an excreted bacterial metabolite) accumulates to a threshold concentration, it will trigger the dissolution of the biofilm matrix and the release of bacteria. This mechanism directly leads to the prediction that natural signal molecules or their analogs can be used to disperse biofilms and clean biofouling surfaces [246]. This biofilm detachment mechanism was originally proposed by observing that blocking the flow of media to the biofilm system caused the biofilm to separate spontaneously within a few days [238]. The cessation of flow presumably allows the accumulation of separated signal molecules, eventually reaching a concentration sufficient to trigger the dispersion of the biofilm. Thus, detachment can occur in two modes when cells are deficient in nutrients and oxygen, it can be mediated by the separation of cells into large streams, or because the sheer force is greater than the cohesive force that holds the biofilm together. The increase in the separation event occurs in the first few seconds of the transient stress, but the value of the shear stress depends on the hydrodynamic growth conditions of the cultured biofilm [238]. For example, Mercier-Bonin et al. designed a flow chamber to remove bacterial detachment and biofilm formation. The chamber consists of a bottom glass plate (210×90×4 mm) and an upper plexiglass plate (210×90×10 mm) used as a substrate, and a hollow stainless-steel gasket (210×90×0.2± 0.0025 mm). The three plates are fixed together with aluminum clips. The fluid enters the chamber through a 1-mm wide slit that penetrates the upper plate vertically and exits the chamber through a 2-mm diameter hole. The third orifice (0.26 mm diameter) with a syringe valve on the top is used to inject medium (Figure 2.22) [3]. Aeri Park et al. demonstrated that optimum shear stress for the formation of *P.aeruginosa* PAO1 biofilm is 0.170 dyn s/cm^2 in the PDMS microfluidic channel after 24-hour culture. The low shear stress means low flow rates can cause problems with the delivery of nutrients and oxygen, which can lead to a lack of nutrients and oxygen, although they are critical for bacterial growth and biofilm formation. However, under high shear stress, some cells detach from the surface because the initial attachment is reversible or the adhesion is relatively weak [247].

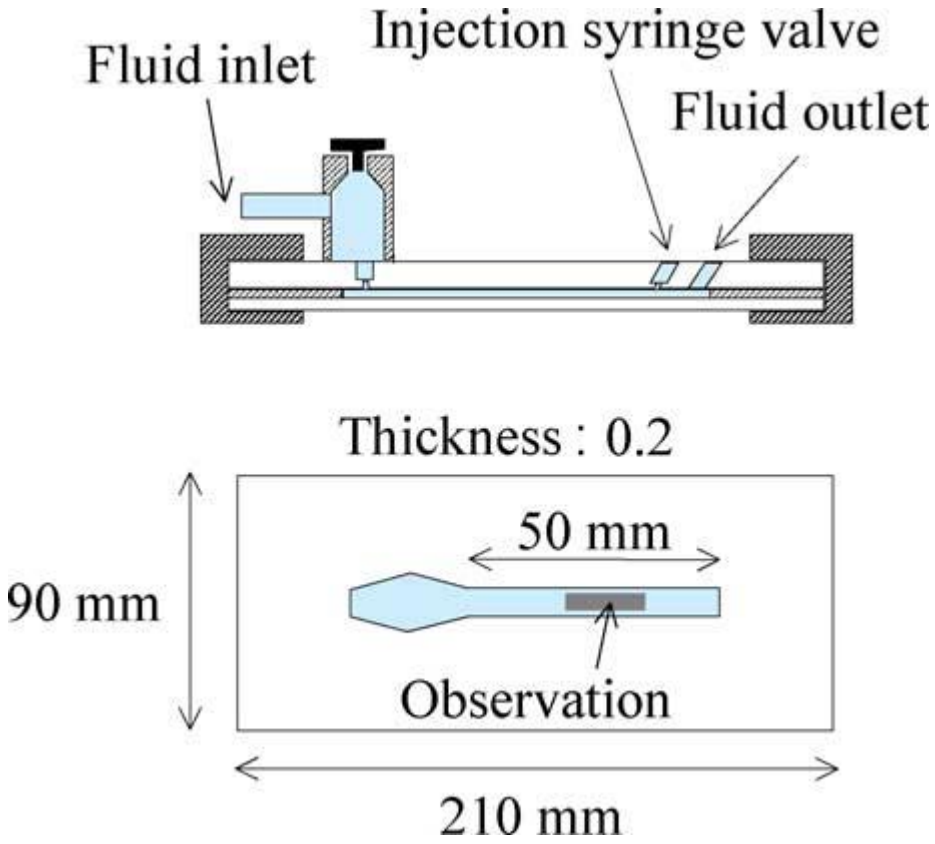

Figure 2.22 Schematic representation of the shear stress flow chamber. [3]

3 General Methodology and Techniques

In this project, we used 6 different surfaces to do the antibiofilm test both in static and dynamic conditions. Thus, in this chapter, general methodologies of surface fabrication, bacterial culture and antibiofilm test, wettability analysis, roughness measurement and flow cell design and setup were summarized. And the techniques for quantifying the biomass and observing the biofilm topography on the surfaces, such as confocal image analysis, critical point drying and SEM analysis are shown.

3.1 Surface fabrication

3.1.1 Control PDMS surface

Polydimethylsiloxane (PDMS) is a biocompatible material with high chemical and thermal stability thanks to the strength of the Si-O bond. To prepare the PDMS, the SYLGARD 184 Elastomer Kit (Dow Corning Corporation, Midland, MI) base and curing agent were mixed with a ratio of 10:1 (wt/wt). After mixing the solution thoroughly, degassing was performed in a vacuum chamber for 1h to remove the bubbles. Then the solution was poured into two bespoke acrylic molds (15mm×15mm×2mm for static culture, 40mm×30mm×2mm for dynamic culture). It was maintained at room temperature for 10mins to distribute evenly, then transferred to a 60°C incubator and cured for 1 day.

3.1.2 Rough PDMS surface

The fabrication method of rough PDMS applies, only by adding a piece of sandpaper with different grits (P120 refers to 120 grits, and P240 refers to 240 grits) to the bottom of the acrylic mold (Figure 3.1). This will enable us to create PDMS with different surface roughness.

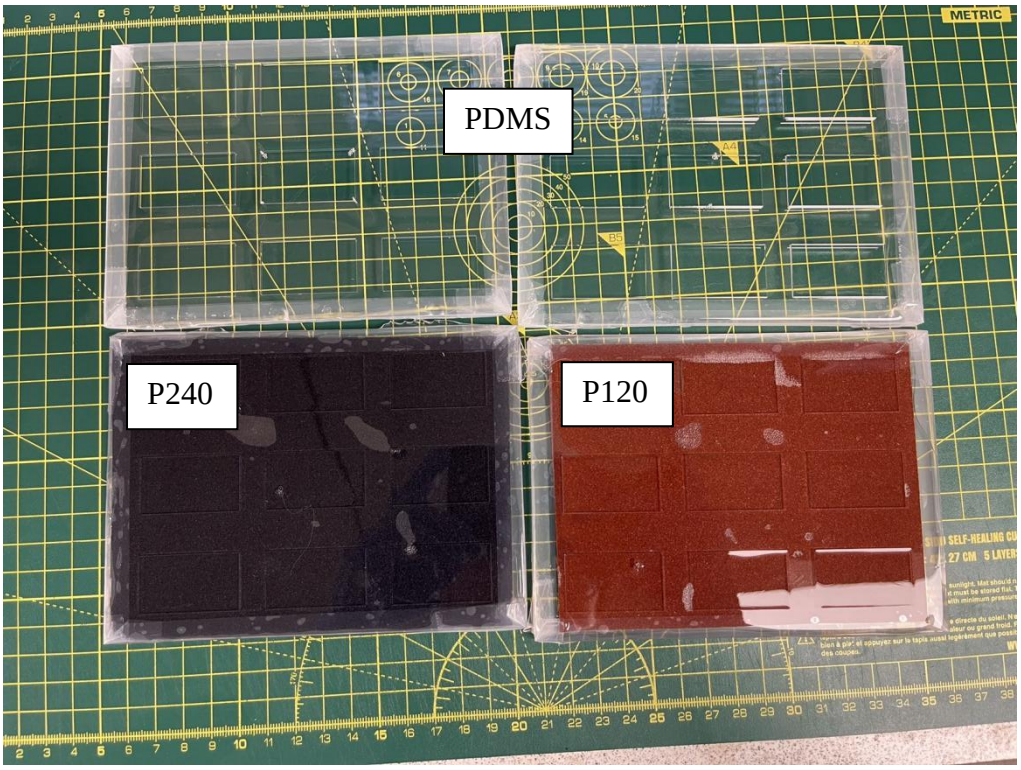

Figure 3.1 The schematic for make the different roughness PDMS.

3.1.3 Different oil thicknesses slippery surfaces

S-PDMS was prepared by immersing cured PDMS into a silicon oil bath (Grade: 10 cSt, 0.93 g/mL, Sigma-Aldrich, Country of origin) and maintaining it at room temperature for 24 hrs, allowing oil to fully penetrate the polymer network to reach equilibrium. The surface was gently wiped with filter paper to remove the excessive oil. The thickness of the surface oil layer can be measured and calculated by confocal microscopy, ellipsometry, or using the weight obtained after layering in the oil. In our case, due to the identical refractive index values of the silicone oil and PDMS, it is difficult to quantify the oil thickness of the S-PMDS optically. Measurements of the weight of the swelling oil cannot be used to determine the thickness of the surface oil layer due to the diffusion of oil into the PDMS polymer chains. The weight (w_1) of S-PDMS after a gentle wipe was measured (same protocol of preparing S-PDMS for surface wetting measurements and antibiofilm tests), followed by the measurement of the weight (w_2) and the dimensions (x, y, z) of the S-PDMS after vigorously wiping off all surface oil. Total of 10 replicates were used. The

thickness of the oil layer of S-PDMS can be adjusted by draining the oil for different duration, i.e., 50μm oil thickness by using samples directly from a well-plate filled with silicone oil; 20μm oil thickness by leaving samples to stand in air for 3 minutes; 5μm oil thickness by leaving samples for 10 minutes; 2μm oil thickness by leaving samples for 10 minutes and applying pressure to squeeze out a small amount of oil inside. The oil thickness (t) is assumed homogeneous in all directions, which can be determined by Equation 9 [60].

$$\frac{w_1 - w_2}{\rho} = (x + 2t)(y + 2t)(z + 2t) - xyz \qquad (9)$$

Where w_1 is the weight of the sample before wiping, w_2 is the weight of the sample after wiping, and x, y, z are the length, width, and height of the wiped sample. ρ is the oil density (0.93g/cm^3). A Matlab code was developed to calculate the oil thickness (seen in the Appendix).

3.1.4 SOCAL surface

Slippery Omniphobic Covalently Attached Liquid (SOCAL) surfaces were created on 25 × 75 mm glass slides using the method detailed by Wang & McCarthy [248]. The protocol was optimized as described by Armstrong et al [249]. The clean glass slides were placed into a Henniker plasma cleaner (HPT-100) at 30% power for 20 minutes, which adds OH bonds to the surface. The slides were then dipped into a reactive solution of isopropanol, dimethyldimethoxysilane and sulphuric acid (90, 9 and 1% wt.) for 5 seconds, then slowly withdrawn. The slides were then placed in a bespoke humidity chamber in a controlled environment at 60% relative humidity and 25 °C for 20 minutes. The acid-catalyzed graft polycondensation of dimethyldimethoxysilane creates a homogeneous layer of polydimethylsiloxane (PDMS) chains, grafted to the surface. The excessive unreacted material was then rinsed away with deionized (DI) water, isopropanol, and toluene. The SOCAL sample prepared is shown in Figure 3.2.

3.1.5 PEG surface

To prepare PEGylated surfaces, a clean glass sample is exposed to air plasma for 40 mins, which deposits OH radicals to allow the PEG chains to adhere to the surface. The sample is then immersed completely inside a solution of 2 (methoxy(polyethyleneoxy6-9propyl) trimeoxysilane, hydrochloric acid and Toluene, volumetric part of 1:8:10000 respectively.

The reaction is left to take place for a period of 18hrs, then it is carefully removed from the solution and rinsed thoroughly with de-ionized water, isopropanol and toluene. This step is important to ensure that any reactive solution is removed from the coated surface. The sample is then dried with compressed air and stored in a petri dish before use. The PEG surface is shown in Figure 3.2. For PEG samples, we divided them into two groups: PEG1 refers to the surfaces with CAH about 2 degrees and PEG2 refers to the surfaces with CAH about 6 degrees.

3.1.6 AgNPs-coated PDMS

AgNPs coating was synthesized on the PDMS surfaces using a protocol detailed by Joong Hyun Kim [250]. Based on the dimension of the PDMS sample, we optimized the methods to acquire a more uniform AgNPs coating (Figure 3.2). The sterilized clean PDMS surfaces were placed in a plasma cleaner (PDC-002-CE) and treated for 12 mins under vacuum. The treated PDMS surfaces must be immediately immersed in 150mL $AgNO_3$ (10mM) solution at room temperature for 1h to form Ag seeds on the surface. Then 3.5mL NaBH4 (50mM) solution was injected into 150mL $AgNO_3$ (10mM) solution and it was incubated for 15 minutes. On the other side, we prepared 150mL 0.0167% $AgNO_3$ solution to grow Ag seeds and preheated it to 80°C in the water bath. After 15 mins incubation, the PDMS surfaces were placed into the preheated solution for 5 mins. Then 3mL 1% (by weight) sodium citrate (Sigma-Aldrich) was injected as a reducing agent of silver ions. The AgNPs growth reaction should be incubated for 2hrs and a repeat was conducted to get a uniform and thicker coating. Finally, the AgNPs coating was rinsed with acetone, isopropanol, and deionized water to remove the residues on the surface such as the organic solvent from the elastomers. Then the sample was kept at 37°C incubation overnight to be dried.

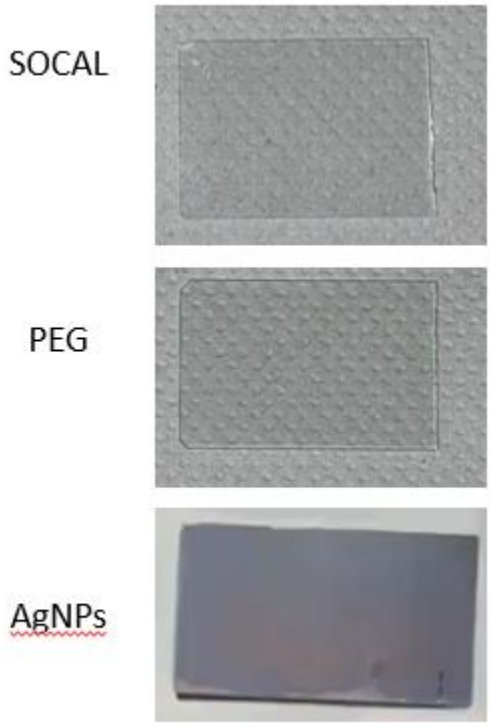

Figure 3.2 The images for SOCAL, PEG and AgNPs-coated PDMS.

3.2 Bacterial culture and antibiofilm test

Staphylococcus epidermidis FH8 isolated from a patient with chronic rhinosinusitis at Freeman Hospital (Newcastle upon Tyne) was used [251]. *Pseudomonas aeruginosa* (PAO1) was also selected, which is the biofilm-forming bacterial pathogen resulting in many infections [252]. For bacterial adhesion and biofilm formation assays, bacteria were routinely cultured in Tryptic Soy Broth (TSB) (Melford Laboratories Ltd, UK), in a shaker at 180rpm, 37°C for 16 hours. *S. epidermidis* FH8 was diluted to OD600=0.2 with a spectrophotometer (Biochrom Libra S11, Biochrom Ltd., Cambridge, UK). *P.aerugniosa* PAO1 was diluted to OD600=0.01 due to its rapidly colonizing surface and overloading the system if at high concentration. Before seeding, samples (PDMS, S-PDMS, AgNPs coating PDMS and Rough-PDMS) were placed in a 12-well plate. 3 ml diluted bacterial broth was added into each cell, which was then incubated at 37 °C for 2 hours (bacterial adhesion assay), 2 days, 7 days, and 14 days (biofilm assay) respectively. Other samples (SOCAL and PEG) were

placed in a petri dish. 20 ml diluted bacterial broth was added and the overall was cultured for 2 hours, 2 days, 7 days, and 14 days. For the bacterial culture lasting 7 days and 14 days, half of the TSB medium needs to be replaced every 3 days to guarantee enough nutrients for bacteria to grow. At least three independent repeats were performed for each surface type.

Flow is an important factor in many applications which should be considered when evaluating anti-biofilm effects. For dynamic culture, a syringe pump together with flow cells was placed inside a 37°C incubator. For 2 hours' bacterial culture, the diluted bacterial broth was pumped into the flow cell chamber at a flow rate of 0.01 ml/min, resulting in a relative wall shear stress (τ_w) of 0.007 Pa, comparable to the typical wall shear stress in urinary catheter [253] and ventricular catheter [254]. For 2 days, 7 days, and 14 days of bacterial culture, diluted bacterial broth culture was supplied into the flow cell for 2 hours to seed. Fresh TSB media was then used for the required time at the same flow rate (0.01 ml/min) at 37°C.

3.3 Wettability analysis

Surface wettability plays a critical role in bacterial adhesion and biofilm formation, which has been discussed in detail in Chapter 2, Section 2.8.2. The static contact angle (CA) and the contact angle hysteresis (CAH) are key parameters for water repellence and the ability of a surface to shed water, which could be correlated with the repellence of bacterial adhesion.

Wetting is usually characterized by the contact angle, which is defined as the angle between the tangent to the liquid-air interface at the three-phase contact line and the solid surface (Figure 3.3) [11]. Regarding a solid surface as atomically smooth, chemically homogeneous, non-reactive, and nondeformable by the liquid, the contact angle between the liquid and an ideal solid surface can be defined by Young's equation (Equation 10) [255, 256]:

$$\cos\theta_{Young} = \frac{\gamma_{SV} - \gamma_{SL}}{\gamma} \qquad (10)$$

Where θ_{Young} the Young is contact angle, γ_{SV} and γ_{Sl} is the solid-vapor and solid-liquid interfacial tensions, respectively; γ is the surface tension of the liquid. By this equation, a solid surface with a high surface energy γ_{SV} tends to show a low contact angle, otherwise a high contact angle with a low-energy surface.

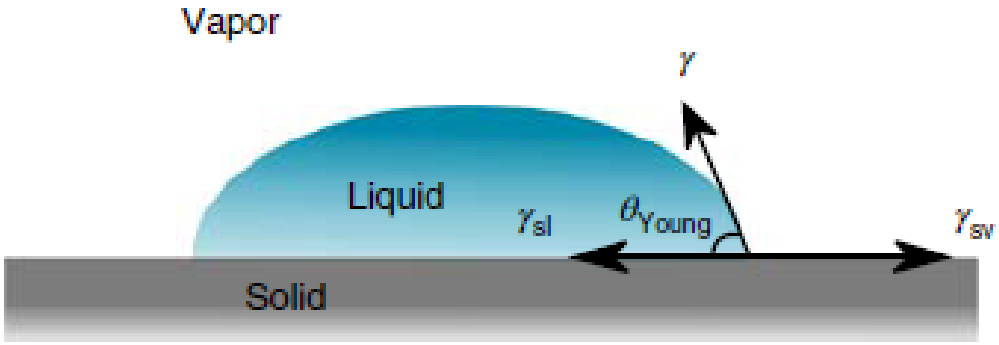

Figure 3.3 A water droplet on an ideal solid surface. Young's contact angle (θ_{Young}) is determined by a balance of the horizontal projection of the surface tension of the water along the solid surface ($\gamma \cos\theta_{Young}$) and interfacial tensions γ_{sv} and γ_{sl}. [11]

The static droplet contact angle method is often used to analyze surface wettability with a contact angle meter, allowing the measurement of the contact angle intuitively [7]. Equipped with an optical subsystem and a backlight, the contours of pure water droplets on a solid substrate can be captured. Surfaces can generally be classified into four categories based on the measured CA of water droplets, as shown in Figure 3.4 [7]:

1. Superhydrophilic surfaces, with a CA<5° in 0.5 Sec.
2. Hydrophilic surface, with a CA between 5° to 90°.
3. Hydrophobic surface, with a CA between 90° to 150°.
4. Superhydrophobic surface, with a CA>150°.

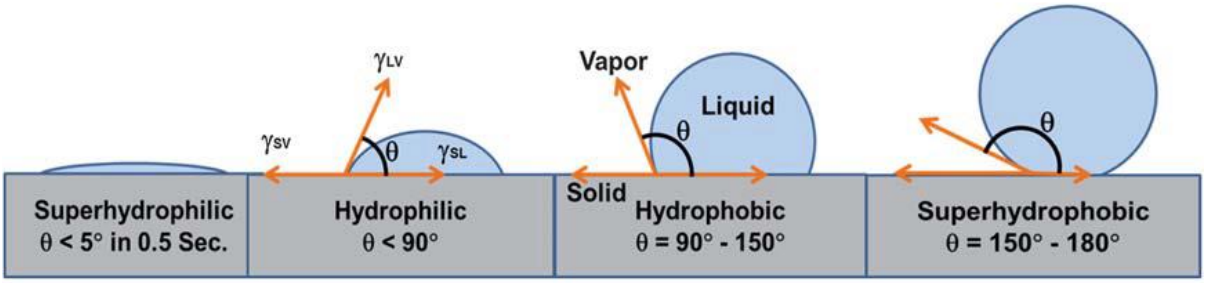

Figure 3.4 Schematic views of different superhydrophilic, hydrophilic, hydrophobic, and superhydrophobic surfaces. [7]

This method assumes that the deposited droplet stays at a global energy minimum thus in a stable state corresponding to Young's contact angle. However, the droplet can be metastable causing nonreproducible static contact angle measurement [11]. It leads to another important parameter for evaluating surface wettability, the contact angle hysteresis (CAH), which is crucial for the mobility of the droplet on the surface, reflecting the movement of the droplet on the solid surface from Activation energy metastability to move a surface to another state (Figure 3.5) [6]. For example, if the CAH is small, raindrops tend to fall off windows, whereas if the CAH is high, raindrops can be fixed on the surface [257]; water droplets on lotus leaves can easily move and roll along the surface because the low CAH [258].

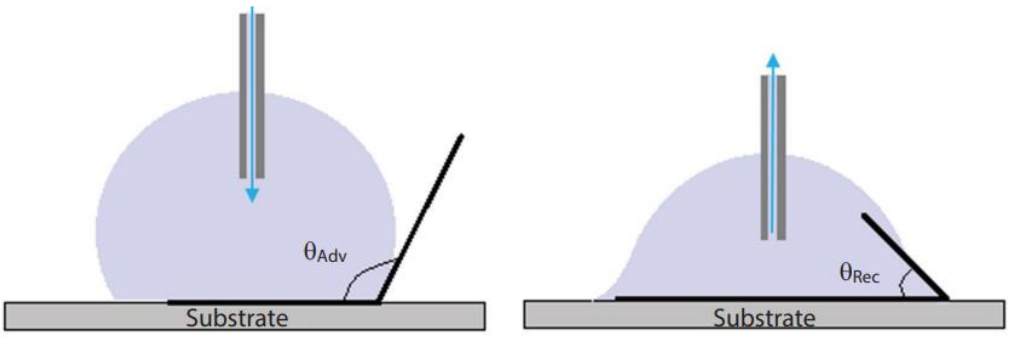

Figure 3.5 Schematic of the sessile-drop method to measure contact angle hysteresis (CAH). [6]

An in-house goniometer [11, 60, 259] was employed to measure the static water contact angle and contact angle hysteresis at ambient conditions (Figure 3.6). Advancing angles on slippery surfaces (needle gauge size ~25, water droplet ~8µl, the maximum volume change of 4µl, using the protocol described in [260]) and receding angles were measured by withdrawing the liquid by a syringe pump system. After inserting and withdrawing the 4µl water droplet, we kept the new droplet for around 10 seconds to become equilibrium. However, this method sometime will cause an advancing angle smaller than the original contact angle. So, in the future, we need to measure the advancing angle and receding angle as soon as possible after the water droplet changes. Contact angle hysteresis (CAH) was determined by the difference between advancing and receding contact angles. For each CA and CAH measurement, at least five repeats were conducted.

Figure 3.6 The in-house goniometer

3.4 Roughness measurement

A roughness meter, surface roughness meter was used to measure the smoothness (roughness) of a target surface. Traditional meters used diamond probes whilst optical types are becoming more popular as diamond probes could damage the surface of semiconductors and similar objects during measurement. In this study, we used the roughness meter to measure the surface of PDMS, P240, and P120. The measured linear

distance is set as 4 mm and the scanning speed is 0.5mm/s. Other set parameters of λs=2.5μm and λc=0.8mm (λs), or 'S-filter', played as a filter eliminating the smallest scale elements from the surface (low-pass filter). This filter is equivalent to the cut-off value of λs in JIS B 0601-2001. For the contact-type surface roughness measurements, noise due to edges is removed. λc, or 'L-filter', is a filter eliminating the largest scale elements from the surface (high-pass filter), which is used to remove undulations and other lateral components from the surface, and thus allows for the extraction of only the roughness components. L-filter is equivalent to the cut-off value λc in JIS B 0633-2001. Finally, Ra was obtained.

3.5 Confocal image analysis

The standard practice of counting planktonic cells is to measure the colony-forming units (CFU) [261]. It confronts a great difficulty to count bacteria in biofilms on surfaces by removing all cells from the surface and dissolving the aggregates into individual cells without killing them [261]. As an alternative, confocal laser scanning microscopy (CLSM) and quantitative image analysis have been widely used to enumerate bacterial cells in biofilms and assess their distribution on surfaces.

CLSM is an invaluable tool to study biofilm matrices, as it enables real-time visualization of fully hydrated living specimens [262]. Due to its easy lab accessibility, CLSM-based methods have been used to retrieve information on the composition and properties of biofilm matrices [262]. It allows a quantitative assessment of bacterial surface coverage or biofilm biomass by a cost-effective staining method [261]. For example, the green, fluorescent nucleic acid dye (SYTO-9) can be used to stain RNA and DNA in live and dead Gram-positive and Gram-negative bacteria [263], which produces rapid quantitative analysis by imaging. Based on the linear relationship between the intensities of the pixels in the biofilm images captured in the x-y plane and the corresponding cell numbers in the z-direction, the thickness and volume of the biofilm can be calculated[261].

After bacterial adhesion or biofilm formation culture, the surface was gently washed with Phosphate Buffered Saline (PBS, pH=7.4) three times to remove weakly adhered bacteria. Then the bacterial cells were stained with Syto9 and the confocal images were taken on NikonA1 with a 20x objective (N.A. =0.75). For AgNPs coated PDMS, bacterial cells were

stained with Syto9 and PI (1:1) and Live/Dead confocal images were taken on NikonA1 with a 20x objective (N.A. =0.75) whilst PDMS as the control sample. 2 hours incubated bacterial cells were visualized by acquiring 2D confocal images. Quantified the surface coverage was presented by using ImageJ (ImageJ(nih.gov)). For *S. epidermidis* and *P. aeruginosa*, surface coverage was converted to volume (referred to as biomass in the COMSTAT software) by direct comparison with bacteria cultured for longer periods. For biofilm or multi-layered bacteria, Z-stack confocal images were taken from biofilms at 5 random locations on the surface. The biomass under each field of view was determined using the COMSTAT2 plugin in ImageJ (Lyngby, Denmark).

For 2 hours of bacterial adhesion confocal images analysis, we used an automatic threshold to select all the bacteria on the image. If the selected threshold contains lots of background noise, need to manually adjust the threshold until only bacteria are selected which can be seen in Figure 3.7a, b. Then we got the pure bacteria image with a white background can be seen in Figure 3.7c. Finally, we analyze the particles to gain surface coverage can be seen in Figure 3.7 The example images for analysing the bacterial surface coverage. (a) automatically threshold the bacteria; (b) manually threshold the bacteria; (c) after applying the threshold; (d) 'Analyze Particles' parameters setting; (e) the results contain the surface coverage '%Area'.d, e. After gaining the bacterial surface coverage, we can convert the surface coverage to biomass by using Equation 11.

$$\mathbf{B} = \frac{\mathbf{V_{single}} \times \frac{\mathbf{C} \times \mathbf{S_{total}}}{\mathbf{S_{single}}}}{\mathbf{S_{total}}} \qquad (11)$$

Where B is biomass, V_{single} is the volume of the single bacteria, C is surface coverage, S_{total} is total surface area, and S_{single} is the single bacteria surface area. We assumed that *S.epidermidis* is a sphere with a diameter of 1um, and *P. aeruginosa* is an ellipsoid that consists of a sphere with a radius of 0.375 um and a cylinder with a radius of 0.375 um and a length of 2.15 um (in Appendix Figure S1).

For biofilm Z-stack confocal images analysis at 2 days, 7 days and 14 days, the detailed steps are shown below. Firstly, we saved the original confocal images as OME-TIFF files in a new folder. Then used the Comstat2 plugin to open the newly saved file to automatically analyzed biomass which can be seen in Figure 3.8.

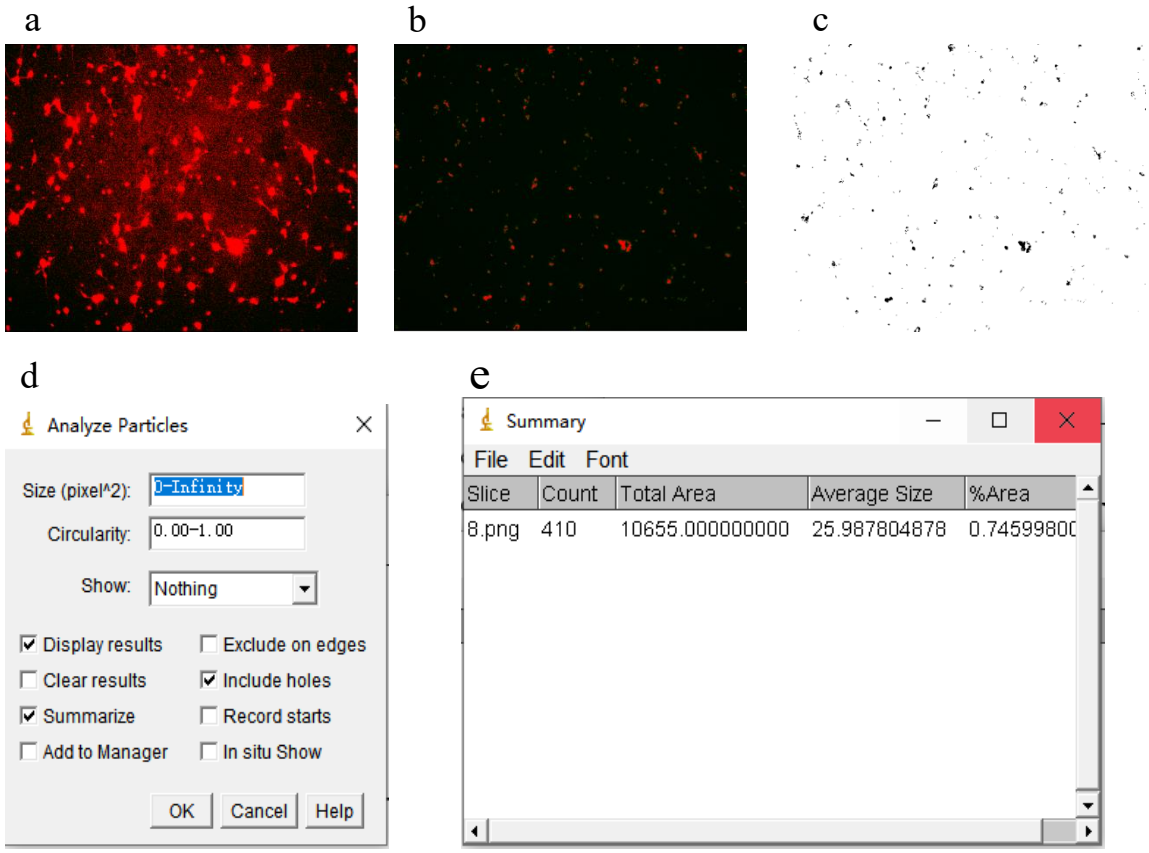

Figure 3.7 The example images for analysing the bacterial surface coverage. (a) automatically threshold the bacteria; (b) manually threshold the bacteria; (c) after applying the threshold; (d) 'Analyze Particles' parameters setting; (e) the results contain the surface coverage '%Area'.

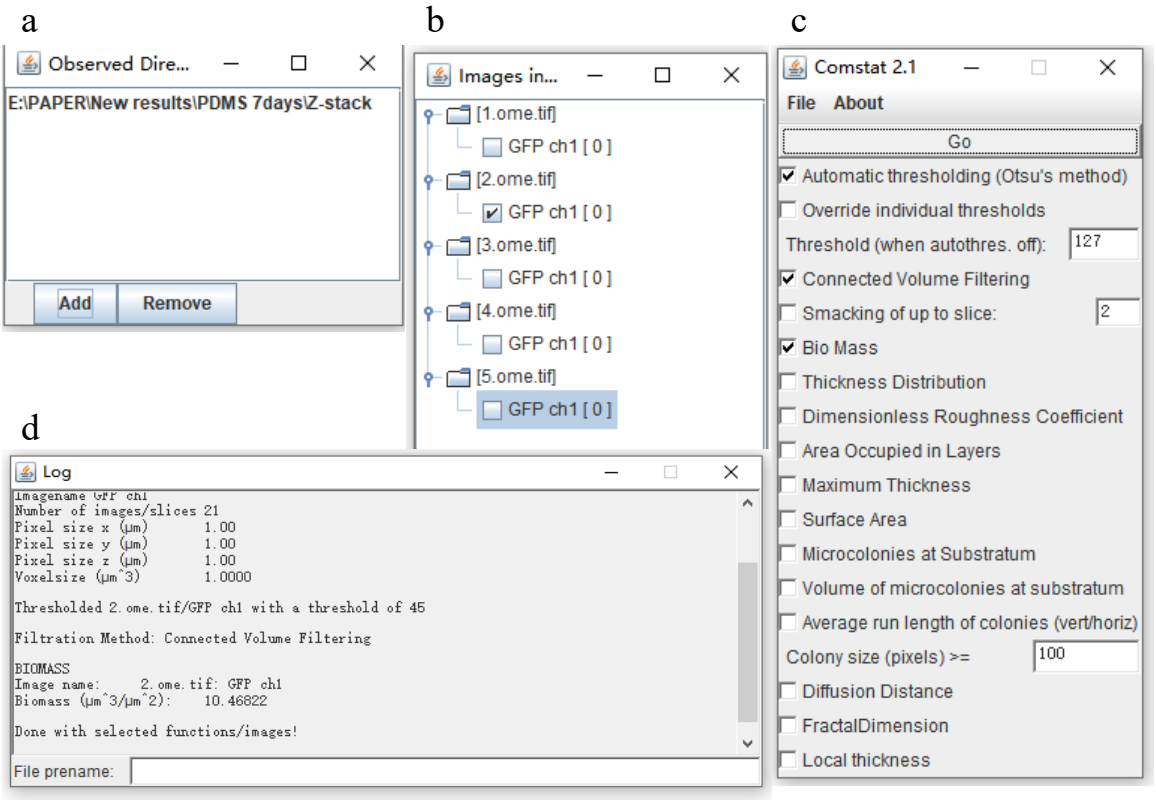

Figure 3.8 The detailed protocol for measure the Z-stack biofilm biomass. (a) 'Observed directions' to select the images folder; (b) select the images you want to measure in 'images in directions'; (c) tick the information you want in 'Comstat 2.1' window; (d) gain the results in 'Log' window.

3.6 Critical point drying and SEM analysis

Scanning electron microscopy (SEM) is an approach to scanning a surface with a focused electron beam that interacts with the atoms of the sample. SEM can detect the secondary electrons emitted by the sample atoms, thereby generating an image of the surface topography of the sample.

Due to the large depth of field, SEM can provide a 3-D appearance or morphology of a sample, which is useful for visualizing and studying sample topography. There are three key advantages of SEM summarized by Azerdo et al.: (a) samples can be visualized at a

high resolution down to 50-100 nm and a large depth of field; (b) qualitative or quantitative data analysis in a 3D manner; (c) various magnifications (20 x to 30,000 x) for analyzing biofilm samples [261].

SEM has proven a suitable tool not only for observing substrate morphology in detail but also tracking bacterial adhesion and biofilm formation on abiotic surfaces, which has been used since a very early age to examine and characterize biofilms on medical devices [264]. It is currently used to study anti-biofilm materials for biomedical applications [264]. SEM has the level of magnification and resolution required to observe the overall shape of the microorganisms that make up biofilms and their spatial organization [264].

The drying method is another important factor in preparing SEM samples. The common methods of drying biological cells include air drying, freeze drying, Hexamethyltiisilizane (HMDS) drying and critical point drying. Air drying is the only way to keep loosely attached bacteria in place on mineral surfaces, whereas chemical fixation and drying can dislocate cells. In contrast, chemical fixation preserves cell morphology but air drying causes most laboratory-grown cells to collapse [265]. Different species can behave completely differently during freeze-drying, even for different strains of the same species which may destroy the surface structure of bacteria. Some bacteria are freeze-resistant and may not dry out completely, so you won't get a good view in the SEM [266]. Critical point drying (CPD) (BAL-TEC CPD 030 (Figure 3.9) is an efficient method of drying delicate samples for SEM applications. It preserves the surface structure of a specimen to avoid damage due to surface tension when changing from a liquid to a gaseous state. Due to the critical point of water at 374°C and 229 bar, any biological samples would be destroyed. So, for the CPD, water can be replaced with liquid CO_2 whose critical point lies at 31 °C and 74 bar which is more appropriate for all biological applications. As CO_2 cannot be miscible with water, water has to be replaced by exchange fluids like ethanol or acetone which are miscible in both water and liquid CO_2 (need to use different concentration series to dehydrate: 25%, 50%, 75%, and 100%). Both exchange fluids cannot be used for critical point drying due to their high critical point temperatures (Ethanol: Pc 60 bar/Tc 241 °C; Acetone: Pc 46 bar/Tc 235 °C). They should be replaced with liquid CO_2. The liquid CO_2 is brought to its critical point and converted to the gaseous phase by decreasing the pressure

at a constant critical point temperature (Figure 3.10) [4]. Hexamethyltiisilizane (HMDS) is an excellent method of chemical drying hydrated specimens. It can easily control the number of transitional steps from 100% ethanol (EtOH) to 100% HMDS and the drying temperature. Fixation and dehydration are the same for both HMDS and CPD. Once the specimen is in the final 100% ethanol, it must be transferred to 100% HMDS through a graded series of ethanol-HMDS mixtures. Due to the high volatility of HMDS, it can dry naturally in a fume hood. Unlike CPD, HMDS does not involve expensive machinery but manual handling that is gentler on the specimens. It is also relatively quicker, and cheaper and results in similar if not higher quality results based on previous comparative studies [267]. One disadvantage is the color of the coating will be strange and the image going to charging due to the porosity of the sample when applying the gold coating on the surface of the sample (Figure 3.11).

Figure 3.9 The critical point drying machine.

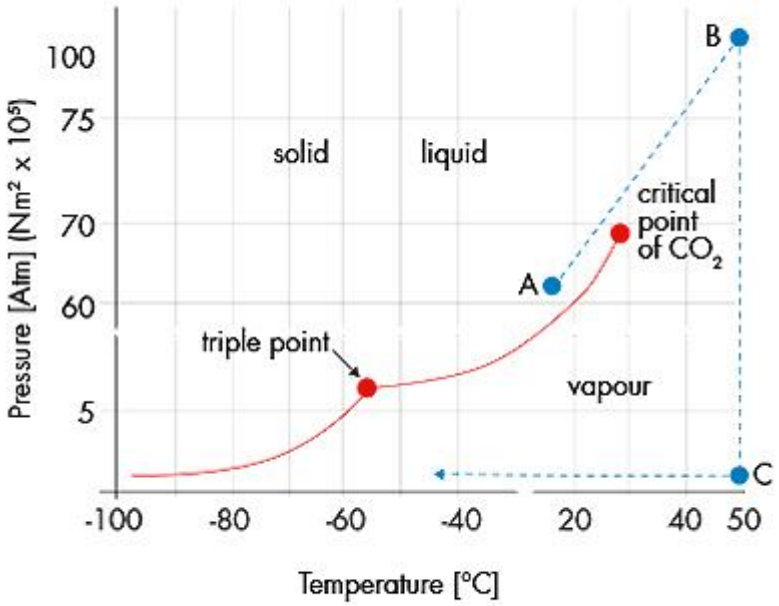

Figure 3.10 Pressure/temperature phase diagram for CO_2. Triple point: Same physical characteristics of solid, liquid, and gaseous. [4]

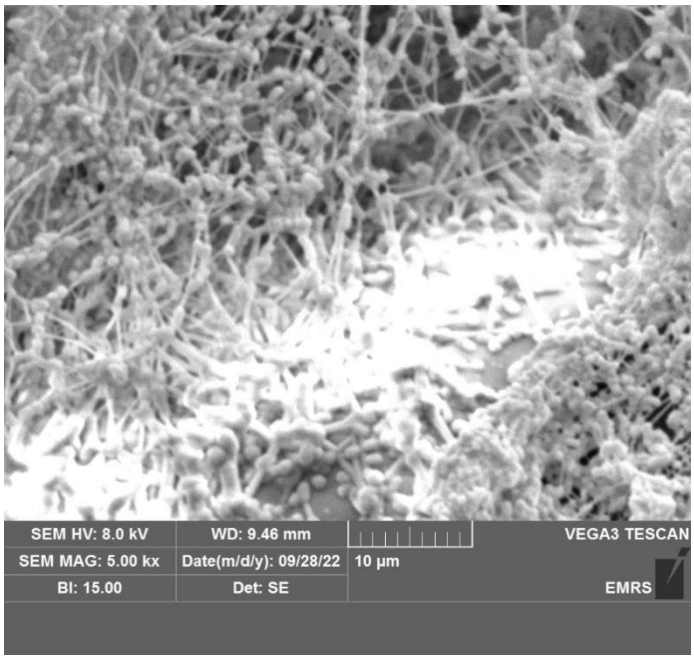

Figure 3.11 The example SEM image which dying by HMDS.

Due to the structure of the rough PDMS, imaging with the confocal microscope is extremely challenging. To gain insight into the possible EPS in biofilms, high-resolution SEM (Tescan Vega LMU) was used to visualize 2 hrs bacterial adhesion samples, 2 days, 7 days and 14 days biofilm samples in a static and dynamic culture. Beam voltage and current were set to 8 kV and 62 µA, respectively. Before SEM imaging, samples were washed with PBS and fixed with 2% glutaraldehyde in 3M Sorenson's phosphate buffer overnight at 4°C, then transferred to new plates and passed through a series of 25% (v/v) dehydration in ethanol solutions 30mins, 50% 30mins, 75% 30mins, 100% 1h and 100% 1h, followed by critical point drying. After drying, the samples were sputter coated with a 5 nm gold coating using a Polaron SEM Coating Unit.

For the plain or silicone oil-infused rough PDMS 2 hours bacteria attachment, SEM imaging was used due to the structure of the samples and automatically using a threshold to select the bacteria where a large amount of background and noise will be selected in Figure 3.12a. Therefore, we need to split a graph into several parts to measure the surface coverage and then combined to acquire the rough total surface coverage due to manual measurement error (Figure 3.12b). Finally, the surface coverage was converted to the total biomass. Each sample has at least 10 images to quantify to minimize the manual measurement error.

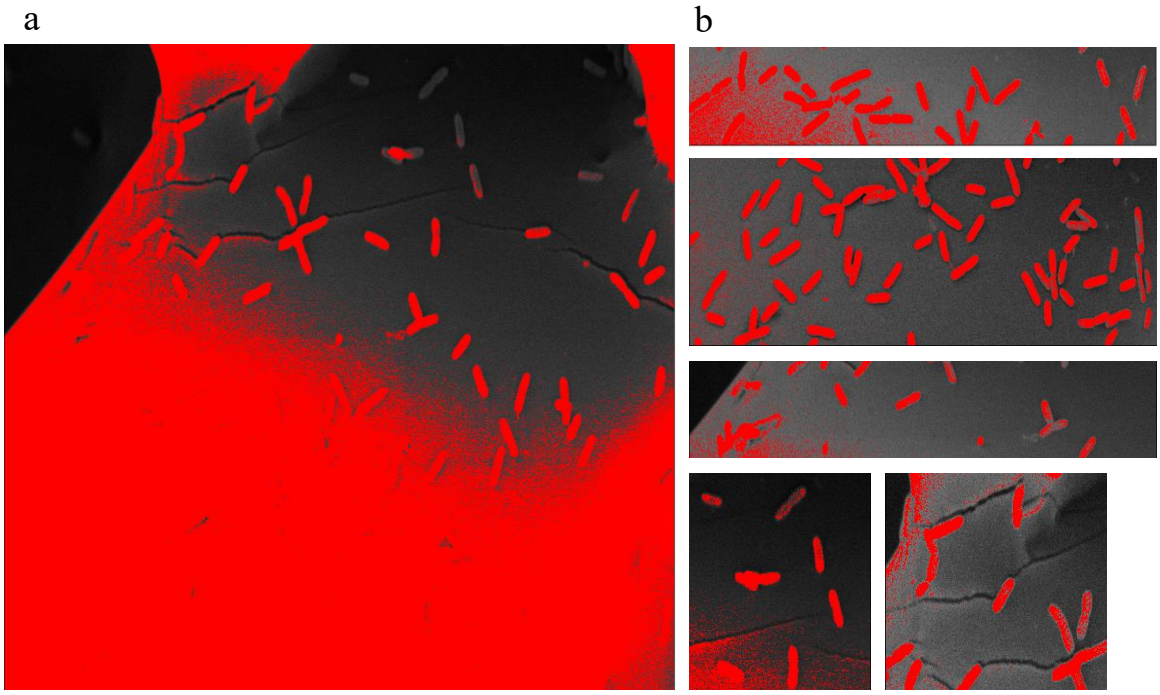

Figure 3.12 The example to analyse the 2 hours bacterial adhesion surface coverage on rough PDMS SEM images. (a) automatically threshold the bacteria; (b) split the whole image to several parts to measure the bacterial surface coverage.

3.7 Flow cell design and setup

Most biofilm formation occurs under a variety of flow conditions such as catheters, and implant surfaces. Thus, the bacterial culture is also performed under flow conditions. A parallel plate flow cell (PPFC) is designed with an inlet long enough to allow fully developed flow for the dynamic bacterial culture [268]. The flow cell (length=10 mm, width=10 mm, height=0.1 mm) was made of PDMS (Figure 3.13) and fabricated by the pattern forming on a milled acrylic block, which is connected to a syringe pump. The sample (PDMS, S-PDMS, SOCAL, NPEG, AgNPs coating PDMS, and Rough-PDMS) used as the bottom surface is attached to the top chamber using a press fit (Figure 3.14). Three holes were created in the flow cell chamber: one for pumping the bacteria-inoculated broth, one for fresh TSB medium, and another one for collecting waste (Figure 3.15). The bacterial culture was pumped into the flow chamber until the trapped air is eliminated, then the pump runs at 37ºC for the required time. When laminar flow is well established in a parallel plate flow cell, the wall shear rate σ is given by Equation 12 [269]:

$$\boldsymbol{\sigma = \frac{3Q}{2(\frac{h}{2})^2 * w}} \qquad (12)$$

The wall shear stress τ_w is given by Equation 13:

$$\boldsymbol{\tau_w = \eta\sigma} \qquad (13)$$

Where Q is the volumetric flow rate, h and w are the height and width of the parallel plate chamber, respectively, and η is the viscosity of the culture medium at 37°C. TSB medium exhibits nearly the same rheological properties as deionized water at 37°C and an average viscosity value of 0.7 mPas of TSB medium measured by a rheometer (Malvern Kinexus Pro+) were used to calculate the wall shear stress.

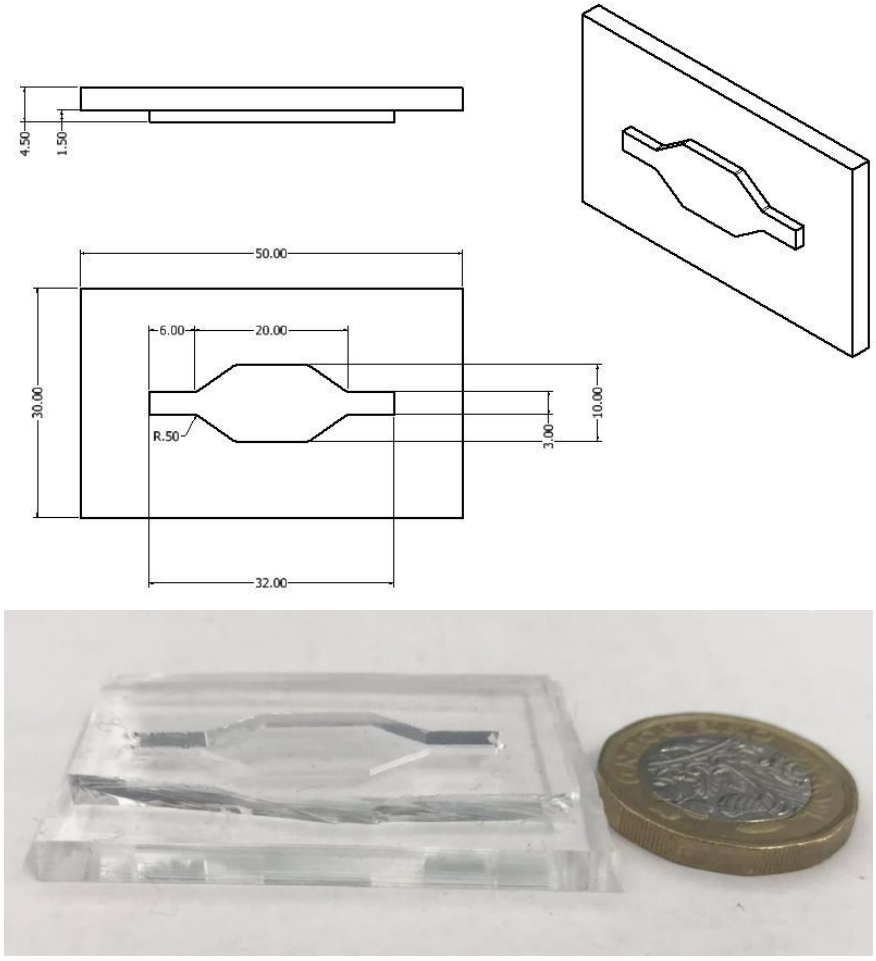

Figure 3.13 (A) Flow cell design diagram; (B) Flow cell made by PDMS compared with 1 pound coin.

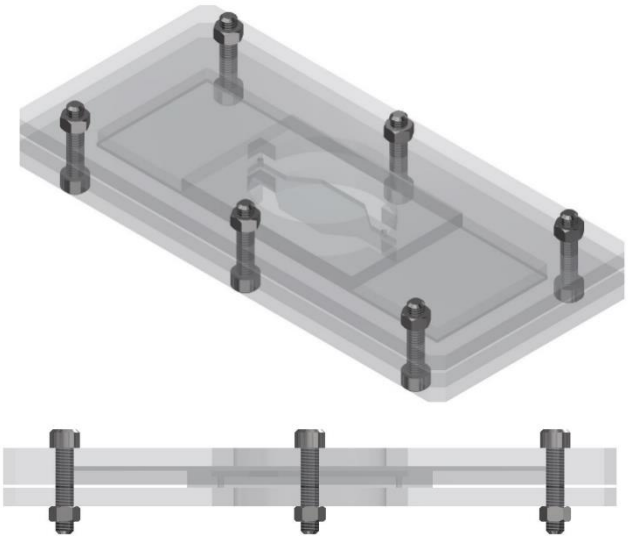

Figure 3.14 Schematic of Press-fit.

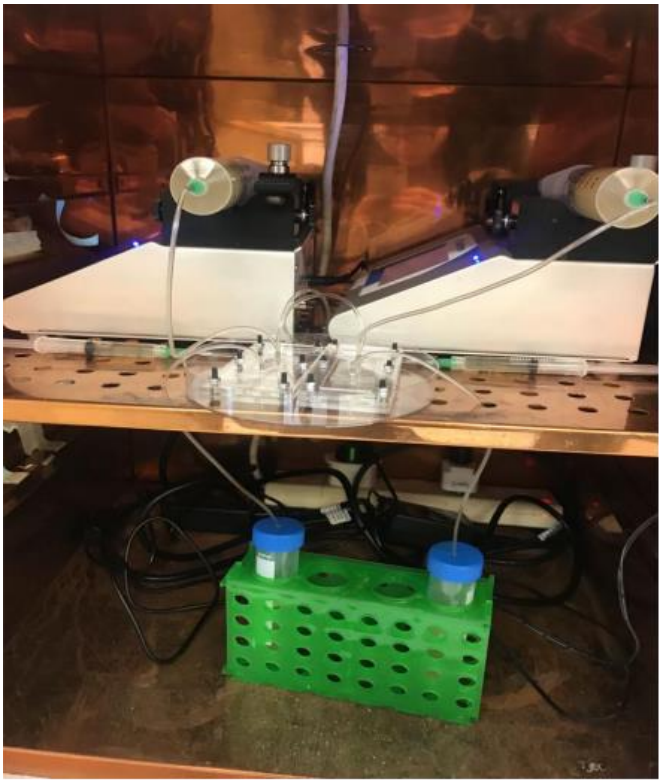

Figure 3.15 Schematic illustration of the flow cell system.

4 The surface roughness effect on bacterial attachment and biofilm formation

4.1 Introduction

The interaction between bacteria and solid surfaces has been comprehensively studied in the past decade. Bacteria move towards material surfaces through the action of physical forces such as Brownian diffusion, gravitational settling, and hydrodynamic forces, as well as their motility [270]. The short-range effects of electrostatic interactions (always repulsive), Acid-Base (AB) Lewis interactions (accounting for hydrophobic effects, repulsion, or attraction) and van der Waals interactions (always attractive) are critical to determining whether bacterial adhesion occurs importantly or whether the bacteria are repelled by the surface [271]. As stated in Kastsikogianni and Missirlis's comments, these effects are intrinsically linked to properties of the material surface such as the Hamaker constant (for van der Waals interactions, depending on the chemical composition), surface charge and hydrophobicity [272]. Alnnsouri et al. investigated the effect of surface roughness on the long-term development of biofilms [273]. They studied the response of biofilms to changes in rotational speed in a laboratory-scale rotating bio-contactor and concluded that surface irregularities introduced in the biofilm bed generally improved adhesion and increased hydraulic loss. More recently, work by Katsikogianni and Missirlis [272] showed that bacteria preferentially adhere to surface irregularities that are typical of a size comparable to their diameter.

This study aims to pinpoint the effect of surface roughness on the growth of *S.epidermidis* and *P. aeruginosa* on PDMS, P120, and P240 surfaces. We set the different culture times of 2 hours, 2 days, 7 days, and 14 days in static conditions, and the long-term (7,14 days) biofilm formation in dynamic conditions. Confocal microscopy and scanning electron microscopy (SEM) were employed to perform characterization. At the beginning of the experiment, we also chose P400 as one of the variables. After culturing 2 hours, 2 days and 7 days in *P. aeruginosa*, the results are similar to the PDMS control sample without further need for experiment.

4.2 Methodology

4.2.1 Rough PDMS fabrication

The detailed fabrication method can be seen in Chapter 3.1.1.

4.2.2 Confocal microscope analysis

The substrates were removed from the well plate with sterile tweezers and gently washed three times with PBS to remove non-adherent or weakly adhered bacteria. The samples were placed onto the glass slide covered with the coverslips and visualized by Nikon A1 upright confocal microscope with a 20x lens. Due to the structure of the rough PDMS, 2 hours of bacterial attachment confocal imaging is a big challenge. For the 2 days, 7 days and 14 days biofilm, bacteria almost covered all the surface and holes, so the morphology of the biofilm is visible. The detailed protocol is shown in Chapter 3.3.

4.2.3 Scanning electron microscope analysis

The SEM sample preparation and drying method are shown in Chapter 3.4. In this study, due to the height difference on the sample surface, ImageJ's automatic threshold to select the bacteria may cause some surfaces to be selected as well. Therefore, the bacteria were manually selected and then converted to biomass, which can greatly reduce the error. Here we use P240 and P120 to represent the PDMS molded on sandpaper with 240 and 120 grits, respectively. It is mainly used to quantify the biomass of P240 and P120 surfaces after 2 hours of bacterial adhesion culture. To ensure the accuracy of the data obtained by SEM image processing, the biomass obtained by PDMS 2-hour bacterial culture in confocal and SEM should be similar, so we use the same method to quantify the biomass of P240 and P120 in 2-hour bacterial culture.

4.2.4 Statistical analysis

Data were represented by mean values with standard errors. The statistical differences among different samples were determined by Student’s t-test assuming unequal variations. And $p < 0.05$ was considered statistically significant in this study, as indicated by the symbols in the representative figures.

4.3 Results and Discussion

4.3.1 Surface wettability and roughness

The static contact angle (CA) and the contact angle hysteresis (CAH) are important parameters for water repellency and the ability of a surface to shed water, which could be correlated with the repellency of bacterial adhesion. Both CA and CAH of DI water droplets on PDMS, P120 and P240 are summarized in Table 4.1 (Figure 4.1, Figure 4.2). The contact angle of PDMS, P240 and P120 is consistent with theoretical predictions based on the surface free energy approach [274, 275]. The CAH of PDMS, P240 and P120 indicates the rougher surface shows a smaller CAH, but there is no evident difference (the detailed roughness of PDMS, P120, P240 is shown in Table 4.2.

Table 4.1 The static contact angle and the contact angle hysteresis of DI water droplets on different surfaces. Data represent the mean and SD of five independent measurements.

Surface	Contact angle (°)	Advancing angle (°)	Receding angle (°)	Contact angle hysteresis (°)
PDMS	117.5 ± 1.1	116.8 ± 1.5	95.4 ± 1.3	21.4 ±2.1
P240	129 ± 5.0	128.5 ± 3.3	107.9 ± 2.9	20.6 ± 3.5
P120	115.0 ± 3.1	117.2 ± 3.8	100.1 ± 6.2	17.1 ± 5.8

Table 4.2 The roughness on different surfaces. Data represent the mean and SD of ten independent measurements.

Surface	Roughness Ra (μm)
PDMS	0.0768 ± 0.033
P240	10.28 ± 0.94
P120	15.51 ± 1.62

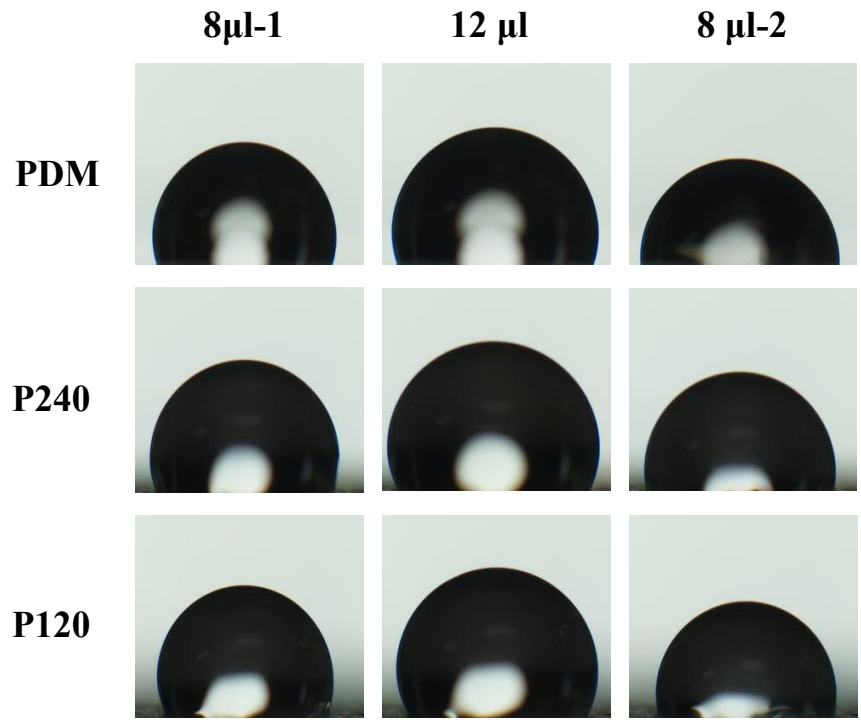

Figure 4.1 The water droplets on different roughness surfaces. 8µl-1 is the initial water contact angle, 12µl is advancing contact angle, 8µl-2 is receding contact angle.

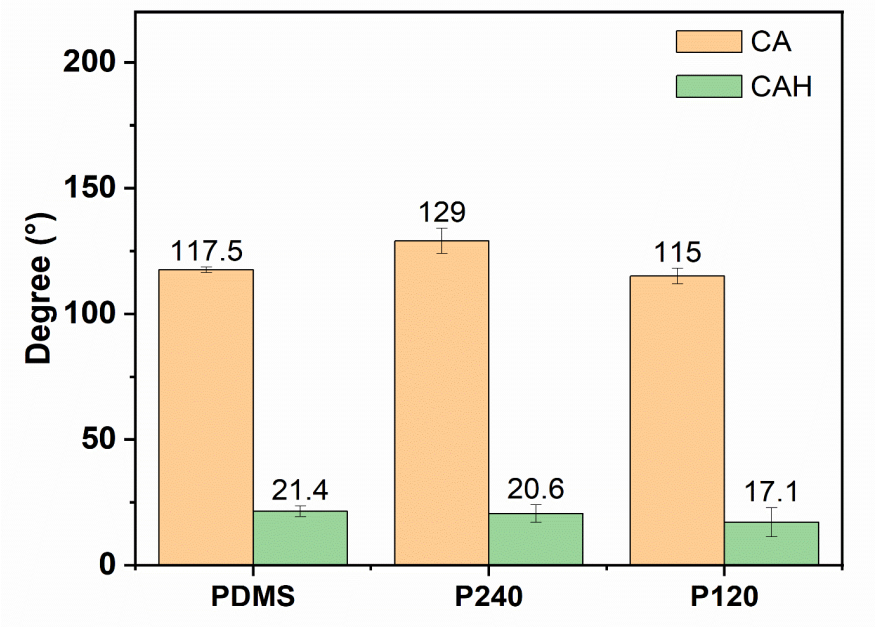

Figure 4.2 The bar chart for different roughness surfaces CA and CAH.

4.3.2 Staphylococcus epidermidis bacterial culture on different Roughness PDMS

The growth of *S.epidermidis* FH8, a recent clinical isolate from a mucosal biofilm, was examined on PDMS, P240 and P120 after 2hrs, 2days, 7 days and 14 days under static conditions, 7 days and 14days under dynamic conditions. Figure 4.3a displays the SEM images after the growth of *S.epidermidis* for 2 hours, 2 days, 7 days and 14 days on PDMS, P240 and P120 surfaces, showing the distribution of bacteria on the surfaces clearly and intuitively. For 2 days, 7 days and 14 days of biofilm formation the Z-stack images cannot be gained from SEM, implanted by using Nikon A1 confocal microscope to quantify the total biomass (Figure 4.3b).

After 2 hours, the PDMS, P240, and P120 surfaces were covered by bacteria with some bacterial aggregates or clusters. The total biomass is relatively similar between P120 and P240 surfaces, but around 3 times more than on PDMS.

After 2 days of culture, a large amount of biofilm had formed on these three surfaces. By quantifying the biomass on these surfaces based on confocal imaging, it was found that the total biomass on PDMS, P240 and P120 is 5.3 $\mu m^3/\mu m^2$, 7.2 $\mu m^3/\mu m^2$, and 9.2 $\mu m^3/\mu m^2$, respectively.

A thick biofilm formed at 7 days and 14 days of bacterial culture. Whereas for 14 days of total biomass, the difference between the PDMS and P240 or P120 was significantly larger than the total biomass in 7 days (Figure 4.4).

For the dynamic bacterial culture under continuous flow, a wall shear stress (τ_w) of 0.007 Pa was chosen to match the flow conditions present in urinary catheters [253]. From the confocal images of 7 days and 14 days in dynamic conditions, P240 and P120 did not show the dense and thick biofilm-like in the PDMS images (Figure 4.5). This is due to the surface structure and roughness of P240 and P120. For images of Z-stack, P240 and P120 have more layers than PDMS.

After 7 days of bacterial culture, the total biomass on the P240 and P120 surfaces was 3.4 and 4.1 times larger than that on PDMS, respectively (p=1.05e-14, p=8.14e-16). After 14 days of bacterial culture, the total biomass on the P240 and P120 surfaces was 3.6 and 4.5 times larger than that on PDMS, respectively (p=4.2e-11, p=3.5e-13).

Comparing *S.epidermidis* colonization in static and dynamic conditions, there was a significant difference for PDMS, P240 and P120 throughout the 7-day culture and 14-day culture period ($p<0.001$). Under the same duration, the biomass in the dynamic culture conditions is generally smaller than in the static conditions.

In addition, Figure 4.3b and Figure 4.5a show the static and dynamic biofilm formation and low intensity in roughened PDMS confocal images. Due to the height difference on the roughened PDMS, only one specific layer of the biofilm Z-static confocal images is shown.

Figure 4.6 displays the SEM image for 2-hour static *S. epidermidis* culture on the P120 surface. It demonstrated that the bacterial adhesion inside the hole is more than outside the hole which indicated that holes protect the surface from colonization of bacteria, either when rinsed with PBS or when applied CPD drying.

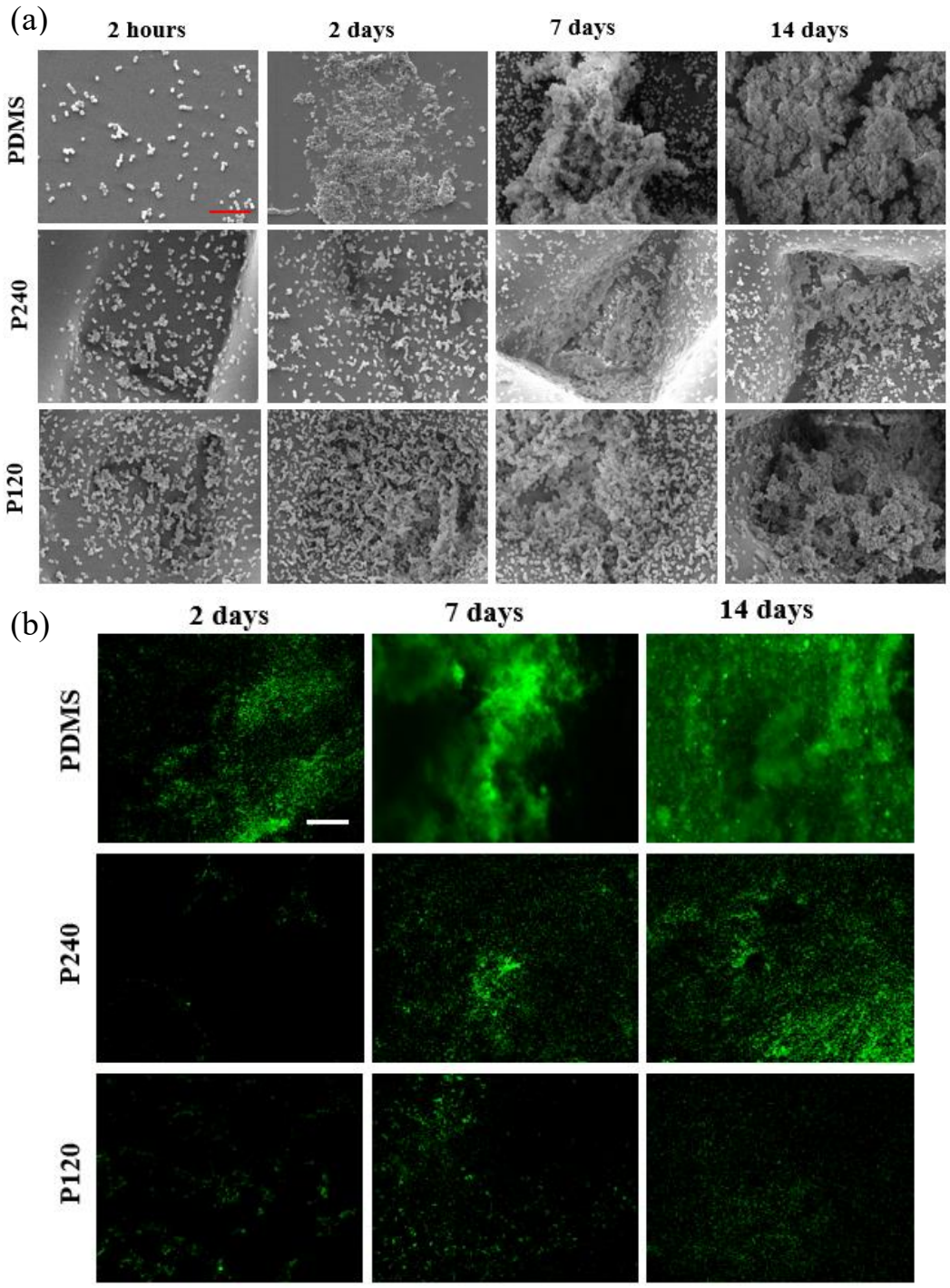

Figure 4.3 Images for *S.epidermidis* 2hours, 2days, 7days and 14days static culture. (a) SEM images for PDMS, P240 and P120 surface, scale bar=10μm; (b) confocal images for PDMS, P240 and P120 surfaces, scale bar=50μm.

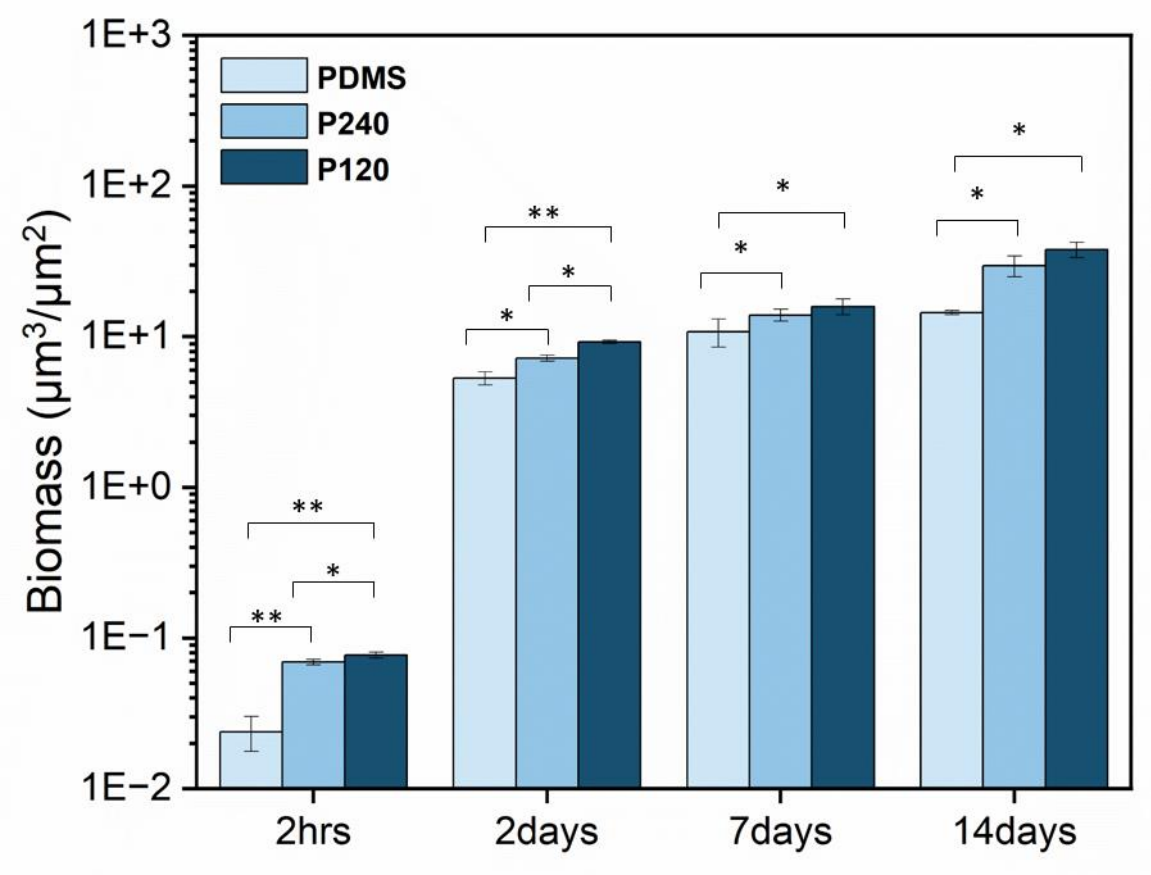

Figure 4.4 The total biomass of *S.epidermidis* on PDMS, P240 and P120 in static with different time scale. * $p<0.05$; ** $p<10^{-10}$; *** $p<10^{-15}$.

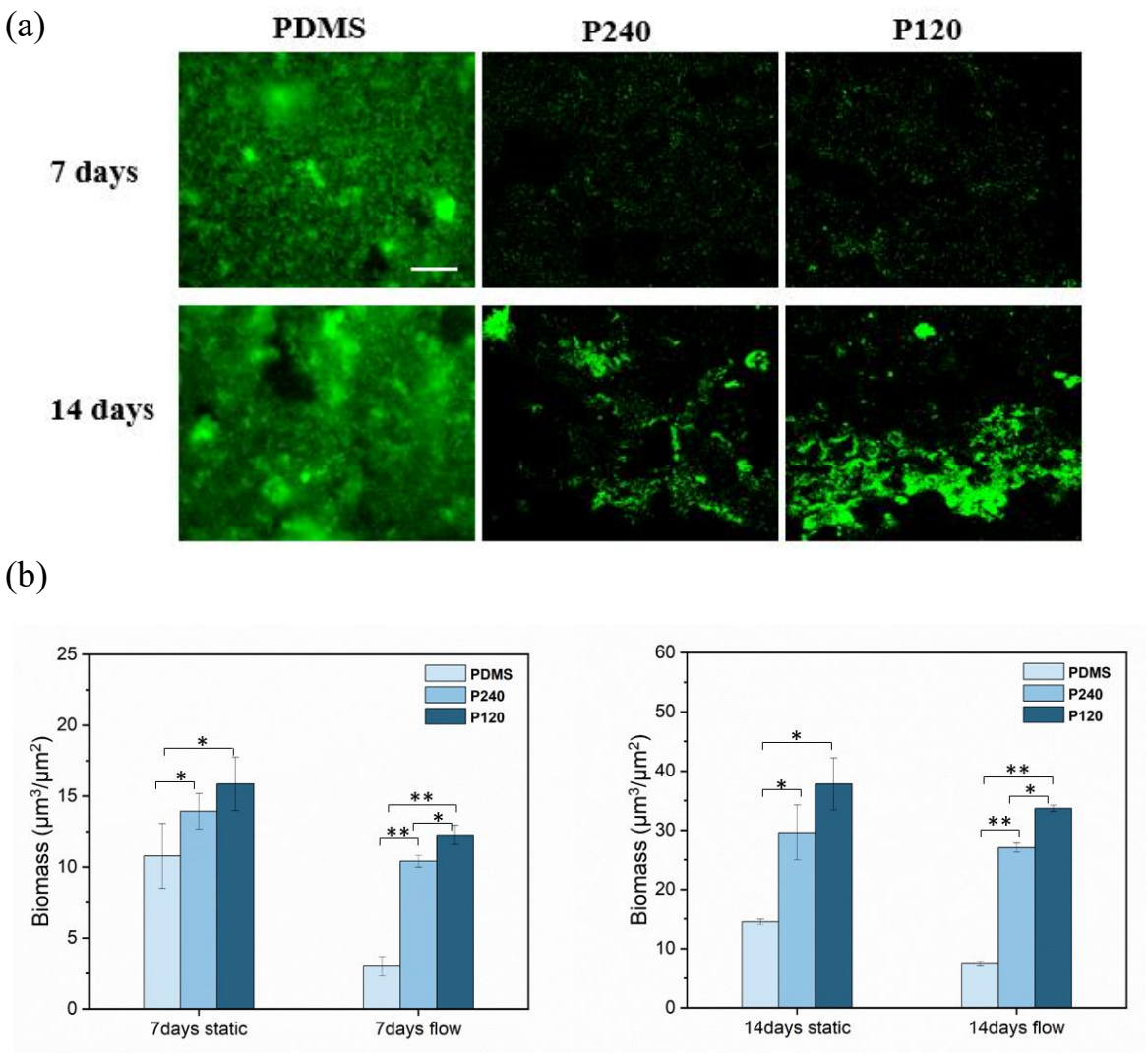

Figure 4.5 (a) Images for *S.epidermidis* 7days and 14days dynamic culture, scale bar=50μm; (b) The total biomass on PDMS, P240 and P120 in 7days and 14days dynamic culture. * $p<0.05$; ** $p<10^{-10}$; *** $p<10^{-15}$.

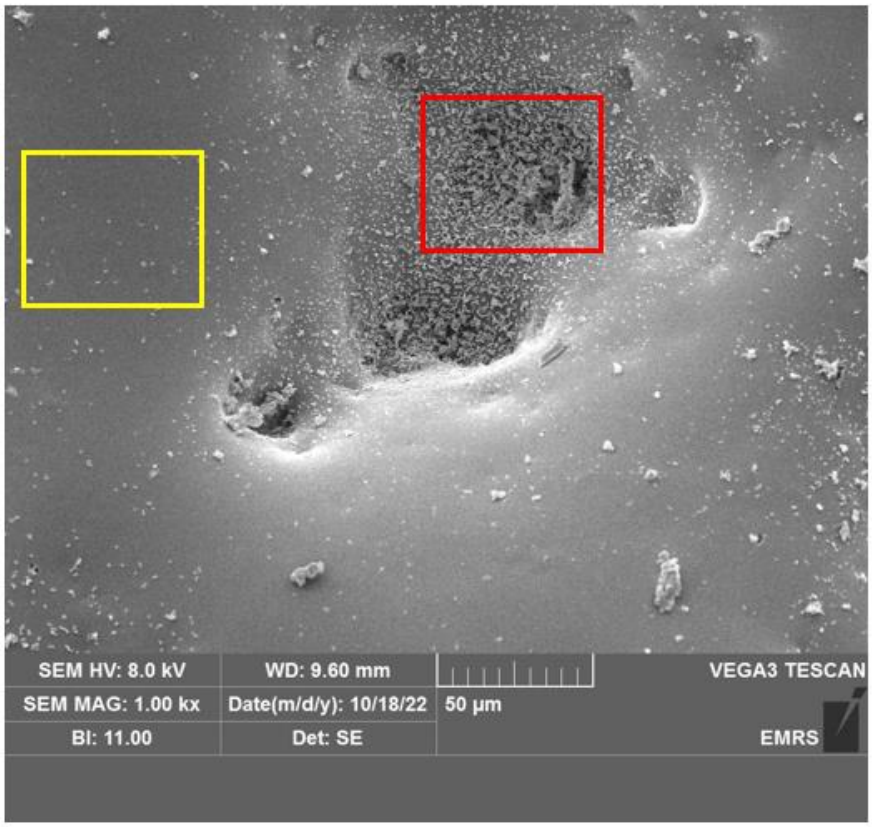

Figure 4.6 Image for 2-hour static *S.epidermidis* culture on P120 surface. **The yellow box** represents outside the hole with a small number of bacteria attached, **the red box** means inside the hole fully covered with bacteria.

4.3.3 *Pseudomonas aeruginosa* bacterial culture on different Roughness PDMS

P. aeruginosa PAO1 was grown on PDMS, P120 and P240 after 2hrs, 2days, 7days and 14days under static condition (Figure 4.7), 7days and 14days under dynamic condition (Figure 4.9a). The *P. aeruginosa* biomass appeared mucoid when removing the PDMS samples from the well-plate in static. While in dynamic conditions, the produced mucoid shows far less than in static. It may be due to the shear stress preventing the large generation of EPS, or due to the smaller flow chamber.

As seen in Figure 4.7 and Figure 4.8, 2 hours of initial bacterial adhesion almost covered the surface on PDMS, P240 and P120, and rougher surfaces have slightly more bacteria than smooth surfaces.

After 2 days, initially thin biofilms formed on these three surfaces, in contrast to the PDMS control sample, the total biomass on P240 and P120 surfaces increased, by 244 ± 3.2 or 340 ± 1.4%, respectively.

After 7 days, a denser and thicker biofilm formed, the total biomass on P240 and P120 surfaces were nearly 3.5 times and 4.5 times larger than that on PDMS surfaces, respectively.

Even after 14 days, the total biomass on P240 and P120 surfaces was nearly 2.5 times and 3.5 times larger than that on PDMS surfaces. There were significant differences ($p<0.05$) at 2 days, 7 days and 14 days, but two rough PDMS showed similar results to the PDMS control at 2 hours ($p=0.90$ and $p=0.29$, respectively).

Under dynamic culture, *P. aeruginosa* grew significantly over time on PDMS, P240, and P120, and dense biofilm was observed after 7 days and 14 days (Figure 4.9b). For 7 days of culture, P240 and P120 surfaces led to 4.5 times and 6 times total biomass larger than the PDMS control surface, respectively. For 14 days culture, compared to PDMS, P240 and P120 surfaces led to at least 3 times and 4.5 times total biomass larger than the PDMS control surface, respectively. In contrast to the 7 days and 14 days of biofilm formation in both static and dynamic conditions, the total biomass on PDMS, P240, and P120 surfaces in static are larger than in dynamic conditions.

A detailed analysis of experimental measurements [276] demonstrated that both convective diffusion and interaction forces can play an important role in bacterial attachment and lead to shear-dependent attachment behaviour. As discussed in our group's previous paper [21], an increase in fluid velocity not only provides a higher bacterial supply rate to the surface but also increases the shear stress exerted on the adherent bacteria. Shear stress was also found to enhance bacterial attachment by a snap-bond mechanism [277, 278]. Therefore, relatively small shear stresses lead to increased bacterial attachment. When the shear stress exceeds a threshold, it will result in a net reduction in bacterial attachment due to shear stress-induced detachment. This threshold depends on the properties of the bacteria and the material surface [279, 280]. Four typical Gram-positive and Gram-negative strains were examined on surfaces with different hydrophobicity and surface roughness, and it was found that the threshold shear stress could range from 0.001 Pa to 0.175 Pa [279]. Depending on the bacteria-surface pairs, gentle flow (0.007Pa in the present work) may promote bacterial attachment or decrease bacterial attachment. In this work, it appears that dynamic culture reduces bacterial attachment and biofilm formation.

Surface roughness is an important factor affecting bacterial adhesion to surfaces before biofilm formation [12]. Surface roughness increases the surface area available for bacterial attachment [65]. Some materials with nanoscale roughness may reduce bacterial adhesion. For example, the adhesion of *Pseudomonas aeruginosa* and *Staphylococcus aureus* on unpolished stainless-steel samples (Ra = 172.5 nm) was significantly reduced compared to electropolished smoother surfaces with an average roughness of 45.2 to 84.4 nm [281]. The roughness of P240 and P120 from sandpaper as a template is above 10 um and the dimension of both *S.epidermidis* and *P. aeruginosa* is much smaller than the roughness of P240 and P120 surfaces. Thus, the bacteria can be easily attached to the P240 and P120 surfaces compared to relatively smooth plain PDMS. Once the bacteria colonize the P240 and P120 surfaces, they can grow a denser and thicker biofilm for long-term culture. Some studies have proposed the idea of threshold arithmetic mean roughness (Ra) of 0.2 μm. For example, an in vitro study claimed that the adhesion threshold of *Streptococcus* mutans and *Streptococcus sobrinus* to composite resin surfaces was estimated to be between 0.15 and 0.35 μm [282]. This further proves that the P240 and P120 attracted more bacteria than PDMS. Hydrodynamic conditions can interfere with or enhance the bacterial perception of

various surface properties, thereby affecting biofilm structure, composition, and mechanical strength [283]. Some studies reported that biofilms grown under dynamic conditions tended to be more elastic, resistant, and denser in matrix proteins and EPS. For example, a study by Hou et al. showed that shear flow enhanced biofilm formation by increasing the EPS production and strength of EPS matrices in *Staphylococcus aureus* on glass-based surfaces [284]. Rodsney et al. found that applying shear stress to biofilms resulted in increased levels of c-di-GMP signal in Pseudomonas aeruginosa on coverslips, thereby promoting biofilm development [285]. We found that in dynamic conditions, *S.epidermidis* and *P. aeruginosa* biofilm formation on all these surfaces were reduced compared to their static counterpart.

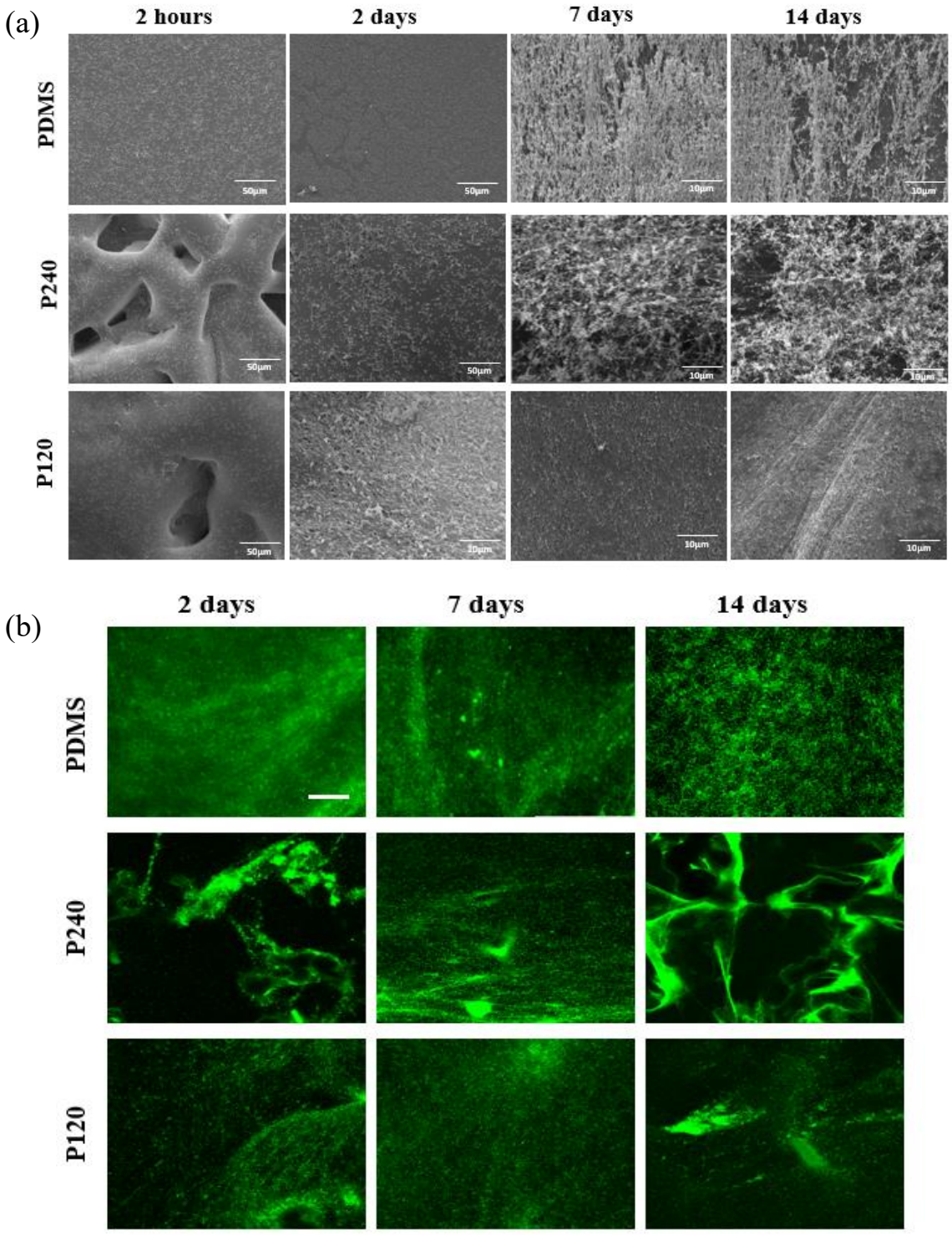

Figure 4.7 Images for *P. aeruginosa* 2 hours, 2 days, 7 days and 14 days static culture. (a) SEM images for PDMS, P240 and P120 surfaces; (b) confocal images for PDMS, P240 and P120 surfaces, scale bar=50μm.

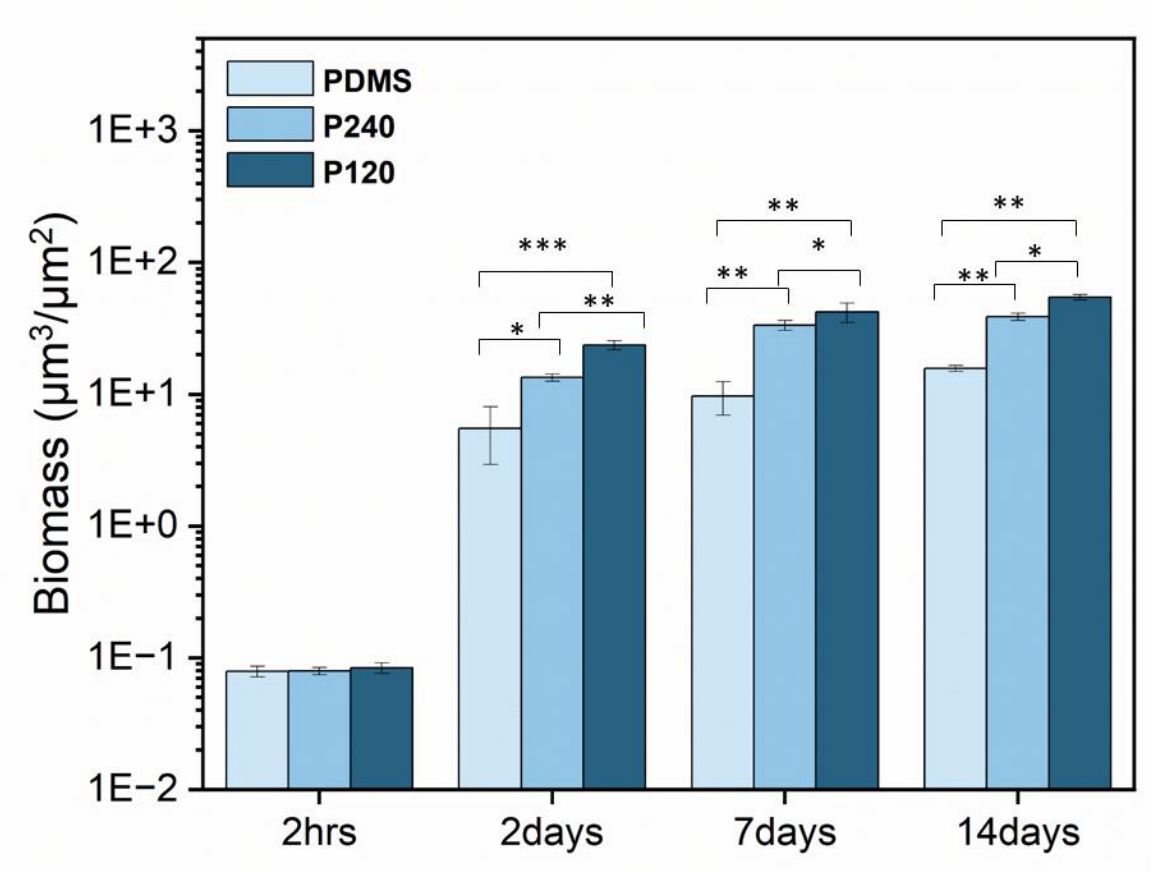

Figure 4.8 The total biomass of *P. aeruginosa* on PDMS, P240 and P120 in static with different time scale. * $p<0.05$; ** $p<10^{-10}$; *** $p<10^{-15}$.

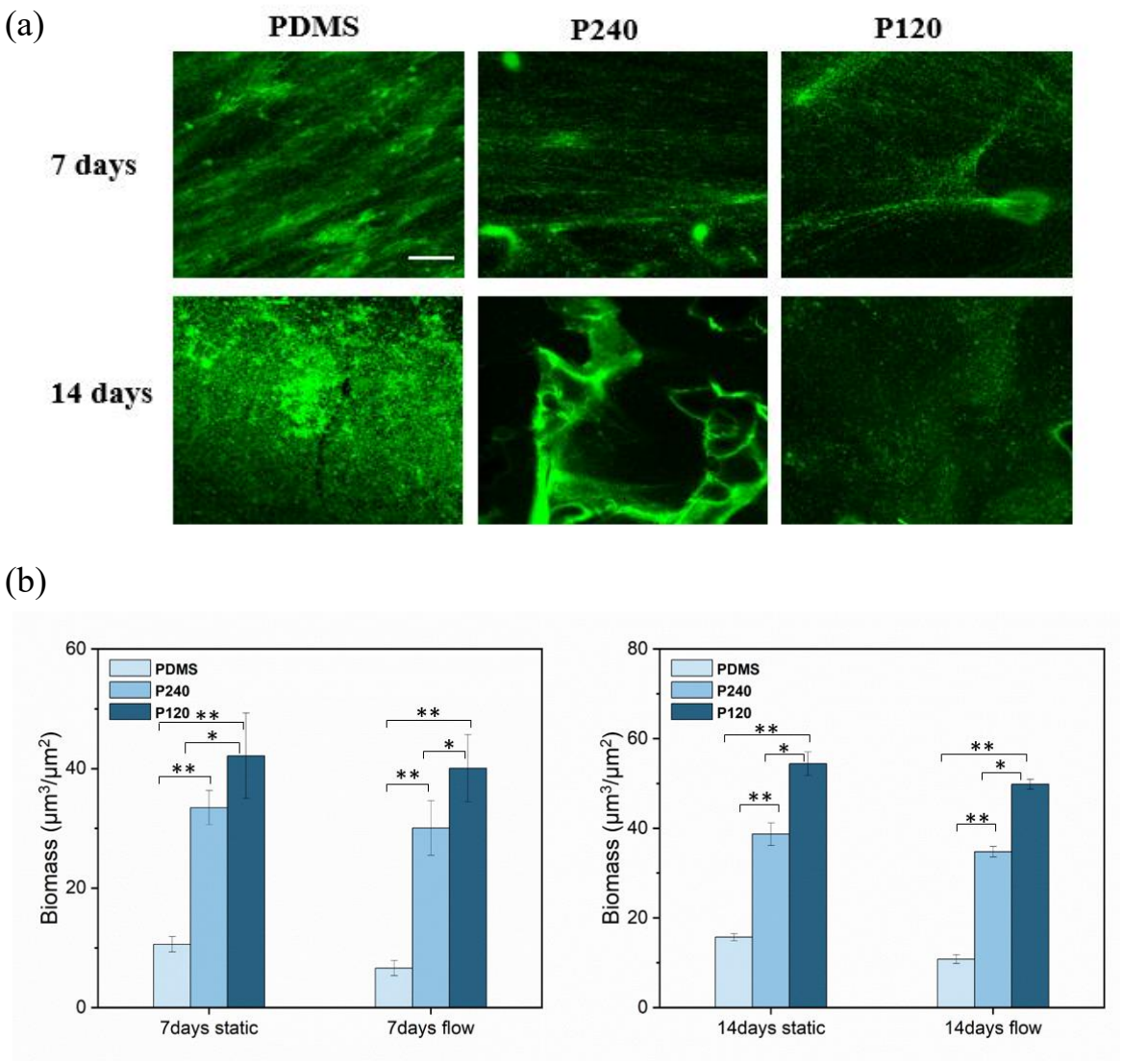

Figure 4.9 (a) Confocal images for *P. aeruginosa* 7days and 14days dynamic culture, scale bar=50μm; (b) The total biomass on PDMS, P240 and P120 in 7days and 14days dynamic culture. * $p<0.05$; ** $p<10^{-10}$; *** $p<10^{-15}$.

4.4 Conclusion

The rougher surface shows easier bacterial adhesion and biofilm formation. With the growth of culture time, denser and thicker biofilms are formed, and the total biomass is increased. Compared to the static culture, biofilm formation and EPS production were reduced because the wall shear stress may be able to detach the bacteria. In terms of the bacteria species, *P. aeruginosa* grew much faster than *S. epidermidis* either in static or dynamic conditions, even though the initial OD of *S. epidermidis* is 20 times larger than that of P. *aeruginosa.*

The change of roughness itself is unlikely to inhibit biofilm formation. In the following chapter, a slippery liquid-infused porous surface (SLIPS) by absorbing silicone oil will be presented.

5 The effect of oil infused surfaces on bacterial attachment and biofilm formation

5.1 Introduction

Anti-biofilm characteristics of material surfaces can be achieved by imparting liquid lubricants to surfaces. Several physical and chemical methods have been developed to maintain a stable lubricant layer through capillary forces, chemical interactions, swelling, or the use of microcapsules to lock in the lubricant [45]. Among these approaches, a porous or textured solid surface can be infused with liquid lubricant to be locked into the structure by capillary forces, thus forming a stable semi-solid/semi-liquid surface [46] or a continuous lubricant coating, i.e., a slippery liquid-infused porous surface (SLIPS) [20, 48]. Alternatively, a liquid lubricant-based supplementation method was used to swell polydimethylsiloxane (PDMS) matrix in silicone oil (S-PDMS) by providing oil reservoirs in the polymer chains [49, 51]. These liquid lubricant-based surfaces are capable of inhibiting bacterial attachment as potential anti-biofilm surfaces but the potential loss of lubricant due to reuse or shearing limits its wider adoption in practice and even poses a safety risk to patients in a clinical setting [286].

In the present work, we fabricated the silicone oil swollen roughened PDMS (P240, P120 with plain PDMS as control) with different oil thicknesses (50, 20, 5, 2µm) and performed anti-biofilm tests against *Staphylococcus epidermidis* and *Pseudomonas aeruginosa* at both static and dynamic conditions. The surface wettability was evaluated by the measurement of the water contact angle and contact angle hysteresis. For dynamic bacterial culture, we focused on the thickest oil layer samples (PDMS 50µm, P240 50µm, and P120 50µm.) for a long-term culture (7 and 14 days).

5.2 Methodology

5.2.1 Different oil thickness slippery surfaces fabrication

The different oil thickness slippery surfaces fabrication methods can be seen in Chapter 3.1.2.

5.2.2 Confocal microscope imaging

After a biofilm formation assay, the substrates were taken out from the flow cell and cut out the interested area with a scalpel, which was gently washed three times with PBS in the well-plate to remove non-adherent or weakly adhered bacteria. All surfaces were visualized and inspected using the Nikon A1 upright confocal microscope with a 20x objective. Due to the relatively large surface features of S-PDMS, SEM imaging was used to observe the distribution of bacteria in a single plane of confocal images.

5.2.3 SEM analysis

The sample surfaces (with bacteria or biofilms) were washed three times with PBS and fixed in 2% glutaraldehyde with 3M Sorenson's phosphate buffer, overnight at 4°C, which were dehydrated through a series of ethanol solutions of 25% (v/v), 50%, 75%, and 100%, followed by critical point drying (BAL-TEC CPD 030) as described in Chapter 3. After drying, the samples were sputter coated by a 5 nm gold coating using a Polaron SEM Coating Unit.

5.2.4 Statistical analysis

Data are represented as mean values with standard error. T-test assuming unequal variations was applied and $p < 0.05$ was considered statistically significant in this study.

5.3 Results and discussion

5.3.1 Surface wettability

The static contact angle (CA) and contact angle hysteresis (CAH) play an important role in bacterial adhesion and biofilm formation. Both CA and CAH of DI water droplets on different oil thickness roughened PDMS samples are summarized in Table 5.1 (Figure 5.1, Figure 5.2). Samples of different roughness with small oil thickness demonstrated a large CA and CAH. For samples with different roughness but the same oil thickness, a similar CA and CAH were observed. Compared to the plain PDMS, P240 and P120 CAH (Chapter

4.3.1), the CAH of samples with the smallest oil thickness (S-PDMS 2, S-P240 2, S-P120 2) reduced around 13°, 8.22°, 5.85°, respectively. It showed that even if the oil is swapped as dry as possible, the surface wettability has already changed, which may affect bacterial adhesion and biofilm formation.

Table 5.1 The static contact angle and the contact angle hysteresis of DI water droplets on different oil thickness roughened surfaces. Data represent the mean and SD of five independent measurements.

Surface	Contact angle (°)	Advancing angle (°)	Receding angle (°)	Contact angle hysteresis (°)
S-PDMS 50	96.33 ± 1.29	94.83 ± 1.16	93.22 ± 1.36	1.61 ± 0.40
S-PDMS 20	96.03 ± 6.91	94.02 ± 5.51	90.01 ± 4.67	4.0 ± 1.36
S-PDMS 5	103.69 ± 2.29	104.30 ± 3.11	99.33 ± 2.04	5.65 ± 2.01
S-PDMS 2	105.27 ± 2.03	105.60 ± 2.32	97.12 ± 4.79	8.48 ± 3.10
S-P240 50	98.77 ± 1.04	95.82 ± 1.75	94.27 ± 1.90	1.56 ± 0.41
S-P240 20	92.0 ± 4.03	91.49 ± 3.49	89.07 ± 4.55	3.88 ± 1.52
S-P240 5	106.34 ± 4.74	114.04 ± 5.75	106.28 ± 5.45	7.77 ± 1.66
S-P240 2	108.40 ± 4.29	113.68 ± 3.95	101.30 ± 5.25	12.38 ± 4.01
S-P120 50	95.44 ± 0.88	98.61 ± 0.73	97.30 ± 0.79	1.31 ± 0.21
S-P120 20	96.88 ± 3.85	96.61 ± 4.24	94.53 ± 3.28	4.43 ± 1.78
S-P120 5	107.23 ± 5.39	106.09 ± 3.42	99.09 ± 3.55	7.00 ± 3.36
S-P120 2	107.88 ± 6.71	111.03 ± 4.19	99.78 ± 4.67	11.25 ± 3.40

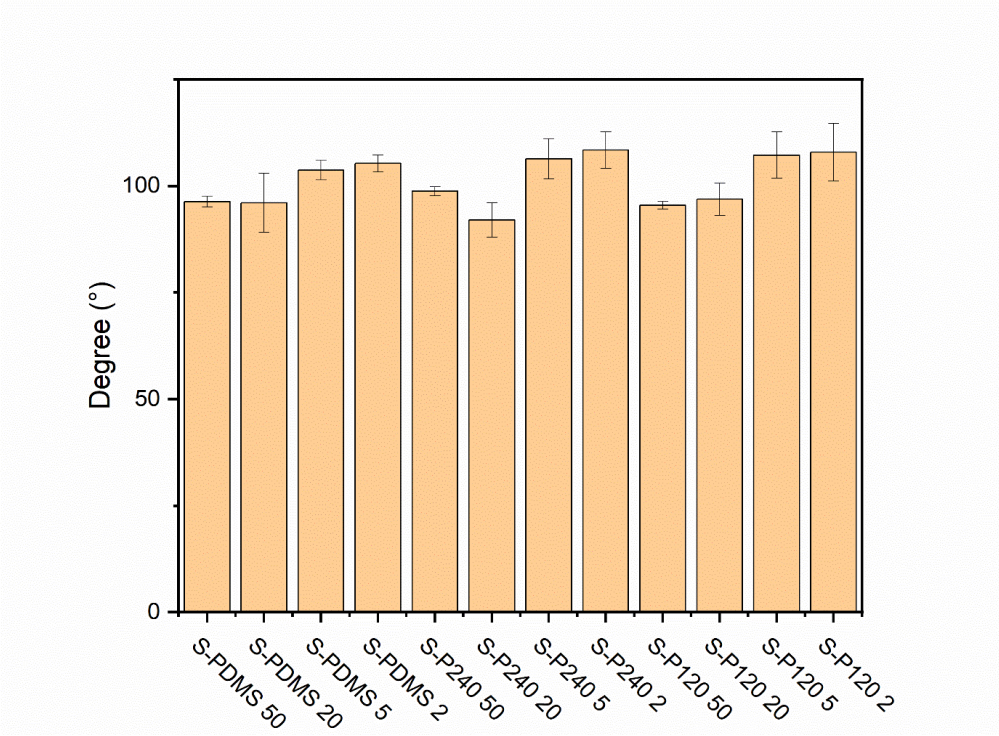

Figure 5.1 Contact angle for different oil thickness roughened PDMS. roughened PDMS.

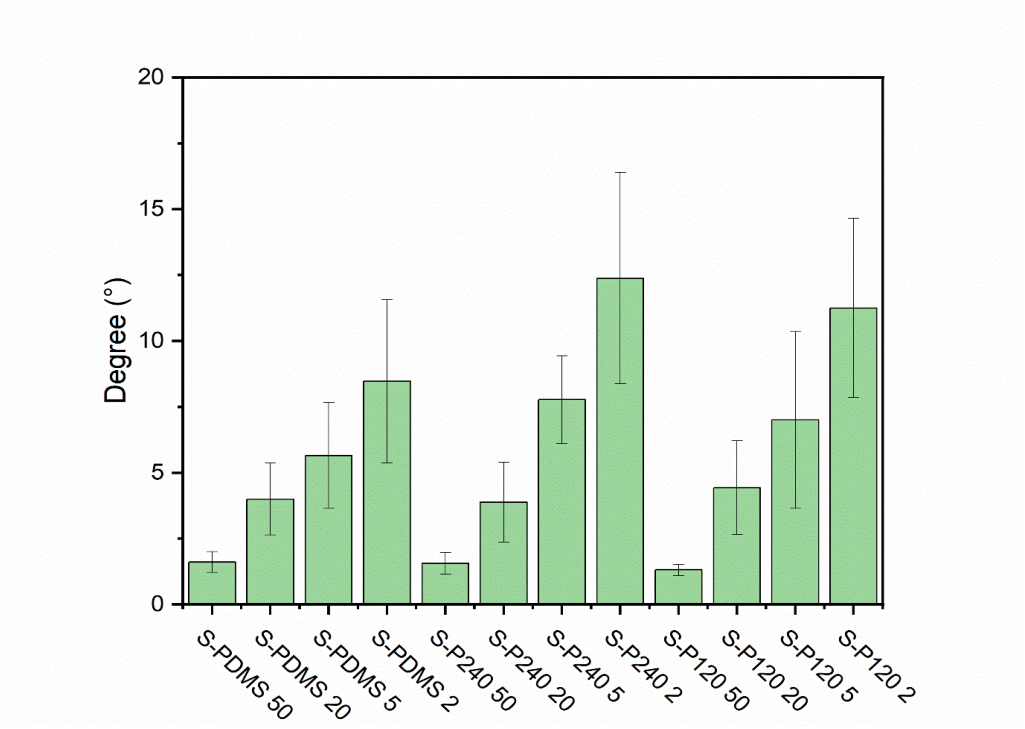

Figure 5.2 Contact angle hysteresis for different oil thickness roughened PDMS.

5.3.2 Anti-biofilm tests against *Staphylococcus epidermidis*

The growth of S. epidermidis FH8 was examined on prepared S-PDMS after different culture periods under static conditions. Figure 5.4A, Figure5.5A and Figure 5.6A display the SEM images after the growth of *S.epidermidis* for 2 hours, 2 days, 7 days and 14 days on plain S-PDMS, S-P240 and S-120 with respective oil thickness (50, 20, 5, 2μm). The total biomass quantification of samples after different culture periods has been shown in Figure 5.4B, Figure 5.5B and Figure 5.6B.

After 2-hour culture, all the samples only showed single bacterial attachment on the surfaces. The total biomass of biofilms on S-PDMS (50, 20, 5, 2μm) is 3.44e-05 $\mu m^3/\mu m^2$, 4.01e-04 $\mu m^3/\mu m^2$, 1.12e-03 $\mu m^3/\mu m^2$, 1.50e-03 $\mu m^3/\mu m^2$, respectively. For the S-P240 (50, 20, 5, 2μm) surfaces, the total biomass is 7.33e-04 $\mu m^3/\mu m^2$, 1.45e-03 $\mu m^3/\mu m^2$, 2.30e-03 $\mu m^3/\mu m^2$, 3.13e-03 $\mu m^3/\mu m^2$, respectively. The total biomass of biofilms on S-P120 (50, 20, 5, 2μm) surfaces is 1.58e-03 $\mu m^3/\mu m^2$, 2.09e-03 $\mu m^3/\mu m^2$, 3.57e-03 $\mu m^3/\mu m^2$, 5.19e-03 $\mu m^3/\mu m^2$, respectively. It demonstrated that the total biomass of biofilms on S-P240 50 and S-P120 50 surface is 1 to 2 orders of magnitude larger than S-PDMS 50. The total biomass of biofilms on S-P240 20 and S-P120 20 surface is 1 order of magnitude larger than S-PDMS 20. While for the samples with oil thicknesses of 5 and 2 μm, the total biomass is in the same order of magnitude. The biomass on the surface of S-P240 and S-P120 is around 2 and 3 times larger than S-PDMS.

After 2-day culture, unlike the plain surfaces with initial biofilm development, only a single bacterial attachment was observed on roughened PDMS surfaces. Even inside the holes on rough surfaces, small amounts of bacteria aggregation were found. The total biomass of biofilms on S-PDMS (50, 20, 5, 2μm) is 1.10e-04 $\mu m^3/\mu m^2$, 3.54e-04 $\mu m^3/\mu m^2$, 2.22e-03 $\mu m^3/\mu m^2$, 4.95e-03 $\mu m^3/\mu m^2$, respectively. For the S-P240 (50, 20, 5, 2μm) surfaces, the total biomass is 1.15e-03 $\mu m^3/\mu m^2$, 2.12e-03 $\mu m^3/\mu m^2$, 3.72e-03 $\mu m^3/\mu m^2$, 4.73e-03 $\mu m^3/\mu m^2$, respectively. And the total biomass of S-P120 (50, 20, 5, 2μm) surfaces is 2.45e-03 $\mu m^3/\mu m^2$, 3.26e-03 $\mu m^3/\mu m^2$, 4.12e-03 $\mu m^3/\mu m^2$, 6.40e-03 $\mu m^3/\mu m^2$, respectively. For the oil thickness is 50 and 20 μm, the total biomass on S-P240 and S-P120 is 1 order of magnitude larger than S-PDMS. While for oil thickness of 5 and 2 μm, the total biomass of rougher surfaces is slightly bigger than smoother ones.

After 7-day culture, the surfaces with oil thicknesses of 50 and 20 μm remain a status of a single bacterium attachment but for the surfaces with oil thicknesses of 5 and 2 μm, bacterial clusters started to form except S-PDMS 5 surface. The total biomass of S-PDMS (50, 20, 5, 2μm) is 1.22e-03 $\mu m^3/\mu m^2$, 1.34e-03 $\mu m^3/\mu m^2$, 3.24e-03 $\mu m^3/\mu m^2$, 8.69e-03 $\mu m^3/\mu m^2$, respectively. For the S-P240 (50, 20, 5, 2μm) surfaces, the total biomass is 2.45e-03 $\mu m^3/\mu m^2$, 2.81e-03 $\mu m^3/\mu m^2$, 1.03e-02 $\mu m^3/\mu m^2$, 1.42e-02 $\mu m^3/\mu m^2$, respectively. And the total biomass of S-P120 (50, 20, 5, 2μm) surfaces is 2.83e-03 $\mu m^3/\mu m^2$, 4.86e-03 $\mu m^3/\mu m^2$, 1.08e-02 $\mu m^3/\mu m^2$, 1.51e-02 $\mu m^3/\mu m^2$, respectively.

After 14-day culture, the surfaces with oil thicknesses of 50 and 20 μm maintained their wettability, only showing a single bacterial attachment on the surfaces. While for the surfaces with 5 and 2 μm oil thickness, the bacterial aggregation or clusters are similar to the plain PDMS, P240 and P120 after 2 hours of static bacterial adhesion in Chapter 4.3.2. The total biomass of S-PDMS (50, 20, 5, 2μm) is 1.63e-03 $\mu m^3/\mu m^2$, 3.06e-03 $\mu m^3/\mu m^2$, 2.89e-02 $\mu m^3/\mu m^2$, 2.98e-02 $\mu m^3/\mu m^2$, respectively. For the S-P240 (50, 20, 5, 2μm) surfaces, the total biomass is 2.53e-03 $\mu m^3/\mu m^2$, 3.60e-03 $\mu m^3/\mu m^2$, 3.25e-02 $\mu m^3/\mu m^2$, 6.23e-02 $\mu m^3/\mu m^2$, respectively. And the total biomass of S-P120 (50, 20, 5, 2μm) surfaces is 3.03e-03 $\mu m^3/\mu m^2$, 5.69e-03 $\mu m^3/\mu m^2$, 3.35e-02 $\mu m^3/\mu m^2$, 9.61e-02 $\mu m^3/\mu m^2$, respectively.

For dynamic bacterial cultures in a continuous flow, we chose flow conditions that can result in a wall shear stress (τ_w) of 0.007 Pa consistent with Chapter 4. When the fluids passed over the surface, the wall shear stress inducing a loss of oil will influence the bacterial adhesion and biofilm formation. We focused on the dynamic bacterial culture on the surface with the thickest oil for the long term (7, 14 days) (Figure 5.7).

After 7 days' dynamic culture, the total biomass of S-PMDS 50, S-P240 50 and S-P120 50 is 1.11e-02 $\mu m^3/\mu m^2$, 4.79e+00 $\mu m^3/\mu m^2$, 1.02e+01 $\mu m^3/\mu m^2$, respectively. It demonstrated that S-PDMS 50 surface under 7 days' dynamic culture showed bacterial adhesion, but 1 order of magnitude larger than S-PDMS 50 under 7 days' static culture.

After 14 days of dynamic culture, the total biomass of S-PMDS 50, S-P240 50 and S-P120 50 is 5.66e+00 $\mu m^3/\mu m^2$, 1.16e+01 $\mu m^3/\mu m^2$, 1.76e+01 $\mu m^3/\mu m^2$, respectively.

All these surfaces showed the growth of thicker biofilm with significant differences. It indicates oil depletion enhanced the biofilm formation, and the bacteria colonizing pores in rough surfaces are not easily washed away by fluids. In our previous work, we demonstrated that significant oil depletion can occur for 2-7 days of flow conditions with a wall shear stress of 0.007Pa (Figure 5.3). It did not cause a change in CA but a significant increase in CAH. As S-PDMS (20μm) was reported to suffer from oil loss in continuous flow [64], we also measured the oil loss and investigated how it may affect the contact angle and CAH, the key results of which are presented in Figure 5.3b. After continuous flow (τ_w = 0.007 Pa) for 7-days, the CA of S-PDMS (20μm) remained unchanged but CAH increased significantly to an average of 8.9 °, which is associated with oil loss (see Figure 5.3c). For the roughened surfaces swollen by silicone oil, their antibiofilm behaviour seems not as good as the S-PDMS. This is probably due to the actual thickness of the surface being less than the S-PDMS as the thickness calculation from Equation 14 assumed a smooth surface.

The plain PDMS, P240 and P120 were used as comparative control surfaces, the details of which are shown in Chapter 4. When comparing to the roughened PDMS surfaces with different oil thicknesses, either in static or dynamic conditions, even for the surfaces with the thinnest silicone oil thickness (2 μm), there was a significant difference for the respective culture period (p<0.001). The total biomass of the roughened PDMS surfaces is 2-4 orders of magnitude less than that of the corresponding plain surfaces.

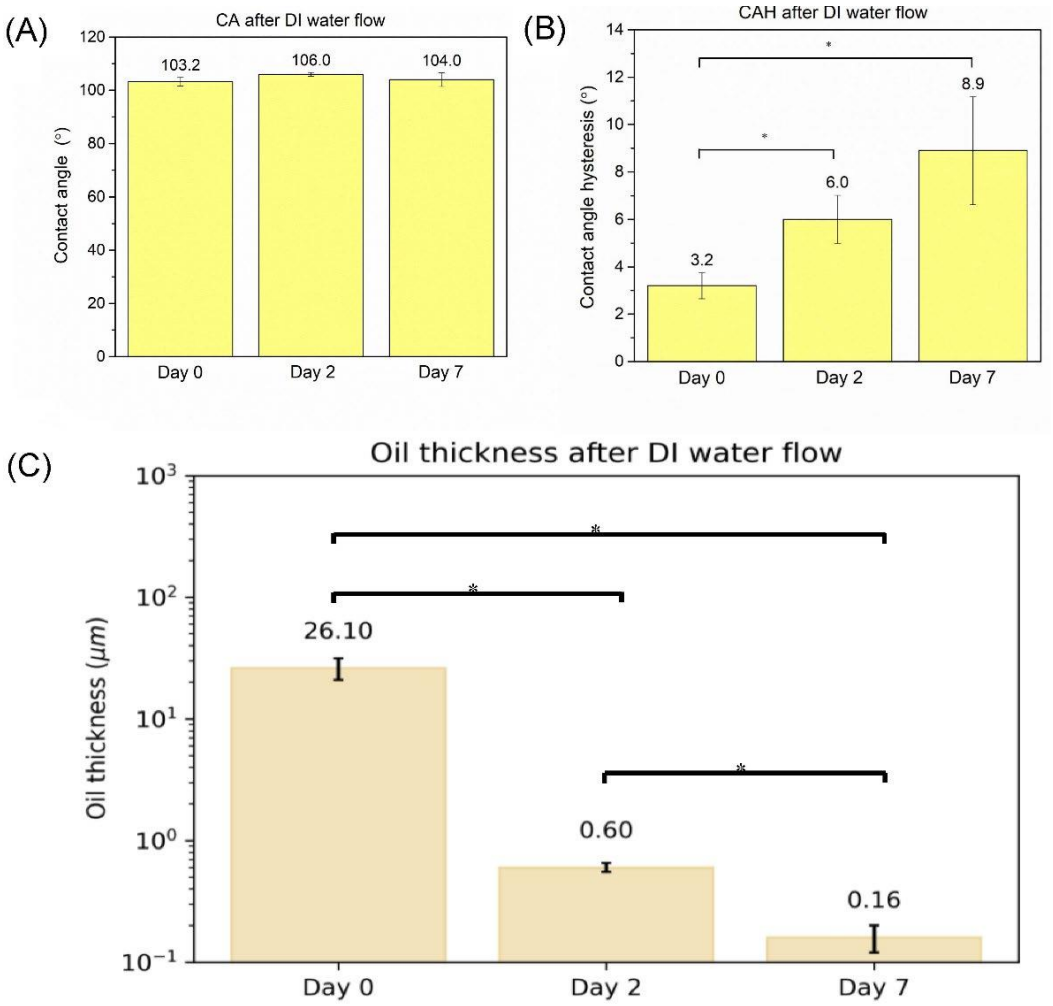

Figure 5.3 (A) The oil thickness atop S-PDMS and the corresponding (B) contact angle and (C) contact angle hysteresis subjected to the continuous flow (τ_w = 0.007 Pa) for 2 days and 7 days. * p<0.05

(A)

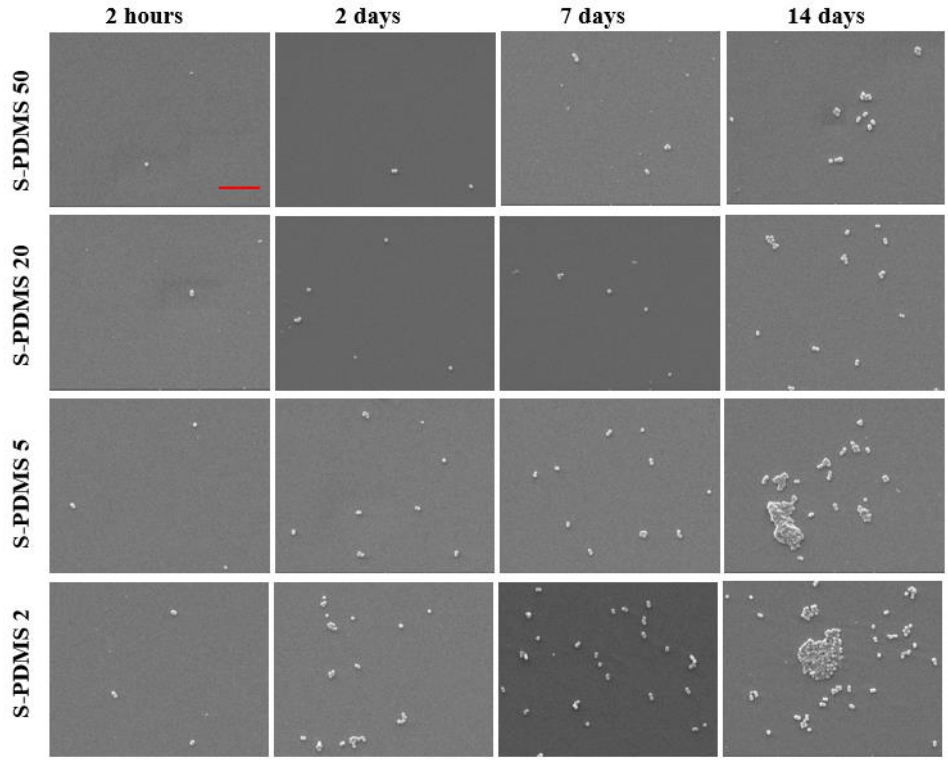

(B)

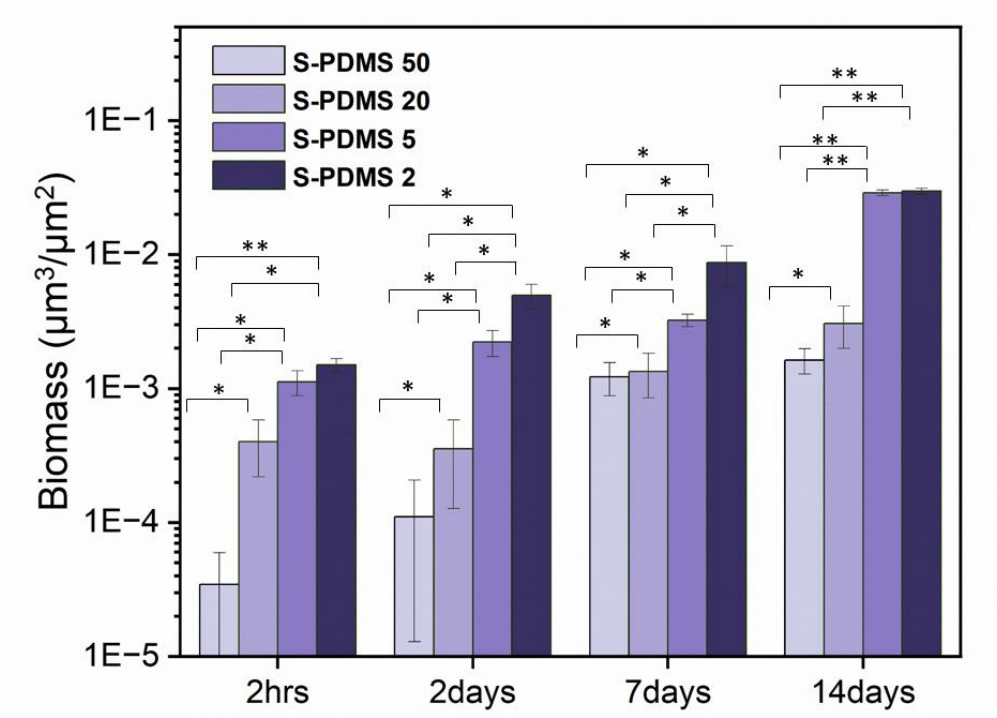

Figure 5.4 (A) Representative SEM images and (B) biomass of the growth of *S. epidermidis* FH8 on different oil thickness S-PDMS for 2 h, 2 days, 7 days, and 14 days in static cell culture. Scale bar = 10μm for all images. In all cases, 10 images were analysed for each surface from 3 independent experiments. Values presented are mean ± SD. * $p<0.05$; ** $p<10^{-10}$; *** $p<10^{-15}$.

(A)

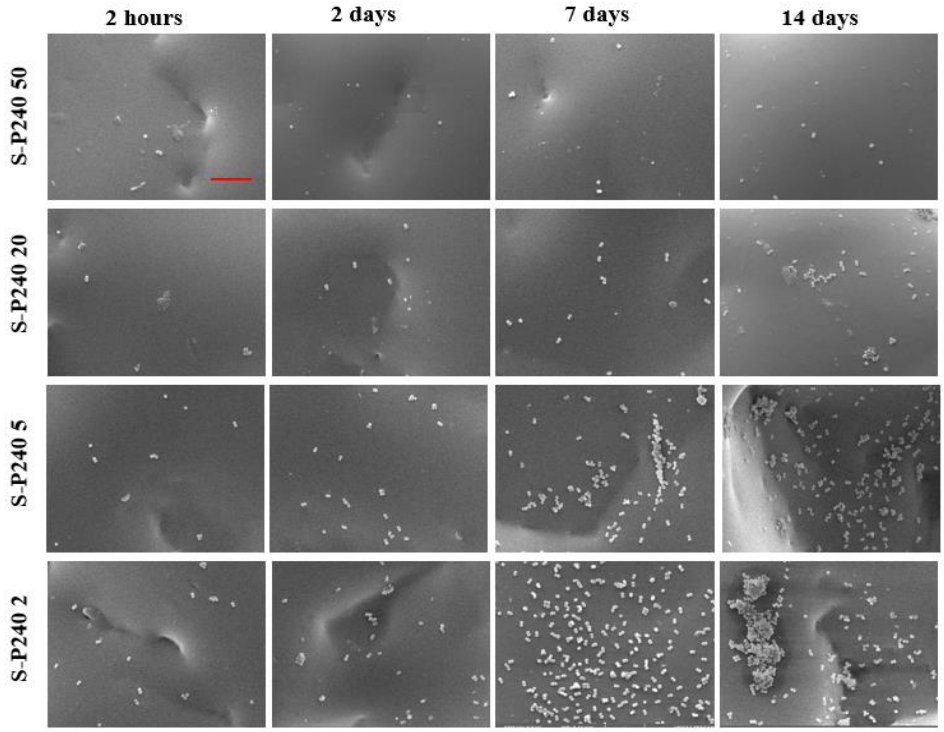

(B)

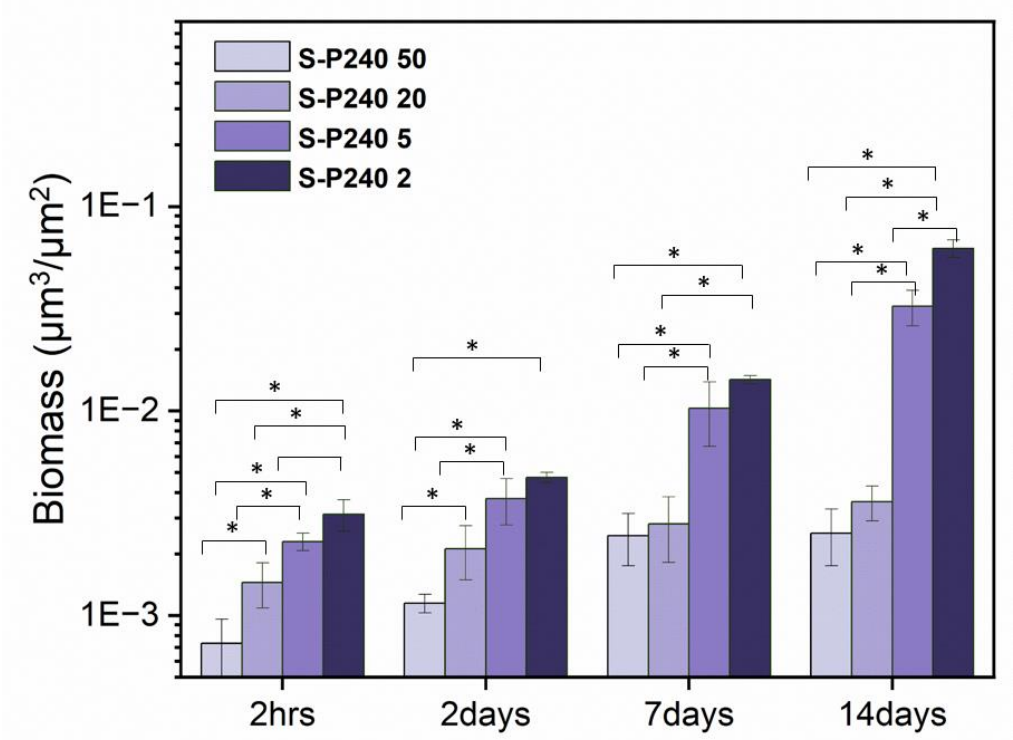

Figure 5.5 (A) Representative SEM images and (B) biomass of the growth of *S. epidermidis* FH8 on different oil thickness S-P240 for 2 h, 2 days, 7 days, and 14 days in static cell culture. Scale bar = 10μm for all images. In all cases, 10 images were analysed for each surface from 3 independent experiments. Values presented are mean ± SD. * $p<0.05$; ** $p<10^{-10}$; *** $p<10^{-15}$.

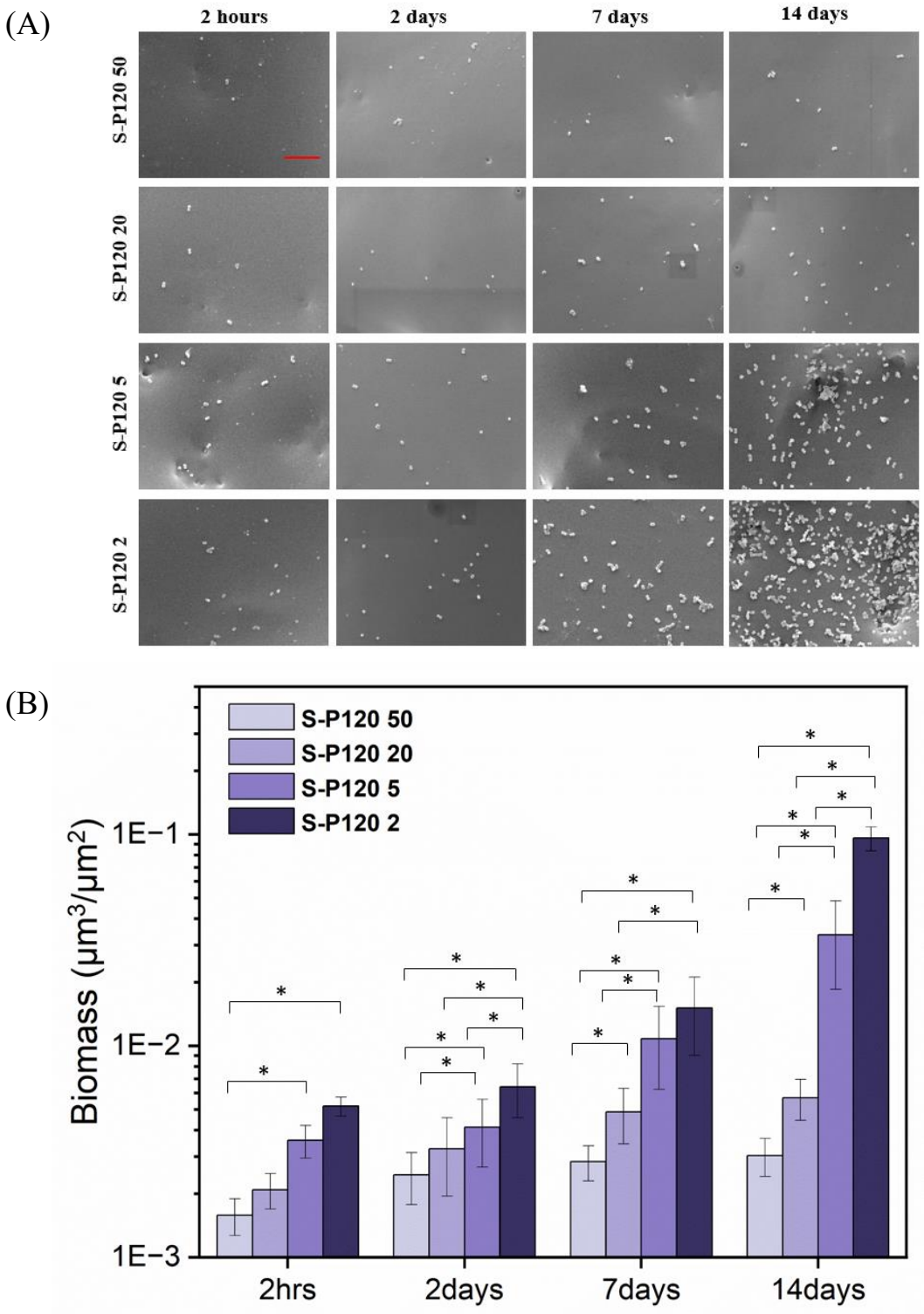

Figure 5.6 (A) Representative SEM images and (B) biomass of the growth of *S. epidermidis* FH8 on different oil thickness S-P120 for 2 h, 2 days, 7 days, and 14 days in static cell culture. Scale bar = 10μm for all images. In all cases, 10 images were analysed for each surface from 3 independent experiments. Values presented are mean ± SD. * $p<0.05$; ** $p<10^{-10}$; *** $p<10^{-15}$.

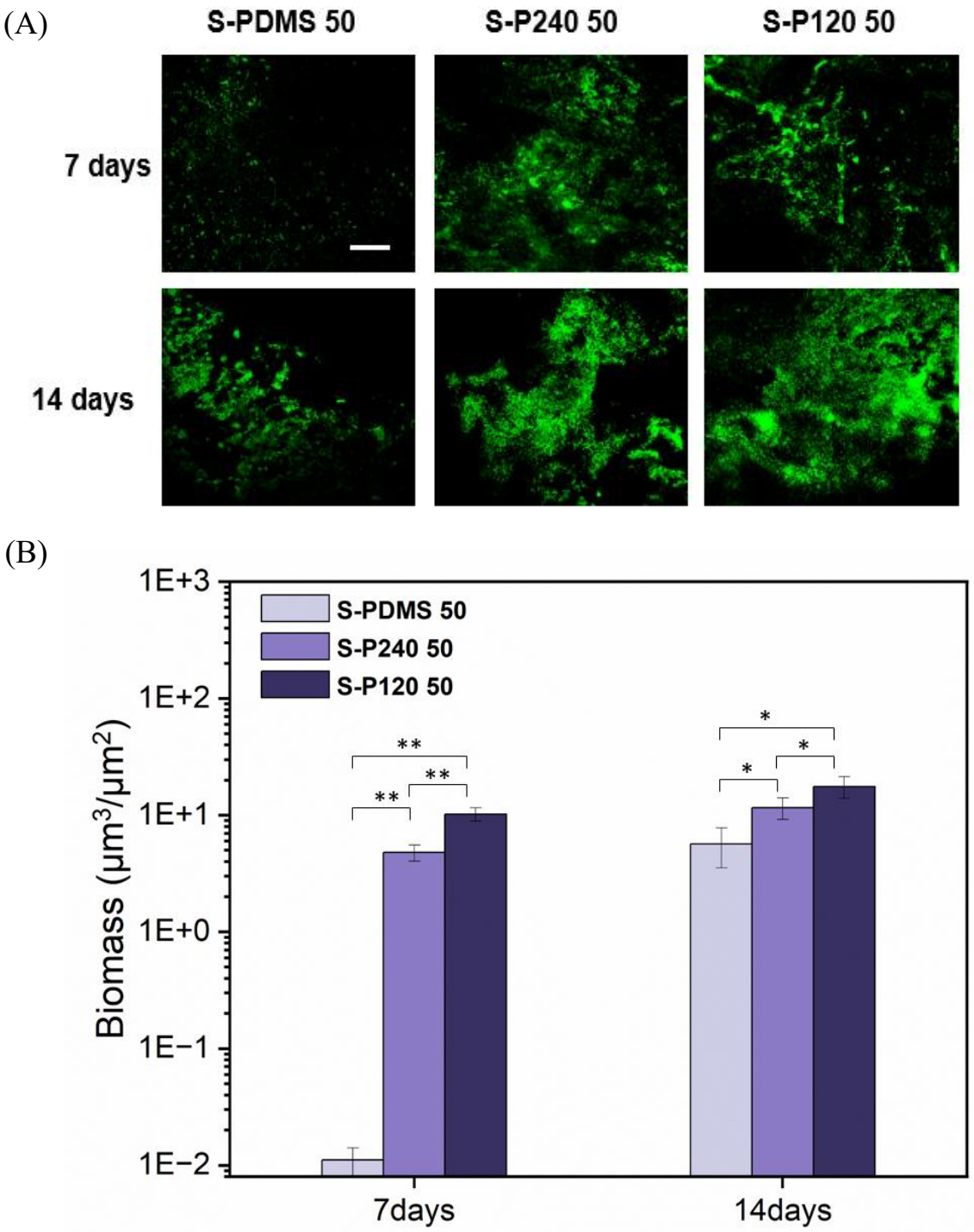

Figure 5.7 (A) Representative confocal images and (B) biomass of the growth of *S. epidermidis* FH8 on S-PDMS 50, S-P240 50 and S-P120 50 surfaces for 7 days and 14 days in dynamic cell culture. Scale bar = 50μm for all images. In all cases, 10 images were analysed for each surface from 3 independent experiments. Values presented are mean ± SD. * $p<0.05$; ** $p<10^{-5}$.

5.3.3 Anti-biofilm tests against *Pseudomonas aeruginosa*

Biofilm-forming strain of *Pseudomonas aeruginosa* (PAO1) isolated from a wound was used in this study. It was cultured on each of the surfaces under static and flow conditions after different culture periods. Figure 5.8A, Figure 5.9A and Figure 5.10A show the SEM images after the growth of PAO1 for 2 hours, 2 days, 7 days and 14 days on S-PDMS, S-P240 and S-120 with different oil thickness (50, 20, 5, 2μm) respectively. The total biomass quantification for different samples after different culture periods is shown in Figure5.8B, Figure 5.9B and Figure 5.10B.

After 2 hours' culture, excluding the aggregation of bacteria on S-P240 2 and S-P120 2 surfaces, the others show single bacteria adhesion. The total biomass on S-PDMS (50, 20, 5, 2μm) is 1.70e-04 $\mu m^3/\mu m^2$, 5.10e-04 $\mu m^3/\mu m^2$, 1.33e-03 $\mu m^3/\mu m^2$, 1.95e-03 $\mu m^3/\mu m^2$, respectively. For the S-P240 (50, 20, 5, 2μm) surfaces, the total biomass is 1.57e-03 $\mu m^3/\mu m^2$, 2.37e-03 $\mu m^3/\mu m^2$, 5.08e-03 $\mu m^3/\mu m^2$, 1.80e-02 $\mu m^3/\mu m^2$, respectively. And the total biomass of S-P120 (50, 20, 5, 2μm) surfaces is 1.99e-03 $\mu m^3/\mu m^2$, 2.56e-03 $\mu m^3/\mu m^2$, 7.99e-03 $\mu m^3/\mu m^2$, 3.78e-02 $\mu m^3/\mu m^2$, respectively. It demonstrated that the total biomass on S-P240 and S-120 surfaces is 1 order of magnitude larger than on S-PDMS surfaces. Comparing S-P240 to S-P120 surfaces, there is a significant difference (p=4.04e-08 (50 μm); p=2.55e-02 (20 μm); p=1.01e-13 (5 μm); p=1.01e-15 (2 μm)).

After 2 days' culture, S-P240 (5 μm) and S-P120 (5 μm) surfaces start to show bacterial aggregation whilst the others only show single bacteria adhesion. The total biomass of S-PDMS (50, 20, 5, 2μm) is 3.63e-04 $\mu m^3/\mu m^2$, 6.02e-04 $\mu m^3/\mu m^2$, 2.54e-03 $\mu m^3/\mu m^2$, 4.14e-03 $\mu m^3/\mu m^2$, respectively. For the S-P240 (50, 20, 5, 2μm) surfaces, the total biomass is 2.19e-03 $\mu m^3/\mu m^2$, 7.80e-03 $\mu m^3/\mu m^2$, 1.24e-02 $\mu m^3/\mu m^2$, 2.49e-02 $\mu m^3/\mu m^2$, respectively. And the total biomass of S-P120 (50, 20, 5, 2μm) surfaces is 4.33e-03 $\mu m^3/\mu m^2$, 9.13e-03 $\mu m^3/\mu m^2$, 2.97e-02 $\mu m^3/\mu m^2$, 3.88e-02 $\mu m^3/\mu m^2$, respectively. The results of the total biomass quantification are the same as that of 2 hours culture.

After 7 days' culture, the bacterial clusters grew on S-PDMS 5 surface, while the others are still under single bacterial attachment, but the total biomass was doubled approximately compared to that of the 2-day culture. The total biomass of S-PDMS (50, 20, 5, 2μm) is 4.25e-04 $\mu m^3/\mu m^2$, 1.10e-03 $\mu m^3/\mu m^2$, 2.37e-02 $\mu m^3/\mu m^2$, 2.92e-02 $\mu m^3/\mu m^2$,

respectively. For the S-P240 (50, 20, 5, 2μm) surfaces, the total biomass is 4.68e-03 $\mu m^3/\mu m^2$, 8.13e-03 $\mu m^3/\mu m^2$, 1.75e-02 $\mu m^3/\mu m^2$, 3.14e-02 $\mu m^3/\mu m^2$, respectively. And the total biomass of S-P120 (50, 20, 5, 2μm) surfaces is 9.97e-03 $\mu m^3/\mu m^2$, 1.64e-02 $\mu m^3/\mu m^2$, 3.42e-02 $\mu m^3/\mu m^2$, 6.40e-02 $\mu m^3/\mu m^2$, respectively. It demonstrated that the total biomass of S-P240 50 and S-120 50 surfaces is 1 order of magnitude larger than the S-PDMS 50 surface. For the surfaces with an oil thickness of 20 μm, the total biomass of the S-P240 (20 μm) surface is 8 times the S-PDMS 20 surface but is half of the S-P120 20 surface. There is abnormal data for the surfaces with 5 μm oil thickness, where the total biomass of the S-P240 (5 μm) surface is smaller than the S-PDMS (5 μm) surface. This may be attributed to the errors in drying bacteria by CPD. This can be improved by designing a new CPD chamber to avoid the flip of samples.

After 14 days' culture, unlike *S.epiderimidis*, bacterial aggregates formed on S-P240 50, S-P240 20, S-P120 50, and S-P120 20 surfaces due to the rapid growth rate and massive EPS production of PAO1. On S-PDMS 50 and S-PDMS 20 surfaces, there is only single bacterial adhesion observed. It implied that roughness could enhance bacterial attachment. The total biomass of S-PDMS (50, 20, 5, 2μm) is 4.66e-04 $\mu m^3/\mu m^2$, 2.42-02 $\mu m^3/\mu m^2$, 6.67e-02 $\mu m^3/\mu m^2$, 6.99e-02 $\mu m^3/\mu m^2$, respectively. For the S-P240 (50, 20, 5, 2μm) surfaces, the total biomass is 1.19e-02 $\mu m^3/\mu m^2$, 2.28e-02 $\mu m^3/\mu m^2$, 4.81e-02 $\mu m^3/\mu m^2$, 6.01e-02 $\mu m^3/\mu m^2$, respectively. And the total biomass of S-P120 (50, 20, 5, 2 μm) surfaces is 1.73e-02 $\mu m^3/\mu m^2$, 6.36e-02 $\mu m^3/\mu m^2$, 4.42e-02 $\mu m^3/\mu m^2$, 8.28e-02 $\mu m^3/\mu m^2$, respectively. It demonstrated that the total biomass of S-P240 50 and S-120 50 surfaces showed 2 orders of magnitude larger than the S-PDMS 50 surface. Another phenomenon observed is that PDMS soaked in ethanol for a long time will cause dehydration, resulting in wrinkles on the surface after CPD drying as seen in Figure 5.8A.

For dynamic bacterial cultures in a continuous flow, we chose flow conditions that result in a wall shear stress (τ_w) of 0.007 Pa consistent with Chapter 4. We focused on the dynamic bacterial culture of the surface with the thickest oil over the long term (7, 14 days) (Figure 5.11).

After 7 days' dynamic culture, the total biomass of S-PMDS 50, S-P240 50 and S-P120 50 is 2.84e-03 $\mu m^3/\mu m^2$, 1.92e+01 $\mu m^3/\mu m^2$, 2.66e+01 $\mu m^3/\mu m^2$, respectively. It

demonstrated that S-PDMS 50 surface under 7 days' dynamic culture only shows bacterial adhesion, but it is 1 order of magnitude larger than the S-PDMS 50 under 7 days' static culture.

After 14 days of dynamic culture, the total biomass of S-PMDS 50, S-P240 50 and S-P120 50 is 6.39e+00 $\mu m^3/\mu m^2$, 2.35e+01 $\mu m^3/\mu m^2$, 3.87e+01 $\mu m^3/\mu m^2$, respectively. All these surfaces grew a thicker biofilm and have a significant difference (p<0.001).

Compared to the *S.epidermidis*, the total biomass of S-PDMS 50 surface is 1 order of magnitude smaller. For the biofilm formation, either 7 days or 14 days underflow, the total biomass of PAO1 is nearly twice larger than that of *S.epidermidis*. When comparing to the roughened PDMS surfaces, either in static or dynamic conditions, even for the surfaces with 2 μm silicone oil thickness, the total biomass of roughened PDMS surfaces is 2-4 orders of magnitude less than that of the corresponding plain surfaces. For 2 hours, 2 days and 7 days of culture of *S.epidermidis* and *P. aeruginosa*, the bacterial attachment was significantly reduced by over 98% on S-PDMS 50 versus the control PDMS which is similar to the other researchers' work [60].

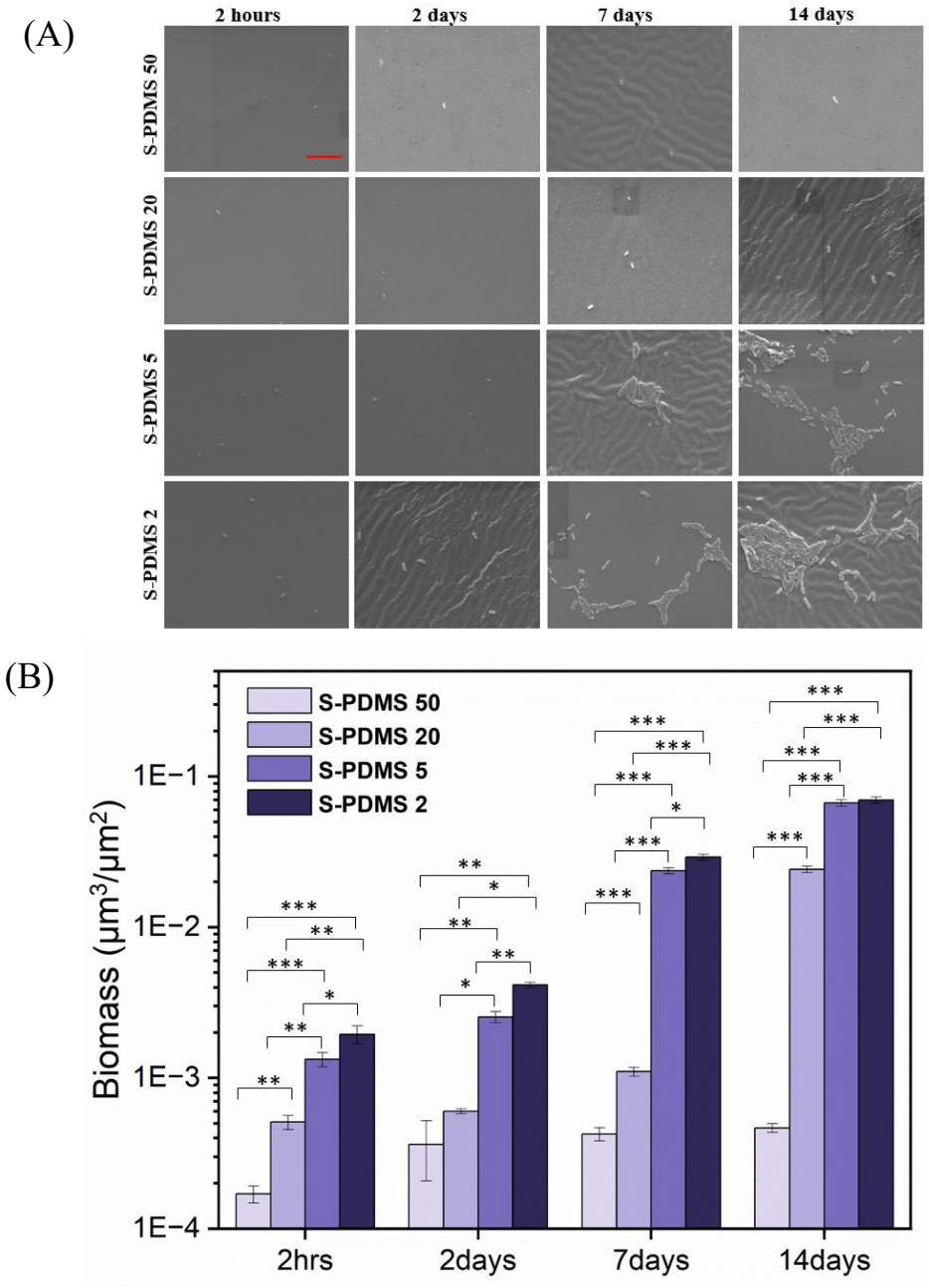

Figure 5.8 (A) Representative SEM images and (B) biomass of the growth of PAO1 on different oil thickness S-PDMS for 2 h, 2 days, 7 days, and 14 days in static cell culture. Scale bar = 10μm for all images. In all cases, 10 images were analysed for each surface from 3 independent experiments. Values presented are mean ± SD. * $p<0.05$; ** $p<10^{-10}$; *** $p<10^{-15}$.

(A)

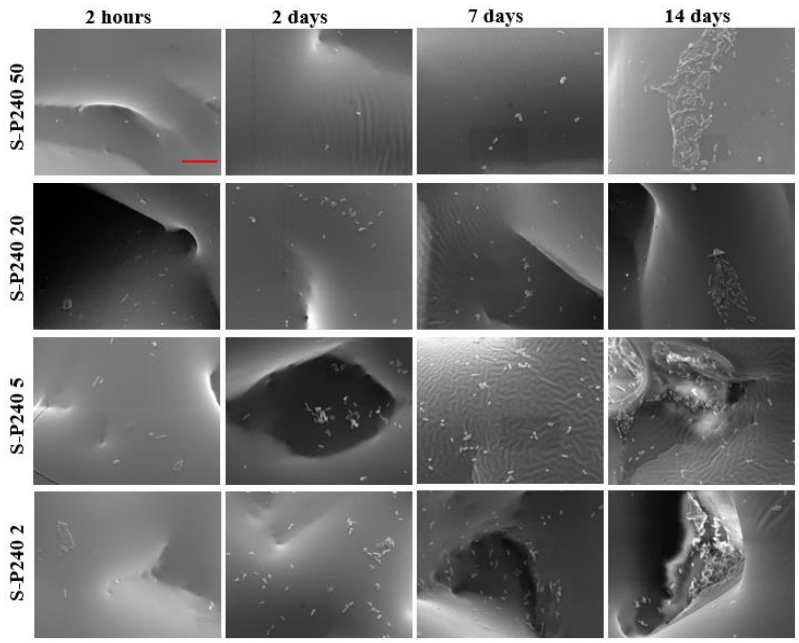

(B)

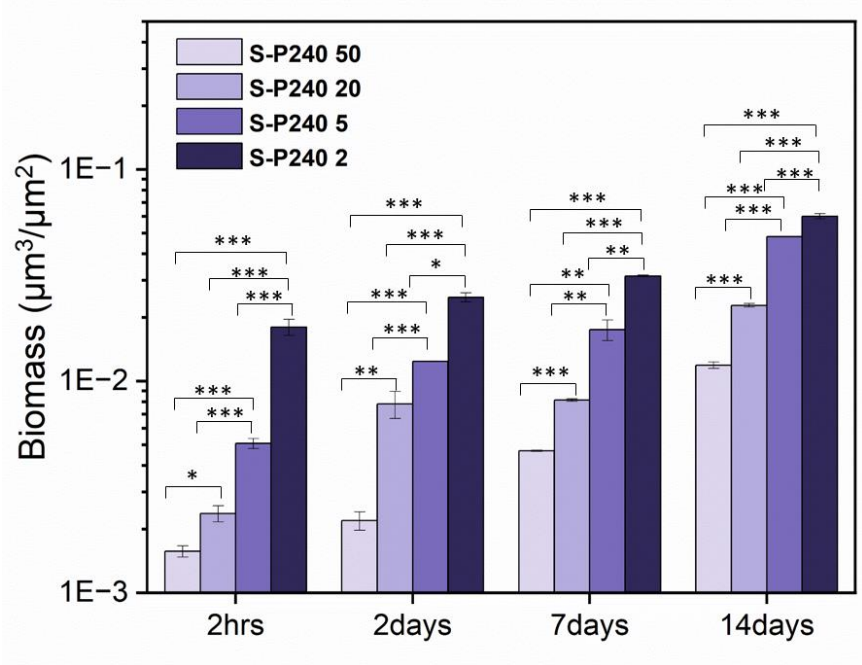

Figure 5.9 (A) Representative SEM images and (B) biomass of the growth of PAO1 on different oil thickness S-P240 for 2 h, 2 days, 7 days, and 14 days in static cell culture. Scale bar = 10μm for all images. In all cases, 10 images were analysed for each surface from 3 independent experiments. Values presented are mean ± SD. * $p<0.05$; ** $p<10^{-10}$; *** $p<10^{-15}$.

(A)

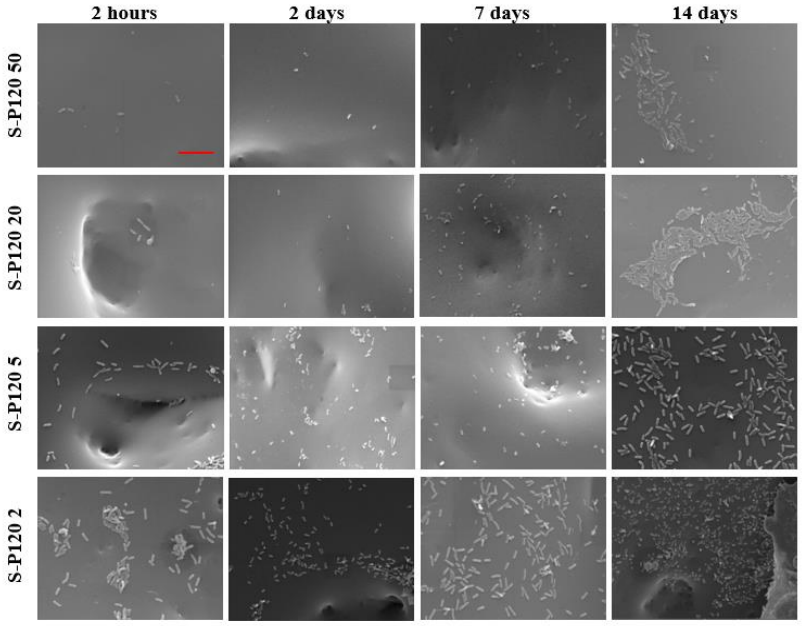

(B)

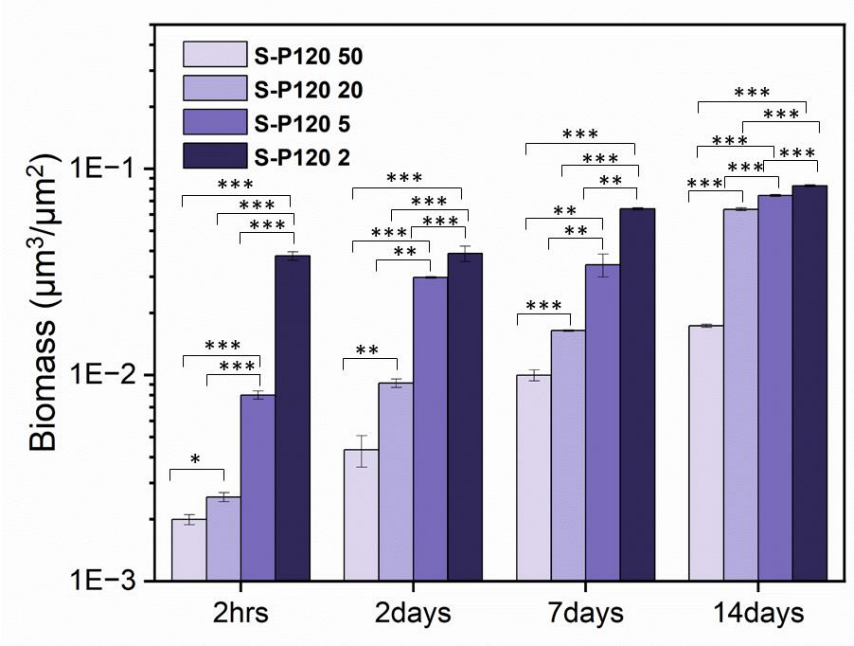

Figure 5.10 (A) Representative SEM images and (B) biomass of the growth of PAO1 on different oil thickness S-P120 for 2 h, 2 days, 7 days, and 14 days in static cell culture. Scale bar = 10μm for all images. In all cases, 10 images were analysed for each surface from 3 independent experiments. Values presented are mean ± SD. * $p<0.05$; ** $p<10^{-10}$; *** $p<10^{-15}$.

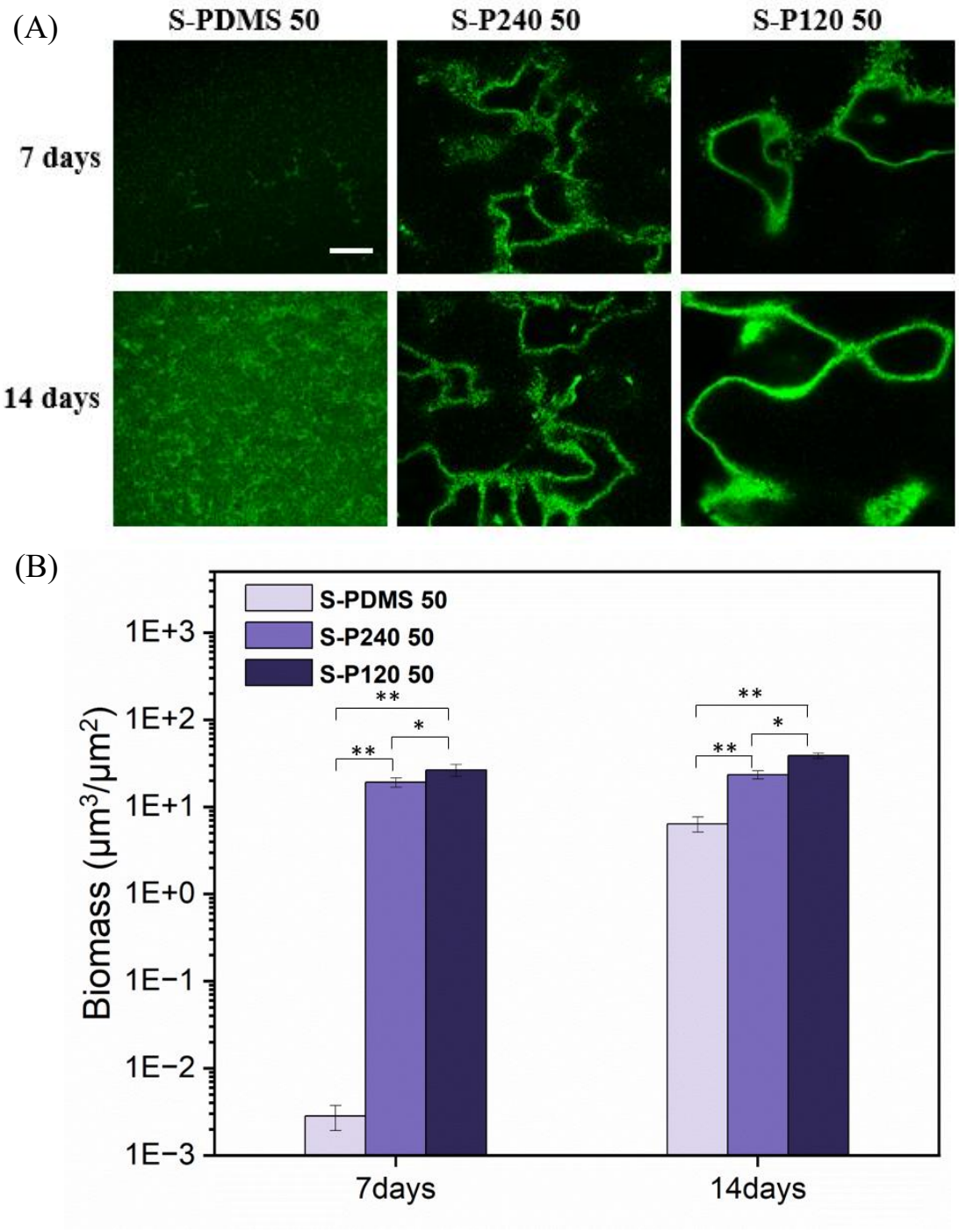

Figure 5.11 (A) Representative confocal images and (B) biomass of the growth of PAO1 on S-PDMS 50, S-P240 50 and S-P120 50 surfaces for 7 days and 14 days in dynamic cell culture. Scale bar = 10μm for all images. In all cases, 10 images were analysed for each surface from 3 independent experiments. Values presented are mean ± SD. * $p<0.05$; ** $p<10^{-5}$.

Based on the above study, we propose the following antibiofilm mechanisms for silicone oil-infused roughened PDMS surfaces (as presented in Figure 5.12): 1) The ultra-low CAH inhibits initial bacterial attachment. 2) The attached bacteria exhibit a planktonic state when they contact with a liquid or liquid surface (i.e., dominated by proliferation with no little or EPS production). 3) Bacterial cells are unable to establish stable, strong interactions with liquid surfaces, resulting in detachment from the surface during growth or by the action of very gentle external forces. 4) Some bacteria will exist in the holes in roughened surface which is difficult to detach. This mechanism would explain why we did not observe cell clusters or biofilms on silicone oil infused roughened PDMS surface even after 2 days, 7 days and 14 days of culture in static and dynamic conditions.

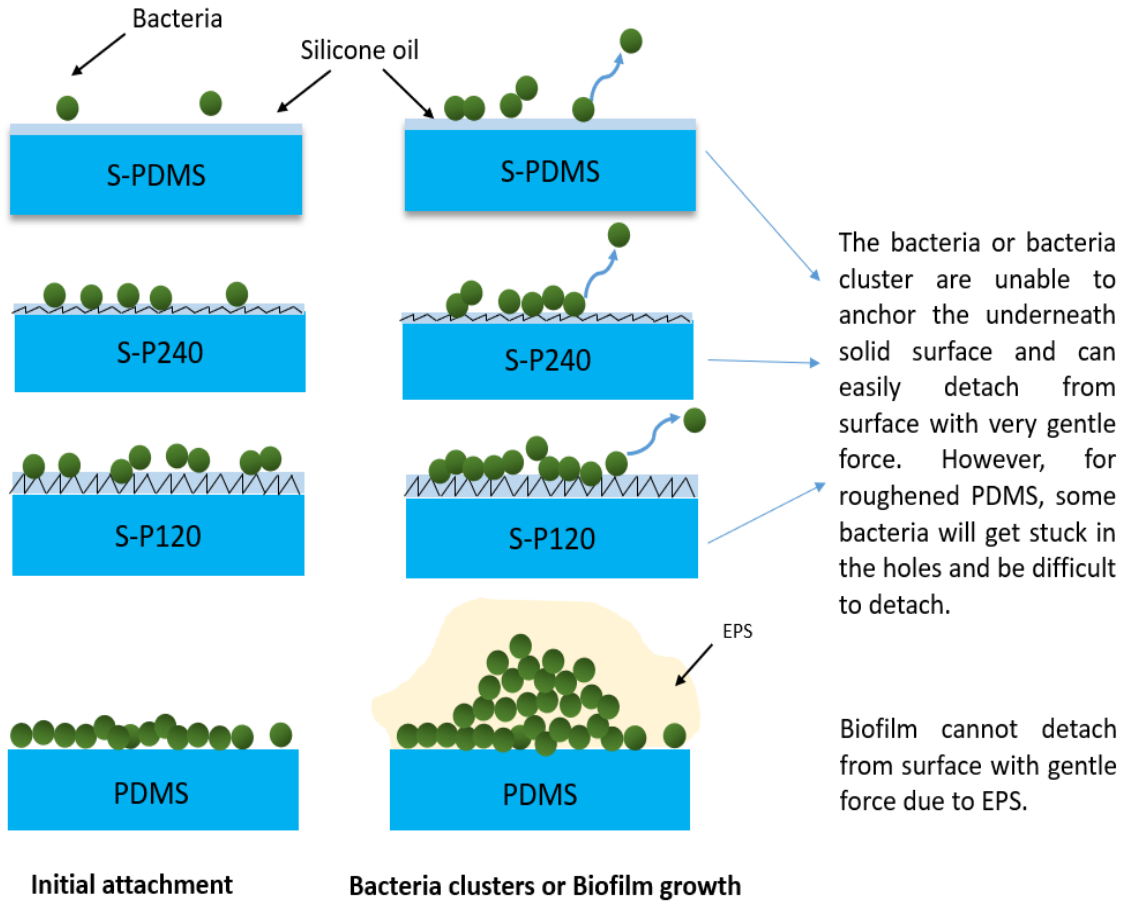

Figure 5.12 Schematic diagram of bacteria attachment on S-PDMS, S-P240, S-P120 and PDMS surfaces.

5.4 Conclusion

In summary, PDMS surfaces roughened with different silicone oil thicknesses showed bacterial adhesion during the 14-day culture of *S. epidermidis* and PAO1 under static conditions. There was a significant difference for plain PDMS, P240 and P120 surfaces ($p<0.01$). Under the same roughness, the thicker the oil layer, the harder it is for bacteria to attach to the surface. While under the same oil thickness, the rougher the surface, the easier it is for bacteria to attach to the surface. It indicated that CAH is affected by oil thickness, and it influenced bacterial adhesion on the surface.

However, in dynamic conditions, due to the wall shear stress induced oil loss which changed the surface wettability, after long-term bacterial culture (7, 14 days), the bacterial aggregates or clusters and biofilms are formed but it remained less than that in the plain surfaces.

Although the silicone oil-infused PDMS surface shows good anti-biofilm resistance in the static bacterial culture condition, if the fluid with high shear stress (>0.1 Pa), it will reduce the anti-biofilm ability. To get the more stable anti-biofilm surfaces, we fabricated two liquid-like solid surfaces (Slippery Omnipobic Covalently Attached Liquid-like (SOCAL) surface, and Polyethylene glycol (PEG) surface). The details are shown in the following chapter.

6 Antibiofilm performance of liquid-like solid surfaces and Sliver nanoparticles coated surfaces

6.1 Introduction

Silver (Ag) is known for its antimicrobial activity against a broad spectrum of pathogenic microorganisms [287], which has been used since ancient times for its medicinal properties. The activity and applications of AgNPs are now being explored in medical research [287]. AgNPs are potent nonspecific antimicrobial agents that inhibit the growth of a broad spectrum of bacterial and fungal species in planktonic form [288]. Their antibacterial activity is attributed to the unique physicochemical properties of AgNPs, such as high surface area, mass ratio, high reactivity, and size in the nanometer range, which endow them with major advantages of developing alternative-resistant microorganisms [288]. Although previous studies reported the embedding of AgNPs into novel composites produced by grafting acrylamide onto polyethersulfone fibers, there is a lack of comparisons in both static and dynamic conditions to slippery surfaces.

Polyethylene glycol (PEG) is a polyether compound consisting of repeating ethylene oxide units [289]. It is a safe compound with a wide range of uses including food additives, pharmaceutical excipients, and stealth coatings in biomedical applications to reduce nonspecific binding and evade the human immune system. And PEG surface has a small CAH like SOCAL, and the difference from SOCAL is hydrophilicity, so in this study, we also performed the test on the PEG surface with a different CAH. As AgNPs are commercially used antimicrobial surfaces. We also prepared AgNPs-coated PDMS as comparisons.

In this study, we fabricated two slippery surfaces (Slippery Omnipobic Covalently Attached Liquid-like (SOCAL) surface, and Polyethylene glycol (PEG) surface) with very low contact angle hysteresis and used AgNPs-coated PDMS as comparisons. We set the different time scales of 2 hours, 2 days, 7 days, and 14 days both in static and dynamic bacterial culture for anti-biofilm test against *Staphylococcus epidermidis* and *Pseudomonas aeruginosa*. The surface wettability was evaluated by measuring the water contact angle and contact angle hysteresis. Due to the limit of the dimension of the prepared

samples not being suitable for the critical point drying (CPD) chamber and the damage to the surface of using the HMDS (Hexamethyltiisilizane) drying method, we only take the confocal images in the present work.

6.2 Methodology

6.2.1 SOCAL surface

The SOCAL surface fabrication method can be seen in Chapter 3.1.3.

To ensure that PDMS was under suitable control for SOCAL surfaces, the surface chemistry of the two materials was assessed by the X-ray photoelectron spectroscopy (XPS) spectrum analysis (Figure 6.1). The XPS of the SOCAL coating prepared by such a dip coating approach was similar to that of PDMS [290]. SOCAL was claimed to be a liquid-like coating which may be expected to be softer than solid PDMS with the lowest crosslinking density [291].

6.2.2 PEG surface

The PEG surface fabrication method can be seen in Chapter 3.1.4.

6.2.3 AgNPs-coated PDMS surface

The AgNPS-coated PDMS surface can be seen in Chapter 3.1.5.

To confirm the AgNPs coating on the surface, we imaged the samples under SEM to measure the single AgNP diameter range and the coating thickness (Figure 6.2). SEM along with energy dispersive spectroscopy (EDS) were employed to identify the presence of gunshot residues (GSR) by the combined information of the morphology and chemical composition of individual particles. The percentage of silver mass on the original AgNPs-coated PDMS is shown in Figure 6.3.

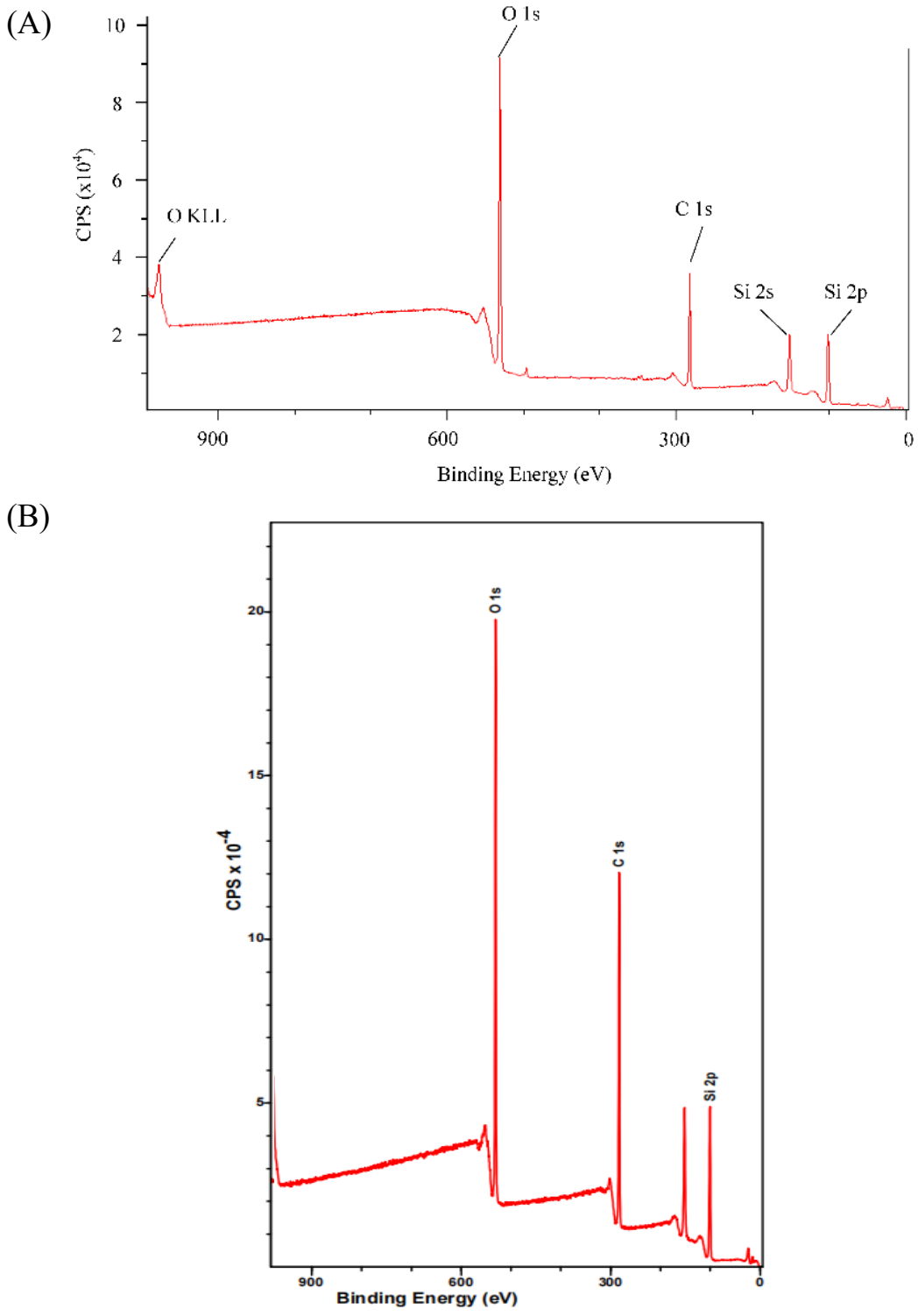

Figure 6.1 The XPS spectrum of (A)SOCAL, (B) PDMS.

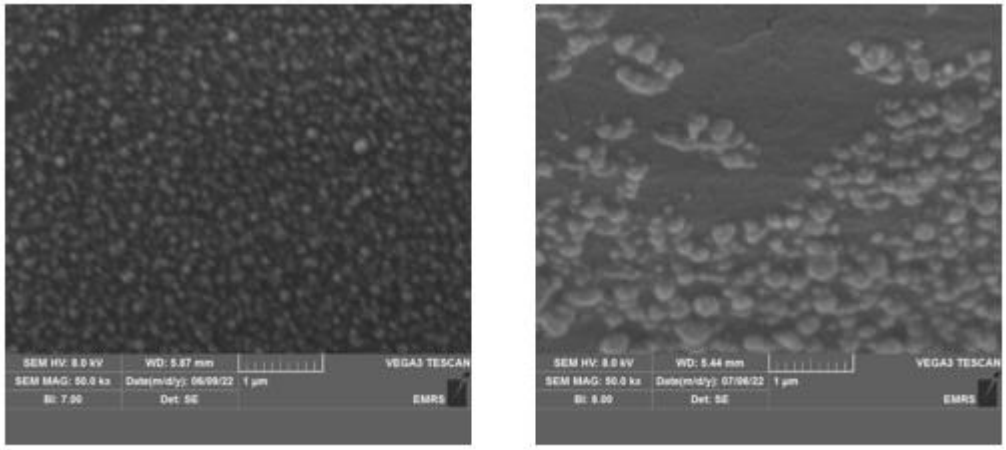

Figure 6.2 The SEM images of AgNPs on PDMS surface (A) 0° tilted, the single AgNP diameter 60nm~140nm, (B) 45° tilted, the coating average thickness ~200nm. In all cases, 5 images were analysed by ImageJ.

6.2.4 Confocal microscope analysis

The surfaces after bacterial adhesion assay, were gently rinsed three times with Phosphate Buffered Saline (PBS, pH=7.4) to remove loosely adhered bacteria. After that, samples were directly observed by NikonA1 upright confocal microscope with a 20x objective lens. As SOCAL, PEG, and AgNPs-coated PDMS surfaces demonstrated excellent resistance against biofilm formation under either static or dynamic conditions, we only need to acquire 2D confocal images on each surface. Then quantified the surface coverage by using ImageJ and covert it to the total biomass.

6.2.5 Statistical analysis

Data are represented as mean values with standard error. T-test assuming unequal variations was applied and $p < 0.05$ was considered statistically significant in this study.

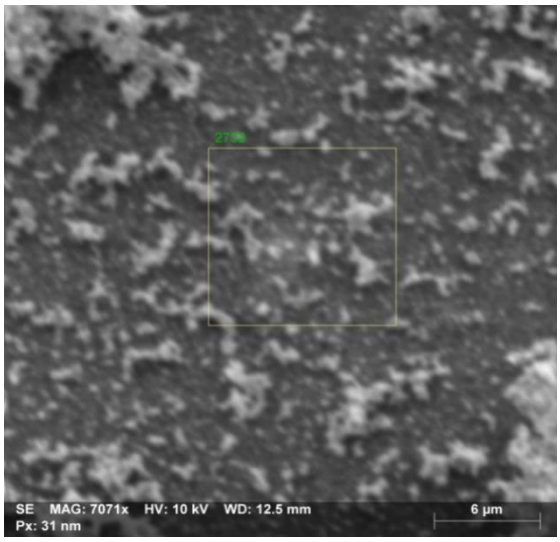

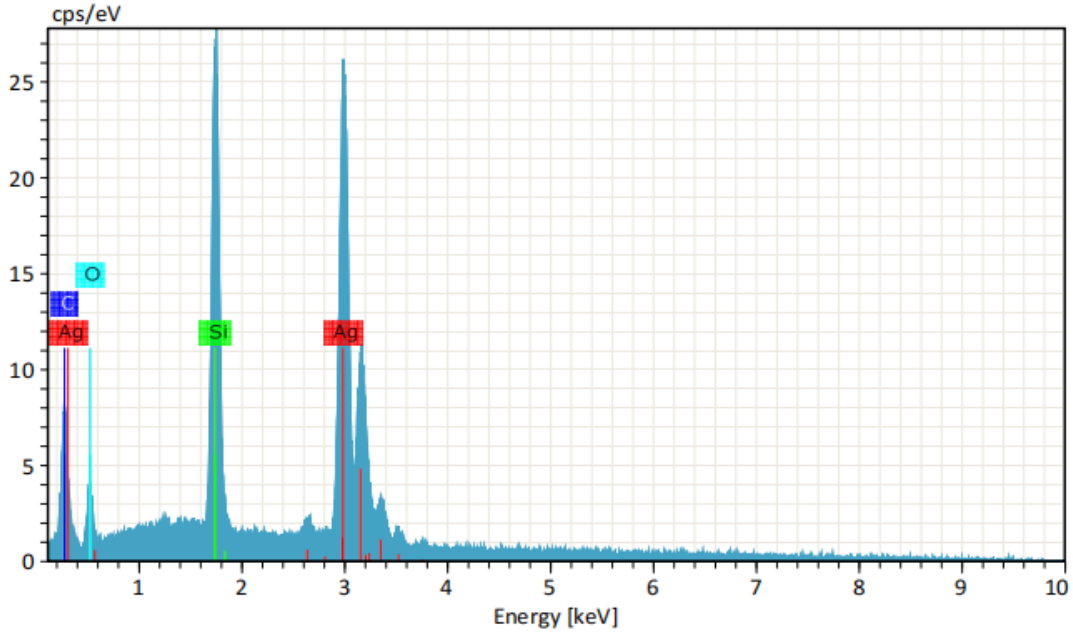

Element	At. No.	Line s.	Netto	Mass [%]	Mass Norm. [%]	Atom [%]	abs. error [%] (3 sigma)	rel. error [%] (3 sigma)
Carbon	6	K-Serie	5185	1.56	3.61	16.11	0.80	51.46
Oxygen	8	K-Serie	3117	1.74	4.03	13.49	0.97	55.80
Silicon	14	K-Serie	35289	7.52	17.39	33.17	1.01	13.39
Silver	47	L-Serie	74821	32.42	74.96	37.22	3.34	10.29
			Sum	**43.25**	**100.00**	**100.00**		

Figure 6.3 SEM image and the corresponding EDS analysis of silver nanoparticles.

6.3 Results and discussion

6.3.1 Surface wettability

The static water contact angle (CA) on SOCAL, PEG1, PEG2 and AgNPs-coated PDMS surfaces were measured in Table 6.1 (Figure 6.4). For the SOCAL sample and AgNPs-coated PDMS, the CA value on the surface indicates they are hydrophobic and AgNPs-coated PDMS showed that surface nanoparticles significantly enhanced the surface hydrophobicity. For PEG1 and PEG2 CA value indicates they are hydrophilicity. Contact Angle Hysteresis (CAH) indicating slip (water-repellence) is measured using the dynamic CA method (increasing or decreasing the volume of a water droplet by using a needle). CAH of the SOCAL, PEG1, PEG2 and AgNPs-coated PDMS is shown in Table 6.1 where both SOCAL and PEG1 have very low CAH. The thickness of SOCAL measured by ellipsometry was 3.9 ± 0.6 nm which is consistent with that previously reported results [286] and such a thickness of SOCAL is important to achieve CAH below 3° [286]. The CAH of PEG1 is around 6 times smaller than PEG2, which may affect the antibiofilm performance. Although the CAH of AgNPs-coated PDMS is close to the plain PDMS, there is the distinct antibacterial mechanism which is detailed explained in Chapter 2.8.3.

Table 6.1 The static contact angle and the contact angle hysteresis of DI water droplets on different slippery surfaces and AgNPs-coated PDMS surfaces. Data represent the mean and SD of five independent measurements.

Surface	Contact angle (°)	Advancing angle (°)	Receding angle (°)	Contact angle hysteresis (°)
SOCAL	104.9 ± 1.6	105.1 ± 0.8	103.0 ± 1.3	2.0 ± 1.0
PEG1	38.04 ± 0.93	38.04 ± 0.93	36.99 ± 0.8	1.1 ± 0.40
PEG2	40.97 ± 12.55	37.93 ± 0.95	31.71 ± 1.03	6.20 ± 0.54
AgNPs	125.14 ± 2.20	124.43 ± 2.54	108.24 ± 2.09	16.20 ± 1.90

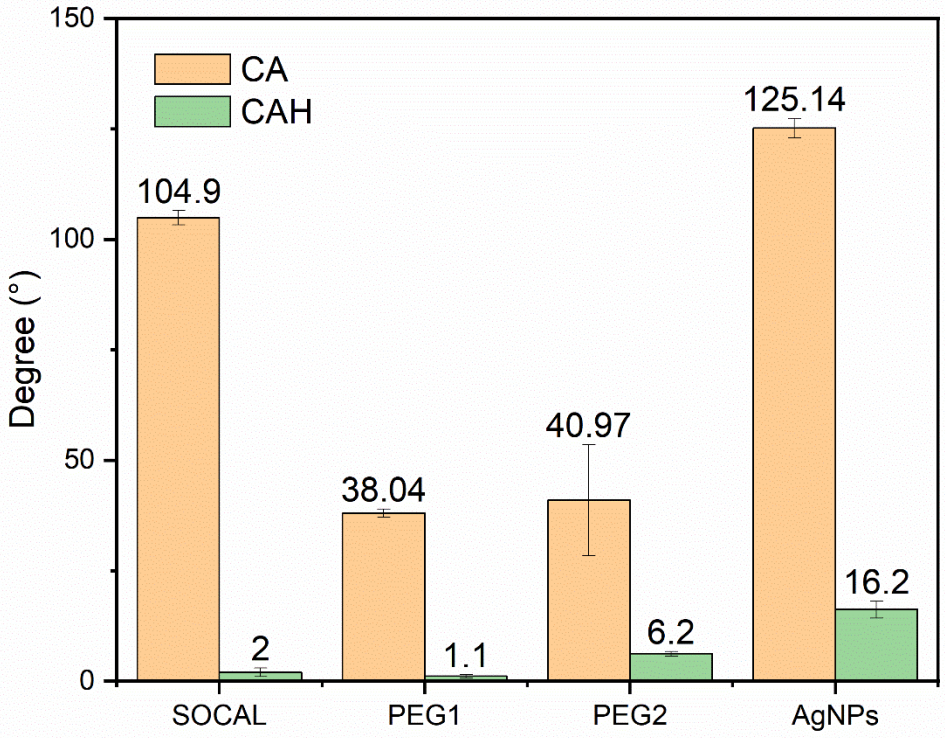

Figure 6.4 The CA and CAH for SOCAL, PEG1, PEG2 and AgNPs-coated PDMS surfaces.

6.3.2 Anti-biofilm tests against *Staphylococcus epidermidis*

Figure 6.5 displays the confocal images after the growth of *S.epidermidis* for 2 hours, 2 days, 7 days and 14 days on SOCAL, PEG1, PEG2 and AgNPs-coated PDMS surfaces in static condition. After 2 hours of culture, only sparse and isolated bacterial cells were present on SOCAL, PEG1 and PEG2 surfaces. Based on the data quantification, the total biomass on SOCAL is 2 orders of magnitude larger than PEG1 (p= 2.78e-08) and PEG2 (p= 1.28e-07). Although the AgNPs-coated PDMS surface was covered by bacteria with some bacterial aggregates or clusters, the total biomass is 1 order of magnitude larger than SOCAL (p=2.04E-12), 77.39% ± 13.81% of the bacteria is dead (Figure 6.7).

After 2 days of culture, there is only single bacterial adhesion on SOCAL, PEG1 and PEG2 surfaces. The total biomass on SOCAL is 2 and 1 orders of magnitude larger than PEG1 (p=4.86e-08) and PEG2 (p=4.03e-07), respectively. While the total biomass of AgNPs-

coated PDMS is 1 order of magnitude larger than SOCAL (p=5.59E-10), 73.28% ± 10.19% of the bacteria is dead (Figure 6.7).

After 7 days of culture, the bacterial aggregates or clusters formed on the SOCAL surface but PEG1 and PEG2 surfaces still show single bacterial attachment. The total biomass of SOCAL is 1 order of magnitude larger than PEG1 (p=2.13e-10) and PEG2 (p=2.75e-10) and 1 order of magnitude less than AgNPs-coated PDMS (p=0.0594). The total biomass of AgNPs-coated PDMS is 5 times less than the 2-day culture and the percentage of dead bacteria dropped to 33.45% ± 14.80%. This may be because some weakly adhered bacteria were washed away and the concentration of silver ions in the liquid was diluted when the fresh culture medium was changed.

After 14 days of culture, the SOCAL surface was covered by a large number of bacterial aggregates or clusters, and the PEG1 and PEG2 surfaces started to form the bacterial aggregates or clusters. The total biomass of the SOCAL surface is 2 orders of magnitude larger than PEG1 (p= 2.24e-09) and PEG2 (p= 2.45e-09). And the total biomass of AgNPs-coated PDMS is 2.5 times larger than that of SOCAL (p= 7.34e-04). The percentage of dead bacteria after 14 days of culture on AgNPs-coated PDMS is 26.62% ± 5.98%.

For the dynamic bacterial culture, we still chose the wall shear stress (τ_w) of 0.007 Pa consistent with the previous experiments. Throughout the experiment (up to 14 days), only sparse and isolated bacteria (with visible EPS) were observed on the SOCAL, PEG1, PEG2, and AgNPs-coated PDMS surfaces under flow conditions. By quantifying the biomass on these surfaces based on confocal imaging (Figure 6.6), it was found that the total biomass on SOCAL is 1 order of magnitude larger than PEG1 (p=2.57e-10) and PEG2 (p= 1.01e-09), and 2 orders of magnitude less than AgNP-coated PDMS (p= 2.37e-11) under 2 hours culture. The percentage of dead bacteria after 2 hours of culture on AgNPs-coated PDMS is 65.01% ± 17.14% (Figure 6.7).

After 2 days of culture, the total biomass on SOCAL is 2 and 1 order of magnitude larger than PEG1 (p= 6.33e-07) and PEG2 (p= 2.66e-04), respectively, and 2 orders of magnitude less than AgNP-coated PDMS (p= 5.59e-10). The percentage of dead bacteria after 2 days of culture on AgNPs-coated PDMS is 72.37% ± 13.66% (Figure 6.7).

After 7 days of culture, the total biomass on SOCAL is 2 and 1 order of magnitude larger than PEG1 (p= 1.92e-03) and PEG2 (p= 4.87e-02), respectively, and there was no significant difference with the AgNP-coated PDMS (p= 0.679). The percentage of dead bacteria after 7 days of culture on AgNPs-coated PDMS is 21.72% ± 17.25% (Figure 6.7).

After 14 days of culture, the total biomass on SOCAL is 2 orders of magnitude larger than PEG1 (p= 4.99e-11) and double that on PEG2 (p= 6.04e-06), and around twice larger than AgNP-coated PDMS (p= 3.58e-04). The percentage of dead bacteria after 7 days of culture on AgNPs-coated PDMS is 26.18% ± 5.20% (Figure 6.7).

When studying *S.epidermidis* colonization in static and flow conditions, the total biomass of these surfaces after 2 hours and 2 days in static culture is a bit larger than under dynamic culture. After 7 days and 14 days of culture, the total biomass under dynamic culture is larger than under static culture. Interestingly, unlike the AgNPs-coated PDMS surface performed in static conditions, in dynamic culture, its total biomass is continuously increased but less than in static culture. The percentage of dead bacteria on AgNPs-coated PDMS in dynamic conditions is smaller than in static conditions under the same culture period.

As the plain PDMS surface has similar surface chemistry characteristics to SOCAL, we regard it as a comparative control sample. To access the anti-biofilm performance of SOCAL and PEG surfaces, we also treated the S-PDMS (50μm) as a control group. The details of the plain PDMS and S-PDMS (50μm) surfaces are shown in Chapter 4 and Chapter 5, respectively. By quantifying the biomass on these surfaces from confocal imaging in static conditions, it was found that SOCAL and S-PDMS significantly reduced initial bacterial attachment (2 h) by 92 ± 3% and 99% ± 3%, respectively.

After 2 days, both SOCAL and S-PDMS (50μm) resulted in 3 and 4 orders of magnitude biomass reduction compared to PDMS, respectively. After 7 days, the total biomass of the SOCAL and S-PDMS (50μm) showed 4 orders of magnitudes less than PDMS. While, after 14 days, the total biomass of the SOCAL and S-PDMS showed 3 and 4 orders of magnitudes less than PDMS, respectively.

After long-term dynamic culture periods, there was no significant difference (p=0.67) between biomass on SOCAL and S-PDMS (50μm) surfaces after 7-day culture. After 14-day culture, the total biomass of the SOCAL was 2 and 3 orders of magnitudes less than S-PDMS (50μm) and PDMS surfaces, respectively. By the previous comparison between SOCAL and PEG, we can conclude that the anti-biofilm performance of the PEG surface with lower CAH (PEG1) is stronger than that of the S-PDMS (50μm) surface, both statically and dynamically.

(A)

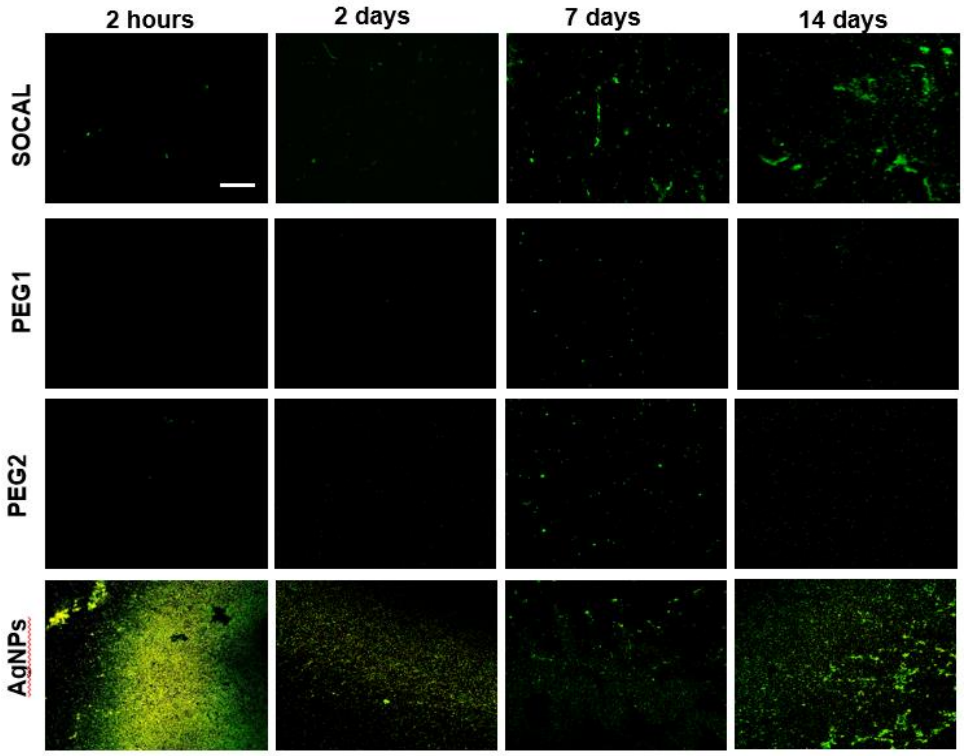

(B)

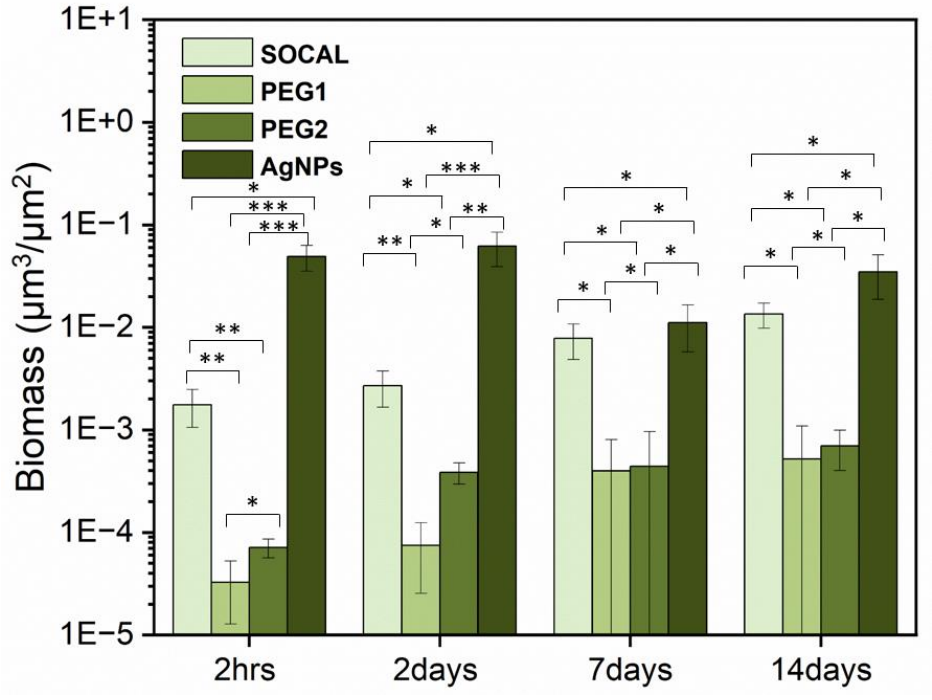

Figure 6.5 (A) Representative confocal images and (B) biomass of the growth of *S. epidermidis* FH8 on SOCAL, PEG1, PEG2 and AgNPs-coated PDMS for 2 h, 2 days, 7 days and 14 days in static cell culture cell culture. Scale bar = 50 μm for all images. In all cases, 10 images were analysed for each surface from 3 independent experiments. Values presented are mean ± SD. * $p<0.05$; ** $p<10^{-10}$; *** $p<10^{-15}$.

(A)

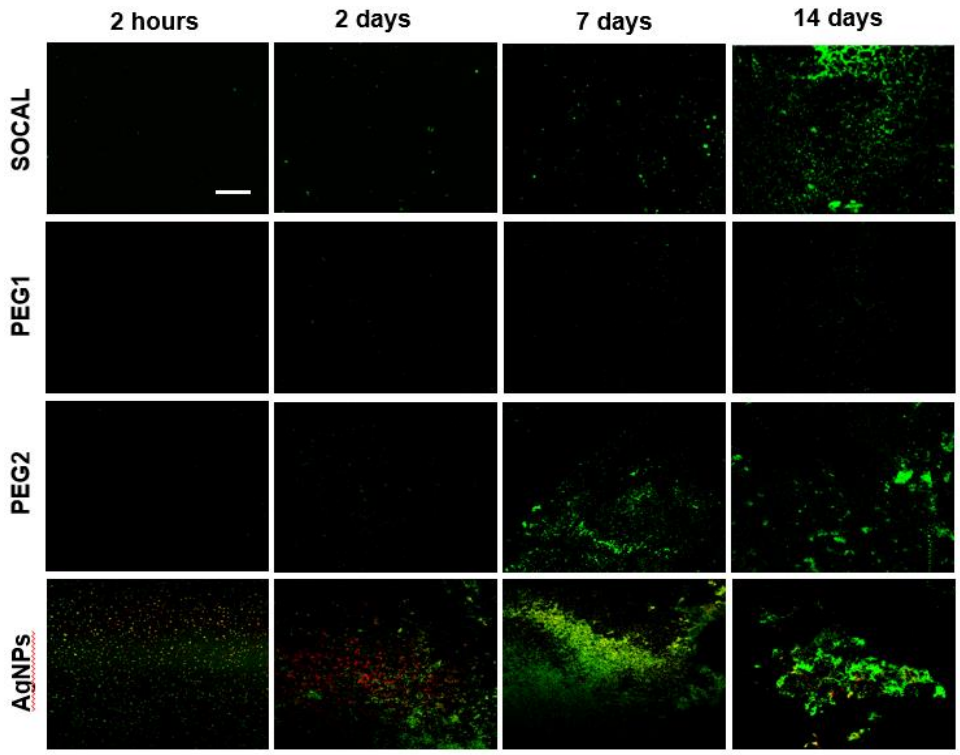

(B)

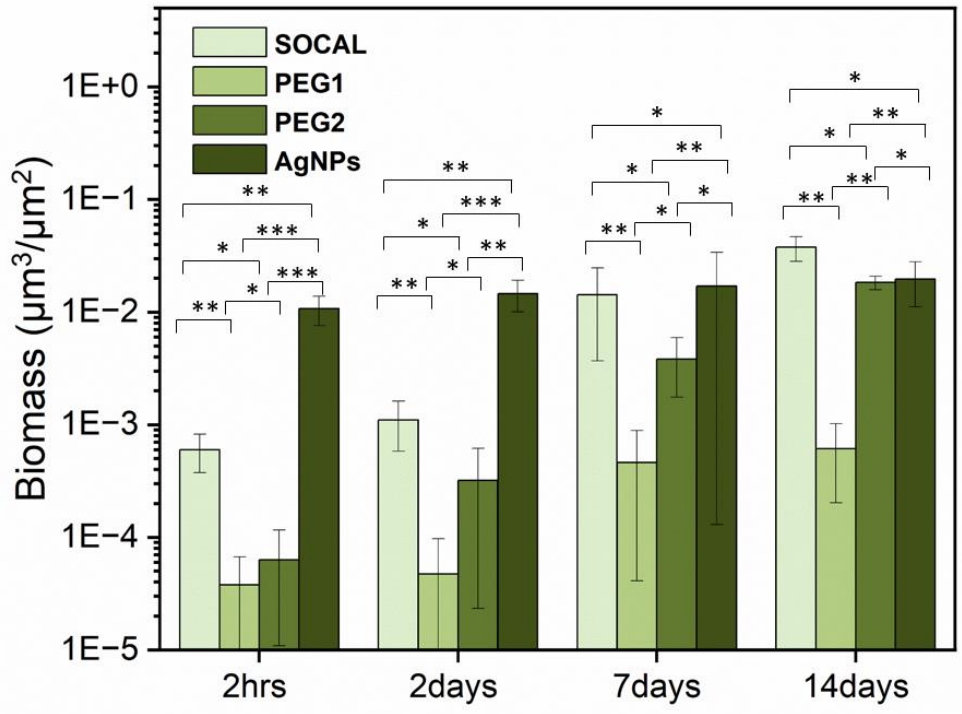

Figure 6.6 (A) Representative confocal images and (B) biomass of the growth of *S. epidermidis* FH8 on SOCAL, PEG<2, PEG>6 and AgNPs-coated PDMS for 2 h, 2 days, 7 days and 14 days in dynamic cell culture cell culture. Scale bar = 50 μm for all images. In all cases, 10 images were analysed for each surface from 3 independent experiments. Values presented are mean ± SD. * * $p<0.05$; ** $p<10^{-10}$; *** $p<10^{-15}$.

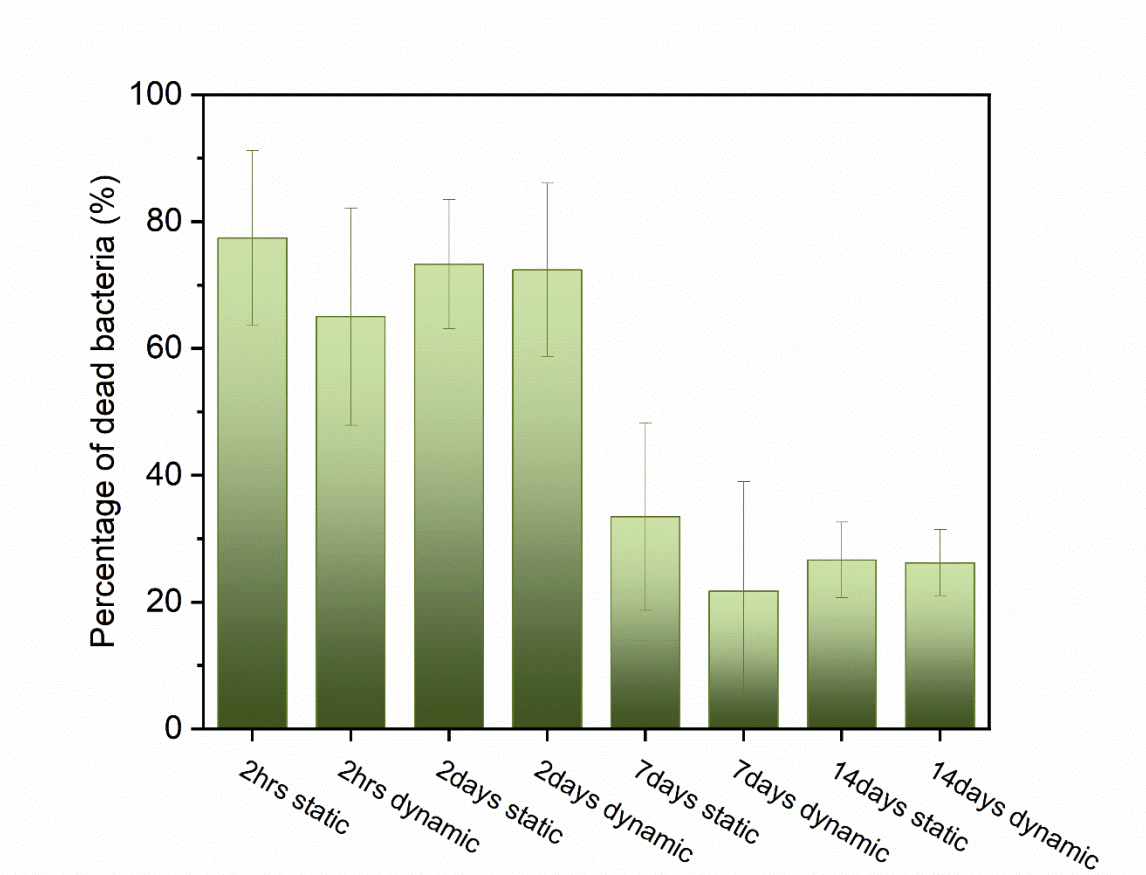

Figure 6.7 The percentage of dead bacteria on AgNP-coated PDMS surface for *S.epidermidis* FH8. In all cases, 10 images were analysed for each surface from 3 independent experiments.

6.3.3 Anti-biofilm tests against *Pseudomonas aeruginosa*

We first cultured PAO1 on SOCAL, PEG1, PEG2 and AgNPs-coated PDMS surfaces in static conditions. The PAO1 biomass appeared mucoid when these samples were removed from the petri dish or well plate. However, over a long-term (up to 14 days) culture, only bacterial adhesion was found on these surfaces (Figure 6.8).

After 2 hours of culture, there were sparse and isolated bacterial cells presented on SOCAL, PEG1, PEG2 and AgNPs-coated PDMS surfaces. By quantifying the data from confocal images, the total biomass on SOCAL is 1 order of magnitude less than PEG1 (p= 2.15e-09), PEG2 (p= 3.92e-11), and AgNPs-coated PDMS (p=5.19e-04). The percentage of dead bacteria after 2 hours of culture on AgNPs-coated PDMS is 90.45% ± 2.40% (Figure 6.10). For example, AgNPs coated with chitosan exhibited high inhibitory activity against *Staphylococcus aureus*, *Pseudomonas aeruginosa*, and *Salmonella typhimurium*, with up to 95% reduction in colony numbers after 4 hours of exposure [292]. Hydrogels were formulated with in situ synthesized AgNPs by using lignin and polyvinyl alcohol. The resulting product exhibited high antimicrobial activity against *E. coli* and *S. aureus*, killing almost 100% of the bacteria after 10 hours of treatment [293].

After 2 days of culture, on SOCAL, PEG1 and PEG2 surfaces only single bacterial adhesion was observed. The total biomass on SOCAL is 1 order of magnitude less than PEG1 (p=6.79e-09) and PEG2 (p=2.79e-13). The total biomass of AgNPs-coated PDMS is 2 orders of magnitude larger than SOCAL (p=2.17e-6) with 55.59% ± 10.95% dead bacteria (Figure 6.10).

After 7 days of culture, the total biomass of SOCAL is approximately 4 times larger than PEG1 (p=7.53e-09) and PEG2 (p=5.61e-13). In this case, the total biomass of AgNPs-coated PDMS is 1 order of magnitude less than SOCAL (p=2.17e-01) with no significant difference. Since the adhesion between EPS and the coating is stronger than that between the coating and the PDMS surface, it leads to peeling off the coating easily when changing the fresh medium. Despite that, silver ions are still present in the solution to kill bacteria. The percentage of dead bacteria dropped to 31.92% ± 12.47% (Figure 6.10).

After 14 days of culture, the total biomass of SOCAL is half of the PEG1 (p=2.07e-05), and 2 orders of magnitude less than PEG2 (p=7.45e-06) and AgNPs-coated PDMS

(p=7.86e-08). The percentage of dead bacteria after 14 days of culture on AgNPs-coated PDMS is 0.66% ± 0.53% (Figure 6.10). Because most of the AgNPs coating was washed away after 3 times of fresh medium replacement during the 14-day culture, it resulted in a large area of bacterial aggregation and reduced bactericidal ability.

Figure 6.9 displays the confocal images after the growth of PAO1 for 2 hours, 2 days, 7 days and 14 days on SOCAL, PEG1, PEG2 and AgNPs-coated PDMS surfaces in dynamic conditions. Notably, the fresh medium is continuously pumped into the flow cell, which can prevent the EPS from being produced in large quantities like in static conditions. Thus, the AgNPs coating was maintained after 2 hours and 2 days of culture. After 7 days and 14 days of culture, however, a small amount of the coatings is washed away through the tube. Silver ions can also move freely in the flow chamber along with the identical fluid, which can kill the bacteria better. Therefore, the percentage of dead bacteria in dynamic conditions is a bit larger than that in static conditions, except in the 2 hours culture (p=0.049 (between static and dynamic 2 hours culture)).

After 2 hours of culture, the total biomass on SOCAL is 2 orders of magnitude less than PEG1 (p= 1.46e-07), PEG2 (p= 2.39e-03), and 1 order of magnitude less than AgNPs-coated PDMS (p=3.39e-12). The percentage of dead bacteria after 2 hours of culture on AgNPs-coated PDMS is 87.16% ± 4.30% (Figure 6.10).

After 2 days of culture, the total biomass on SOCAL is 1 order of magnitude less than PEG1 (p= 1.66e-09), PEG2 (p= 4.74e-07), and 2 orders of magnitude less than AgNPs-coated PDMS (p=7.34e-11). The percentage of dead bacteria after 2 hours of culture on AgNPs-coated PDMS is 61.68% ± 15.14% (Figure 6.10).

After 7 days of culture, the total biomass on SOCAL is 1 order of magnitude less than PEG1 (p= 8.48e-06), PEG2 (p= 2.53e-08), and AgNPs-coated PDMS (p=3.71e-11). The percentage of dead bacteria after 2 hours of culture on AgNPs-coated PDMS is 41.00% ± 12.24% (Figure 6.10).

After 14 days of culture, the total biomass on SOCAL is 3 times less than PEG1 (p= 5.65e-06), 1 order of magnitude less than PEG2 (p= 5.66e-06) and AgNPs-coated PDMS

(p=1.37e-08). The percentage of dead bacteria after 2 hours of culture on AgNPs-coated PDMS is 36.15% ± 12.28% (Figure 6.10).

Figure 6.9 demonstrated that the percentage of dead bacteria decreased with increasing incubation time both in static and dynamic conditions. As PAO1 is Gram-negative bacteria that have narrower cell walls, the AgNPs can easily penetrate the bacterial cell wall and subsequently alter the structure of cell membranes, resulting in cell damage. Compared to *S.epidermidis* (Figure 6.8), the percentage of dead bacteria after 2 hours of static and dynamic conditions of PAO1 is around 12% and 22% higher than *S.epidermidis*. However, after 2 days, 7 days and 14 days of culture, the percentage of dead bacteria of PAO1 is smaller than *S.epidermidis*. It may be because the number of EPS produced by PAO1 is much larger than that of *S.epidermids*, and EPS protects bacteria from the invasion of AgNPs. In static and dynamic culture conditions, sliver nanoparticles performed differently in *S.epidermidis* and PAO1 culture medium as seen in Appendix Figure S. After 2 hours of static culture, the AgNPs coating existed well in both bacteria. After 2 days and 7 days of static culture, when using PBS to wash the samples in PAO1, the AgNPs coating was peeled off with the adhesive EPS. But in *S. epidermidis*, there is an intact coating. After 14 days of static culture, part of the AgNP coatings was removed in *S. epidermidis*. Comparing 7 days and 14 days of dynamic culture, the coating was removed only for the 14 days of PAO1 culture.

Comparing PAO1 colonization in static and flow conditions, the total biomass of SOCAL and PEG1 in static conditions is less than under dynamic culture at the same culture periods. After 7 days of culture, the total biomass of PEG2 surfaces in dynamic conditions is 1.2 times larger than in static. In 14-day culture, the total biomass of PEG2 surfaces in dynamic conditions is 2.5 times larger than that in static. It indicated that CAH is an important parameter affecting bacterial adhesion.

Furthermore, biomass on SOCAL and S-PDMS (50μm) surfaces were 2 orders of magnitude less than the plain PDMS surface after 2 hours of bacterial static culture. After 2 days, compared to the PDMS control surface, the total biomass reduction on the SOCAL and S-PDMS (50μm) surfaces was over 4 orders of magnitude. After 7 days, the total biomass reduction on both SOCAL and S-PDMS (50μm) surfaces was almost 4 orders of

magnitude less, compared to the PDMS control surface. Even after 14 days, the total biomass reduction on both SOCAL and S-PDMS (50μm) surfaces was 4 and 5 orders of magnitude less, respectively, compared to the PDMS control surface. Even though there were significant differences ($p<0.05$) at 2 hours and 2 days, SOCAL and S-PDMS (50μm) surfaces performed equally well ($p=0.11$ for 2 hours; $p=0.54$ for 2 days) at retarding biofilm compared to the PDMS control. For dynamic bacterial culture, the total biomass of SOCAL surface was 1 order and 3 orders of magnitude less than S-PDMS (50μm) and PDMS surfaces after 7-day culture, respectively. After 14-day culture, the total biomass of SOCAL surface was 3 orders and 4 orders of magnitude less than S-PDMS (50μm) and PDMS surfaces, respectively. Similarly, through the comparison of SOCAL and PEG for culturing PAO1, the PEG surface is more likely to form bacterial aggregation than SOCAL and S-PDMS (50μm) surfaces.

The antibiofilm results of SOCAL and PEG surfaces with low CAH presented here were similar to other SLIPs reported in the seminal paper by Epstein et al. [51]. In their paper, SLIPS prevented 99.6% of *P. aeruginosa* biofilm formation over a 7-d period under both static and flow conditions. Other studies also demonstrated that SLIPs surfaces are capable of preventing biofilm formation by 1-3 orders of magnitudes for 1-7 days in static cultures [31, 60, 294, 295]. The antibiofilm results of both slippery surfaces in the present study compare well to commercial antimicrobial agent-coated materials used for catheters. For example, silver-coated silicone (PDMS) has been shown to reduce *P. aeruginosa* biofilm formation by ~97% when grown statically for 1 day, compared to pure silicone [296]. For silicone coated with antibiotics (e.g., rifampin/minocycline, vancomycin, or amikacin), particularly rifampin/minocycline, no significant bacterial colonization was found on these surfaces after seven days of static culture [297]. Therefore, the slippery surfaces presented here are possible alternatives to antibiotics, which will not cause the antimicrobial resistance but achieving equivalent antibiofilm performance.

(A)

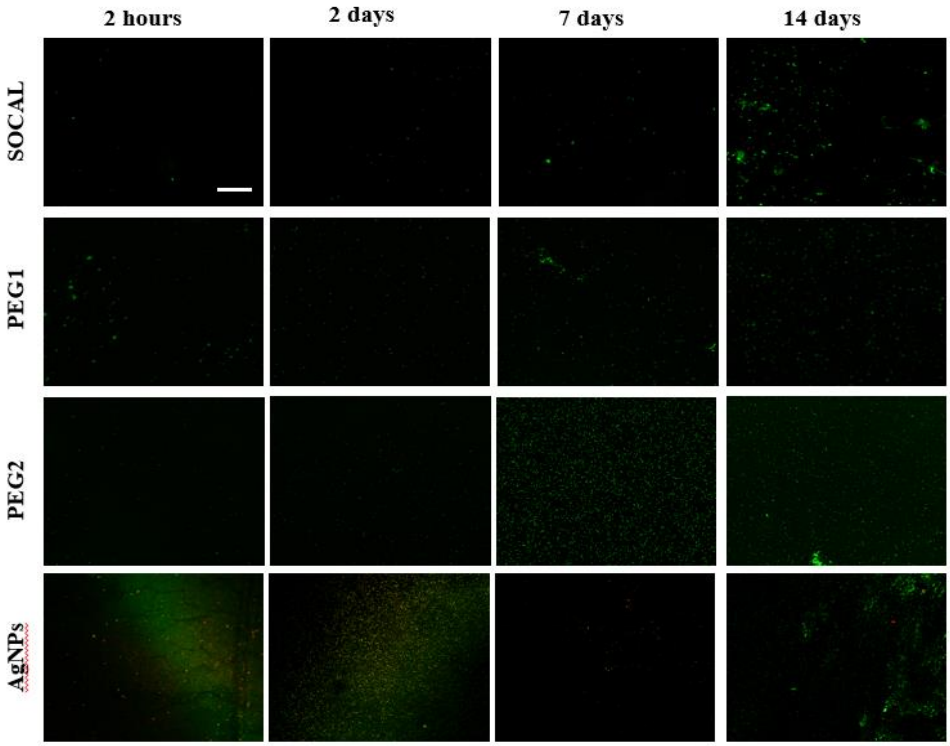

(B)

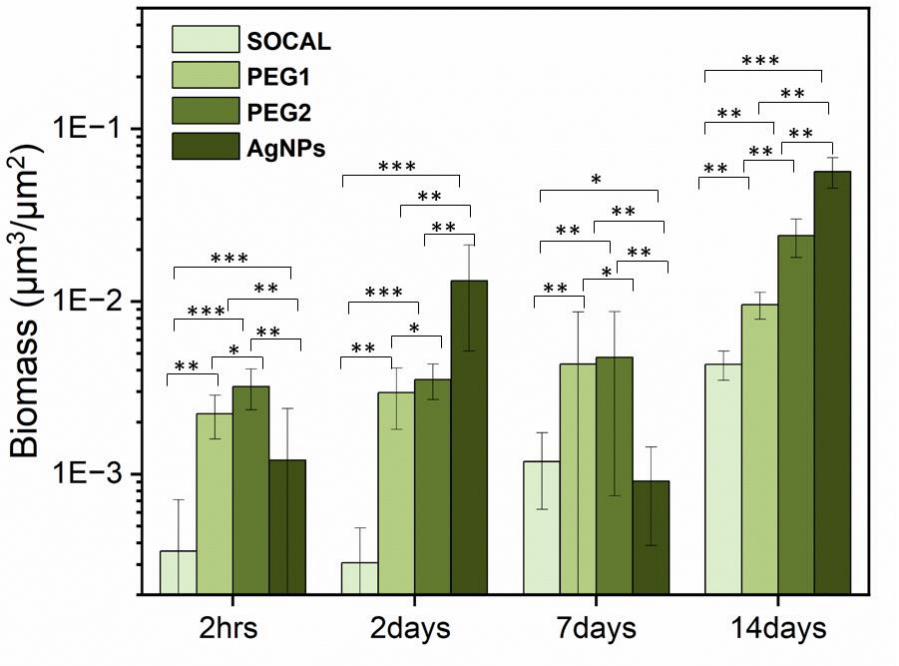

Figure 6.8 (A) Representative confocal images and (B) biomass of the growth of *Pseudomonas aeruginosa* PAO1 on SOCAL, PEG<2, PEG>6 and AgNPs-coated PDMS for 2 h, 2 days, 7 days and 14 days in dynamic cell culture cell culture. Scale bar = 50 µm for all images. In all cases, 10 images were analysed for each surface from 3 independent experiments. Values presented are mean ± SD. * $p<0.05$; ** $p<10^{-10}$; *** $p<10^{-15}$.

(A)

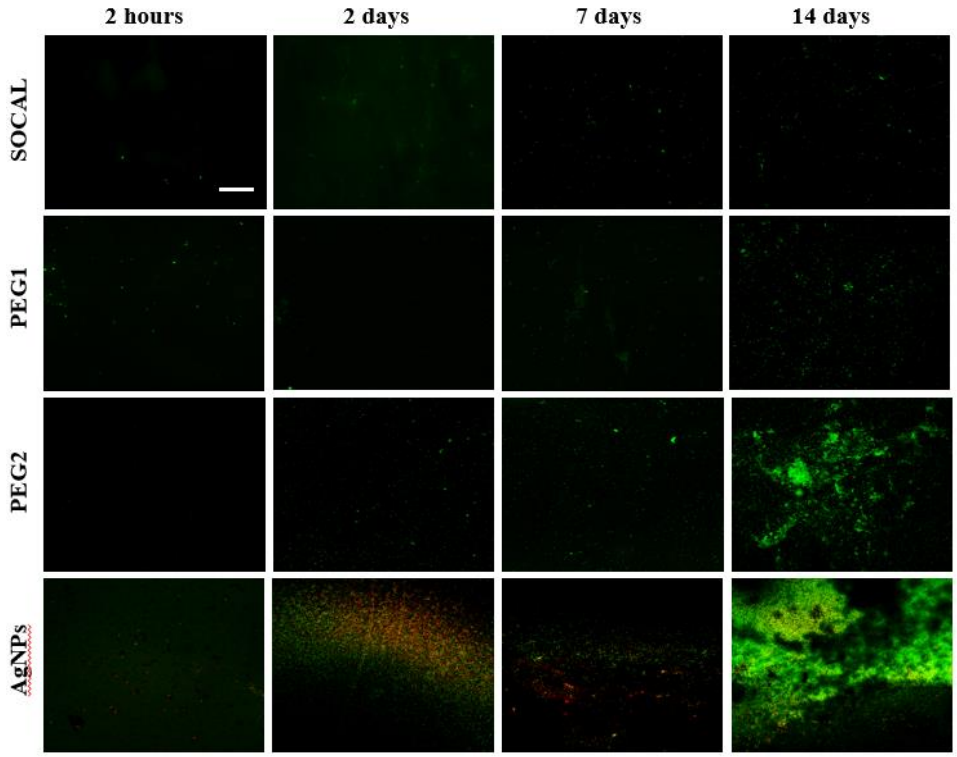

(B)

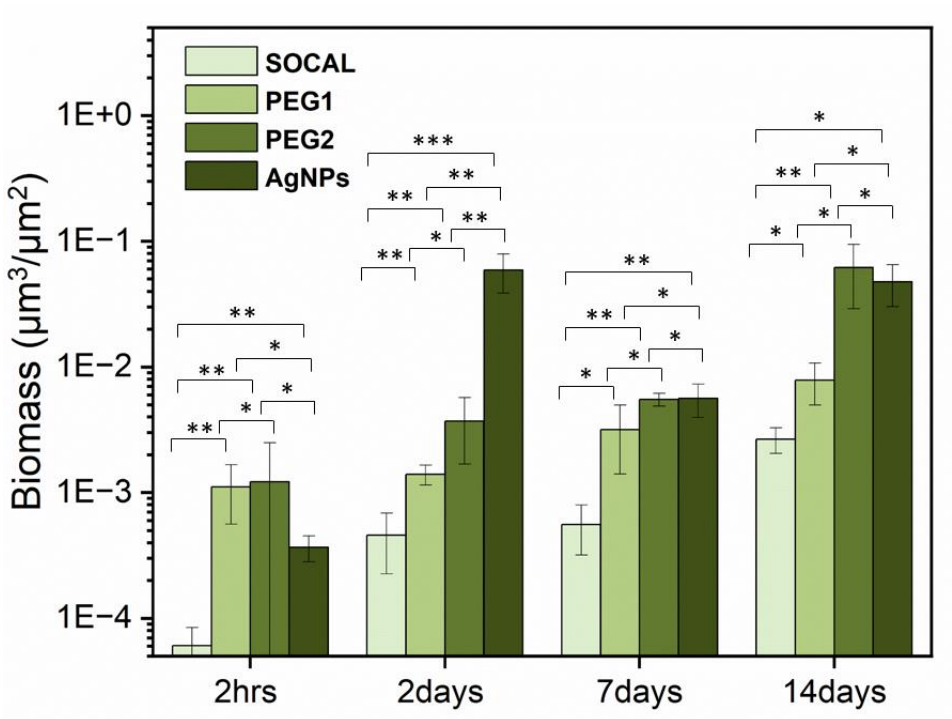

Figure 6.9 (A) Representative confocal images and (B) biomass of the growth of *Pseudomonas aeruginosa* PAO1 on SOCAL, PEG<2, PEG>6 and AgNPs-coated PDMS for 2 h, 2 days, 7 days and 14 days in dynamic cell culture cell culture. Scale bar = 50 μm for all images. In all cases, 10 images were analysed for each surface from 3 independent experiments. Values presented are mean ± SD. * $p<0.05$; ** $p<10^{-10}$; *** $p<10^{-15}$.

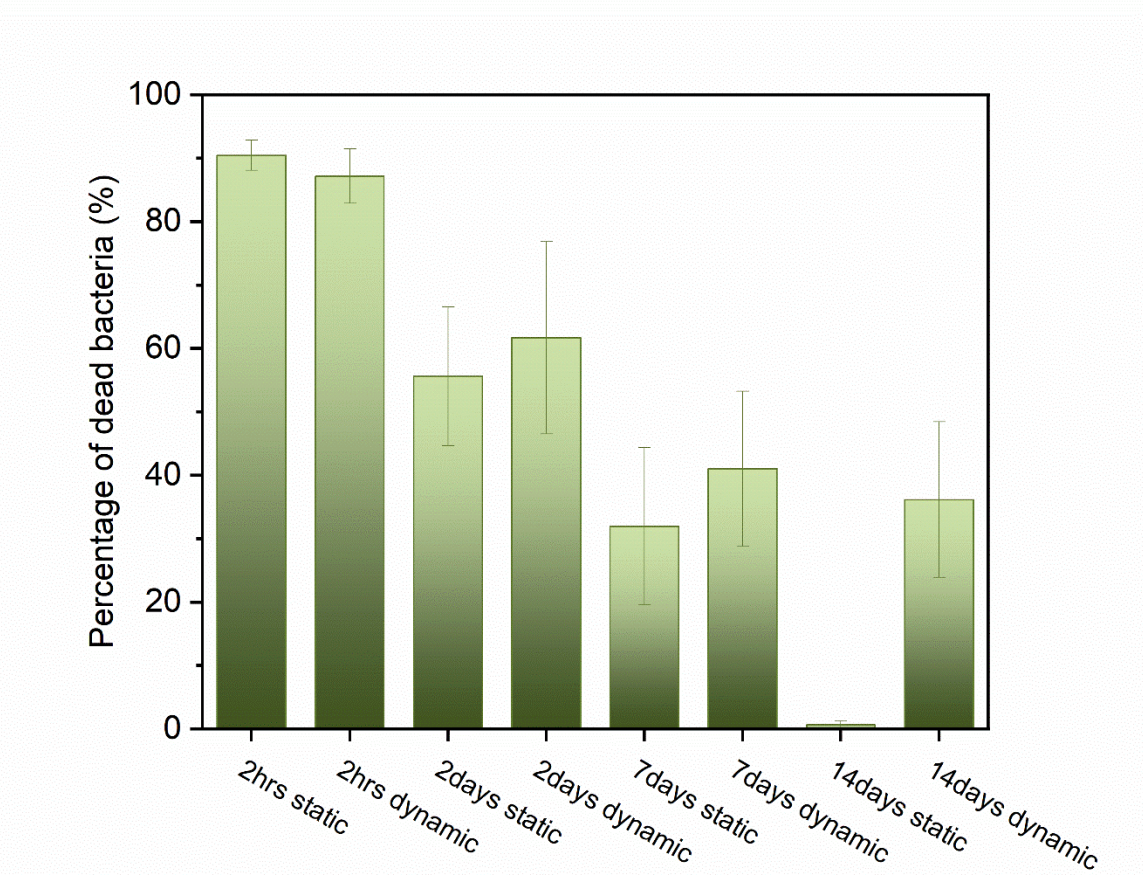

Figure 6.10 The percentage of dead bacteria on AgNP-coated PDMS surface for *Pseudomonas aeruginosa* PAO1. In all cases, 10 images were analysed for each surface from 3 independent experiments.

We propose the following antibiofilm mechanisms for liquid-like surfaces (as presented in Figure 6.11): 1) The ultra-low CAH inhibits initial bacterial attachment. 2) The attached bacteria exhibit a planktonic state when they contact with a liquid-like surface (i.e., dominated by proliferation with no little or EPS production). 3) Bacterial cells are unable to establish stable, strong interactions with liquid-like surfaces, resulting in detachment from the surface during growth or by the action of very gentle external forces. This mechanism would explain why we did not observe cell clusters or biofilms on SOCAL, PEG and AgNPs-coated PDMS surfaces even after 2 days, 7 days and 14 days of culture in static and dynamic conditions.

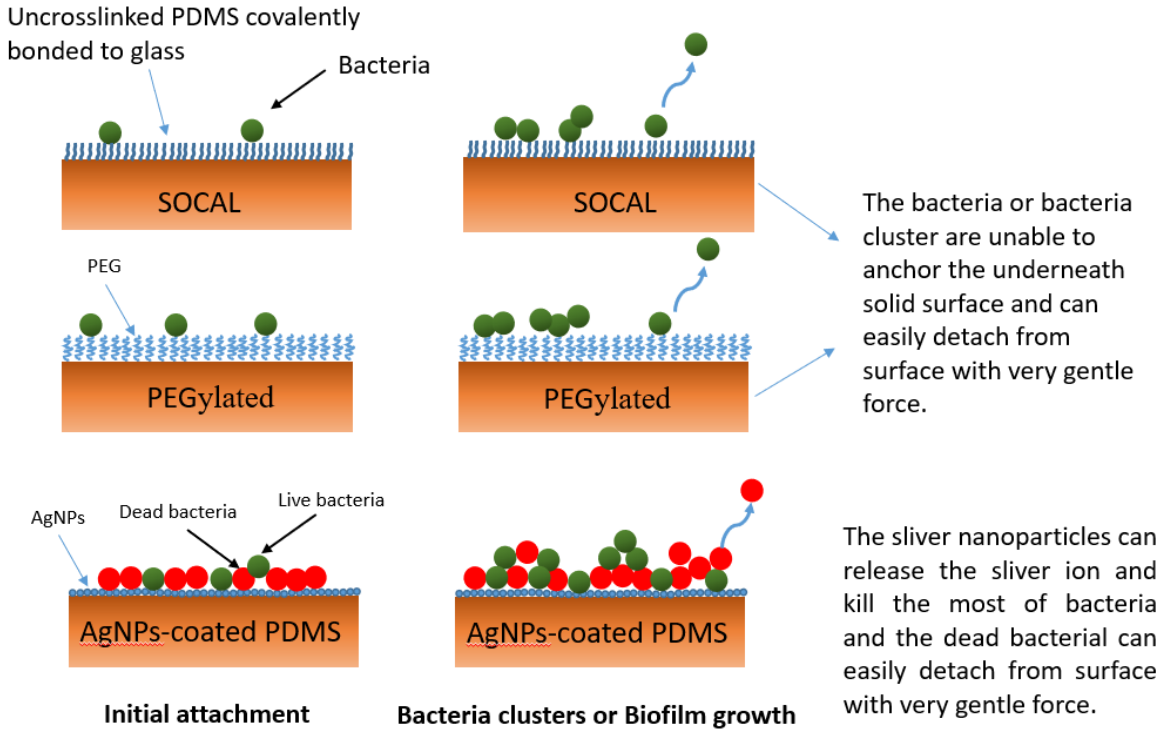

Figure 6.11 Schematic diagram of bacteria attachment on SOCAL (uncrosslinked PDMS covalently bonded to glass substrate), PEG and AgNPs-coated PDMS.

6.4 Conclusion

Both SOCAL and PEG surface with very low CAH (< 2 degrees) exhibited excellent resistance against biofilm for long-term culture periods either in static or dynamic conditions. The performance of the surfaces differs for different bacterial species (*S. epidermidis* and PAO1) due to the surface wettability. In summary, the liquid-like solid surface strategy of SOCAL and PEG shows promising results for applications where continuous flow is important, such as catheters and the transparency of visible light is another advantage of these materials, which adds value for potential use for medical devices requiring excellent optical transmission.

In addition, AgNPs-coated PDMS surface as commercial control sample also shows good anti-biofilm resistance. However, in the long-term bacterial culture process, the antibacterial ability will become weaker and weaker. Strains that produce abundant EPS (such as PAO1) can also affect the adhesion of the AgNPs-coating on the PDMS surface.

7 Conclusion and Future Work

7.1 Conclusions

In this Ph.D. project, we have studied the roughness effect of *S. epidermidis* or *P. aeruginosa* biofilm growth in both static and dynamic cultures. Then a wide range of antibiofilm surfaces, including SLIPs with different oil thicknesses atop the surface, SOCAL, PEG and AgNPs-coated PDMS were fabricated. Their anti-biofilm efficacies were evaluated against clinical bacterial strains (*S. epidermidis* or *P. aeruginosa*) both in static and dynamic conditions, as compared with plain PDMS control surfaces. Based on the main results of this study, the following conclusions can be drawn:

- Katsikogianni and Missirlis have demonstrated bacteria preferentially adhere to surface irregularities whose typical size is comparable to their diameter. In this project, the dimension of PAO1 is around 3μm and *S. epidermidis* is around 1μm which is significantly smaller than the roughened surface roughness. So, these two strains are easily adhered to on the roughened surface [272]. In addition, biofilm growth of *S. epidermidis* and *P. aeruginosa* after 2 hours, 2 days, 7 days and 14 days on different roughness surfaces (P240, P120) compared with the control flat plain PDMS surface, indicating that increasing surface roughness enhanced biofilm formation both in static and dynamic conditions which also confirmed that the roughness larger than the idea of threshold arithmetic mean roughness (Ra) of 0.2 μm, bacteria are easy to adhere [282].
- No one has used roughened PDMS to make SLIPS, nor have they compared the anti-biofilm performance of SLIPS in static and dynamic conditions. This project demonstrated different oil-thickness slippery surfaces have different contact angle hysteresis which influenced bacterial adhesion or biofilm formation. The thicker oil layer slippery surfaces got lower contact angle hysteresis and had better biofilm resistance. While comparing the surfaces with the same nominal oil thickness and different roughness, the antibiofilm performance of rougher surfaces is worse, which can be due to the effect of oil trapped in the surface holes and having less oil atop the material's surface.

- Compared to the control PDMS surfaces, SOCAL, PEG and S-PDMS surfaces have very low contact angle hysteresis and get excellent resistance against biofilm for long-term culture periods either in static or dynamic conditions which were similar to other SLIPs reported in the seminal paper by Epstein et al. [51]. In static conditions, the bacterial attachment was significantly reduced by over 98% on SOCAL, PEG1 and S-PDMS 50 versus the control PDMS which is similar to the other researchers' work [60].
- Compared to the bacterial attachment of *S.epidermidis* and *P.aeruginosa* on SOCAL and PEG surfaces under static and dynamic conditions, the *S.epidermidis* total biomass of SOCAL is 2 orders magnitude larger than that of PEG1 surface, the vice versa on *P.aeruginosa*. It may be due to the bacterial properties and the surface wettability. Normally, hydrophilic bacteria (PAO1 [298]) love hydrophilic surfaces (PEG) while hydrophobic bacteria (*S. epidermidis* [299]) love hydrophobic surfaces (SOCAL).
- Compared to the PEG1 (CAH <2 degrees) and PEG2 (CAH>6 degrees) surfaces antibiofilm test, the total biomass of PEG1 is significantly less than that of PEG2. It indicated that the surfaces with low contact angle hysteresis have better antibiofilm ability than the surfaces with high contact angle hysteresis.
- No one has compared the anti-bacterial attachment and anti-biofilm formation performance of Liquid-like solid surfaces (SOCAL, PEG) to an antimicrobial surface (AgNPs-coated) in both static and dynamic culturing regimes. Silver nanoparticles as the commercially used antimicrobial surfaces also presented excellent resistance against biofilm in short-term [292, 293]. However, in this project, long-term biofilm resistance is worse than SOCAL and PEG surfaces. In addition, the adhesion of the coating to the PDMS surface is not strong enough. It is very easy to peel off with PAO1-produced EPS.
- Based on long-term culture dynamic bacterial, the wall shear stress induced oil loss then changed the surface properties will affect the bacterial attachment and biofilm formation. And the fluids reduced *P.aeruginosa* to produce EPS, and the AgNPs coating existed on the PDMS surface longer than in static conditions. In addition,

the total biomass under dynamic conditions is a bit lower than that under static conditions due to the fluids washing away some weakly adhered bacteria.

7.2 Future work

- Further biofilm testing using the co-culture method

  In this project, we only used *S.epidermidis* and *P.aeruginosa* to culture the biofilm on different surfaces one by one. However, in the in *vivo* environment there are different bacterial co-growth biofilms. For example, *Pseudomonas aeruginosa* and *S. aureus* are the two main species that colonize the airways of CF and are known for their resistance to antibiotic treatment due to their ability to form biofilms [300]. Biofilm growth patterns have been proposed as a survival strategy for environmental bacteria in response to antibiotic treatment and lung immune responses in CF patients. Various factors such as surface appendages, quorum sensing, motility, and extracellular polymeric substance (EPS) composition [e.g., extracellular DNA (eDNA) and polysaccharides have been reported to be required for biofilm development of different bacteria [300]. However, it is unclear how these factors contribute to the development of mixed-species biofilms. We also examine the antibiofilm efficiency of those slippery surfaces in artificial urines.

- Strengthen the adhesion of AgNPs-coated on PDMS

  In this project, the adhesion between silver nanoparticle coatings and PDMS is not very strong. When culturing long-term biofilms or in continuous fluid, the coating is easily detached by washing with PBS. Poor adhesion between AgNPs coatings and silicone substrates remains a problem due to the low surface energy and lack of reactive groups on the silicone substrates, thus limiting the application of AgNPs coatings on silicone implants. Physical (plasma, ultraviolet (UV) radiation, ozone) and chemical (H2SO4/H2O2, polydopamine) methods have been used to activate On the silicone surface (-COOH, -OH), the target coating is fixed on the silicone surface by chemical bonding [301].

- Further comparisons with recently advanced antibiofilm surfaces

  It would also be useful to make a comparison between SOCAL, PEG and other advanced antibiofilm surfaces. For example, Shuai Zhang et al. demonstrated that a slippery liquid-infused silver-polytetrafluoroethylene (AgFP) coating surface exhibits excellent stability and excellent repellency to liquids of various surface tensions. Anti-biofouling properties were investigated by adsorption of Escherichia coli, Staphylococcus aureus, fibrinogen and bovine serum albumin [302]. Due to its self-cleaning properties, AgFP exhibited enhanced antibacterial and protein antiadhesion activities relative to conventional electroless plating, although fibrinogen deposition significantly facilitated bacterial binding [302]. Hogi Kim et al. fabricated and developed a completely transparent, non-toxic and environmentally stable polysulfide-based anti-biofilm coating (PAC) through simple gas-phase synthesis. The polysulfide layer exhibited long-lasting anti-biofilm properties against pathogenic bacteria such as *Escherichia coli:* O157 and *Staphylococcus aureus*. Their excellent anti-biofilm properties are attributed to the non-adhesive smooth surface, and dynamic nature of the polysulfide (-S-S-) chains [303].

- Further designing the new flow cell

  In this study, we need to open the flow cell to take out the experimental surface. This process may affect the actual bacterial attachment or biofilm formation. In the future, it is better to keep the sample in the newly designed flow cell when using PBS to wash the sample, using dyes to stain the bacteria, even for confocal imaging. This can greatly reduce the experimental error.

Reference

1. Hori, K.; Matsumoto, S., Bacterial adhesion: From mechanism to control. *Biochemical engineering journal* **2010,** *48* (3), 424-434.
2. Hou, S.; Gu, H.; Smith, C.; Ren, D., Microtopographic patterns affect Escherichia coli biofilm formation on poly (dimethylsiloxane) surfaces. *Langmuir* **2011,** *27* (6), 2686-2691.
3. Mercier-Bonin, M.; Ouazzani, K.; Schmitz, P.; Lorthois, S., Study of bioadhesion on a flat plate with a yeast/glass model system. *J Colloid Interface Sci* **2004,** *271* (2), 342-50.
4. Design, Q. Manual critical-point dryer. https://qd-europe.com/de/en/product/manual-critical-point-dryer/ (accessed 05/16/2023).
5. Murray, P. R., *Medical microbiology*. Ninth edition.. ed.; Philadelphia, PA : Elsevier: 2021.
6. Hasan, M. S.; Nosonovsky, M., Lotus effect and friction: does nonsticky mean slippery? *Biomimetics* **2020,** *5* (2), 28.
7. Chieng, B. W.; Ibrahim, N. A.; Ahmad Daud, N.; Talib, Z. A., *Functionalization of Graphene Oxide via Gamma-Ray Irradiation for Hydrophobic Materials.* 2019.
8. Rai, M. K.; Deshmukh, S.; Ingle, A.; Gade, A., Silver nanoparticles: the powerful nanoweapon against multidrug‐resistant bacteria. *Journal of applied microbiology* **2012,** *112* (5), 841-852.
9. Crawford, R. J.; Webb, H. K.; Truong, V. K.; Hasan, J.; Ivanova, E. P., Surface topographical factors influencing bacterial attachment. *Advances in colloid and interface science* **2012,** *179*, 142-149.
10. Algburi, A.; Comito, N.; Kashtanov, D.; Dicks, L. M.; Chikindas, M. L., Control of biofilm formation: antibiotics and beyond. *Applied and environmental microbiology* **2017,** *83* (3), e02508-16.
11. Huhtamäki, T.; Tian, X.; Korhonen, J. T.; Ras, R. H., Surface-wetting characterization using contact-angle measurements. *Nature protocols* **2018,** *13* (7), 1521-1538.
12. Ammar, Y.; Swailes, D.; Bridgens, B.; Chen, J., Influence of surface roughness on the initial formation of biofilm. *Surface and Coatings Technology* **2015,** *284*, 410-416.
13. Mohamed, A. M.; Abdullah, A. M.; Younan, N. A., Corrosion behavior of superhydrophobic surfaces: A review. *Arabian journal of chemistry* **2015,** *8* (6), 749-765.
14. Chung, K. K.; Schumacher, J. F.; Sampson, E. M.; Burne, R. A.; Antonelli, P. J.; Brennan, A. B., Impact of engineered surface microtopography on biofilm formation of Staphylococcus aureus. *Biointerphases* **2007,** *2* (2), 89-94.
15. Wang, J.; Wu, Y.; Cao, Y.; Li, G.; Liao, Y., Influence of surface roughness on contact angle hysteresis and spreading work. *Colloid and Polymer Science* **2020,** *298* (8), 1107-1112.
16. Boks, N. P.; Kaper, H. J.; Norde, W.; Busscher, H. J.; van der Mei, H. C., Residence time dependent desorption of Staphylococcus epidermidis from hydrophobic and hydrophilic substrata. *Colloids and Surfaces B: Biointerfaces* **2008,** *67* (2), 276-278.
17. Buddingh, J. V.; Hozumi, A.; Liu, G., Liquid and liquid-like surfaces/coatings that readily slide fluids. *Progress in polymer science* **2021,** *123*, 101468.

18. Nguyen, S. H.; Webb, H. K.; Crawford, R. J.; Ivanova, E. P., Natural antibacterial surfaces. In *Antibacterial Surfaces*, Springer: 2015; pp 9-26.
19. Perera-Costa, D.; Bruque, J. M.; González-Martín, M. a. L.; Gómez-García, A. C.; Vadillo-Rodriguez, V., Studying the influence of surface topography on bacterial adhesion using spatially organized microtopographic surface patterns. *Langmuir* **2014,** *30* (16), 4633-4641.
20. Wong, T. S.; Kang, S. H.; Tang, S. K. Y.; Smythe, E. J.; Hatton, B. D.; Grinthal, A.; Aizenberg, J., Bioinspired self-repairing slippery surfaces with pressure-stable omniphobicity. *Nature* **2011,** *477* (7365), 443-447.
21. Chinnaraj, S. B.; Jayathilake, P. G.; Dawson, J.; Ammar, Y.; Portoles, J.; Jakubovics, N.; Chen, J., Modelling the combined effect of surface roughness and topography on bacterial attachment. *Journal of materials science & technology* **2021,** *81*, 151-161.
22. Muhammad, M. H.; Idris, A. L.; Fan, X.; Guo, Y.; Yu, Y.; Jin, X.; Qiu, J.; Guan, X.; Huang, T., Beyond Risk: Bacterial Biofilms and Their Regulating Approaches. *Front Microbiol* **2020,** *11*, 928.
23. Xu, L.; Wang, Y.-Y.; Huang, J.; Chen, C.-Y.; Wang, Z.-X.; Xie, H., Silver nanoparticles: Synthesis, medical applications and biosafety. *Theranostics* **2020,** *10* (20), 8996-9031.
24. Bai, R.; Peng, L.; Sun, Q.; Zhang, Y.; Zhang, L.; Wei, Y.; Han, B., Metallic antibacterial surface treatments of dental and orthopedic materials. *Materials* **2020,** *13* (20), 4594.
25. Berne, C.; Ellison, C. K.; Ducret, A.; Brun, Y. V., Bacterial adhesion at the single-cell level. *Nature Reviews Microbiology* **2018,** *16* (10), 616-627.
26. Wolcott, R.; Rhoads, D.; Bennett, M.; Wolcott, B.; Gogokhia, L.; Costerton, J.; Dowd, S., Chronic wounds and the medical biofilm paradigm. *Journal of wound care* **2010,** *19* (2), 45-53.
27. Sousa, C.; Henriques, M.; Oliveira, R., Mini-review: antimicrobial central venous catheters–recent advances and strategies. *Biofouling* **2011,** *27* (6), 609-620.
28. Ramstedt, M.; Ribeiro, I. A.; Bujdakova, H.; Mergulhão, F. J.; Jordao, L.; Thomsen, P.; Alm, M.; Burmølle, M.; Vladkova, T.; Can, F., Evaluating efficacy of antimicrobial and antifouling materials for urinary tract medical devices: Challenges and recommendations. *Macromolecular bioscience* **2019,** *19* (5), 1800384.
29. Rupp, M. E.; Karnatak, R., Intravascular catheter–related bloodstream infections. *Infectious Disease Clinics* **2018,** *32* (4), 765-787.
30. Hollenbeak, C. S., The cost of catheter-related bloodstream infections: implications for the value of prevention. *Journal of Infusion Nursing* **2011,** *34* (5), 309-313.
31. Li, J.; Kleintschek, T.; Rieder, A.; Cheng, Y.; Baumbach, T.; Obst, U.; Schwartz, T.; Levkin, P. A., Hydrophobic liquid-infused porous polymer surfaces for antibacterial applications. *ACS applied materials & interfaces* **2013,** *5* (14), 6704-6711.
32. Cao, Y.; Su, B.; Chinnaraj, S.; Jana, S.; Bowen, L.; Charlton, S.; Duan, P.; Jakubovics, N. S.; Chen, J., Nanostructured titanium surfaces exhibit recalcitrance towards Staphylococcus epidermidis biofilm formation. *Scientific reports* **2018,** *8* (1), 1-13.

33. Diu, T.; Faruqui, N.; Sjöström, T.; Lamarre, B.; Jenkinson, H. F.; Su, B.; Ryadnov, M. G., Cicada-inspired cell-instructive nanopatterned arrays. *Scientific reports* **2014,** *4* (1), 1-7.
34. Bhadra, C. M.; Khanh Truong, V.; Pham, V. T.; Al Kobaisi, M.; Seniutinas, G.; Wang, J. Y.; Juodkazis, S.; Crawford, R. J.; Ivanova, E. P., Antibacterial titanium nano-patterned arrays inspired by dragonfly wings. *Scientific reports* **2015,** *5* (1), 16817.
35. Fadeeva, E.; Truong, V. K.; Stiesch, M.; Chichkov, B. N.; Crawford, R. J.; Wang, J.; Ivanova, E. P., Bacterial retention on superhydrophobic titanium surfaces fabricated by femtosecond laser ablation. *Langmuir* **2011,** *27* (6), 3012-3019.
36. Ivanova, E. P.; Hasan, J.; Webb, H. K.; Truong, V. K.; Watson, G. S.; Watson, J. A.; Baulin, V. A.; Pogodin, S.; Wang, J. Y.; Tobin, M. J., Natural bactericidal surfaces: mechanical rupture of Pseudomonas aeruginosa cells by cicada wings. *Small* **2012,** *8* (16), 2489.
37. Cheng, G.; Zhang, Z.; Chen, S.; Bryers, J. D.; Jiang, S., Inhibition of bacterial adhesion and biofilm formation on zwitterionic surfaces. *Biomaterials* **2007,** *28* (29), 4192-4199.
38. Cheng, G.; Li, G.; Xue, H.; Chen, S.; Bryers, J. D.; Jiang, S., Zwitterionic carboxybetaine polymer surfaces and their resistance to long-term biofilm formation. *Biomaterials* **2009,** *30* (28), 5234-5240.
39. Fu, Y.; Jiang, J.; Zhang, Q.; Zhan, X.; Chen, F., Robust liquid-repellent coatings based on polymer nanoparticles with excellent self-cleaning and antibacterial performances. *Journal of Materials Chemistry A* **2017,** *5* (1), 275-284.
40. Howell, C.; Grinthal, A.; Sunny, S.; Aizenberg, M.; Aizenberg, J., Designing liquid‐infused surfaces for medical applications: a review. *Advanced materials* **2018,** *30* (50), 1802724.
41. Truong, V.; Webb, H.; Fadeeva, E.; Chichkov, B.; Wu, A.; Lamb, R.; Wang, J.; Crawford, R.; Ivanova, E., Air-directed attachment of coccoid bacteria to the surface of superhydrophobic lotus-like titanium. *Biofouling* **2012,** *28* (6), 539-550.
42. Ma, J.; Sun, Y.; Gleichauf, K.; Lou, J.; Li, Q., Nanostructure on taro leaves resists fouling by colloids and bacteria under submerged conditions. *Langmuir* **2011,** *27* (16), 10035-10040.
43. Tang, P.; Zhang, W.; Wang, Y.; Zhang, B.; Wang, H.; Lin, C.; Zhang, L., Effect of superhydrophobic surface of titanium on staphylococcus aureus adhesion. *Journal of Nanomaterials* **2011,** *2011*, 1-8.
44. Banerjee, I.; Pangule, R. C.; Kane, R. S., Antifouling coatings: recent developments in the design of surfaces that prevent fouling by proteins, bacteria, and marine organisms. *Advanced materials* **2011,** *23* (6), 690-718.
45. Chen, X.; Wen, G.; Guo, Z., What are the design principles, from the choice of lubricants and structures to the preparation method, for a stable slippery lubricant-infused porous surface? *Materials Horizons* **2020,** *7* (7), 1697-1726.
46. Lafuma, A.; Quéré, D., Slippery pre-suffused surfaces. *Europhysics Letters* **2011,** *96* (5), 56001.
47. Wong, T.-S.; Kang, S. H.; Tang, S. K.; Smythe, E. J.; Hatton, B. D.; Grinthal, A.; Aizenberg, J., Bioinspired self-repairing slippery surfaces with pressure-stable omniphobicity. *Nature* **2011,** *477* (7365), 443-447.

48. Jamil, M. I.; Ali, A.; Haq, F.; Zhang, Q.; Zhan, X.; Chen, F., Icephobic strategies and materials with superwettability: design principles and mechanism. *Langmuir* **2018,** *34* (50), 15425-15444.
49. Wei, C.; Zhang, G.; Zhang, Q.; Zhan, X.; Chen, F., Silicone oil-infused slippery surfaces based on sol–gel process-induced nanocomposite coatings: a facile approach to highly stable bioinspired surface for biofouling resistance. *ACS applied materials & interfaces* **2016,** *8* (50), 34810-34819.
50. Sotiri, I.; Tajik, A.; Lai, Y.; Zhang, C. T.; Kovalenko, Y.; Nemr, C. R.; Ledoux, H.; Alvarenga, J.; Johnson, E.; Patanwala, H. S., Tunability of liquid-infused silicone materials for biointerfaces. *Biointerphases* **2018,** *13* (6), 06D401.
51. Epstein, A. K.; Wong, T.-S.; Belisle, R. A.; Boggs, E. M.; Aizenberg, J., Liquid-infused structured surfaces with exceptional anti-biofouling performance. *Proceedings of the National Academy of Sciences* **2012,** *109* (33), 13182-13187.
52. Zhao, L.; Li, R.; Xu, R.; Si, D.; Shang, Y.; Ye, H.; Zhang, Y.; Ye, H.; Xin, Q., Antifouling slippery liquid-infused membrane for separation of water-in-oil emulsions. *Journal of Membrane Science* **2020,** *611*, 118289.
53. Ouyang, Y.; Zhao, J.; Qiu, R.; Hu, S.; Chen, M.; Wang, P., Liquid-infused superhydrophobic dendritic silver matrix: A bio-inspired strategy to prohibit biofouling on titanium. *Surface and Coatings Technology* **2019,** *367*, 148-155.
54. Xiao, Y.; Zhao, J.; Qiu, R.; Shi, Z.; Niu, S.; Wang, P., Slippery liquid-infused surface from three-dimensional interconnecting net structure via breath figure approach and its usage for biofouling inhibition. *Progress in Organic Coatings* **2018,** *123*, 47-52.
55. Kratochvil, M. J.; Welsh, M. A.; Manna, U.; Ortiz, B. J.; Blackwell, H. E.; Lynn, D. M., Slippery liquid-infused porous surfaces that prevent bacterial surface fouling and inhibit virulence phenotypes in surrounding planktonic cells. *ACS infectious diseases* **2016,** *2* (7), 509-517.
56. Tenjimbayashi, M.; Park, J.-Y.; Muto, J.; Kobayashi, Y.; Yoshikawa, R.; Monnai, Y.; Shiratori, S., In situ formation of slippery-liquid-infused nanofibrous surface for a transparent antifouling endoscope lens. *ACS Biomaterials Science & Engineering* **2018,** *4* (5), 1871-1879.
57. Ware, C. S.; Smith-Palmer, T.; Peppou-Chapman, S.; Scarratt, L. R.; Humphries, E. M.; Balzer, D.; Neto, C., Marine antifouling behavior of lubricant-infused nanowrinkled polymeric surfaces. *ACS applied materials & interfaces* **2018,** *10* (4), 4173-4182.
58. Yong, J.; Chen, F.; Yang, Q.; Fang, Y.; Huo, J.; Zhang, J.; Hou, X., Nepenthes inspired design of self‐repairing omniphobic slippery liquid infused porous surface (SLIPS) by femtosecond laser direct writing. *Advanced Materials Interfaces* **2017,** *4* (20), 1700552.
59. Zhou, X.; Lee, Y.-Y.; Chong, K. S. L.; He, C., Superhydrophobic and slippery liquid-infused porous surfaces formed by the self-assembly of a hybrid ABC triblock copolymer and their antifouling performance. *Journal of Materials Chemistry B* **2018,** *6* (3), 440-448.
60. Cao, Y.; Jana, S.; Tan, X.; Bowen, L.; Zhu, Y.; Dawson, J.; Han, R.; Exton, J.; Liu, H.; McHale, G., Antiwetting and antifouling performances of different Lubricant-Infused slippery surfaces. *Langmuir* **2020,** *36* (45), 13396-13407.

61. Peppou-Chapman, S.; Neto, C., Mapping depletion of lubricant films on antibiofouling wrinkled slippery surfaces. *ACS applied materials & interfaces* **2018,** *10* (39), 33669-33677.
62. Cao, Y.; Jana, S.; Bowen, L.; Tan, X.; Liu, H.; Rostami, N.; Brown, J.; Jakubovics, N. S.; Chen, J., Hierarchical rose petal surfaces delay the early-stage bacterial biofilm growth. *Langmuir* **2019,** *35* (45), 14670-14680.
63. Adera, S.; Alvarenga, J.; Shneidman, A. V.; Zhang, C. T.; Davitt, A.; Aizenberg, J., Depletion of lubricant from nanostructured oil-infused surfaces by pendant condensate droplets. *ACS nano* **2020,** *14* (7), 8024-8035.
64. Howell, C.; Vu, T. L.; Johnson, C. P.; Hou, X.; Ahanotu, O.; Alvarenga, J.; Leslie, D. C.; Uzun, O.; Waterhouse, A.; Kim, P., Stability of surface-immobilized lubricant interfaces under flow. *Chemistry of Materials* **2015,** *27* (5), 1792-1800.
65. Zheng, S.; Bawazir, M.; Dhall, A.; Kim, H.-E.; He, L.; Heo, J.; Hwang, G., Implication of surface properties, bacterial motility, and hydrodynamic conditions on bacterial surface sensing and their initial adhesion. *Frontiers in Bioengineering and Biotechnology* **2021,** *9*, 643722.
66. Bardell, D., The roles of the sense of taste and clean teeth in the discovery of bacteria by Antoni van Leeuwenhoek. *Microbiological reviews* **1983,** *47* (1), 121-126.
67. Shiffman, M. A., Biofilm: History, Cause, and Treatment. In *Biofilm, Pilonidal Cysts and Sinuses*, 2017; pp 3-5.
68. Dobell, C., *Antony van Leeuwenhoek and his "little animals" : being some account of the father of protozoology and bacteriology and his multifarious discoveries in these disciplines*. London : J. Bale, Sons & Danielson: London, 1932.
69. Hoiby, N., A short history of microbial biofilms and biofilm infections. *APMIS* **2017,** *125* (4), 272-275.
70. Hoiby, N., A personal history of research on microbial biofilms and biofilm infections. *Pathogens and disease* **2014,** *70* (3), 205-211.
71. Henrici, A. T.; Johnson, D. E., Studies of Freshwater Bacteria: II. Stalked Bacteria, a New Order of Schizomycetes. *Journal of bacteriology* **1935,** *30* (1), 61-93.
72. Zobell, C. E.; Allen, E. C., The Significance of Marine Bacteria in the Fouling of Submerged Surfaces. *Journal of bacteriology* **1935,** *29* (3), 239-251.
73. Hoiby, N.; Flensborg, E. W.; Beck, B.; Friis, B.; Jacobsen, S. V.; Jacobsen, L., Pseudomonas aeruginosa infection in cystic fibrosis. Diagnostic and prognostic significance of Pseudomonas aeruginosa precipitins determined by means of crossed immunoelectrophoresis. *Scand J Respir Dis* **1977,** *58* (2), 65-79.
74. Lam, J.; Chan, R.; Lam, K.; Costerton, J. W., Production of mucoid microcolonies by Pseudomonas aeruginosa within infected lungs in cystic fibrosis. *Infection and Immunity* **1980,** *28* (2), 546-556.
75. Costerton, J. W.; Irvin, R. T.; Cheng, K. J., The bacterial glycocalyx in nature and disease. *Annual review of microbiology* **1981,** *35* (1), 299-324.
76. Costerton, J. W.; Cheng, K. J.; Geesey, G. G.; Ladd, T. I.; Nickel, J. C.; Dasgupta, M.; Marrie, T. J., Bacterial biofilms in nature and disease. *Annual review of microbiology* **1987,** *41* (1), 435-464.
77. Mack, W. N.; Mack, J. P.; Ackerson, A. O., Microbial Film Development in a Trickling Filter. *Microbial ecology* **1975,** *2* (3), 215-226.

78. Jendresen, M. D.; Glantz, P.-O., Clinical Adhesiveness of Selected Dental Materials: An in-vivo study. *Acta odontologica Scandinavica* **1981,** *39* (1), 39-45.
79. Jendresen, M. D.; Glantz, P.-O.; Baier, R. E.; Eick, J. D., Microtopography and Clinical Adhesiveness of an Acid Etched Tooth Surface: An in-vivo study. *Acta odontologica Scandinavica* **1981,** *39* (1), 47-53.
80. McCoy, W. F.; Bryers, J. D.; Robbins, J.; Costerton, J. W., Observations of fouling biofilm formation. *Can J Microbiol* **1981,** *27* (9), 910-7.
81. Nickel, J. C.; Ruseska, I.; Wright, J. B.; Costerton, J. W., Tobramycin resistance of Pseudomonas aeruginosa cells growing as a biofilm on urinary catheter material. *Antimicrobial Agents and Chemotherapy* **1985,** *27* (4), 619-624.
82. Costerton, J. W.; Geesey, G. G.; Cheng, K. J., How bacteria stick. *Sci Am* **1978,** *238* (1), 86-95.
83. Jensen, E. T.; Kharazmi, A.; Lam, K.; Costerton, J. W.; Hoiby, N., Human polymorphonuclear leukocyte response to Pseudomonas aeruginosa grown in biofilms. *Infection and Immunity* **1990,** *58* (7), 2383-2385.
84. Giwercman, B.; Jensen, E. T.; Hoiby, N.; Kharazmi, A.; Costerton, J. W., Induction of beta-lactamase production in Pseudomonas aeruginosa biofilm. *Antimicrobial Agents and Chemotherapy* **1991,** *35* (5), 1008-1010.
85. Brown, M. R. W.; Collier, P. J.; Gilbert, P., Influence of growth rate on susceptibility to antimicrobial agents: Modification of the cell envelope and batch and continuous culture studies. *Antimicrobial agents and chemotherapy* **1990,** *34* (9), 1623-1628.
86. Lawrence, J. R.; Korber, D. R.; Hoyle, B. D.; Costerton, J. W.; Caldwell, D. E., Optical sectioning of microbial biofilms. *Journal of Bacteriology* **1991,** *173* (20), 6558-6567.
87. Moller, S.; Kristensen, C. S.; Poulsen, L. K.; Carstensen, J. M.; Molin, S., Bacterial growth on surfaces: automated image analysis for quantification of growth rate-related parameters. *Applied and Environmental Microbiology* **1995,** *61* (2), 741-748.
88. Bagge, N.; Schuster, M.; Hentzer, M.; Ciofu, O.; Givskov, M.; Greenberg, E. P.; Høiby, N., Pseudomonas aeruginosa biofilms exposed to imipenem exhibit changes in global gene expression and beta-lactamase and alginate production. *Antimicrob Agents Chemother* **2004,** *48* (4), 1175-87.
89. Pamp, S. J.; Gjermansen, M.; Johansen, H. K.; Tolker-Nielsen, T., Tolerance to the antimicrobial peptide colistin in Pseudomonas aeruginosa biofilms is linked to metabolically active cells, and depends on the pmr and mexAB-oprM genes. *Mol Microbiol* **2008,** *68* (1), 223-40.
90. Lopez, D.; Vlamakis, H.; Kolter, R., Biofilms. *Cold Spring Harb Perspect Biol* **2010,** *2* (7), a000398.
91. Peterson, B. W.; He, Y.; Ren, Y.; Zerdoum, A.; Libera, M. R.; Sharma, P. K.; Van Winkelhoff, A.-J.; Neut, D.; Stoodley, P.; Van Der Mei, H. C., Viscoelasticity of biofilms and their recalcitrance to mechanical and chemical challenges. *FEMS microbiology reviews* **2015,** *39* (2), 234-245.
92. Garrett, T. R.; Bhakoo, M.; Zhang, Z., Bacterial adhesion and biofilms on surfaces. *Progress in natural science* **2008,** *18* (9), 1049-1056.
93. Peterson, B. W.; He, Y.; Ren, Y.; Zerdoum, A.; Libera, M. R.; Sharma, P. K.; van Winkelhoff, A.-J.; Neut, D.; Stoodley, P.; van der Mei, H. C.; Busscher, H. J.,

Viscoelasticity of biofilms and their recalcitrance to mechanical and chemical challenges. *FEMS microbiology reviews* **2015,** *39* (2), 234-245.
94. Donlan, R. M., Biofilms on Central Venous Catheters: Is Eradication Possible? *Bacterial Biofilms* **2008,** *322*, 133-161.
95. Hatt, J. K.; Rather, P. N., Role of Bacterial Biofilms in Urinary Tract Infections. *Bacterial Biofilms* **2008,** *322*, 163-192.
96. de Carvalho, C. C., Biofilms: recent developments on an old battle. *Recent Pat Biotechnol* **2007,** *1* (1), 49-57.
97. Poulsen, L. V., Microbial Biofilm in Food Processing. *LWT - Food Science and Technology* **1999,** *32* (6), 321-326.
98. Palmer, J.; Flint, S.; Brooks, J., Bacterial cell attachment, the beginning of a biofilm. *Journal of industrial microbiology & biotechnology* **2007,** *34* (9), 577-588.
99. Ramstedt, M.; Ribeiro, I. A. C.; Bujdakova, H.; Mergulhão, F. J. M.; Jordao, L.; Thomsen, P.; Alm, M.; Burmølle, M.; Vladkova, T.; Can, F.; Reches, M.; Riool, M.; Barros, A.; Reis, R. L.; Meaurio, E.; Kikhney, J.; Moter, A.; Zaat, S. A. J.; Sjollema, J., Evaluating Efficacy of Antimicrobial and Antifouling Materials for Urinary Tract Medical Devices: Challenges and Recommendations. *Macromolecular bioscience* **2019,** *19* (5), e1800384-n/a.
100. HPA (London Health protection Agency), National Point Prevalence Survey on Healthcare-associated Infections and Antimicrobial Use. https://www.london.gov.uk/who-we-are/what-london-assembly-does/questions-mayor/find-an-answer/health-protection-agency (accessed 05/16/2023)**.**
101. Preedy, E.; Perni, S.; Nipiĉ, D.; Bohinc, K.; Prokopovich, P., Surface Roughness Mediated Adhesion Forces between Borosilicate Glass and Gram-Positive Bacteria. *Langmuir* **2014,** *30* (31), 9466-9476.
102. Sharma, S.; Jaimes-Lizcano, Y. A.; McLay, R. B.; Cirino, P. C.; Conrad, J. C., Subnanometric Roughness Affects the Deposition and Mobile Adhesion of Escherichia coli on Silanized Glass Surfaces. *Langmuir* **2016,** *32* (21), 5422-5433.
103. Ebrey, R.; Shea Hamilton, M.; Cairns, G.; Lappin‐Scott, H. M., Biofilms and hospital‐acquired infections. *Microbial biofilms* **2004**, 294-313.
104. Mohamed, J. A.; Huang, D. B., Biofilm formation by enterococci. *Journal of medical microbiology* **2007,** *56* (12), 1581-1588.
105. Otto, M., Staphylococcal biofilms. *Bacterial biofilms* **2008**, 207-228.
106. Cramton, S. E.; Götz, F., Biofilm development in Staphylococcus. *Microbial biofilms* **2004**, 64-84.
107. Vidyasagar A. What Are Biofilms? https://www.livescience.com/57295-biofilms.html (accessed 05/16/2023).
108. Jayathilake, P. G.; Gupta, P.; Li, B.; Madsen, C.; Oyebamiji, O.; González-Cabaleiro, R.; Rushton, S.; Bridgens, B.; Swailes, D.; Allen, B.; McGough, A. S.; Zuliani, P.; Ofiteru, I. D.; Wilkinson, D.; Chen, J.; Curtis, T., A mechanistic Individual-based Model of microbial communities. *PloS one* **2017,** *12* (8), e0181965-e0181965.
109. Wanner, O., New experimental findings and biofilm modelling concepts. *Water science and technology* **1995,** *32* (8), 133-140.
110. Donlan, R. M.; Costerton, J. W., Biofilms: Survival Mechanisms of Clinically Relevant Microorganisms. *Clinical Microbiology Reviews* **2002,** *15* (2), 167-193.

111. Flemming, H.-C.; Wingender, J.; Griegbe, T.; Mayer, C., Physico-chemical properties of biofilms. *Biofilms: recent advances in their study and control. Amsterdam: Harwood Academic Publishers* **2000**, 19-34.
112. Sutherland, I. W., Biofilm exopolysaccharides: A strong and sticky framework. *Microbiology (Society for General Microbiology)* **2001,** *147* (1), 3-9.
113. Hussain, M.; Wilcox, M. H.; White, P. J., The slime of coagulase-negative staphylococci: Biochemistry and relation to adherence. *FEMS microbiology letters* **1993,** *104* (3-4), 191-208.
114. Leriche, V.; Sibille, P.; Carpentier, B., Use of an Enzyme-Linked Lectinsorbent Assay To Monitor the Shift in Polysaccharide Composition in Bacterial Biofilms. *Applied and Environmental Microbiology* **2000,** *66* (5), 1851-1856.
115. Donlan, R. M., Role of biofilms in antimicrobial resistance. *ASAIO journal* **2000,** *46* (6), S47-S52.
116. Tsai, B. N.; Chang, C. H.; Lee, D. J., Fractionation of soluble microbial products (smp) and soluble extracellular from wastewater sludge. *Environmental technology* **2008,** *29* (10), 1127-1138.
117. Liao, B. Q.; Allen, D. G.; Droppo, I. G.; Leppard, G. G.; Liss, S. N., Surface properties of sludge and their role in bioflocculation and settleability. *Water research (Oxford)* **2001,** *35* (2), 339-350.
118. Otto, M., Staphylococcus epidermidis - the 'accidental' pathogen. *Nature reviews. Microbiology* **2009,** *7* (8), 555-567.
119. Foster, T. J., Surface Proteins of Staphylococcus epidermidis. *Frontiers in microbiology* **2020,** *11*, 1829-1829.
120. Kasetty, S.; Katharios-Lanwermeyer, S.; O'Toole, G. A.; Nadell, C. D., Differential surface competition and biofilm invasion strategies of Pseudomonas aeruginosa PA14 and PAO1. *Journal of bacteriology* **2021,** *203* (22), e0026521-e0026521.
121. BYJU'S Difference Between Gram-positive and Gram-negative Bacteria. https://byjus.com/biology/difference-between-gram-positive-and-gram-negative-bacteria/#:~:text=Gram%2Dpositive%20bacteria%20produce%20exotoxins,Gram%2Dnegative%20bacteria%20produce%20endotoxins. (accessed 05/16/2023).
122. Muhsin Jamal1 *, U. T., Tahir Hussain1 and Saadia Andleeb, Bacterial biofilm: its composition formation and role in human infections. *Research & Reviews: Journal of Microbiology and Biotechnology* **2015,** *4*, 1-14.
123. Masahiro, O.; Isao, S.; Soo Jeong, C.; Hidehisa, I.; Toshihiko, N.; David, D.; Youji, S., Structure of the Bacillus subtilis quorum-sensing peptide pheromone ComX. *Nature chemical biology* **2005,** *1* (1), 23.
124. Sauer, F. G.; Remaut, H.; Hultgren, S. J.; Waksman, G., Fiber assembly by the chaperone–usher pathway. *BBA - Molecular Cell Research* **2004,** *1694* (1), 259-267.
125. Donlan, R. M., Biofilm Formation: A Clinically Relevant Microbiological Process. *Clinical infectious diseases* **2001,** *33* (8), 1387-1392.
126. PUIU, T. What are biofilms and how they form. https://www.zmescience.com/science/what-are-biofilms/ (accessed 05/16/2023).
127. Lorite, G. S.; Rodrigues, C. M.; de Souza, A. A.; Kranz, C.; Mizaikoff, B.; Cotta, M. A., The role of conditioning film formation and surface chemical changes on

Xylella fastidiosa adhesion and biofilm evolution. *Journal of colloid and interface science* **2011,** *359* (1), 289-295.
128. Kanematsu, H.; Barry, D. M., Conditioning films. In *Biofilm and Materials Science*, Springer: 2015; pp 9-15.
129. Loeb, G. I.; Neihof, R. A., Marine conditioning films. ACS Publications: 1975.
130. Mittelman, M. W., Adhesion to biomaterials. *Bacterial adhesion: molecular and ecological diversity. New York: Wiley-Liss, Inc* **1996**, 89-127.
131. Hermansson, M., The DLVO theory in microbial adhesion. *Colloids and surfaces, B, Biointerfaces* **1999,** *14* (1), 105-119.
132. An, Y. H.; Dickinson, R. B.; Doyle, R. J., Mechanisms of bacterial adhesion and pathogenesis of implant and tissue infections. In *Handbook of bacterial adhesion*, Springer: 2000; pp 1-27.
133. Dufour, D.; Leung, V.; Lévesque, C. M., Bacterial biofilm: structure, function, and antimicrobial resistance: Bacterial biofilm. *Endodontic topics* **2010,** *22* (1), 2-16.
134. Kaplan, J. B.; Ragunath, C.; Ramasubbu, N.; Fine, D. H., Detachment of Actinobacillus actinomycetemcomitans Biofilm Cells by an Endogenous β-Hexosaminidase Activity. *Journal of Bacteriology* **2003,** *185* (16), 4693-4698.
135. Izano, E. A.; Amarante, M. A.; Kher, W. B.; Kaplan, J. B., Differential Roles of Poly-N-Acetylglucosamine Surface Polysaccharide and Extracellular DNA in Staphylococcus aureus and Staphylococcus epidermidis Biofilms. *Applied and Environmental Microbiology* **2008,** *74* (2), 470-476.
136. Vigeant, M. A. S.; Ford, R. M.; Wagner, M.; Tamm, L. K., Reversible and Irreversible Adhesion of Motile Escherichia coli Cells Analyzed by Total Internal Reflection Aqueous Fluorescence Microscopy. *Applied and Environmental Microbiology* **2002,** *68* (6), 2794-2801.
137. Arjmandi-Tash; Omid; Koyalchuk; Nina, M.; Trybala; Anna; Kuchin; Igor, V.; Starov; Victor, Kinetics of Wetting and Spreading of Droplets over Various Substrates.
138. McClaine, J. W.; Ford, R. M., Reversal of flagellar rotation is important in initial attachment of Escherichia coli to glass in a dynamic system with high-and low-ionic-strength buffers. *Applied and environmental microbiology* **2002,** *68* (3), 1280-1289.
139. Boks, N. P.; Busscher, H. J.; van der Mei, H. C.; Norde, W., Bond-strengthening in staphylococcal adhesion to hydrophilic and hydrophobic surfaces using atomic force microscopy. *Langmuir* **2008,** *24* (22), 12990-12994.
140. Chen, J., 7 - Thin film coatings and the biological interface. Elsevier Ltd, 2016, 143-164.
141. Song, F.; Koo, H.; Ren, D., Effects of Material Properties on Bacterial Adhesion and Biofilm Formation. *Journal of Dental Research* **2015,** *94* (8), 1027-1034.
142. Campoccia, D.; Montanaro, L.; Arciola, C. R., A review of the biomaterials technologies for infection-resistant surfaces. *Biomaterials* **2013,** *34* (34), 8533-8554.
143. Mabboux, F.; Ponsonnet, L.; Morrier, J.-J.; Jaffrezic, N.; Barsotti, O., Surface free energy and bacterial retention to saliva-coated dental implant materials—an in vitro study. *Colloids and surfaces, B, Biointerfaces* **2004,** *39* (4), 199-205.
144. Wang, H.; Sodagari, M.; Chen, Y.; He, X.; Newby, B.-m. Z.; Ju, L.-K., Initial bacterial attachment in slow flowing systems: Effects of cell and substrate surface properties. *Colloids and surfaces, B, Biointerfaces* **2011,** *87* (2), 415-422.

145. Pasmore, M.; Todd, P.; Pfiefer, B.; Rhodes, M.; Bowman, C. N., Effect of Polymer Surface Properties on the Reversibility of Attachment of Pseudomonas aeruginosa in the Early Stages of Biofilm Development. *Biofouling (Chur, Switzerland)* **2002,** *18* (1), 65-71.
146. Tang, P.; Zhang, W.; Wang, Y.; Zhang, B.; Wang, H.; Lin, C.; Zhang, L., Effect of Superhydrophobic Surface of Titanium on Staphylococcus aureus Adhesion. *Journal of nanomaterials* **2011,** *2011*.
147. Dai, S.; Zhang, D.; Shi, Q.; Han, X.; Wang, S.; Du, Z., Biomimetic fabrication and tunable wetting properties of three-dimensional hierarchical ZnO structures by combining soft lithography templated with lotus leaf and hydrothermal treatments. *CrystEngComm* **2013,** *15* (27), 5417-5424.
148. Bracco, G.; Holst, B., *Surface science techniques*. Springer Science & Business Media: 2013.
149. Si, Y.; Yu, C.; Dong, Z.; Jiang, L., Wetting and spreading: Fundamental theories to cutting-edge applications. *Current opinion in colloid & interface science* **2018,** *36*, 10-19.
150. Chau, T. T.; Bruckard, W. J.; Koh, P. T. L.; Nguyen, A. V., A review of factors that affect contact angle and implications for flotation practice. *Advances in colloid and interface science* **2009,** *150* (2), 106-115.
151. Kuchin, I.; Starov, V., Hysteresis of contact angle of sessile droplets on smooth homogeneous solid substrates via disjoining/conjoining pressure. *Langmuir* **2015,** *31* (19), 5345-5352.
152. Arjmandi-Tash, O.; Kovalchuk, N. M.; Trybala, A.; Kuchin, I. V.; Starov, V., Kinetics of Wetting and Spreading of Droplets over Various Substrates. *Langmuir* **2017,** *33* (18), 4367-4385.
153. Girifalco, L.; Good, R. J., A theory for the estimation of surface and interfacial energies. I. Derivation and application to interfacial tension. *The Journal of Physical Chemistry* **1957,** *61* (7), 904-909.
154. Nishino, T.; Meguro, M.; Nakamae, K.; Matsushita, M.; Ueda, Y., The lowest surface free energy based on− CF3 alignment. *Langmuir* **1999,** *15* (13), 4321-4323.
155. Nakajima, A.; Hashimoto, K.; Watanabe, T., Recent studies on super-hydrophobic films. *Molecular Materials and Functional Polymers* **2001**, 31-41.
156. Nilsson, M. A.; Daniello, R. J.; Rothstein, J. P., A novel and inexpensive technique for creating superhydrophobic surfaces using Teflon and sandpaper. *Journal of Physics D: Applied Physics* **2010,** *43* (4), 045301.
157. Watson, G. S.; Gellender, M.; Watson, J. A., Self-propulsion of dew drops on lotus leaves: a potential mechanism for self cleaning. *Biofouling* **2014,** *30* (4), 427-434.
158. Miwa, M.; Nakajima, A.; Fujishima, A.; Hashimoto, K.; Watanabe, T., Effects of the surface roughness on sliding angles of water droplets on superhydrophobic surfaces. *Langmuir* **2000,** *16* (13), 5754-5760.
159. Kim, J.-H.; Kavehpour, H. P.; Rothstein, J. P., Dynamic contact angle measurements on superhydrophobic surfaces. *Physics of Fluids* **2015,** *27* (3), 032107.
160. Taylor, R. L.; Verran, J.; Lees, G. C.; Ward, A. P., The influence of substratum topography on bacterial adhesion to polymethyl methacrylate. *Journal of Materials Science: Materials in Medicine* **1998,** *9* (1), 17-22.

161. Truong, V. K.; Lapovok, R.; Estrin, Y. S.; Rundell, S.; Wang, J. Y.; Fluke, C. J.; Crawford, R. J.; Ivanova, E. P., The influence of nano-scale surface roughness on bacterial adhesion to ultrafine-grained titanium. *Biomaterials* **2010,** *31* (13), 3674-3683.
162. Bagherifard, S.; Hickey, D. J.; de Luca, A. C.; Malheiro, V. N.; Markaki, A. E.; Guagliano, M.; Webster, T. J., The influence of nanostructured features on bacterial adhesion and bone cell functions on severely shot peened 316L stainless steel. *Biomaterials* **2015,** *73*, 185-197.
163. Liu, L.; Ercan, B.; Sun, L.; Ziemer, K. S.; Webster, T. J., Understanding the role of polymer surface nanoscale topography on inhibiting bacteria adhesion and growth. *ACS Biomaterials Science & Engineering* **2016,** *2* (1), 122-130.
164. Lüdecke, C.; Roth, M.; Yu, W.; Horn, U.; Bossert, J.; Jandt, K. D., Nanorough titanium surfaces reduce adhesion of Escherichia coli and Staphylococcus aureus via nano adhesion points. *Colloids and Surfaces B: Biointerfaces* **2016,** *145*, 617-625.
165. Rizzello, L.; Sorce, B.; Sabella, S.; Vecchio, G.; Galeone, A.; Brunetti, V.; Cingolani, R.; Pompa, P. P., Impact of nanoscale topography on genomics and proteomics of adherent bacteria. *Acs Nano* **2011,** *5* (3), 1865-1876.
166. Wu, S.; Zhang, B.; Liu, Y.; Suo, X.; Li, H., Influence of surface topography on bacterial adhesion: A review. *Biointerphases* **2018,** *13* (6), 060801.
167. Ramón-Torregrosa, P.; Rodríguez-Valverde, M.; Amirfazli, A.; Cabrerizo-Vílchez, M., Factors affecting the measurement of roughness factor of surfaces and its implications for wetting studies. *Colloids and surfaces a: physicochemical and engineering aspects* **2008,** *323* (1-3), 83-93.
168. Kubiak, K.; Wilson, M.; Mathia, T.; Carval, P., Wettability versus roughness of engineering surfaces. *Wear* **2011,** *271* (3-4), 523-528.
169. Karim, A. M.; Rothstein, J. P.; Kavehpour, H. P., Experimental study of dynamic contact angles on rough hydrophobic surfaces. *Journal of colloid and interface science* **2018,** *513*, 658-665.
170. Chau, T.; Bruckard, W.; Koh, P.; Nguyen, A., A review of factors that affect contact angle and implications for flotation practice. *Advances in colloid and interface science* **2009,** *150* (2), 106-115.
171. Cheng, K.; Naccarato, B.; Kim, K. J.; Kumar, A., Theoretical consideration of contact angle hysteresis using surface-energy-minimization methods. *International Journal of Heat and Mass Transfer* **2016,** *102*, 154-161.
172. Quéré, D., Wetting and roughness. *Annu. Rev. Mater. Res.* **2008,** *38*, 71-99.
173. Lafuma, A.; Quéré, D., Superhydrophobic states. *Nature materials* **2003,** *2* (7), 457-460.
174. Cassie, A. B. D., Skyler Baxter, Wettability of porous surfaces. *Transactions of the Faradya society* **1994,** *40*, 546-551.
175. Ramiasa, M.; Ralston, J.; Fetzer, R.; Sedev, R., The influence of topography on dynamic wetting. *Advances in colloid and interface science* **2014,** *206*, 275-293.
176. Xu, L.-C.; Siedlecki, C. A., Staphylococcus epidermidis adhesion on hydrophobic and hydrophilic textured biomaterial surfaces. *Biomedical materials* **2014,** *9* (3), 035003.
177. Lorenzetti, M.; Dogša, I.; Stošicki, T. a.; Stopar, D.; Kalin, M.; Kobe, S.; Novak, S. a., The influence of surface modification on bacterial adhesion to titanium-based substrates. *ACS applied materials & interfaces* **2015,** *7* (3), 1644-1651.

178. Sakamoto, A.; Terui, Y.; Horie, C.; Fukui, T.; Masuzawa, T.; Sugawara, S.; Shigeta, K.; Shigeta, T.; Igarashi, K.; Kashiwagi, K., Antibacterial effects of protruding and recessed shark skin micropatterned surfaces of polyacrylate plate with a shallow groove. *FEMS Microbiology letters* **2014,** *361* (1), 10-16.
179. Hayes, M. J.; Levine, T. P.; Wilson, R. H., Identification of nanopillars on the cuticle of the aquatic larvae of the drone fly (Diptera: Syrphidae). *Journal of Insect Science* **2016,** *16* (1).
180. Solga, A.; Cerman, Z.; Striffler, B. F.; Spaeth, M.; Barthlott, W., The dream of staying clean: Lotus and biomimetic surfaces. *Bioinspiration & biomimetics* **2007,** *2* (4), S126.
181. Bixler, G. D.; Bhushan, B., Fluid drag reduction and efficient self-cleaning with rice leaf and butterfly wing bioinspired surfaces. *Nanoscale* **2013,** *5* (17), 7685-7710.
182. Hasan, J.; Webb, H. K.; Truong, V. K.; Watson, G. S.; Watson, J. A.; Tobin, M. J.; Gervinskas, G.; Juodkazis, S.; Wang, J. Y.; Crawford, R. J., Spatial variations and temporal metastability of the self-cleaning and superhydrophobic properties of damselfly wings. *Langmuir* **2012,** *28* (50), 17404-17409.
183. Friedlander, R. S.; Vlamakis, H.; Kim, P.; Khan, M.; Kolter, R.; Aizenberg, J., Bacterial flagella explore microscale hummocks and hollows to increase adhesion. *Proceedings of the National Academy of Sciences* **2013,** *110* (14), 5624-5629.
184. Gu, H.; Chen, A.; Song, X.; Brasch, M. E.; Henderson, J. H.; Ren, D., How Escherichia coli lands and forms cell clusters on a surface: a new role of surface topography. *Scientific reports* **2016,** *6* (1), 1-14.
185. Jahed, Z.; Lin, P.; Seo, B. B.; Verma, M. S.; Gu, F. X.; Tsui, T. Y.; Mofrad, M. R., Responses of Staphylococcus aureus bacterial cells to nanocrystalline nickel nanostructures. *Biomaterials* **2014,** *35* (14), 4249-4254.
186. Berne, C.; Ducret, A.; Hardy, G. G.; Brun, Y. V., Adhesins involved in attachment to abiotic surfaces by Gram‐negative bacteria. *Microbial biofilms* **2015**, 163-199.
187. Dufrêne, Y. F.; Martínez-Martín, D.; Medalsy, I.; Alsteens, D.; Müller, D. J., Multiparametric imaging of biological systems by force-distance curve–based AFM. *Nature methods* **2013,** *10* (9), 847-854.
188. Lemon, K. P.; Higgins, D. E.; Kolter, R., Flagellar motility is critical for Listeria monocytogenes biofilm formation. *Journal of bacteriology* **2007,** *189* (12), 4418-4424.
189. Petrova, O. E.; Sauer, K., Sticky situations: key components that control bacterial surface attachment. *Journal of bacteriology* **2012,** *194* (10), 2413-2425.
190. Song, F.; Brasch, M. E.; Wang, H.; Henderson, J. H.; Sauer, K.; Ren, D., How bacteria respond to material stiffness during attachment: a role of Escherichia coli flagellar motility. *ACS applied materials & interfaces* **2017,** *9* (27), 22176-22184.
191. Conrad, J. C.; Gibiansky, M. L.; Jin, F.; Gordon, V. D.; Motto, D. A.; Mathewson, M. A.; Stopka, W. G.; Zelasko, D. C.; Shrout, J. D.; Wong, G. C., Flagella and pili-mediated near-surface single-cell motility mechanisms in P. aeruginosa. *Biophysical journal* **2011,** *100* (7), 1608-1616.
192. Jin, F.; Conrad, J. C.; Gibiansky, M. L.; Wong, G. C., Bacteria use type-IV pili to slingshot on surfaces. *Proceedings of the National Academy of Sciences* **2011,** *108* (31), 12617-12622.

193. Maier, B.; Wong, G. C., How bacteria use type IV pili machinery on surfaces. *Trends in microbiology* **2015,** *23* (12), 775-788.
194. Jayathilake, P. G.; Li, B.; Zuliani, P.; Curtis, T.; Chen, J., Modelling bacterial twitching in fluid flows: a CFD-DEM approach. *Scientific reports* **2019,** *9* (1), 1-10.
195. Davies, D., Understanding biofilm resistance to antibacterial agents. *Nature reviews Drug discovery* **2003,** *2* (2), 114-122.
196. Luppens, S. B.; Reij, M. W.; van der Heijden, R. W.; Rombouts, F. M.; Abee, T., Development of a standard test to assess the resistance of Staphylococcus aureus biofilm cells to disinfectants. *Applied and Environmental Microbiology* **2002,** *68* (9), 4194-4200.
197. Huang, C.-T.; Yu, F. P.; McFeters, G. A.; Stewart, P. S., Nonuniform spatial patterns of respiratory activity within biofilms during disinfection. *Applied and environmental microbiology* **1995,** *61* (6), 2252-2256.
198. Tripathy, A.; Sen, P.; Su, B.; Briscoe, W. H., Natural and bioinspired nanostructured bactericidal surfaces. *Advances in colloid and interface science* **2017,** *248*, 85-104.
199. Maisch, T.; Baier, J.; Franz, B.; Maier, M.; Landthaler, M.; Szeimies, R.-M.; Bäumler, W., role of singlet oxygen and oxygen concentration in photodynamic inactivation of bacteria. *Proceedings of the National Academy of Sciences - PNAS* **2007,** *104* (17), 7223-7228.
200. Ahmed, Y.; Zhong, J.; Yuan, Z.; Guo, J., Roles of reactive oxygen species in antibiotic resistant bacteria inactivation and micropollutant degradation in Fenton and photo-Fenton processes. *Journal of hazardous materials* **2022,** *430*, 128408-128408.
201. Bismuth, H. D.; Brasseur, G.; Ezraty, B.; Aussel, L., Bacterial Genetic Approach to the Study of Reactive Oxygen Species Production in Galleria mellonella During Salmonella Infection. *Frontiers in cellular and infection microbiology* **2021,** *11*, 640112-640112.
202. Hajipour, M. J.; Fromm, K. M.; Ashkarran, A. A.; de Aberasturi, D. J.; de Larramendi, I. R.; Rojo, T.; Serpooshan, V.; Parak, W. J.; Mahmoudi, M., Antibacterial properties of nanoparticles. *Trends in biotechnology* **2012,** *30* (10), 499-511.
203. Martinez-Gutierrez, F.; Boegli, L.; Agostinho, A.; Sánchez, E. M.; Bach, H.; Ruiz, F.; James, G., Anti-biofilm activity of silver nanoparticles against different microorganisms. *Biofouling* **2013,** *29* (6), 651-660.
204. Ju-Nam, Y.; Lead, J. R., Manufactured nanoparticles: an overview of their chemistry, interactions and potential environmental implications. *Science of the total environment* **2008,** *400* (1-3), 396-414.
205. Yadav, T. P.; Yadav, R. M.; Singh, D. P., Mechanical milling: a top down approach for the synthesis of nanomaterials and nanocomposites. *Nanoscience and Nanotechnology* **2012,** *2* (3), 22-48.
206. Khayati, G.; Janghorban, K., The nanostructure evolution of Ag powder synthesized by high energy ball milling. *Advanced Powder Technology* **2012,** *23* (3), 393-397.
207. Tien, D.; Liao, C.; Huang, J.; Tseng, K.; Lung, J.; Tsung, T.; Kao, W.; Tsai, T.; Cheng, T.; Yu, B., Novel technique for preparing a nano-silver water suspension by the arc-discharge method. *Rev. Adv. mater. sci* **2008,** *18* (8), 752-758.

208. Amendola, V.; Meneghetti, M., Laser ablation synthesis in solution and size manipulation of noble metal nanoparticles. *Physical chemistry chemical physics* **2009,** *11* (20), 3805-3821.
209. Stagon, S. P.; Huang, H., Syntheses and applications of small metallic nanorods from solution and physical vapor deposition. *Nanotechnology Reviews* **2013,** *2* (3), 259-267.
210. Bapat, R. A.; Chaubal, T. V.; Joshi, C. P.; Bapat, P. R.; Choudhury, H.; Pandey, M.; Gorain, B.; Kesharwani, P., An overview of application of silver nanoparticles for biomaterials in dentistry. *Materials Science and Engineering: C* **2018,** *91*, 881-898.
211. Khorrami, S.; Zarrabi, A.; Khaleghi, M.; Danaei, M.; Mozafari, M., Selective cytotoxicity of green synthesized silver nanoparticles against the MCF-7 tumor cell line and their enhanced antioxidant and antimicrobial properties. *International journal of nanomedicine* **2018,** *13*, 8013.
212. Yin, I. X.; Zhang, J.; Zhao, I. S.; Mei, M. L.; Li, Q.; Chu, C. H., The Antibacterial Mechanism of Silver Nanoparticles and Its Application in Dentistry. *Int J Nanomedicine* **2020,** *15*, 2555-2562.
213. Liao, C.; Li, Y.; Tjong, S. C., Bactericidal and cytotoxic properties of silver nanoparticles. *International journal of molecular sciences* **2019,** *20* (2), 449.
214. Li, L.; Li, L.; Zhou, X.; Yu, Y.; Li, Z.; Zuo, D.; Wu, Y., Silver nanoparticles induce protective autophagy via Ca2+/CaMKKβ/AMPK/mTOR pathway in SH-SY5Y cells and rat brains. *Nanotoxicology* **2019,** *13* (3), 369-391.
215. Noronha, V. T.; Paula, A. J.; Durán, G.; Galembeck, A.; Cogo-Müller, K.; Franz-Montan, M.; Durán, N., Silver nanoparticles in dentistry. *Dental Materials* **2017,** *33* (10), 1110-1126.
216. Khorrami, S.; Jafari Najafabadi, F.; Zarepour, A.; Zarrabi, A., Is Astragalus gossypinus honey a natural antibacterial and cytotoxic agent? An investigation on A. gossypinus honey biological activity and its green synthesized silver nanoparticles. *BioNanoScience* **2019,** *9*, 603-610.
217. Jacob, J. M.; John, M. S.; Jacob, A.; Abitha, P.; Kumar, S. S.; Rajan, R.; Natarajan, S.; Pugazhendhi, A., Bactericidal coating of paper towels via sustainable biosynthesis of silver nanoparticles using Ocimum sanctum leaf extract. *Materials Research Express* **2019,** *6* (4), 045401.
218. Meikle, T. G.; Dyett, B. P.; Strachan, J. B.; White, J.; Drummond, C. J.; Conn, C. E., Preparation, characterization, and antimicrobial activity of cubosome encapsulated metal nanocrystals. *ACS applied materials & interfaces* **2020,** *12* (6), 6944-6954.
219. Saravanan, M.; Arokiyaraj, S.; Lakshmi, T.; Pugazhendhi, A., Synthesis of silver nanoparticles from Phenerochaete chrysosporium (MTCC-787) and their antibacterial activity against human pathogenic bacteria. *Microbial pathogenesis* **2018,** *117*, 68-72.
220. Yin, I. X.; Yu, O. Y.; Zhao, I. S.; Mei, M. L.; Li, Q.-L.; Tang, J.; Chu, C.-H., Developing biocompatible silver nanoparticles using epigallocatechin gallate for dental use. *Archives of Oral Biology* **2019,** *102*, 106-112.
221. Pugazhendhi, A.; Prabakar, D.; Jacob, J. M.; Karuppusamy, I.; Saratale, R. G., Synthesis and characterization of silver nanoparticles using Gelidium amansii and its antimicrobial property against various pathogenic bacteria. *Microbial pathogenesis* **2018,** *114*, 41-45.

222. Gu, H.; Ren, D., Materials and surface engineering to control bacterial adhesion and biofilm formation: A review of recent advances. *Frontiers of Chemical Science and Engineering* **2014,** *8* (1), 20-33.
223. Bazaka, K.; Jacob, M.; Chrzanowski, W.; Ostrikov, K., Anti-bacterial surfaces: natural agents, mechanisms of action, and plasma surface modification. *Rsc Advances* **2015,** *5* (60), 48739-48759.
224. Elbourne, A.; Crawford, R. J.; Ivanova, E. P., Nano-structured antimicrobial surfaces: From nature to synthetic analogues. *Journal of Colloid and Interface Science* **2017,** *508*, 603-616.
225. Fotakis, C.; Barberoglou, M.; Zorba, V.; Stratakis, E.; Papadopoulou, E.; Ranella, A.; Terzaki, K.; Farsari, M. In *Applications of ultrafast lasers in materials processing: fabrication on self-cleaning surfaces and scaffolds for tissue engineering*, 15th International School on Quantum Electronics: Laser Physics and Applications, International Society for Optics and Photonics: 2008; p 702702.
226. Damodaran, V. B.; Murthy, N. S., Bio-inspired strategies for designing antifouling biomaterials. *Biomaterials research* **2016,** *20* (1), 1-11.
227. Dickson, M. N.; Liang, E. I.; Rodriguez, L. A.; Vollereaux, N.; Yee, A. F., Nanopatterned polymer surfaces with bactericidal properties. *Biointerphases* **2015,** *10* (2), 021010.
228. Yeh, S.-B.; Chen, C.-S.; Chen, W.-Y.; Huang, C.-J., Modification of silicone elastomer with zwitterionic silane for durable antifouling properties. *Langmuir* **2014,** *30* (38), 11386-11393.
229. Linklater, D. P.; Juodkazis, S.; Ivanova, E. P., Nanofabrication of mechano-bactericidal surfaces. *Nanoscale* **2017,** *9* (43), 16564-16585.
230. Feng, L.; Zhang, Z.; Mai, Z.; Ma, Y.; Liu, B.; Jiang, L.; Zhu, D., A super-hydrophobic and super-oleophilic coating mesh film for the separation of oil and water. *Angewandte Chemie* **2004,** *116* (15), 2046-2048.
231. Long, Y.; Yin, X.; Mu, P.; Wang, Q.; Hu, J.; Li, J., Slippery liquid-infused porous surface (SLIPS) with superior liquid repellency, anti-corrosion, anti-icing and intensified durability for protecting substrates. *Chemical Engineering Journal* **2020,** *401*.
232. Zhang, X.; Wu, G.; Peng, X.; Li, L.; Feng, H.; Gao, B.; Huo, K.; Chu, P. K., Mitigation of corrosion on magnesium alloy by predesigned surface corrosion. *Scientific reports* **2015,** *5* (1), 1-11.
233. Sun, X.; Damle, V. G.; Liu, S.; Rykaczewski, K., Bioinspired stimuli-responsive and antifreeze-secreting anti-icing coatings. *Advanced Materials Interfaces* **2015,** *2* (5), 1400479.
234. Liu, M.; Hou, Y.; Li, J.; Tie, L.; Guo, Z., Transparent slippery liquid-infused nanoparticulate coatings. *Chemical Engineering Journal* **2018,** *337*, 462-470.
235. Xiang, T.; Zhang, M.; Sadig, H. R.; Li, Z.; Zhang, M.; Dong, C.; Yang, L.; Chan, W.; Li, C., Slippery liquid-infused porous surface for corrosion protection with self-healing property. *Chemical Engineering Journal* **2018,** *345*, 147-155.
236. Jing, X.; Guo, Z., Durable lubricant-impregnated surfaces for water collection under extremely severe working conditions. *ACS applied materials & interfaces* **2019,** *11* (39), 35949-35958.

237. Basu, S.; Hanh, B. M.; Isaiah Chua, J. Q.; Daniel, D.; Ismail, M. H.; Marchioro, M.; Amini, S.; Rice, S. A.; Miserez, A., Green biolubricant infused slippery surfaces to combat marine biofouling. *J Colloid Interface Sci* **2020,** *568*, 185-197.
238. Hunt, S. M.; Werner, E. M.; Huang, B.; Hamilton, M. A.; Stewart, P. S., Hypothesis for the role of nutrient starvation in biofilm detachment. *Appl Environ Microbiol* **2004,** *70* (12), 7418-25.
239. Allison, D. G.; Ruiz, B.; SanJose, C.; Jaspe, A.; Gilbert, P., Extracellular products as mediators of the formation and detachment of Pseudomonas fluorescens biofilms. *FEMS microbiology letters* **1998,** *167* (2), 179-184.
240. Ohashi, A.; Harada, H., Characterization of detachment mode of biofilm developed in an attached-growth reactor. *Water Science and Technology* **1994,** *30* (11), 35.
241. Applegate, D. H.; Bryers, J. D., Effects of carbon and oxygen limitations and calcium concentrations on biofilm removal processes. *Biotechnology and bioengineering* **1991,** *37* (1), 17-25.
242. Peyton, B. M.; Characklis, W. G., A statistical analysis of the effect of substrate utilization and shear stress on the kinetics of biofilm detachment. *Biotechnology and bioengineering* **1993,** *41* (7), 728-735.
243. Chang, H. T.; Rittmann, B. E.; Amar, D.; Heim, R.; Ehlinger, O.; Lesty, Y., Biofilm detachment mechanisms in a liquid-fluidized bed. *Biotechnology and Bioengineering* **1991,** *38* (5), 499-506.
244. Webb, J. S.; Thompson, L. S.; James, S.; Charlton, T.; Tolker-Nielsen, T.; Koch, B.; Givskov, M.; Kjelleberg, S., Cell death in Pseudomonas aeruginosa biofilm development. *Journal of bacteriology* **2003,** *185* (15), 4585-4592.
245. Kaplan, J. B.; Meyenhofer, M. F.; Fine, D. H., Biofilm growth and detachment of Actinobacillus actinomycetemcomitans. Am Soc Microbiol: 2003.
246. Hentzer, M.; Riedel, K.; Rasmussen, T. B.; Heydorn, A.; Andersen, J. B.; Parsek, M. R.; Rice, S. A.; Eberl, L.; Molin, S.; Høiby, N., Inhibition of quorum sensing in Pseudomonas aeruginosa biofilm bacteria by a halogenated furanone compound. *Microbiology* **2002,** *148* (1), 87-102.
247. Park, A.; Jeong, H.-H.; Lee, J.; Kim, K. P.; Lee, C.-S., Effect of shear stress on the formation of bacterial biofilm in a microfluidic channel. *Biochip journal* **2011,** *5* (3), 236-241.
248. Wang, L.; McCarthy, T. J., Covalently attached liquids: instant omniphobic surfaces with unprecedented repellency. *Angewandte Chemie International Edition* **2016,** *55* (1), 244-248.
249. Armstrong, S.; McHale, G.; Ledesma-Aguilar, R.; Wells, G. G., Pinning-Free Evaporation of Sessile Droplets of Water from Solid Surfaces. *Langmuir* **2019,** *35* (8), 2989-2996.
250. Kim, J. H.; Park, H.; Seo, S. W., In situ synthesis of silver nanoparticles on the surface of PDMS with high antibacterial activity and biosafety toward an implantable medical device. *Nano Convergence* **2017,** *4* (1), 33.
251. Shields, R. C.; Mokhtar, N.; Ford, M.; Hall, M. J.; Burgess, J. G.; ElBadawey, M. R.; Jakubovics, N. S., Efficacy of a marine bacterial nuclease against biofilm forming microorganisms isolated from chronic rhinosinusitis. *PLoS One* **2013,** *8* (2), e55339.

252. Cole, S. J.; Lee, V. T., Cyclic di-GMP signaling contributes to Pseudomonas aeruginosa-mediated catheter-associated urinary tract infection. *Journal of Bacteriology* **2016,** *198* (1), 91-97.
253. Nowatzki, P. J.; Koepsel, R. R.; Stoodley, P.; Min, K.; Harper, A.; Murata, H.; Donfack, J.; Hortelano, E. R.; Ehrlich, G. D.; Russell, A. J., Salicylic acid-releasing polyurethane acrylate polymers as anti-biofilm urological catheter coatings. *Acta Biomaterialia* **2012,** *8* (5), 1869-1880.
254. Lee, S.; Kwok, N.; Holsapple, J.; Heldt, T.; Bourouiba, L., Enhanced wall shear stress prevents obstruction by astrocytes in ventricular catheters. *Journal of the Royal Society Interface* **2020,** *17* (168), 20190884.
255. Young, T., III. An essay on the cohesion of fluids. *Philosophical transactions of the royal society of London* **1805,** (95), 65-87.
256. Zhang, X.; Wang, L.; Levänen, E., Superhydrophobic surfaces for the reduction of bacterial adhesion. *Rsc Advances* **2013,** *3* (30), 12003-12020.
257. Eral, H. B.; 't Mannetje, D.; Oh, J. M., Contact angle hysteresis: a review of fundamentals and applications. *Colloid and polymer science* **2013,** *291*, 247-260.
258. Marmur, A., The lotus effect: superhydrophobicity and metastability. *Langmuir* **2004,** *20* (9), 3517-3519.
259. Gart, S.; Mates, J. E.; Megaridis, C. M.; Jung, S., Droplet impacting a cantilever: A leaf-raindrop system. *Physical Review Applied* **2015,** *3* (4), 044019.
260. Barrio-Zhang, H.; Ruiz-Gutierrez, E.; Armstrong, S.; McHale, G.; Wells, G. G.; Ledesma-Aguilar, R., Contact-angle hysteresis and contact-line friction on slippery liquid-like surfaces. *Langmuir* **2020,** *36* (49), 15094-15101.
261. Azeredo, J.; Azevedo, N. F.; Briandet, R.; Cerca, N.; Coenye, T.; Costa, A. R.; Desvaux, M.; Di Bonaventura, G.; Hébraud, M.; Jaglic, Z., Critical review on biofilm methods. *Critical reviews in microbiology* **2017,** *43* (3), 313-351.
262. Schlafer, S.; Meyer, R. L., Confocal microscopy imaging of the biofilm matrix. *Journal of Microbiological Methods* **2017,** *138*, 50-59.
263. Stiefel, P.; Schmidt-Emrich, S.; Maniura-Weber, K.; Ren, Q., Critical aspects of using bacterial cell viability assays with the fluorophores SYTO9 and propidium iodide. *BMC microbiology* **2015,** *15*, 1-9.
264. Gomes, L. C.; Mergulhão, F. J., SEM analysis of surface impact on biofilm antibiotic treatment. *Scanning* **2017,** *2017*.
265. Hynninen, A.; Külaviir, M.; Kirsimäe, K., Air-drying is sufficient pre-treatment for in situ visualization of microbes on minerals with scanning electron microscopy. *Journal of microbiological methods* **2018,** *146*, 77-82.
266. Gaidhani, K. A.; Harwalkar, M.; Bhambere, D.; Nirgude, P. S., Lyophilization/freeze drying–a review. *World journal of pharmaceutical research* **2015,** *4* (8), 516-543.
267. Hazrin-Chong, N. H.; Manefield, M., An alternative SEM drying method using hexamethyldisilazane (HMDS) for microbial cell attachment studies on sub-bituminous coal. *Journal of microbiological methods* **2012,** *90* (2), 96-99.
268. Bakker, D.; Van der Plaats, A.; Verkerke, G.; Busscher, H.; Van der Mei, H., Comparison of velocity profiles for different flow chamber designs used in studies of microbial adhesion to surfaces. *Applied and environmental microbiology* **2003,** *69* (10), 6280-6287.

269. Elimelech, M., Particle deposition on ideal collectors from dilute flowing suspensions: Mathematical formulation, numerical solution, and simulations. *Separations technology* **1994,** *4* (4), 186-212.
270. Morisaki, H.; Nagai, S.; Ohshima, H.; Ikemoto, E.; Kogure, K., The effect of motility and cell-surface polymers on bacterial attachment. *Microbiology* **1999,** *145* (10), 2797-2802.
271. Gottenbos, B.; Busscher, H.; Van Der Mei, H.; Nieuwenhuis, P., Pathogenesis and prevention of biomaterial centered infections. *Journal of Materials Science: Materials in Medicine* **2002,** *13*, 717-722.
272. Katsikogianni, M.; Missirlis, Y., Concise review of mechanisms of bacterial adhesion to biomaterials and of techniques used in estimating bacteria-material interactions. *Eur Cell Mater* **2004,** *8* (3), 37-57.
273. Alnnasouri, M.; Lemaitre, C.; Gentric, C.; Dagot, C.; Pons, M.-N., Influence of surface topography on biofilm development: experiment and modeling. *Biochemical engineering journal* **2011,** *57*, 38-45.
274. McHale, G.; Orme, B. V.; Wells, G. G.; Ledesma-Aguilar, R., Apparent contact angles on lubricant-impregnated surfaces/slips: From superhydrophobicity to electrowetting. *Langmuir* **2019,** *35* (11), 4197-4204.
275. Semprebon, C.; McHale, G.; Kusumaatmaja, H., Apparent contact angle and contact angle hysteresis on liquid infused surfaces. *Soft matter* **2017,** *13* (1), 101-110.
276. Wang, H.; Sodagari, M.; Ju, L.-K.; Newby, B.-m. Z., Effects of shear on initial bacterial attachment in slow flowing systems. *Colloids and Surfaces B: Biointerfaces* **2013,** *109*, 32-39.
277. Thomas, W. E.; Trintchina, E.; Forero, M.; Vogel, V.; Sokurenko, E. V., Bacterial Adhesion to Target Cells Enhanced by Shear Force. *Cell* **2002,** *109* (7), 913-923.
278. Whitfield, M.; Ghose, T.; Thomas, W., Shear-Stabilized Rolling Behavior of E. coli Examined with Simulations. *Biophysical journal* **2010,** *99* (8), 2470-2478.
279. Wang, H.; Sodagari, M.; Ju, L.-K.; Zhang Newby, B.-m., Effects of shear on initial bacterial attachment in slow flowing systems. *Colloids and Surfaces B: Biointerfaces* **2013,** *109*, 32-39.
280. Nejadnik, M. R.; van der Mei, H. C.; Busscher, H. J.; Norde, W., Determination of the Shear Force at the Balance between Bacterial Attachment and Detachment in Weak-Adherence Systems, Using a Flow Displacement Chamber. *Applied and Environmental Microbiology* **2008,** *74* (3), 916-919.
281. Wu, S.; Altenried, S.; Zogg, A.; Zuber, F.; Maniura-Weber, K.; Ren, Q., Role of the surface nanoscale roughness of stainless steel on bacterial adhesion and microcolony formation. *ACS omega* **2018,** *3* (6), 6456-6464.
282. Park, J.-W.; An, J.-S.; Lim, W. H.; Lim, B.-S.; Ahn, S.-J., Microbial changes in biofilms on composite resins with different surface roughness: An in vitro study with a multispecies biofilm model. *The Journal of prosthetic dentistry* **2019,** *122* (5), 493.e1-493.e8.
283. Ali, S. M. F.; Tanwir, F., Oral microbial habitat a dynamic entity. *Journal of oral biology and craniofacial research* **2012,** *2* (3), 181-187.
284. Hou, J.; Veeregowda, D. H.; van de Belt-Gritter, B.; Busscher, H. J.; van der Mei, H. C., Extracellular polymeric matrix production and relaxation under fluid shear

and mechanical pressure in Staphylococcus aureus biofilms. *Applied and environmental microbiology* **2018,** *84* (1), e01516-17.
285. Rodesney, C. A.; Roman, B.; Dhamani, N.; Cooley, B. J.; Katira, P.; Touhami, A.; Gordon, V. D., Mechanosensing of shear by Pseudomonas aeruginosa leads to increased levels of the cyclic-di-GMP signal initiating biofilm development. *Proceedings of the National Academy of Sciences - PNAS* **2017,** *114* (23), 5906-5911.
286. Zhu, Y.; McHale, G.; Dawson, J.; Armstrong, S.; Wells, G.; Han, R.; Liu, H.; Vollmer, W.; Stoodley, P.; Jakubovics, N., Slippery Liquid-Like Solid Surfaces with Promising Antibiofilm Performance in both Static and Flow Conditions. *ACS applied materials & interfaces* **2022,** *14*, 6307-6319.
287. Martinez-Gutierrez, F.; Boegli, L.; Agostinho, A.; Sánchez, E. M.; Bach, H.; Ruiz, F.; James, G., Anti-biofilm activity of silver nanoparticles against different microorganisms. *Biofouling (Chur, Switzerland)* **2013,** *29* (6), 651-660.
288. de Lacerda Coriolano, D.; de Souza, J. B.; Bueno, E. V.; Medeiros, S. M. d. F. R. d. S.; Cavalcanti, I. D. L.; Cavalcanti, I. M. F., Antibacterial and antibiofilm potential of silver nanoparticles against antibiotic-sensitive and multidrug-resistant Pseudomonas aeruginosa strains. *Brazilian journal of microbiology* **2021,** *52* (1), 267-278.
289. Xu, Q.; Ensign, L. M.; Boylan, N. J.; Schön, A.; Gong, X.; Yang, J.-C.; Lamb, N. W.; Cai, S.; Yu, T.; Freire, E.; Hanes, J., Impact of Surface Polyethylene Glycol (PEG) Density on Biodegradable Nanoparticle Transport in Mucus ex Vivo and Distribution in Vivo. *ACS nano* **2015,** *9* (9), 9217-9227.
290. Louette, P.; Bodino, F.; Pireaux, J.-J., Poly (dimethyl siloxane)(PDMS) XPS reference core level and energy loss spectra. *Surface Science Spectra* **2005,** *12* (1), 38-43.
291. Chen, J.; Bull, S., On the factors affecting the critical indenter penetration for measurement of coating hardness. *Vacuum* **2009,** *83* (6), 911-920.
292. Jena, P.; Mohanty, S.; Mallick, R.; Jacob, B.; Sonawane, A., Toxicity and antibacterial assessment of chitosancoated silver nanoparticles on human pathogens and macrophage cells. *International journal of nanomedicine* **2012**, 1805-1818.
293. Bruna, T.; Maldonado-Bravo, F.; Jara, P.; Caro, N., Silver Nanoparticles and Their Antibacterial Applications. *Int J Mol Sci* **2021,** *22* (13).
294. MacCallum, N.; Howell, C.; Kim, P.; Sun, D.; Friedlander, R.; Ranisau, J.; Ahanotu, O.; Lin, J. J.; Vena, A.; Hatton, B., Liquid-infused silicone as a biofouling-free medical material. *ACS Biomaterials Science & Engineering* **2015,** *1* (1), 43-51.
295. Kovalenko, Y.; Sotiri, I.; Timonen, J. V.; Overton, J. C.; Holmes, G.; Aizenberg, J.; Howell, C., Bacterial interactions with immobilized liquid layers. *Advanced healthcare materials* **2017,** *6* (15), 1600948.
296. Wang, R.; Neoh, K. G.; Kang, E. T.; Tambyah, P. A.; Chiong, E., Antifouling coating with controllable and sustained silver release for long-term inhibition of infection and encrustation in urinary catheters. *Journal of Biomedical Materials Research Part B: Applied Biomaterials* **2015,** *103* (3), 519-528.
297. LI, H.; FAIRFAX R, M.; DUBOCQ, F.; DAROUICHE, R. O.; RAJPURKAR, A.; THOMPSON, M.; TEFILLI, M. V.; Dhabuwala, C., Antibacterial activity of antibiotic coated silicone grafts. *The Journal of urology* **1998,** *160* (5), 1910-1913.
298. Guilbaud, M.; Bruzaud, J.; Bouffartigues, E.; Orange, N.; Guillot, A.; Aubert-Frambourg, A.; Monnet, V.; Herry, J. M.; Chevalier, S.; Bellon-Fontaine, M. N.,

Proteomic Response of Pseudomonas aeruginosa PAO1 Adhering to Solid Surfaces. *Front Microbiol* **2017,** *8*, 1465.
299. F. REIFSTECK, S. W. a. B. J. W., Hydrop hobicity-hydrop hilicity of staphylococci. *J. Med. Microbiol.* **1987,** *24*, 65-73.
300. Yang, L.; Liu, Y.; Markussen, T.; Høiby, N.; Tolker-Nielsen, T.; Molin, S., Pattern differentiation in co-culture biofilms formed by Staphylococcus aureus and Pseudomonas aeruginosa. *FEMS Immunology & Medical Microbiology* **2011,** *62* (3), 339-347.
301. Yassin, M. A.; Elkhooly, T. A.; Elsherbiny, S. M.; Reicha, F. M.; Shokeir, A. A., Facile coating of urinary catheter with bio–inspired antibacterial coating. *Heliyon* **2019,** *5* (12), e02986.
302. Zhang, S.; Liang, X.; Teng, X.; Gadd, G. M.; McGrath, J. W.; McCoy, C. P.; Zhao, Q., Enhanced anti-biofilm and anti-protein adsorption properties of liquid-infused silver-polytetrafluoroethylene coatings. *Applied Surface Science* **2023,** *616*, 156463.
303. Kim, H.; Park, S.; Song, Y.; Jang, W.; Choi, K.; Lee, K. G.; Lee, E.; Im, S. G., Vapor-phase synthesis of a robust polysulfide film for transparent, biocompatible, and long-term stable anti-biofilm coating. *Korean Journal of Chemical Engineering* **2023**, 1-7.

Appendix

Figure S1 The SEM images for *S.epidermidis and P. aeruginosa* dimension.

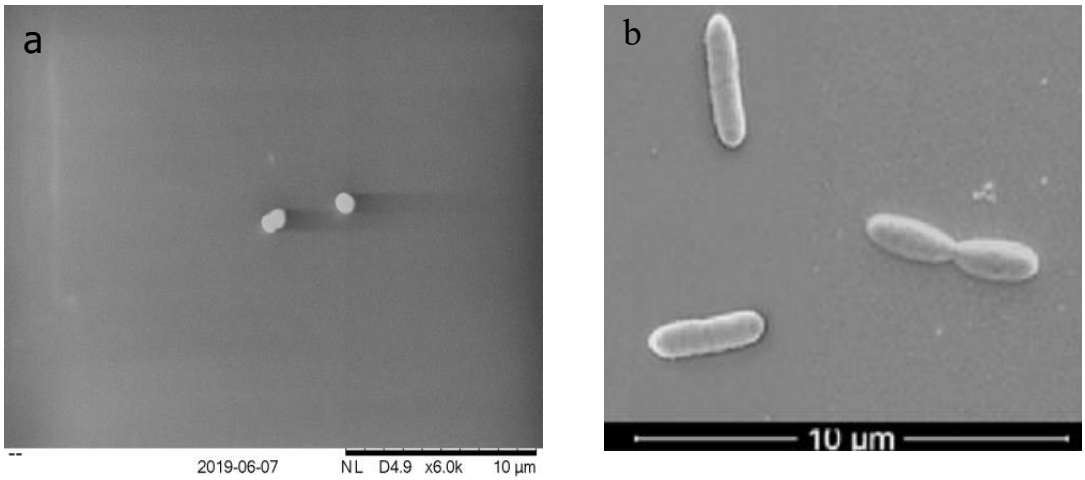

Figure S1 The SEM images for *S.epidermidis and P. aeruginosa* dimension. (a) *S.epidermidis*; (b) *P. aeruginosa*. Used for converting surface coverage to biomass.

A Matlab code for calculating the oil thickness

```
Input Data
widths = [10; 9; 9; 9; 8; 7; 10; 8.5; 8; 9]; % Input values into array in mm
lengths = [10; 9; 9; 9; 7.5; 8; 9; 8.5; 9; 9]; % Input values into array in mm
heights = [0.7; 0.7; 0.7; 0.7; 0.7; 0.7; 0.7; 0.7; 0.7; 0.7]; % Input values into array in mm
swollenWeights = [0.0615; 0.0519; 0.0505; 0.0529; 0.0362; 0.0332; 0.0561; 0.0415; 0.0495; 0.0503]; % Final units are kg. Input values into array in g
wipedWeights = [0.0521; 0.0462; 0.0428; 0.0417; 0.0325; 0.0306; 0.0441; 0.0381; 0.0411; 0.0423]; % Input values into array in g
oilDensity = 0.93; % Units are g/ml
Solve for the Oil Thickness
Cubic coefficients
tCubedCoefs = 8*ones(length(widths),1); % Unitless
tSquaredCoefs = 4*(lengths + widths + heights)/1E3; % Units m
tCoefs = 2*(lengths.*heights + lengths.*widths + widths.*heights)/1E6; %Units m^3
constants = -1E-6*(swollenWeights - wipedWeights)/oilDensity; % Units m^3
combinedEquations = [tCubedCoefs, tSquaredCoefs, tCoefs, constants];
Solve cubic equation to find thickness
for ii = length(tCubedCoefs):-1:1
   equationRoot = roots(combinedEquations(ii,:))*1E6;
oilThicknesses(ii,1) = equationRoot(imag(equationRoot)==0 & equationRoot > 0);
end
```

Figure S2 Characterization of AgNPs-coated PDMS after bacterial culture.

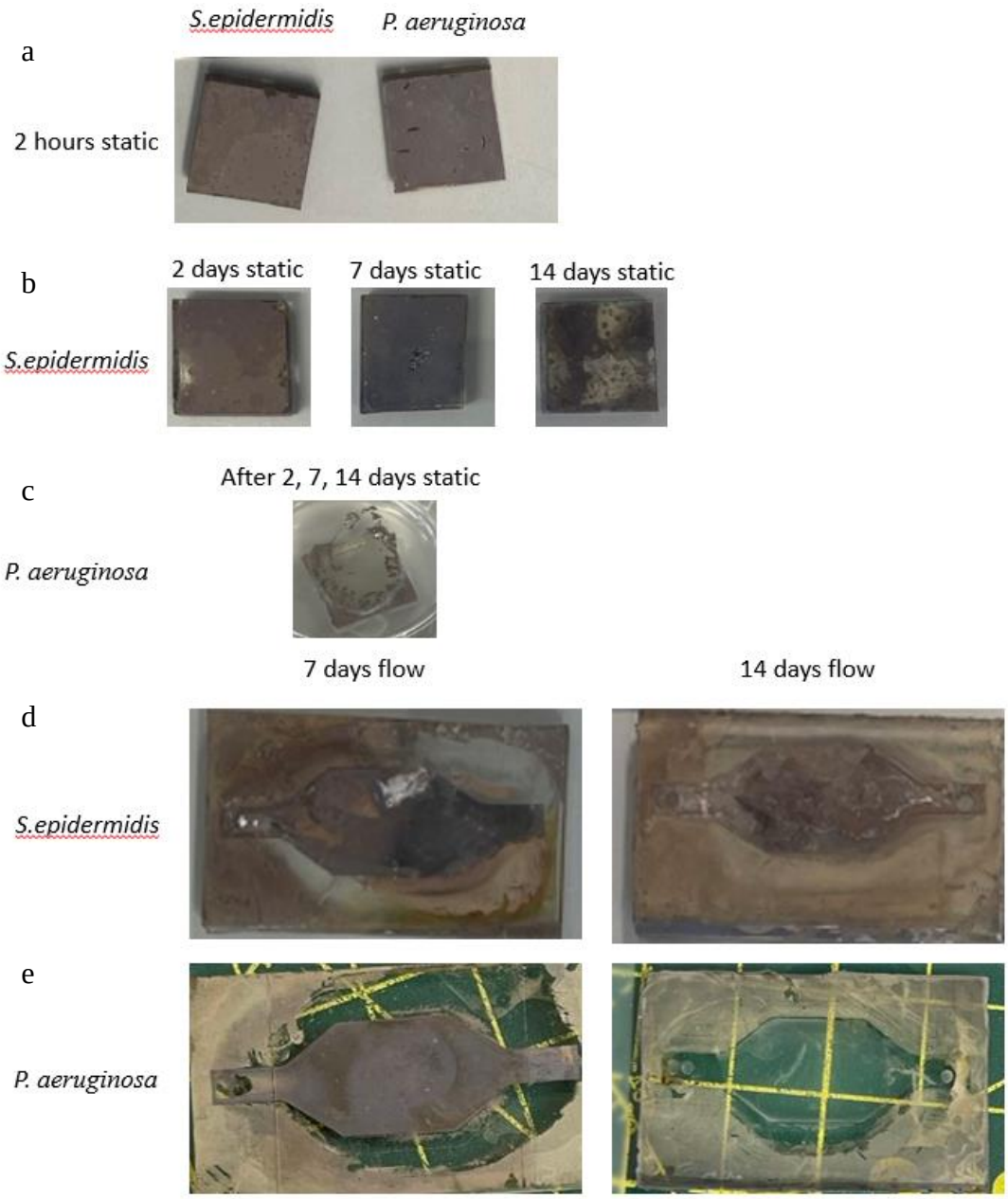

Figure S2 Characterization of AgNPs-coated PDMS after bacterial culture. (a) 2 hours static bacterial adhesion, no coating peeled. (b) 2days, 7days S.epidermidis static biofilm formation, no coating peeled; 14days around half coating peeled. (c) 2days, 7days and 14days PAO1 static biofilm formation, almost all the coating peeled. (d) 7days and 14days S.epidermidis dynamic biofilm formation, no coating peeled. (e) 7days PAO1 dynamic biofilm formation, no coating peeled; 14days all coating peeled.